



# Self-assembled monolayers and patterned surfaces derived from them as templates for the growth of chiral crystals

Ángela Bejarano Villafuerte

**ADVERTIMENT.** La consulta d'aquesta tesi queda condicionada a l'acceptació de les següents condicions d'ús: La difusió d'aquesta tesi per mitjà del servei TDX ([www.tdx.cat](http://www.tdx.cat)) i a través del Dipòsit Digital de la UB ([diposit.ub.edu](http://diposit.ub.edu)) ha estat autoritzada pels titulars dels drets de propietat intel·lectual únicament per a usos privats emmarcats en activitats d'investigació i docència. No s'autoritza la seva reproducció amb finalitats de lucre ni la seva difusió i posada a disposició des d'un lloc aliè al servei TDX ni al Dipòsit Digital de la UB. No s'autoritza la presentació del seu contingut en una finestra o marc aliè a TDX o al Dipòsit Digital de la UB (framing). Aquesta reserva de drets afecta tant al resum de presentació de la tesi com als seus continguts. En la utilització o cita de parts de la tesi és obligat indicar el nom de la persona autora.

**ADVERTENCIA.** La consulta de esta tesis queda condicionada a la aceptación de las siguientes condiciones de uso: La difusión de esta tesis por medio del servicio TDR ([www.tdx.cat](http://www.tdx.cat)) y a través del Repositorio Digital de la UB ([diposit.ub.edu](http://diposit.ub.edu)) ha sido autorizada por los titulares de los derechos de propiedad intelectual únicamente para usos privados enmarcados en actividades de investigación y docencia. No se autoriza su reproducción con finalidades de lucro ni su difusión y puesta a disposición desde un sitio ajeno al servicio TDR o al Repositorio Digital de la UB. No se autoriza la presentación de su contenido en una ventana o marco ajeno a TDR o al Repositorio Digital de la UB (framing). Esta reserva de derechos afecta tanto al resumen de presentación de la tesis como a sus contenidos. En la utilización o cita de partes de la tesis es obligado indicar el nombre de la persona autora.

**WARNING.** On having consulted this thesis you're accepting the following use conditions: Spreading this thesis by the TDX ([www.tdx.cat](http://www.tdx.cat)) service and by the UB Digital Repository ([diposit.ub.edu](http://diposit.ub.edu)) has been authorized by the titular of the intellectual property rights only for private uses placed in investigation and teaching activities. Reproduction with lucrative aims is not authorized nor its spreading and availability from a site foreign to the TDX service or to the UB Digital Repository. Introducing its content in a window or frame foreign to the TDX service or to the UB Digital Repository is not authorized (framing). Those rights affect to the presentation summary of the thesis as well as to its contents. In the using or citation of parts of the thesis it's obliged to indicate the name of the author.



**CSIC**

CONSEJO SUPERIOR DE INVESTIGACIONES CIENTÍFICAS



INSTITUT DE NANOCIÈNCIA  
I NANOTECNOLOGIA



UNIVERSITAT DE BARCELONA



FACULTAT DE  
FARMÀCIA

Research performed at the Institut de Ciència de Materials de Barcelona  
(ICMAB-CSIC) in the framework of the  
Nanosciences Doctoral Programme

of the

UNIVERSITAT DE BARCELONA

FACULTAT DE FARMÀCIA

DEPARTAMENT DE FARMACOLOGIA I QUÍMICA TERAPÈUTICA

**Self-assembled monolayers and patterned surfaces derived  
from them as templates for the growth of chiral crystals.**

Presented by

Ángela Bejarano Villafuerte

Under the supervision of

David B. Amabilino (ICMAB-CSIC)

and Tutored by

Ma Lluïsa Pérez García (Facultat de Farmàcia)

**2013**

# Contents

<b>1</b>	<b>Chapter 1: General introduction.</b>	
1.1	Chirality	2
1.2	Resolution	4
1.2.1	Conglomerate crystallisation	6
1.2.2	Resolution by entrainment	7
1.2.3	Classical resolution	8
1.2.4	Dutch resolution	9
1.3	Crystallisation	10
1.3.1	Nucleation theory	10
1.3.1.1	Classical nucleation theory	12
1.3.1.2	Two-step nucleation theory	13
1.3.1.3	Homogeneous nucleation	14
1.3.1.4	Heterogeneous nucleation	16
1.4	Crystallisation on self-assembled monolayers	18
1.4.1	Self-assembled monolayers (SAMs)	18
1.4.2	Nucleation on SAMs	18
1.4.3	Crystal growth on SAMs	22
1.5	Crystallisation on micropatterned surfaces.	26
<b>2</b>	<b>Chapter 2. Objectives.</b>	<b>31</b>

# Contents

<b>3</b>	<b>Chapter 3. Crystal Structure analysis.</b>	
3.1	Introduction	33
3.2	Phencyphos derives	33
3.3	Diastereomeric salts	38
3.3.1	New structures	38
3.3.2	Crystalline diastereomeric salt structures retrieved from the CSD	48
3.4	Conclusions	58
<b>4</b>	<b>Chapter 4. Self-assembled monolayers.</b>	
4.1	Introduction	64
4.2	SAMs	66
4.3	(+) Phencyphos 4-Methylenethiol SAMs on monocrystalline gold.	68
4.3.1	XPS Analysis	68
4.3.2	Contact angle measurement	69
4.3.3	STM	70
4.4	Dodecanethiol SAMs on monocrystalline gold	71
4.4.1	XPS Analysis	72
4.4.2	Contact angle measurement	72
4.4.3	STM	73
4.5	11-Mercaptoundecanoic acid SAMs on Monocrystalline gold.	

## Contents

4.5.1	XPS Analysis	74
4.5.2	Contact angle measurement	75
4.6	Experimental section	75
<b>5</b>	<b>Chapter 5: Multilayer formation through complementary Interactions on SAMs</b>	
5.1	Introduction	77
5.2	Room temperature adsorption	80
5.2.1	Neutral multilayer growth on a SAM of (+)-PMT at r. t.	80
5.2.2	Neutral multilayers growth on MUA monolayer at r. t.	84
5.2.3	Charged multilayers for growth on SAM of (+) PMT at r. t.	87
5.3	Formation of multilayers at higher temperature	
5.3.1	Neutral multilayer. Monocrystalline gold on mica. (Higher temperature, 40°C)	93
5.3.1.1	AFM study	97
5.4	Conclusions	99
<b>6</b>	<b>Chapter 6: Self-assembled monolayers as templates for crystal nucleation and growth</b>	
6.1	SAMs as templates for crystal nucleation and growth	101
6.2	Crystallisation of phencyphos on SAMs of (+) PMT.	103

## Contents

6.2.1	Fast solvent evaporation method	104
6.2.1.1	Chloroform series	104
6.2.1.2	Isopropanol series	108
6.2.2	Slow solvent (under control) evaporation method	
6.2.2.1	Chloroform series	114
6.2.2.2	Isopropanol series	117
6.3	Infrared spectroscopy analysis	119
6.4	Experimental section	122
6.5	Conclusions	123
<b>7</b>	<b>Chapter 7: Preparation of Micropatterned Surfaces</b>	
7.1	Introduction	125
7.2	Optimising a microcontact printing protocol	128
7.2.1	Mask design	128
7.2.2	Photolithography for preparation of Silicon Wafer Master	132
7.2.3	Profilometry	135
7.2.4	Preparation of PDMS Stamps	139
7.2.5	Substrates	140
7.3	Chemical Patterning with Thiols	141
7.4	Microcontact printing Stamping Protocol and Patterning	142

# Contents

7.5	Conclusions	146
<b>8</b>	<b>Chapter 8: Micropatterned surfaces as templates for crystal growth</b>	
8.0	Introduction	149
<b>8.1</b>	<b>Preferential Phencyphos crystallisation on micropatterned surfaces</b>	
8.1.1	Introduction	151
8.1.2	Crystallization methods	
8.1.2.1	Drop casting	155
8.1.2.2	Fast solvent evaporation method	156
8.1.2.3	Slow solvent evaporation method	162
8.1.2.3.1	Powder X-ray microdiffraction characterisation	170
8.1.2.4	Micropatterned surface for a prolonged time the in solution with stirring method	
8.1.2.4.1	Chloroform series	173
8.1.2.4.2	Isopropanol series	175
8.1.3	Pattern shape and size influence	183
8.1.4	Chirality and Polarity on surface	185
8.1.5	Contrasting solvents in the heterogeneous nucleation of PMT on micropatterned surfaces	186
8.1.6	Conclusions	190

# Contents

## 8.2 Preferential Diastereomeric Salts crystallisation on micropatterned surfaces

8.2.1	Introduction	191
8.2.2	Influence in the diastereomeric salt crystallisation on micropatterned surfaces	195
8.2.2.1	Concentration of the ink solution influence	195
8.2.2.2	Control experiments	197
8.2.2.3	Incubation time of the micropatterned surface in solution influence	198
8.2.2.3.1	Powder X-ray microdiffraction characterisation	200
8.2.2.4	Shape and size of the motif printed influence	203
8.2.3	Crystallisation method	206
8.2.3.1	Slow solvent evaporation	206
8.2.3.2	Drop casting	207
8.2.3.2.1	Dry drop casting (5 mM, 10 mM, 25 and 40 mM)	207
8.2.3.2.2	Wet casting incubation-growth method	211
8.2.4	Chirality at surface	213
8.2.4.1	Same chirality on surface (full surface)	213
8.2.4.2	Different chirality on surface: <i>Half</i> and <i>crossed printing</i>	217
8.2.5	Crystallisation in the Crystallisation Mushroom®	218



## Contents

8.2.5.1	Different chirality on surface: <i>Half printing</i>	219
8.2.5.2	Different chirality on surface: <i>Crossed printing</i>	221
8.2.6	(+)-PMPP/(+)-PEA salt crystallisation	223
8.2.7	Characterisation of (-)-PMPP/(-)-PEA salt crystals on micropatterned surfaces.	226
8.2.7.1	Powder X-ray microdiffraction characterisation	226
8.2.7.2	Raman confocal characterisation	228
8.2.8	Conclusions	231
<b>8.3</b>	<b>Dutch Resolution on micropatterned surfaces</b>	
8.3.1	Dutch Resolution	232
8.3.1.1	Fast solvent evaporation method	234
8.3.1.2	Slow solvent evaporation method	238
8.3.2	Conclusions	246
<b>9</b>	<b>Chapter 9: Final Conclusions</b>	<b>248</b>

## Agradecimientos

El camino recorrido hasta hoy no ha sido un camino de rosas, muchos han sido los obstáculos que he tenido que superar, muchos me producían más pánico que satisfacción y aun así seguí adelante, siempre luchando contra todos mis miedos por conseguir lo que quería. Al fin, he conseguido terminar lo que tanto me ha costado, muchos quebraderos de cabeza, muchas horas dedicadas y muchos sofocones ante cada nuevo paso. No habría podido conseguirlo sin todas las personas que me habéis dedicado vuestro tiempo y esfuerzo, y espero que el resultado os guste tanto como a mí.

Todo esto no habría sido posible sin la oportunidad que mi director me ofreció. Por esta fantástica oportunidad, por su gran paciencia, su dirección, por exigirme tanto, por saber tratarme, por sus consejos y críticas constructivas, agradezco enormemente a David B. Amabilino haberme ayudado tanto en el desarrollo de esta tesis doctoral y haber apostado por mí. Agradecer también, a mi tutora en la Universitat de Barcelona, María Lluïsa Pérez García, por su gran asesoramiento tanto burocrático, científico y personal durante la realización de esta tesis.

I would to thank to the financial support of the European Community's Seventh Framework Programme for the RESOLVE Project under Grant Agreement No. NMP4-SL-2008-214340. I would to thank to all the people involved in the RESOLVE Project, I have learnt much with them: Rasmita Raval, David Beljonne, Roberto Lazzaroni, Steven de Feyter, Albert Schenning, especially to Richard M. Kellogg and Maarten W. van der Meijden for their hospitality during my stay in Syncom and for the nice collaboration. Thank you very much Maarten for your help and for the funny time together.

Difícilmente habría podido realizar este proyecto sin la ayuda de dos personas fundamentales con las que he tenido el honor de trabajar. En primer lugar, por ayudarme a situarme con el cambio de tema, por enseñarme todo lo que ella sabía, por su paciencia, quiero agradecer a Maggie toda la ayuda y el tiempo que me ha dedicado. Dicen que *no hay camino más oscuro que el que se recorre con los ojos cerrados*, y por un tiempo cerré los ojos por no saber bien cómo hacer, hasta que

apareció Arancha, se remangó las mangas y dijo “¿Qué pasa aquí?” y volvió la luz. Muchas gracias a todos los niveles, gracias por ser tan paciente y comprometida, trabajar mano a mano conmigo, por tratarme de tú a tú, plantearme dilemas que se me escapaban, por reñirme, por mostrarme el camino y explicarme las cosas. Me has dedicado mucho tiempo y me has ayudado mucho más de lo que piensas, gracias.

Me gustaría agradecer a todos los integrantes de mi grupo y del despacho que cada uno ha contribuido en algo y me han hecho pasar momentos geniales. François, Filippo, Wojtek (mi ying en el grupo, gracias por compensar la balanza con tu positividad), Josep (me has ayudado en todo lo que podías, muchas gracias!), María, Queralt, Dani y Markos, que hemos aprendido mucho uno del otro, gracias por las charlas y los sermones filosóficos. A Marta y Cristina, muchas gracias por apoyarme y animarme. Por ser mis manos cuando andaba vendada hasta el codo, y sacarme sonrisas siempre que me veis, tenéis un pedacito de mí.

A mis técnicas favoritas Judith Oro y Ana Crespi, que siempre me habéis ayudado mucho, por las sesiones arreglando el mundo y por paraos a conocerme y dejarme conocerlos. Al técnico que nos mantiene a raya y a la vez nos escucha y ayuda en todo lo que puede, Amable. Muchas gracias a los integrantes de Sala Blanca, por su apoyo y ayuda, por su paciencia con mis cambios y por ir siempre a contrarreloj, gracias Neus, Edgar y Quique. Da gusto trabajar con vosotros. A todo el personal del ICMAB, que hacen de este instituto un lugar fantástico para trabajar.

Muchas gracias a “los orgánicos”, con lo que he tenido el placer de compartir con vosotros miles de historias, y rollos de laboratorio, César, Eli, Ingrid (gracias por tan buenos momentos), Elena, Carlos, Jose, Javi, Lidia, Matt, Victor... A Eve, que me has ayudado tanto cristalográfica y personalmente, y me costará tenerte lejos. A Paco, por las conversaciones acaloradas llevándonos la contraria como si no hubiese mañana, por ayudarme con la química (que para eso eres un crack!), por los momentos bancos y por lo bien que nos lo hemos pasado!

A mis amigos, que siempre han confiado en mí aunque no sabían muy bien que estaba haciendo, especialmente a María y Carlos que son los que más me han apoyado y siempre me han estado dando ánimos. A Nina, por mostrarme el camino, acogerme

cuando llegué, enseñarme la Barcelona “gambitera” y ayudarme a relativizar los problemas que me encontraba.

Al despacho OnFire! que lo forman muchos, punto cardinal de reunión y donde salen los mejores momentos improvisados!! Javi, AnaMi, Ana Lopez (A.Lo), PoppyLau, Nerea, Nina, Stefanía, Jessica, Jullieith, Tomate, Raül, Marisa ... Gracias por ser mi familia y sentirme que tengo un hueco entre vosotros, me habéis hecho sentir como en casa, me habéis dado mucha fuerza y me faltaréis vaya donde vaya.

Muchas gracias a toda mi familia, que siempre me han apoyado, a los que ya no están, especialmente a mi abuela que siempre me mandaba fuera a que conociese mundo y no me conformase con lo de siempre. A mis padres, Antonio y Mari Carmen, por haberme tejido tan bien las alas que me han permitido volar. Gracias por haber sido tan insistentes conmigo siempre, por transmitirme este instinto de superación que me hace tirar hacia delante contra viento y marea, por no daros por vencidos luchando contra el genio que llevo dentro. A mi padre, por escucharme, enseñarme a razonar y reducir los problemas difíciles a un simple contratiempo. Siempre me has sabido desenredar. A mi madre, por ser mi modelo a seguir, por hacerme multifunción y confiar en mí incondicionalmente. Siempre sabes hacer que saque de donde no hay. A mis hermanos que siempre me han echado un cable y han ido amoldándose el terreno. Alejandro, gracias por tus locuras, racionalidad, por mostrarme cómo se pueden combinar ambas cosas sin perderse en el intento y jamás dudar que pudiera con esto. Adelaida, por llamarme la atención sobre las cosas que no veía, por darme varios puntos de vista y por estar siempre conmigo animándome en cada paso. A mis tíos, mis primos, a Paloma y Enrique, por interesaros tanto y seguir la evolución con emoción. A mi pequeña Julia.

Quisiera agradecer a mi pareja, David, todo el apoyo que me ha dado, nunca me ha dejado caer, por su infinita paciencia y por darme fuerzas cada día. Agradecer también a su familia por acogerme como uno más y pasar por todo conmigo.

Ángela

## **Abbreviation list**

AFM = Atomic Force Microscopy

CA = Contact angle

CNT = Classical Nucleation Theory.

DT = Dodecanethiol

MUA = 11-Mercaptoundecanoic acid.

PMT = Phencyphos 4-Methylenethiol

SAMs = Self-assembled monolayer

SEM = Scanning Electron Microscopy

STM = Scanning Tunneling Microscopy

TNT = Two-step nucleation theory

XPS = X-ray Photoelectron spectroscopy

# Chapter 1

## Introduction

---

This chapter introduces the main concepts in the fields studied in this Thesis that are chirality, resolution and crystallisation on functionalised surfaces.

## 1.1. Chirality

Chiral phenomena are ubiquitous in the natural world from the macroscopic to the microscopic scale. The handedness of biological systems has resulted in chirality being termed “the signature of life”.<sup>1</sup> The high preference for chirality of small biomolecules, the particular secondary structures in the conformations of biomacromolecules induced by it, as well as chirality-triggered biological and physiological processes bear witness to this assertion. Life also shows chirality in most of the processes it carries out because they involve chiral molecules in their biological routes, and is expressed from the molecular level to the form of living things. But what does chirality mean? The word *chirality* derived from the Greek *χειρ* (*kheir*), hand, a familiar chiral object. Chirality is a property of structural dissymmetry of an object that is non-superimposable on its mirror image.<sup>2</sup> A well-known example of chirality in nature is quartz crystals. Four quartz crystals are shown in Figure 1.1. The two crystals of each set are of opposite chirality. Chirality arises in quartz from the nature of bonding between tetrahedral ( $\text{SiO}_4$ ) silicate groups, which results in either right- or left-handed helices running through these network-covalent solids (with space groups  $P3_121$  and  $P3_221$  for  $\alpha$ -quartz and  $P6_222$  and  $P6_422$  for  $\beta$ -quartz, respectively).

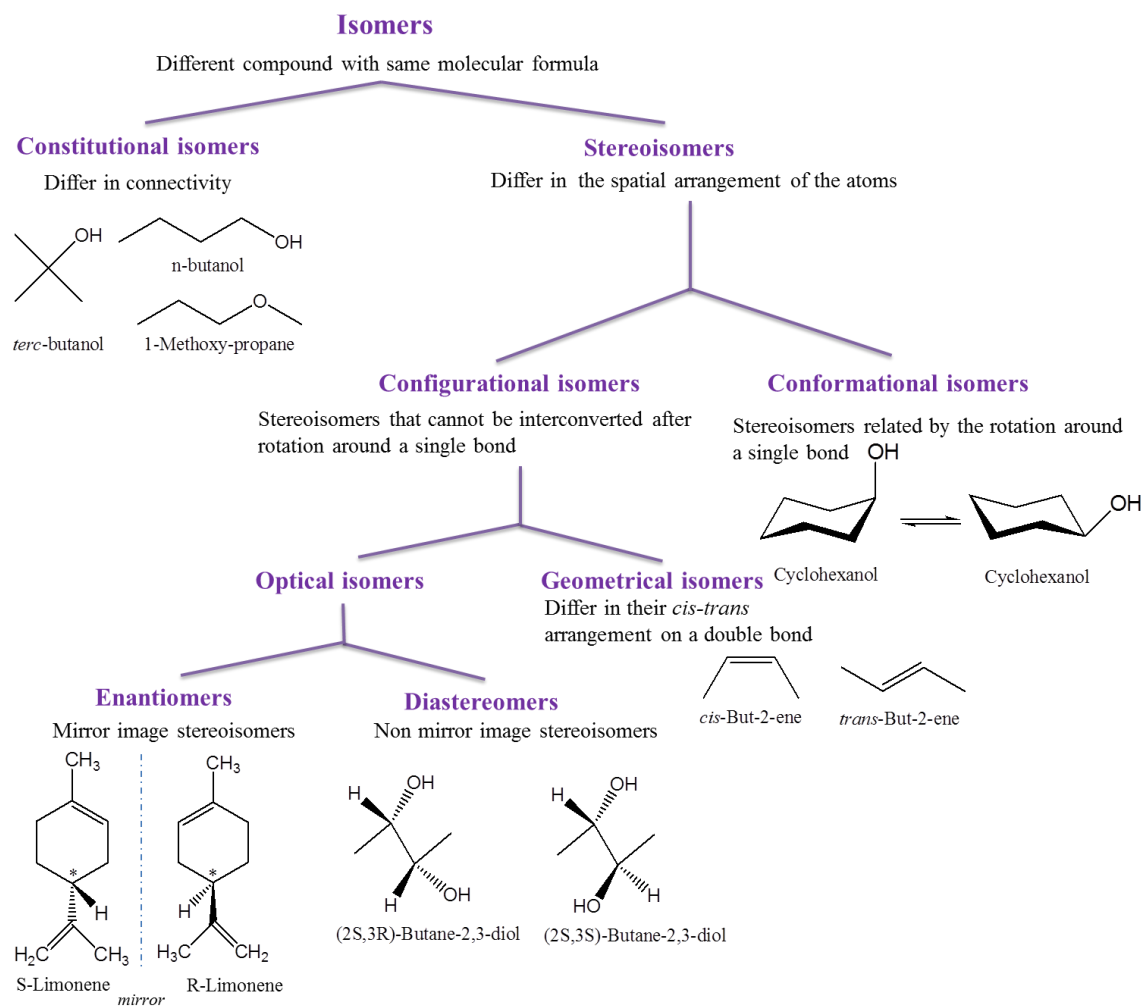


**Figure 1.1.** Enantiomorphic quartz crystals grown in nature.

<sup>1</sup> A. J. MacDermott, L. D. Barron, A. Brack, T. Buhse, A. F. Drake, R. Emery, G. Gottarelli, J. M. Greenberg, R. Haberle, R. A. Hegstrom, K. Hobbs, D. K. Kondepudi, C. McKay, S. Moorbath, F. Raulin, M. Sandford, D. W. Schwartzman, W. H.-P. Thiemann, G. E. Tranter, J. C. Zarnecki, *Planet. Space Sci.*, **1996**, *44*, 1441-1446.

<sup>2</sup> R. Bentley, *Chirality*, **2010**, *22*, 1–2.

Quartz crystals are formed by pure enantiomers which are optical isomers. The *isomers* are compounds with the same molecular formula but differ in their chemical structures, in the case of enantiomers with a mirror-image relationship. There is an isomer classification which is shown in the Figure 1.2.



**Figure 1.2.** An isomer classification.

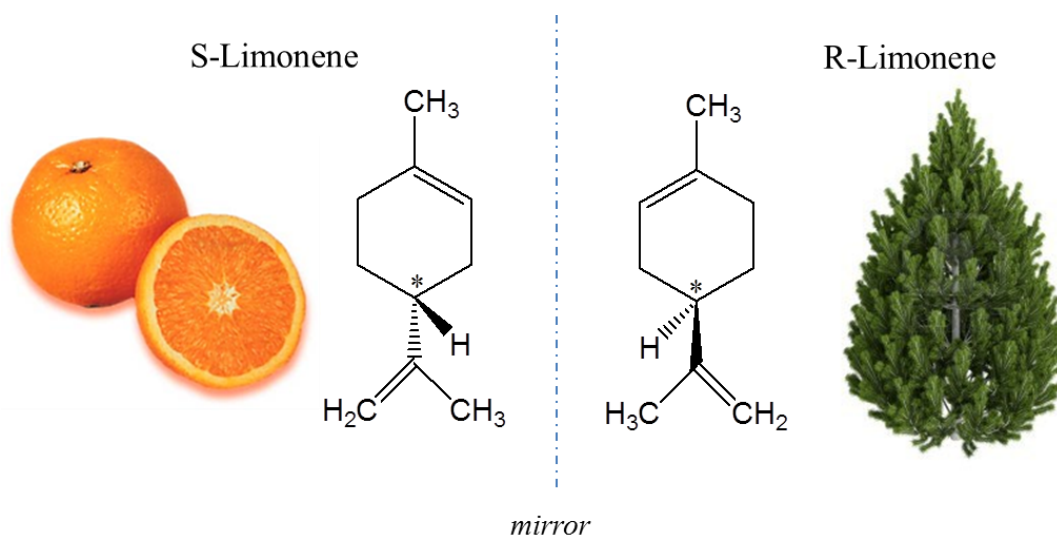
Enantiomers have identical energy content and physical properties such as colour, weight, density, melting point, solubility, etc. in a symmetrical environment.<sup>3</sup> However, there are some atomistic effects to take into account in order to calculate the energy of each enantiomer which conclude there is a tiny difference in energy between both enantiomers. For example, calculations of some sugar molecules observe that there is a difference of  $10^{-13}$ - $10^{-14}$  J between the L-sugar and the D-sugar (discriminated in nature).<sup>4</sup> In a non-symmetrical (chiral) environment enantiomers behave very differently, because

<sup>3</sup> G. Pályi, C. Zucchi, L. Caglioti, *Progress in Biological Chirality*, **2004**, Elsevier Ltd.

<sup>4</sup> L. D. Barron, *J. Am. Chem. Soc.*, **1986**, *108*, 5539.



the combination of chiralities gives rise to different energies for a system in the form of *diastereoisomers*. For example, we (who are chiral!) can distinguish enantiomers of certain compounds by smell and taste, is the case of the molecule Limonene, its smell is different for each enantiomer, D-Limonene smells of pine and L-Limonene smells of citrus fruit (Figure 1.3).



**Figure 1.3.** L-Limonene orange-like smell and D-Limonene pine-like smell.

## 1.2. Resolution

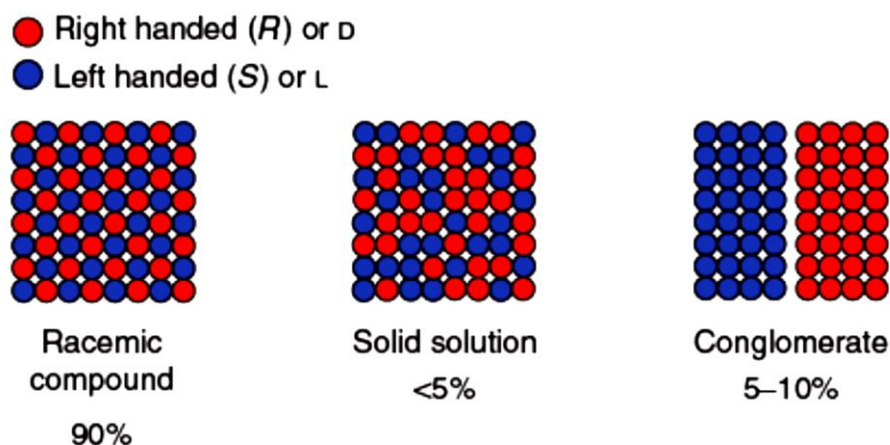
The importance of chirality in medicine is utmost because the enantiomers of chiral drugs can have very different biological activities,<sup>5</sup> and for this reason the separation of enantiomers in a racemate – a mixture of molecules of opposite chirality – using a chiral environment is of utmost importance.<sup>6</sup> As stated, this combination of chiralities is termed diastereoisomerism. Diastereomers are not related as image and mirror image, and differ in energy content and consequently in all properties including solubility. The diastereomeric relationship between systems is used for the separation – or *resolution* – of enantiomers in a racemate with the help of enantiomerically pure resolving agents.<sup>7</sup>

<sup>5</sup> A. R. Fassihi, *Int. J. Pharmac.*, 1993, 92, 1-14.

<sup>6</sup> T. J. Wozniak, R. J. Bopp, E. C. Jensen, *J. Pharma. Biomed. Anal.*, **1991**, 9, 363-382.

<sup>7</sup> A. Mannschreck, R. Kiesswetter, *J. Chem. Ed.*, **2005**, 82, 1034-1039.

The separation of enantiomers is most effectively achieved from the mixture of the two on a large scale through crystallisation. A solid racemate could fall into one of the three forms (Figure 1.4); as a racemic compound (crystals containing both enantiomers in a periodic array), a conglomerate (where enantiomers are contained in separate crystals), and a solid solution (crystals containing both enantiomers in a non-periodic array). Approximately 90% of organic compounds crystallise as racemic compounds and less than 5% as solid solutions. Conglomerates constitute the remaining 5-10% of neutral organic compounds.<sup>8</sup> In the case of salts, the percentage is higher, probably around 30%.<sup>9</sup> Thus, crystallisation from a solution containing enantiomers will follow one of these cases: conglomerate crystallisation, racemate crystallisation and crystallisation of a solid solution.



**Figure 1.4.** Scheme of the symmetry relationships between molecules in the types of racemates: crystallisation as racemic compound, solid solution or conglomerates.<sup>3</sup>

For the pharmaceutical industry, it is vitally important to separate both enantiomers from a racemic mixture (racemates); the reason lies in the final products of the organic synthesis to get the drugs. Normally, these final products (or compounds on route to them) form racemates. Thus, taking into account that a pair of chiral drugs may exhibit very different medical effects toward a patient – one enantiomer may be effective for a kind of disease, while the other one may be ineffective or even toxic – their separation is mandatory.<sup>10</sup>

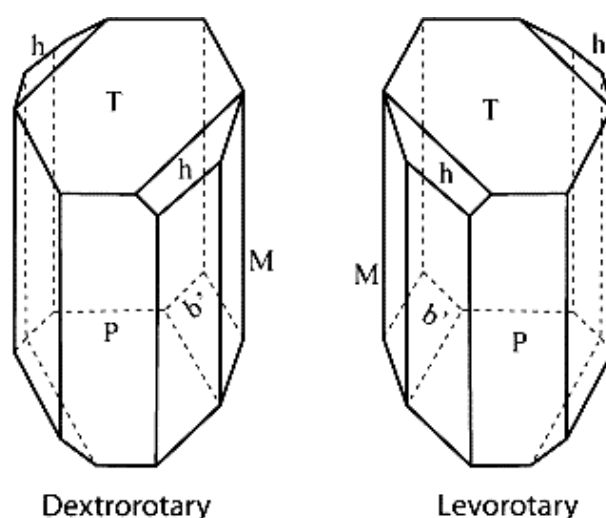
<sup>8</sup> J. Jacques, A. Collet, S. H. Wilen, *Enantiomers, Racemates and Resolution*, Krieger, Florida, **1994**.

<sup>9</sup> R. M. Kellogg, M. Leeman, *Crystallization as a Tool in Industrial Applications of Asymmetric Synthesis*. *Comprehensive Chirality*, **2012**, 9, 367-399. Elsevier.

<sup>10</sup> M. Zhang, G. Qing, T. Sun. *Chem. Soc. Rev.*, **2012**, 41, 1972-1984.

### 1.2.1. Conglomerate crystallisation

A compound is a *conglomerate* if both enantiomers of a racemate crystallize in two separate mirror imaged crystals. A *conglomerate crystallisation* consists in the spontaneous crystallisation of each enantiomer separately. The most famous conglomerate crystallisation was in 1848, when Louis Pasteur crystallised an aqueous solution of sodium ammonium tartrate and obtained mirror image single crystals (Figure 1.5) which he could separate with a looking glass and tweezers.<sup>11</sup> Enantiomeric crystals are formed by one pure enantiomer and they are mirror images non-superimposable.



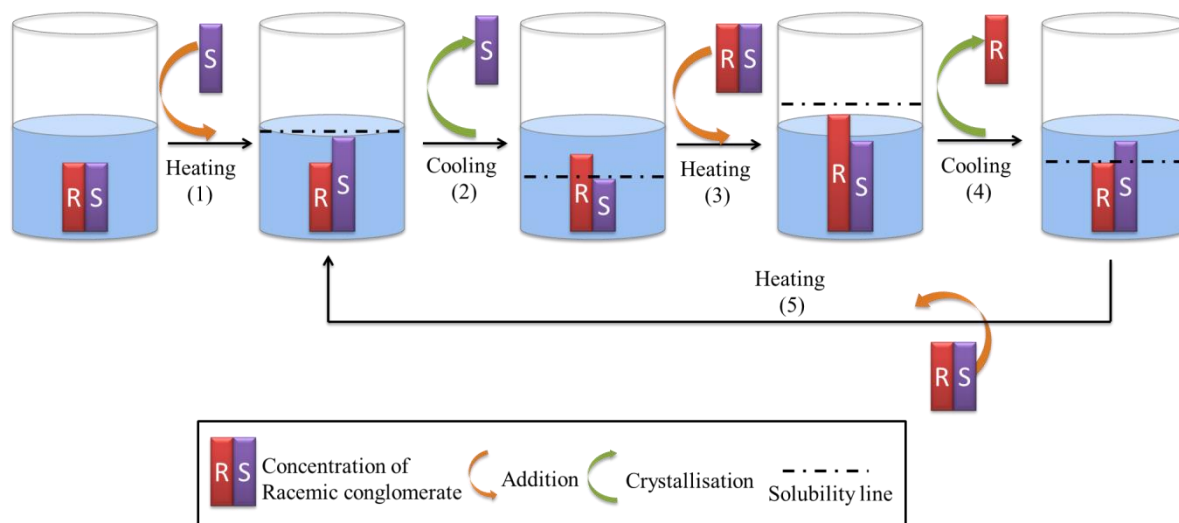
**Figure 1.5.** Sodium ammonium tartrate enantiomeric crystals results of Pasteur's chiral separation of racemic sodium ammonium tartrate. The crystal's morphology revealed the chirality of the molecules of which it was composed.

As only roughly 10% of all racemates crystallize as conglomerates there are two different techniques which can be applied in preferential crystallisation: *simultaneous crystallisation* and *resolution by entrainment*. In *simultaneous crystallisation*, from a supersaturated solution of a racemic conglomerate is allowed to crystallise in two separate enantiomeric crystals, simultaneously.

<sup>11</sup> L. Pasteur, *L. Ann. Chim. Phys.*, **1848**, 24, 442-459.

### 1.2.2. Resolution by entrainment<sup>12</sup>

The resolution by entrainment consists in the separation of both enantiomers from a racemate solution playing with the difference in the solubility of each enantiomer due to enantiomeric excess. The supersaturated solution of a racemic conglomerate contains seeds of the respective enantiomer (Figure 1.6). In the *step 1*: The resolution starts with the (*S*)-enantiomer addition to the racemic mixture in a solvent and heated to dissolution. The *step 2* consists in cooling down the mixture of enantiomers, promoting the crystallisation of the enantiomer with the highest concentration (*S*) and its concentration will return to the saturation point (saturation line). The (*S*)-enantiomer is collected by filtration before the supersaturated (*R*)-enantiomer starts to crystallize. In the *step 3* the racemate is added with the same weight as the (*S*)-enantiomer collected in the previous step 2, and the mixture is heated to dissolution. The *step 4* cold down again the mixture to supersaturate both enantiomer, but now the *R*-enantiomer crystallises. The amount of crystals collected after filtration is the same as the amount of racemate added in the previous step. The racemate would be added to the mixture which would be heated to dissolution, then cooled down to get the same results as after the first step.



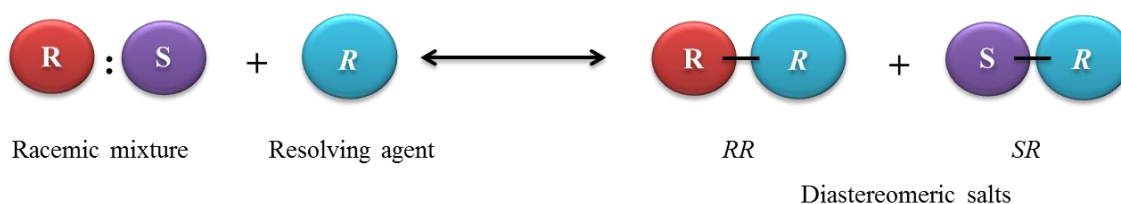
**Figure 1.6.** Scheme of resolution by entrainment process of a saturated solution of a racemic conglomerate.

<sup>12</sup> M. S. Leeman, *Resolutions of Racemates by Crystallization*, 2009, University of Groningen (The Netherlands) (ISBN: 978-90-367-3842-2).

Resolution by entrainment is useful because no additional agents are required. Thus, enantiopure crystals could be added as template for the same handedness enantiomer to crystallise on. This method is denominated *seeding* and may be repeated as needed. The mother liquor limits the number of repetitions because when this liquor is reused it accumulates impurities that can affect to the crystallisation process.

### 1.2.3. Classical Resolution

Racemates do not resolve easily, but if the racemate has an acid or basic group, a salt can be formed by the reaction with an enantiopure acid or basic compound (resolving agent). This is the most used method to obtain optically pure enantiomers called *Classical Resolution* (Figure 1.7). The resolving agent reacts with one enantiomer, forming a *diastereomeric salt*, which precipitates – while the other enantiomer stays in solution – and the pure enantiomer can be liberated by addition of acid or base.<sup>13</sup> This method is useful in order to resolve equal mixture of racemates, playing with the diastereomeric salts solubility.<sup>14</sup>



**Figure 1. 7.** Classical resolution scheme. Racemic mixture is resolved by a resolving agent (enantiomerically pure, *R* or *S*) forming diastereomeric salts (*RR*, *RS*), one crystallises and the other one keep in solution.

There are compounds whose resolution is complicated because they do not have acid or basic groups such as, for example, alcohols. To resolve alcohols by classical resolution the formation of an inclusion complex with a chiral host or the reaction with an enantiopure compound producing covalently bound diastereomers is needed, changing their physical properties and allowing its success separation.<sup>15</sup>

<sup>13</sup> D. Kozma, *Optical Resolutions via diastereomeric salt formation*, CRC Press; 1st edition, 2012.

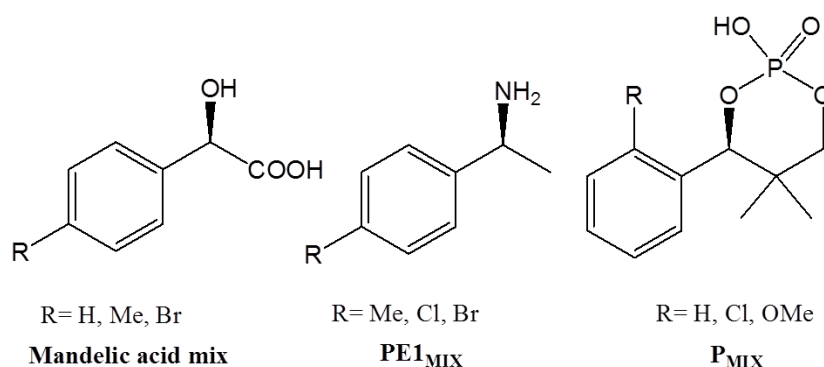
<sup>14</sup> Q. He, H. Goma, S. Rohani, J. Zhu, M. Jennings. *Chirality*, 2010, 22, 707-716.

<sup>15</sup> S. Müller, M. Cyrus, R. de Gelder, G.J.A. Ariaans, B. Kaptein, Q.B. Boxterman, A. Bruggink, *Eur. J. Org. Chem.* 2005, 25, 1082–1096.

### 1.2.4. Dutch Resolution

In 1998,<sup>16</sup> a research team in Holland presented an improvement of classical resolution (by diastereomeric salt formation), called *Dutch Resolution*.<sup>17</sup> This term is given to the use of mixtures of enantiopure resolving agents in classical resolutions. Racemates would be resolved by diastereomeric salt formation faster by adding stoichiometric amounts of a homochiral mixture of resolving agents, called *family members* (Figure 1.8).

The first major effect of the *Dutch resolution* is due to the presence of a resolving agent family, which improves dramatically the chance of success in the search of diastereomeric salts. With three resolving agents and one racemate, the combination of least soluble diastereomers would crystallise first, reducing the chance of encountering a salt that will not form crystalline salts.<sup>18</sup> Even if these family members are not incorporated in the growing crystal, their presence in solution can still have a positive effect on nucleation.



**Figure 1.8.** Three examples of resolving agent families used in Dutch resolution.

The second major effect of the Dutch resolution is nucleation inhibition. It was noticed that if a family of three resolving agents was used that often one of the resolving agents was only slightly incorporated into the precipitated salts. The diastereomer that is not wanted is kept in solution longer, since nucleation inhibition is a kinetic effect.

<sup>16</sup> T. Vries, H. Wynberg, E. van Echten, J. Koek, W. ten Hoeve, R. M. Kellogg, Q. B. Broxterman, A. Minnard, B. Kaptein, S. van der Sluis, L. Hulshof, J. Kooistra, *Angew. Chem. Int. Ed.*, **1998**, *37*, 2349-2354.

<sup>17</sup> R. M. Kellogg, J. W. Nieuwenhuijzen, K. Pouwer, T. R. Vries, Q. B. Broxterman, R. F. P. Grimbergen, B. Kaptein, R. M. La Crois, E. de Wever, K. Zwaagstra, A. C. van der Laan. *Synthesis*, **2003**, *10*, 1626-1638.

<sup>18</sup> M. Leeman, G. Brasile, E. Gelens, T. Vries, B. Kaptein, R. M. Kellogg, *Angew. Chem. Int. Ed.*, **2008**, *47*, 1287-1290.

Both classical and Dutch resolutions rely on crystallization of diastereomeric salts. Therefore, in order to advance in the area of resolutions of this type, it is essential to understand the crystallization process in organic compounds.

### 1.3. Crystallisation

Crystallisation is crucial to many processes occurring in nature, chemical, pharmaceutical, and food industries. Solution crystallisation is an intensely used process for separation and purification in the chemical and pharmaceutical industry.<sup>9, 18</sup> The crystallisation process consists of two stages: *Nucleation* and *Crystal growth*. The nucleation stage is a stochastic process in which the nucleus (clusters of molecules) would be formed until they reach the critical size and rearrange to overcome the critical energy to form crystals which gives an ordered nucleus that then increases in size in the crystal growth stage.

#### 1.3.1. Nucleation theory

In a first-order phase transition, there is a discontinuous change in some order parameter between the two phases. Nucleation is a first order transition process in which a metastable phase (liquid) transforms into a new stable phase (solid). The thermodynamic definition of the first-order phase transitions according to which at the point of phase equilibrium the chemical potentials of the old and the new phases are equal, but their derivatives of first order  $\left(\frac{\partial\mu_{liquid}}{\partial p}\right)_T \neq \left(\frac{\partial\mu_{solid}}{\partial p}\right)_T$  are not since any variation on pressure or temperature can affect them.

Thus, phase equilibrium or coexistence between the old and the new phases is possible when the corresponding minima of the free energy of these phases are equally deep, i.e. when  $\mu_{liquid,e} = \mu_{solid,e} \equiv \mu_e$  -here  $\mu_{liquid,e}$  and  $\mu_{solid,e}$  are, respectively, the chemical potentials of the old and the new phases at equilibrium, and  $\mu_e$  the equilibrium chemical potential<sup>19</sup>.

The *driving force of nucleation*<sup>21</sup> is the *supersaturation* ( $\Delta\mu$ ), which thermodynamically is defined by the difference between the chemical potentials of both phases:

---

<sup>19</sup> D. Kashchiev, *Nucleation Basic Theory with Applications*, 2000, Butterworth-Heinemann Ed.

$$S \equiv \Delta\mu \equiv (G_{liquid} - G_{solid})/M = \mu_{liquid} - \mu_{solid} \quad (1.1)$$

Physically, the supersaturation ( $S$ ) is the gain in free energy per molecule (or atom) associated with the change of the phase from the minimum with higher Gibbs free energy ( $G_{liquid}$ ) to the minimum with lower Gibbs free energy ( $G_{solid}$ ).  $\mu_{liquid}$  and  $\mu_{solid}$  are, respectively, the chemical potentials of the old and the new phases at the corresponding minima;  $M$  is the total number of molecules in the system.

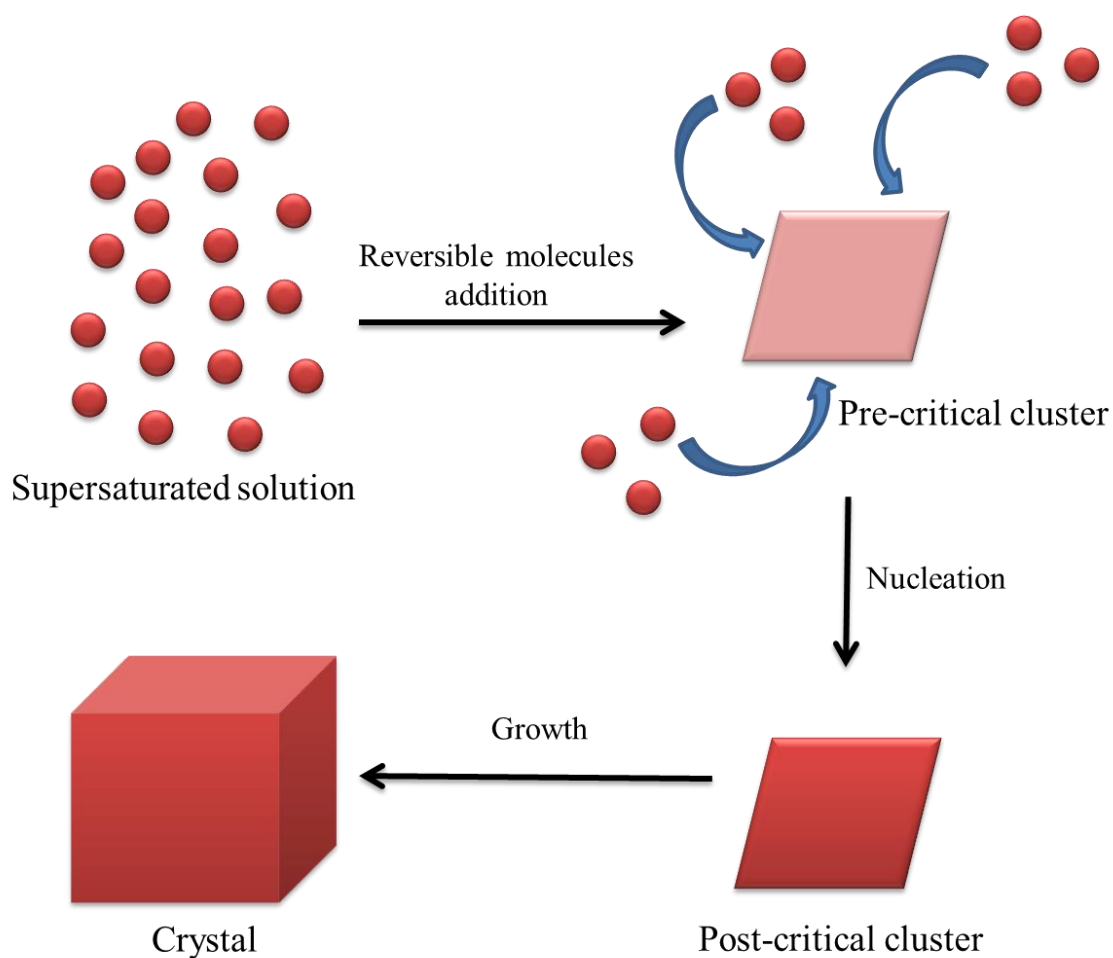
If  $\Delta\mu=0$  at phase equilibrium there exists no driving force for first-order phase transition and, hence, for nucleation. Then it is said that the liquid phase is saturated. Obviously, nucleation is impossible as well when  $\Delta\mu < 0$ : the liquid phase is then undersaturated (its  $G$  minimum is lower than that of the solid phase and  $\mu_{liquid} < \mu_{solid}$ ). Changing the thermodynamic variables such as temperature, volume or pressure makes it possible to reach supersaturation and promote the nucleation event.

Nowadays, there are two main theories to explain the nucleation process, which differ mainly in the nucleation stage description. They are *classical nucleation theory* and *two-step nucleation theory*.



### 1.3.1.1. Classical nucleation theory (CNT)

*CNT* provides a simple model of how crystals nucleate, so, it is the most used theory to explain the process. *CNT* describes a structural model of the dynamics of cluster formation during the nucleation, explained in the Figure 1.9. From a supersaturated solution, an ordered pre-critical cluster would be formed by a molecule's reversible addition to reach the critical size. Once the cluster has this size, the nucleation energetic barrier ( $\Delta G_{\text{crit}}$ ) would be overcome. Post-critical clusters (nuclei) keep growing until they form a macroscopic crystal.<sup>20</sup>

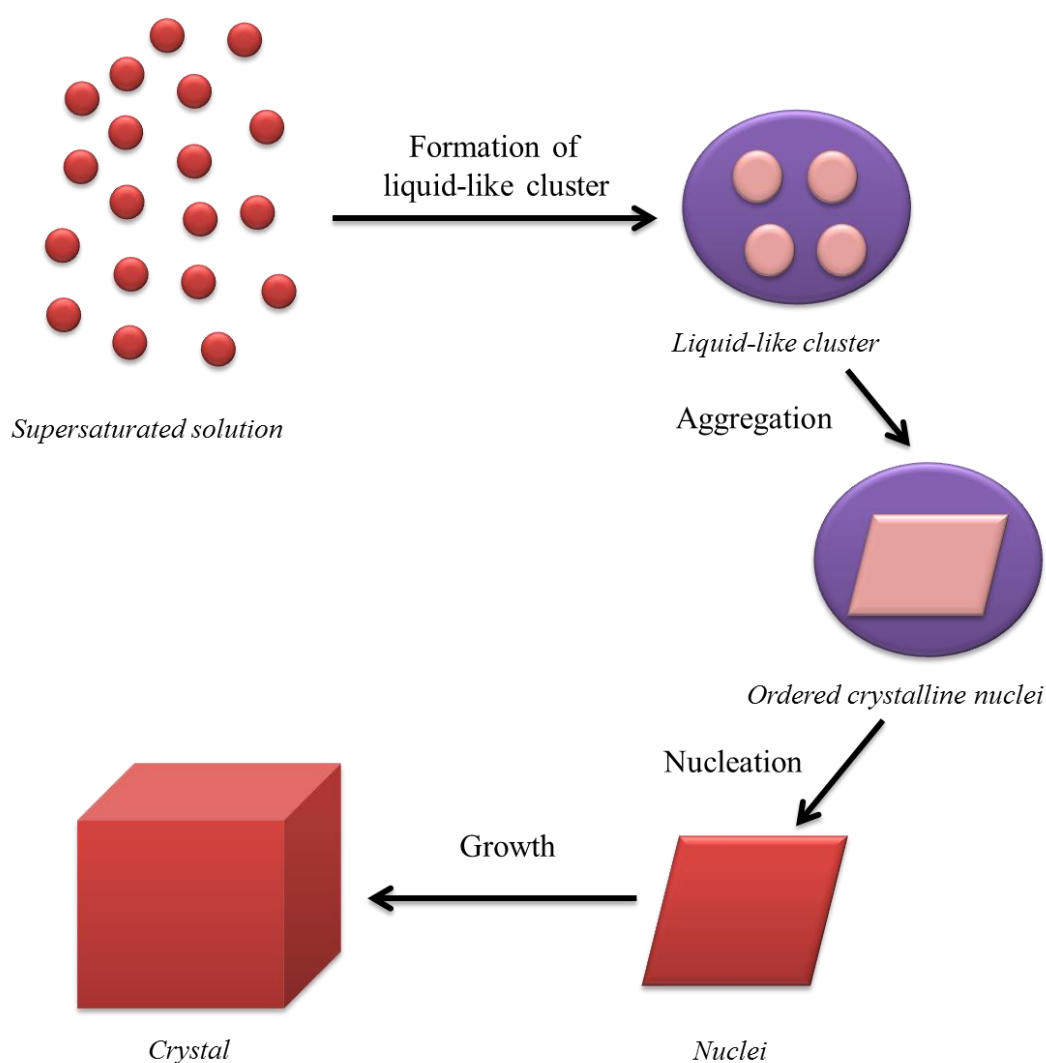


**Figure 1.9.** Scheme describes the structural model of the dynamics of cluster formation during nucleation according to the *CNT*.

<sup>20</sup> P. G. Vekilov, *Cryst. Growth. Des.*, **2010**, *10*, 5007-5019.

### 1.3.1.2. Two-step nucleation theory

Wolde and Frenkel reported two-step nucleation theory in 1997 as one of the first computational studies in this area.<sup>21</sup> Two-step nucleation theory suggests a structural model of the dynamics of cluster formation during the nucleation, explained in the Figure 1.10. From a supersaturated solution, the formation of liquid-like clusters by the aggregation of molecules provides a dense and more disordered intermediate than in CNT. The aggregation of these liquid-like clusters and their re-organisation forming ordered crystalline nuclei, which keep growing until form a macroscopic crystal, is the proposed mechanism.<sup>22</sup>



**Figure 1.10.** Scheme describes the structural model of the dynamics of cluster formation during nucleation according to the *two-step nucleation theory*.

<sup>21</sup> P. R. ten Wolde, D. Frenkel, *Science*, **1997**, 277, 1975-1978.

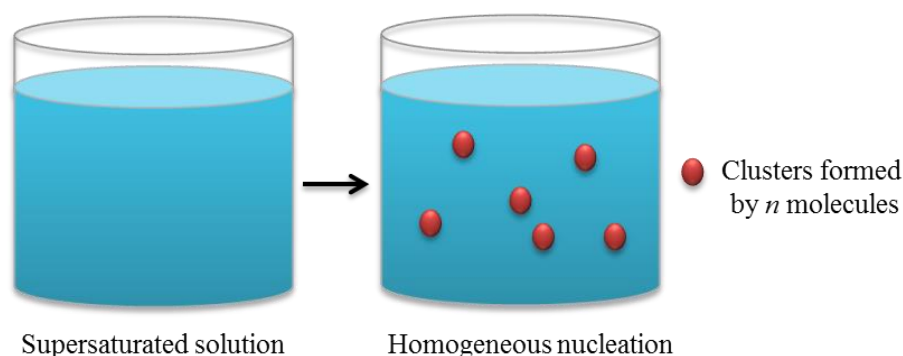
<sup>22</sup> D. Erdemir, A. Y. Lee, A. S. Myerson, *Acc. Chem. Res.*, **2009**, 42, 621-629.

A priori, it is not possible to know which theory fits better with the experiment done. Recent studies<sup>23</sup> show techniques such as Small angle X-Ray Scattering (SAXS) can “see” the nuclei in solution,<sup>24</sup> and on self-assembled monolayers in order to distinguish which theory govern the nucleation process.<sup>25</sup>

Nucleation is the first stage in the crystallisation process and it is influenced greatly by the free energy barrier to be overcome by the clusters formed in the supersaturated solution. In a saturated solution there are two types of nucleation: *homogeneous* and *heterogeneous nucleation*.

### 1.3.1.3. Homogeneous nucleation<sup>26</sup>

The nucleation of any crystal in solution starts with a microscopic fluctuation, which usually occurs at the interface between the solution and a solid impurity. *Homogeneous nucleation* implies the creation of a nucleus formation in the interior of a uniform substance (Figure 1.11) creating a new interface, generally this type of nucleation occurs with much more difficulty due to the high energetic costs of a new surface formation.



**Figure 1. 11.** Homogeneous nucleation.

<sup>23</sup> D. Erdemir, S. Chattopadhyay, L. Guo, J. Ilavsky, H. Amenitsch, C. U. Segre, A. S. Myerson, *Phys. Rev. Lett.*, **2007**, 99, 115702.

<sup>24</sup> S. Chattopadhyay, D. Erdemir, J. M.B. Evans, J. Ilavsky, H. Amenitsch, C. U. Segre, A. S. Myerson, *Cryst. Growth Des.*, **2005**, 5, 523-527.

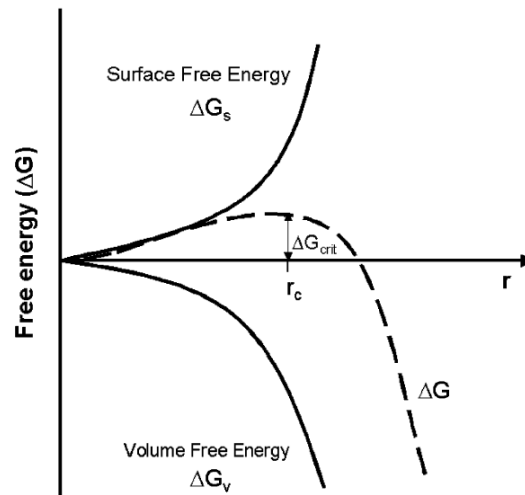
<sup>25</sup> P C.J. Stephens, Y.Y. Kim, S.D. Evans, F.C. Meldrum, H.K. Christenson, *J. Am. Chem. Soc.*, **2011**, 133, 5210-5213.

<sup>26</sup> (a) D. W. Oxtoby, *J. Phys. Condens. Matter*, **1992**, 4, 7627-7650. (b) D. Kashchiev, *Nucleation Basic Theory with Applications*, **2000**, 20-29, Butterworth-Heinemann Ed.

Gibbs, who defined the free energy change required for cluster formation ( $\Delta G$ ) as a sum of the free energy change for the phase transformation ( $\Delta G_V$ ) and the free energy change for the formation of a surface ( $\Delta G_S$ ), equation 1.2, developed the thermodynamic description of this process at the end of the 19th century.

$$\Delta G = -\Delta G_V + \Delta G_S \quad (1.2)$$

Larger clusters have a greater probability of dissolving than of continuing to grow. There are two forces involved in the cluster growth:  $F_A$ , is the force to maintain the cluster united, and  $F_S$  is the force to separate the group, dissolving the clusters. Thus, the growth of clusters depends on the competition between decreases in  $\Delta G_V$  that favour growth and an increase in  $\Delta G_S$ , which favours dissolution. All these energetic factors are represented in Figure 1.12.

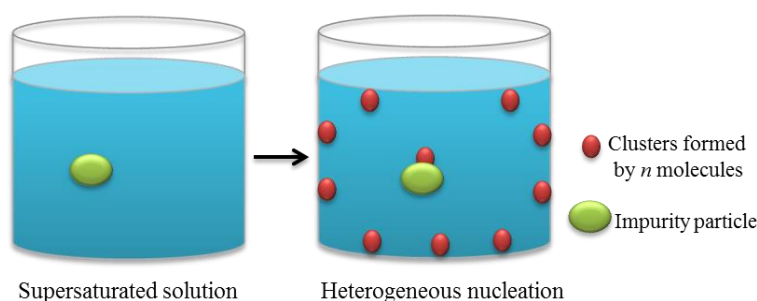


**Figure 1.12.** Gibbs free energy diagram represents the nucleation stage.

The homogeneous nucleation occurs when the clusters of the new phase are in contact only with the old phase and with no other phases and/or molecular species. Nucleation of droplets in the bulk of ideally pure supersaturated vapours is a classic example of homogeneous nucleation.

### 1.3.1.4. Heterogeneous nucleation

*Heterogeneous nucleation* takes place when the nucleus formation is at the solution-surface interface, which presents lower energetic costs than homogeneous nucleation when the liquid phase is in contact or contains other phases and/or molecular species. Heterogeneous nucleation is much more extensive in nature and technology than homogeneous nucleation is. The liquid phase often has solid impurities itself, or bubbles and even it has to be in a container, normally glass container. All these impurities and interfaces can result in a place on which the formation of the clusters of the new phase is preferred to the bulk state (Figure 1.13).<sup>27</sup>



**Figure 1.13.** Heterogeneous nucleation. The nucleus appears at the interfaces, glass-solution, solution-impurity particle, and solution-air.

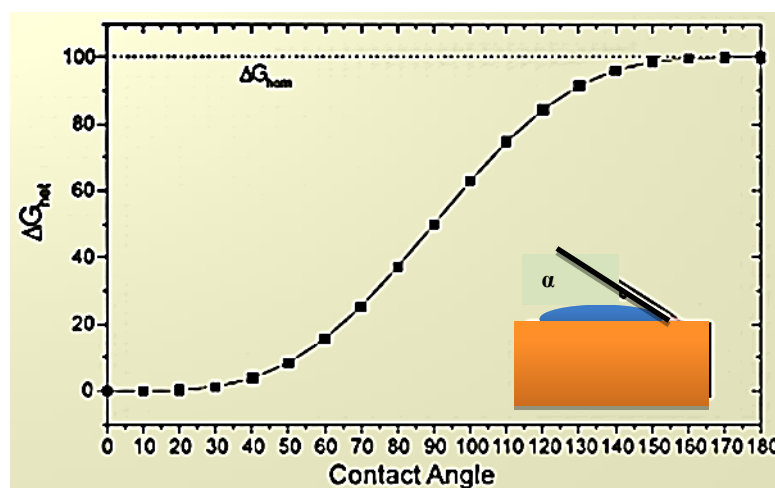
When there is a hydrophobic or hydrophilic surface in the system, this surface will decrease the work required to create critical nuclei and will increase the probability of heterogeneous nucleation with respect to the homogenous case. The interaction between solute and substrate is governed by the *wettability* – a property used to represent the affinity between the substrate and the solution- which is normally measured by the contact angle formed by the interaction solution-substrate. Thus, the reduction of the activation energy is given by the equation (1.3).<sup>28</sup>

$$\Delta G_{het} = \Delta G_{hom} \left( \frac{1}{2} - \frac{3}{4} \cos\alpha + \frac{1}{4} \cos^3\alpha \right) \quad (1.3)$$

<sup>27</sup> X. Y. Liu, *J. Chem. Phys.*, **2000**, *112*, 9949- 9955.

<sup>28</sup> J.M. García-Ruíz, *J. Struc. Bio.*, **2003**, *142*, 22–31.

Plotting this expression to a fixed value of  $\Delta G_{\text{hom}}$  – to compare the wettability effect in the heterogeneous nucleation – when the nucleus wets the substrate ( $\alpha = 180^\circ$ ) any nucleation is favoured, that is the  $\Delta G_{\text{het}} = \Delta G_{\text{hom}}$ ; when the contact angle is  $\alpha = 90^\circ$ , the activation energy barrier for the heterogeneous nucleation is  $\Delta G_{\text{het}} = \frac{1}{2} \Delta G_{\text{hom}}$ . Thus, for smaller the value of  $\alpha$  (contact angle) -high wettability- the activation energy for the heterogeneous nucleation would be smaller, even if it tends to zero for  $\alpha = 0$ .



**Figure 1.14.** Graphic representation of how the activation energy barrier of the heterogeneous nucleation ( $\Delta G_{\text{het}}$ ) varies with the contact angle ( $\alpha$ ) for a given  $\Delta G_{\text{hom}}$  value.<sup>28</sup>

Heterogeneous nucleation on the foreign bodies will be favoured when there is a good structural match with the nucleating phase and will be dominant at low supersaturation, while the heterogeneous nucleation on foreign bodies that have a weak interaction and poor structural match with the nucleating phase will control the kinetics at high supersaturation.<sup>29</sup> This is the main reason that self-assembled monolayers on a substrate would favour the heterogeneous nucleation on them.

<sup>29</sup> D. Turnbull, *J. Chem. Phys.*, **1950**, *18*, 198-203.

## 1.4. Crystallisation on self-assembled monolayers

### 1.4.1. Self-assembled monolayers (SAMs)

When a substrate – usually metallic – is placed in contact with a solution of organic molecules, which then spontaneously align themselves with respect to the whole substrate's surface and bond to it, SAMs are formed. SAMs provide a convenient, flexible and simple system with which to tailor the interfacial properties of metals, semiconductors<sup>30</sup>, ceramics and polymers.<sup>31</sup> The SAMs can dramatically change the surface interface properties.

In the SAM formation of the most common type, the strong affinity between sulphur and gold hold the molecules on the surface<sup>32</sup>, and lateral van der Waals interactions between alkyl chains and the dipole interaction between polar end groups help drive the alkanethiols order. The coincidence of the lattices of the gold surface (generally 111) and the alkyl chains means that well ordered structures are formed.<sup>33</sup> The structures of well-ordered alkyl thiol 2D SAMs contain molecules with positional and orientational order, at least in the small domains that are formed. The headgroup binding at the surface controls the location, and whether the chain lies flat on the surface or adopts some vertical orientation is determined by coverage and intermolecular interactions. Positional order does not necessarily imply the existence of orientational order (and vice versa).<sup>34</sup>

### 1.4.2. Nucleation on SAMs

The control of homogeneous nucleation is difficult on a small scale, as it is a stochastic process requiring high supersaturation and the activation energy barrier for the nucleation process is relatively high.<sup>35</sup> SAMs can dramatically change interface properties, and the wettability plays a key role in order to reduce the energetic barrier associated with heterogeneous nucleation, (Figure 1. 14). Combining these factors it is possible reach controlled nucleation on a functionalised surface due to the high affinity between the

---

<sup>30</sup> S. Sek, R. Bilewicz, K. Slowinski, *Chem. Commun.*, **2004**, 404–405.

<sup>31</sup> C. Vericat, M. E. Vela, R. C. Salvarezza, *Phys. Chem. Chem. Phys.*, **2005**, 7, 3258 – 3268.

<sup>32</sup> J. C. Love, L. A. Estroff, J. K. Kriebel, R. G. Nuzzo, G. M. Whitesides, *Chem. Rev.*, **2005**, 105, 1103-1139.

<sup>33</sup> G. E. Poirier, *Chem. Rev.*, **1997**, 97, 1117-1127.

<sup>34</sup> A. Badia, R. B. Lenox, L. Reven, *Acc. Chem. Res.* **2000**, 33, 475-481.

<sup>35</sup> R.J. Davey, S.L.M. Schroeder, J.H. ter Horst, *Angew. Chem. Int. Ed.*, **2013**, 52, 2166-2179.

SAMs and the solution, where the growing nucleus can be anchored and act as a point of growth for the nascent crystal.<sup>36</sup> Indeed, SAMs have proven their ability to act as nucleation points in a number of chemical systems, both inorganic<sup>25,37</sup> and organic<sup>38</sup> mainly in water or aqueous solvents.

SAMs on surfaces apparently act as nucleation points by lowering the energy required for nucleation, since the SAMs potentially provide an ordered template to the nucleus that has high geometric complementarity at the solution-SAM interface.<sup>39</sup> These factors correspond to an epitaxial model to explain crystal orientation on surfaces.<sup>40</sup> The geometric complementarities have been assigned as the driving force to favour the nucleation and the crystal growth on the SAMs rather than the homogeneous nucleation inside the bulk solution.

In any case, SAMs can be used as controlled heterogeneous nucleation centres to create chiral polar surfaces that might show diastereoselectivity in this process as it is also explain applying both nucleation theories. Figures 1.15 and 1.16 show schematically the nucleation theories to the nucleation on SAMs process.

Figure 1.15 represents the difference between both nucleation processes following the CNT basis, which conclude that heterogeneous nucleation is dramatically favoured in contrast to the homogeneous nucleation (Equation 1.3). Figure 1.16 explains that also the heterogeneous nucleation is favoured on the functionalised surface since these would provide an order template to the liquid-like cluster doing its self-reorganisation step faster.

---

<sup>36</sup> xK. Ino, I. Udagawa, K. Iwabata, Y. Takakusagi, M. Kubota, K. Kurosaka, K. Arai, Y. Seki, M. Nogawa, A. Mariaux, M. Rappaz, *Acta Mater.*, **2011**, *59*, 927-933.

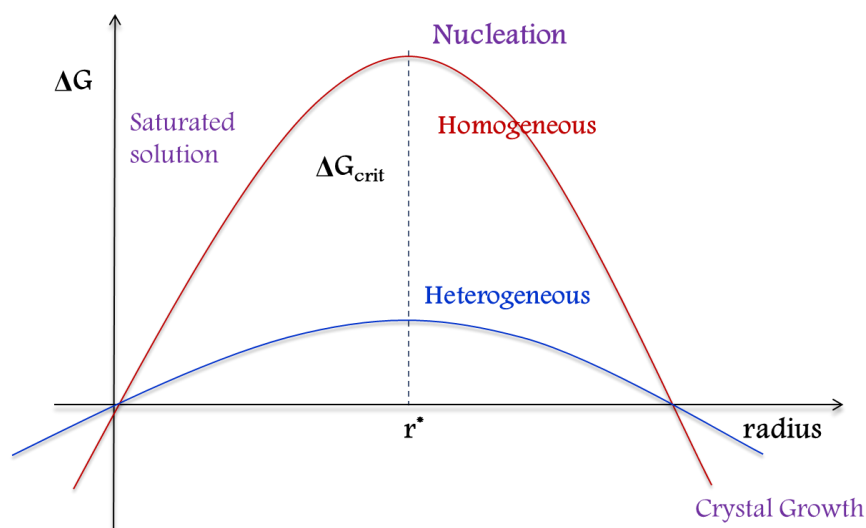
<sup>37</sup> J. Kuther, R. Seshadri, W. Knoll, W. Tremel, *J. Mater. Chem.*, **1998**, *8*, 641-650.

<sup>38</sup> B. Pokroy, V.F. Chernow, J. Aizenberg, *Langmuir*, **2009**, *25*, 14002-14006.

<sup>39</sup> A. Y. Lee, I. S. Lee, A. S. Myerson, *Chem. Eng. Technol*, **2006**, *29*, 281-285.

<sup>40</sup> J. R. Cox, M. Dabros, J. A. Shaffer, V. R. Thalladi, *Angew. Chem. Int. Ed.*, **2007**, *46*, 1988-1991.

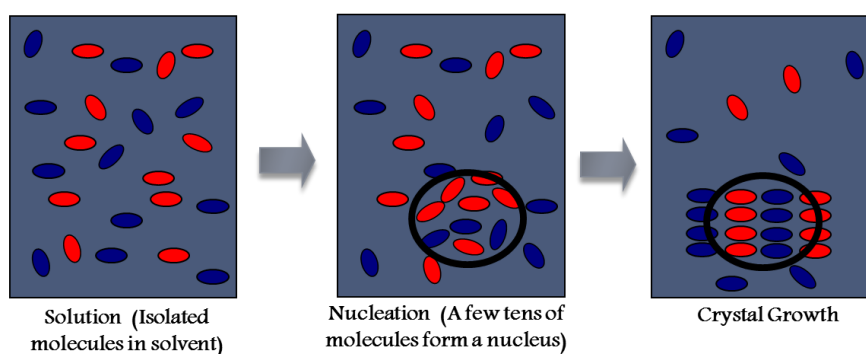




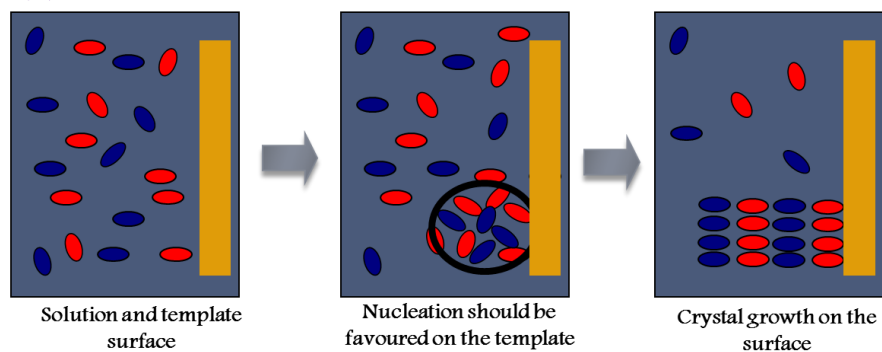
**Figure 1.15.** Free energy diagram for crystallisation process according to classical theory of crystallisation, points out the free energy difference between homogeneous and heterogeneous nucleation. ( $r^*$  is the cluster critical size  $\sim 50$  nm).

### Two step nucleation theory

#### (A) Homogeneous nucleation

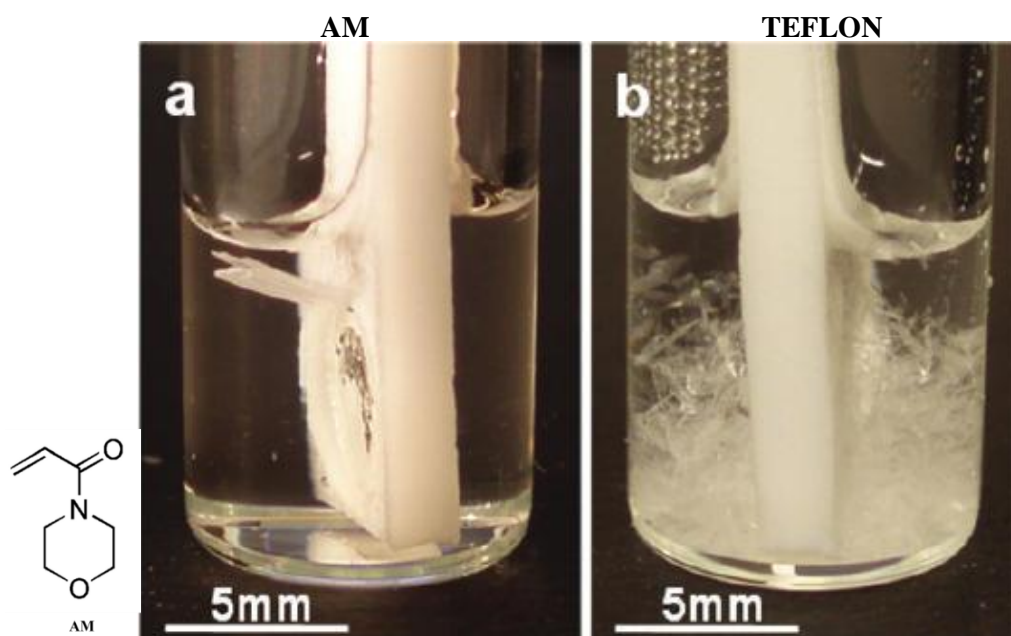


#### (B) Heterogeneous nucleation



**Figure 1.16.** Two step nucleation theory applied to (A) homogeneous and (B) heterogeneous nucleation on a functionalised surface.

Both theories support the potentially dramatic influence of a functionalised surface on the crystallisation process. Heterogeneous nucleation sites are highly favoured; a study by Myerson and co-workers described very well this fact, who used different functionalised polymers for the nucleation of aspirin (2-acetoxybenzoic acid) crystals in toluene (3 mg aspirin/ml toluene).<sup>41</sup> They observed a negative effect when only the Teflon plates were inserted into the solution while the Teflon functionalised with 4-acryloylmorpholine (AM) polymer has an enormous effect on heterogeneous nucleation. Figure 1.17 shows typical scenarios observed in vials with the polymer AM (Figure 1.17a) and without (Figure 1.17b). Clearly, a few large crystals nucleated and grew from the polymer surface, while numerous small crystals precipitated out from the bulk. This implies that nucleation on polymers occurred much earlier than in the bulk and the rapid crystal growth depleted aspirin molecules from the solution, which suppressed crystallization from the bulk, supporting the heterogeneous nucleation prevalence. The heterogeneous nucleation on the polymer and the Teflon cannot be due to epitaxy/commensurate nature of the surface since the polymers are not crystalline. This experiment opens new routes for the crystallisation on modified surfaces.



**Figure 1.17.** Comparison of aspirin crystals from (a) the surface of AM and (b) the bulk with Teflon only. (Compound structures on the right).

<sup>41</sup> Y. Diao, A. S. Myerson, T. A. Hatton, B. L. Trout, *Langmuir*, **2011**, 27, 5324-5334.

The method most used for the crystallisation of the organic molecules on the SAMs surfaces was a casting technique, whereby a drop of a solution of the target compound was deposited on the clean SAMs. The reason for this approach is that attempted crystallisation on the surface immersed in a warm supersaturated solution of the compound to crystallise did not afford reliable crystallisation on the SAM, but rather in the bulk of the solution, meaning that under those conditions homogeneous nucleation is preferred over heterogeneous nucleation according to both crystallisation theories. Many experiments have been carried out in this Thesis in order to probe all these assumptions.

### 1.4.3. Crystal growth on SAMs

The controlled growth of crystals of organic compounds on surfaces is an area of increasing interest because of the many fundamental questions it might answer as well as for the many applications it could have.<sup>42</sup> The possibility to control crystallization processes using self-assembled monolayers (SAMs) is an increasingly interesting and promising approach for the selective growth of ordered organic materials.<sup>43</sup>

The use of chiral surfaces for resolution - thanks to local stereoselective recognition - is commonplace in chiral chromatography where weak non-specific interactions are responsible for the separation.<sup>44</sup> However, the possibility of using chiral surfaces in crystallisations is challenging because of the difficulty in nucleating species at a surface.<sup>45</sup> Dressler and Mastai have shown that enantiomerically enriched crystals of glutamic acid are attached to chiral self-assembled monolayers of cysteine on gold when the racemate of the acid is crystallised from aqueous solution,<sup>46</sup> although the precise mechanism is not entirely clear (Figure 1.18). In other cases, metastable phases can be

---

<sup>42</sup> (a) D.S. Tsekova, D.R. Williams, J.Y.Y. Heng, *Chem. Eng. Sci.*, **2012**, *77*, 201-206.

(b) O. Werzer, N. Boucher, J.P. de Silva, G. Gbabode, Y.H. Geerts, O. Kononov, A. Moser, J. Novak, R. Resel, M. Sferrazza, *Langmuir*, **2012**, *28*, 8530-8536.

(c) C. Weber, C. Frank, S. Bommel, T. Rukat, W. Leitenberger, P. Schafer, F. Schreiber, S. Kowarik, *J. Chem. Phys.*, **2012**, *136*, Art. No. 204709.

(d) J. Martinez-Blanco, A. Mascaraque, Y.S. Dedkov, K. Horn, *Langmuir*, **2012**, *28*, 3840-3844.

(e) X.L. Qiao, Y.H. Geng, D.H. Yan, *J. Phys. Chem. B*, **2012**, *116*, 1812-1818.

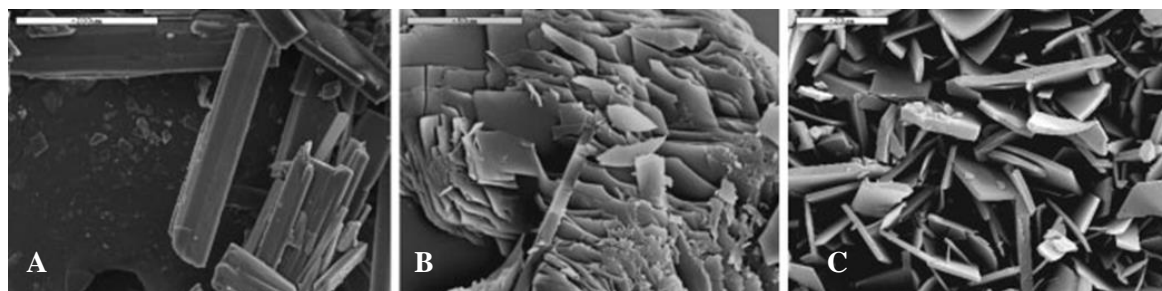
<sup>43</sup> A. Singh, I.S. Lee, K. Kim, A.S. Myerson, *CrystEngComm*, **2011**, *13*, 24-32.

<sup>44</sup> R. Sancho, C. Minguillon *Chem. Soc. Rev.*, **2009**, *38*, 797-805.

<sup>45</sup> Y. Mastai, *Chem. Soc. Rev.*, **2009**, *38*, 772-780.

<sup>46</sup> D. H. Dressler, Y. Mastai, *Chirality*, **2007**, *19*, 358-365.

stabilised<sup>47</sup> and a conglomerate was successfully formed on a chiral monolayer, although no stereoselectivity was observed.<sup>48</sup>



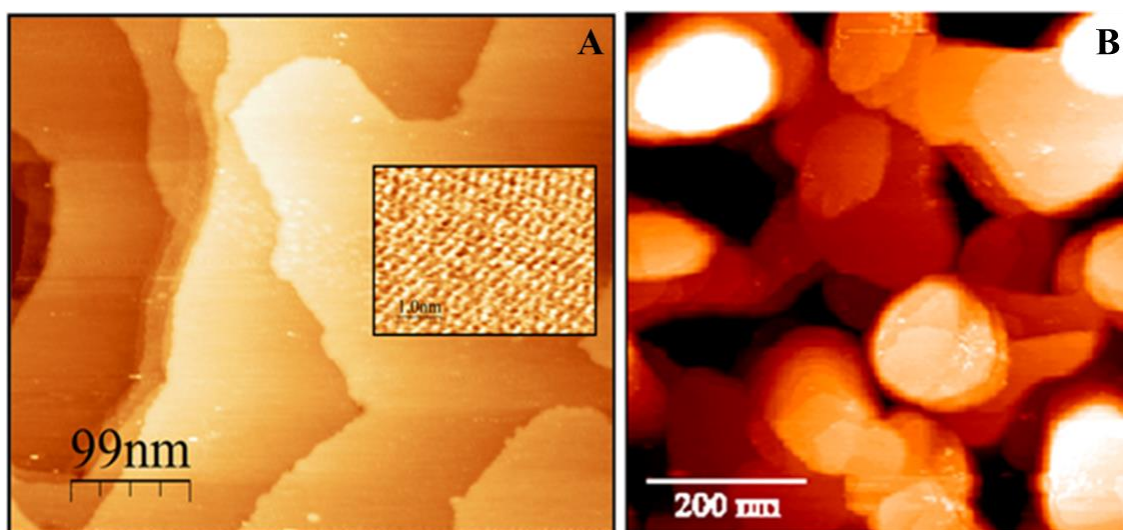
**Figure 1.18.** Scanning electron micrographs of *rac*-Glutamic acid crystals: (A) Crystal morphology of *rac*-Glutamic acid crystallized from solution (Scalebar 200 $\mu$ m). (B) Crystal morphology of *rac*-Glutamic acid crystallized onto a chiral (-)-D-Cysteine surface, plate like (Scalebar 50 $\mu$ m). (C) Crystal morphology of *rac*-Glutamic acid crystallized onto a chiral (+)-L-Cysteine surface, rectangular (Scalebar 200 $\mu$ m).<sup>46</sup>

The crystal growth on SAMs is dramatically influenced by the combination of several parameters (that would be studied and discussed in depth in this Thesis). The evaporation rate of the solvent and the roughness of the surface are the most important parameters involved in the nucleation and in the crystal growth stage. The Figure 1.19 shows the topography of the both gold substrates used, monocrystalline gold – mainly the (1 1 1) surface – on mica and polycrystalline gold on a glass substrate. The topography of a substrate is not modified drastically during SAM formation, since these SAMs adopt approximately the same roughness as the clean substrate (although at the nanometre scale small pits and changes at the step edges can take place)<sup>49</sup>. Monocrystalline gold substrates are very flat and offer mainly flat (1 1 1) terraces where well-organised SAMs can grow, while the polycrystalline gold substrates have smaller terraces which mean that the roughness of this kind of substrates is relatively high. Crystal growth on SAMs on a rougher surface – such as polycrystalline gold – offer more nucleation points at the SAMs-solution interface than on a very flat surface that the crystal growth favoured would be the epitaxial.

<sup>47</sup> D.H. Dressler, I. Hod, Y. Mastai, *J. Cryst. Growth*, **2008**, *310*, 1718-1724.

<sup>48</sup> M. Ejgenberg, Y. Mastai, *Chem. Commun.*, **2011**, *47*, 12161-12163.

<sup>49</sup> (a) S. Franzen, *Chem. Phys. Lett.*, **2003**, *381*, 315-321. (b) X. Li, J. Huskens, D. N. Reinhoudt, *J. Mater. Chem.*, **2004**, *14*, 2954-2971.



**Figure 1.19.** STM micrographs of gold substrates (A) monocrystalline gold on mica (111) and (B) polycrystalline gold on glass. Monocrystalline gold offer plane and bigger terraces of (111) than polycrystalline gold that order is random.

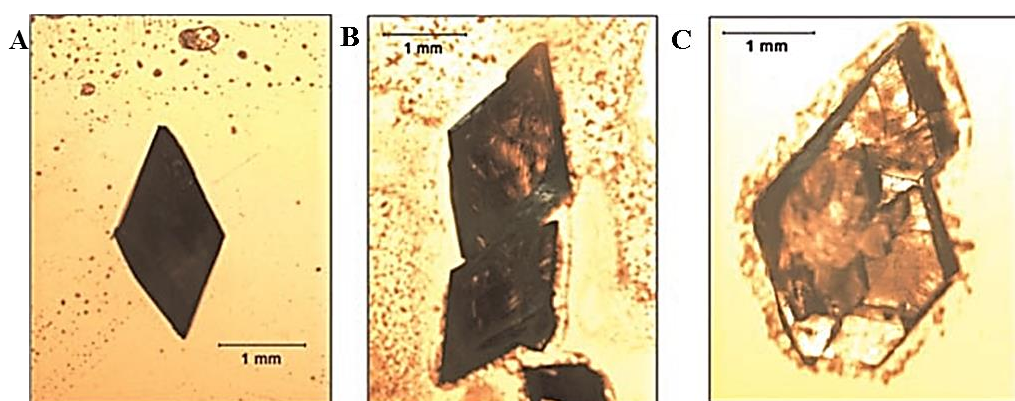
The evaporation rate has a great influence on the crystallization process. Growing crystals on surfaces from volatile organic solvents presents considerable challenges. The wetting behaviour on the surface is completely different to water, because of the high surface tension of the latter. The evaporation rate of a solution has a great influence on the nucleation process (because supersaturation point can be approached very quickly) and the crystal growth, and so the processes taking place from volatile organics are particularly hard to control on small scales.<sup>50</sup>

Solvent evaporation rate is an effect related with the diffusion of the molecules over the SAMs, lower evaporation rate of the solvent allows more time for diffusion (mass transport). Under these conditions, weak interactions can become more significant, providing bigger and differently oriented crystals – polymorphs in many cases<sup>51</sup> – grown off different crystalline planes. A very fast evaporation of the solvent prevents the efficient diffusion of the molecules over the SAMs, so that the crystals grow – due to the strongest interaction at the interface – smaller and from the most related crystal plane to the SAMs.

<sup>50</sup> M. D. Eddleston, W. Jones, *Cryst. Grow. Design*, **2010**, *10*, 365–370.

<sup>51</sup> K. Kim, A. Centrone, T. A. Hatton, A. S. Myerson, *CrystEngComm*, **2011**, *13*, 1127-1131.

Dressler and Mastai<sup>52</sup> and Nakanishi et al.<sup>53</sup> have shown the separation of enantiomers from aqueous solutions on SAMs, although the generality of the approach is not evident. For example, Myerson's group showed that for valine crystallization on SAMs the enantiomer formed at the monolayer surface depended on the one that was in excess in the crystallizing system (Figure 1.20),<sup>54</sup> although separation was achieved with reversal with respect to the monolayer from racemic mixtures in line with observations in conceptually similar systems.<sup>55</sup> Figure 1.20 shows an optical microscope image of the pure L-valine crystals obtained on the L-Glutathione chiral monolayer (Figure 1.20.A), on the N-Acetyl L-Cysteine chiral monolayer (Figure 1.20.B) from supersaturated solutions having varying enantiomeric excess (L-valine) values. Figure 1.20.C corresponds to the pure D-valine crystals obtained on the D-cysteine chiral monolayers from supersaturated solutions having varying enantiomeric excess (D-valine) values.



**Figure 1.20.** Optical micrographs of (A) pure L-valine crystals on L-Glutathione chiral monolayer; (B) pure L-valine crystals on the N-Acetyl L-Cysteine chiral monolayer, and (C) pure D-valine crystals obtained on the D-cysteine chiral monolayers.<sup>50</sup>

Nevertheless, in the long term, it should be possible that a surface functionalized with a resolving agent could provide a preferential template to get chiral recognition and favour the nucleation on it of one enantiomer in a conglomerate.<sup>56</sup>

<sup>52</sup> D.H. Dressler, Y. Mastai, *J. Colloid Interface Sci.*, **2007**, *310*, 653–660.

<sup>53</sup> T. Nakanishi, N. Bannob, M. Matsunaga, T. Asahi, T. Osaka, *Colloids Surf. A: Physicochem. Eng. Aspects*, **2006**, *284–285*, 270–275.

<sup>54</sup> A. Singh, A.S. Myerson, *J. Pharm. Sci.*, **2010**, *99*, 3931–3940.

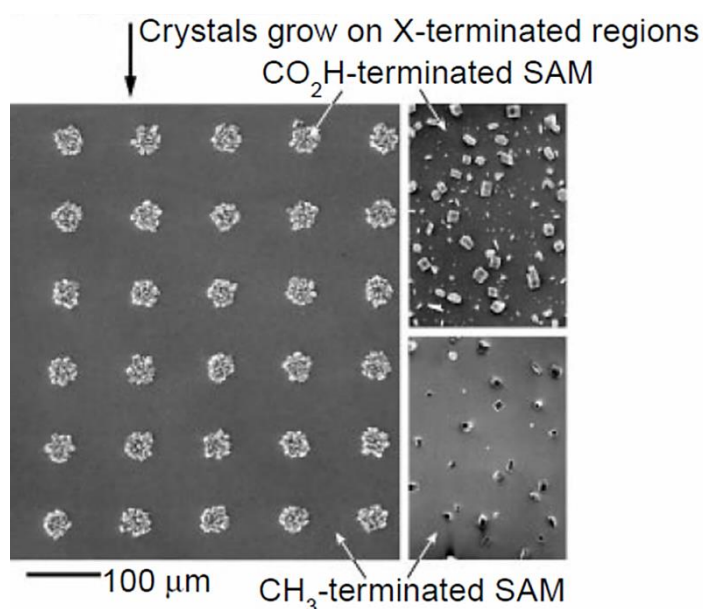
<sup>55</sup> L. Addadi, S. Weinstein, E. Gati, I. Weissbuch, M. Lahav, *J. Am. Chem. Soc.*, **1982**, *104*, 4610–4617.

<sup>56</sup> M. Ejgenberg, Y. Mastai, *Chem. Commun.*, **2011**, *47*, 12161–12163.

## 1.5. Crystallisation on micropatterned surfaces

The  $\mu$ CP method is a very appropriate soft lithographic technique that can create patterned features of SAMs on both planar and non-planar surfaces, functionalising in a controlled way the desired surface with the molecules selected.<sup>57</sup>

The  $\mu$ CP method has been successfully used to generate layers upon which crystallization can be achieved as in 1999, when Aizenberg and Whitesides presented a good method to perform controlled crystallisation on micropatterned surfaces by thiols of different nature – polar groups and methyl-terminated SAMs – in the crystallisation of Calcite from ethanolic solution (Figure 1.21).<sup>58</sup>



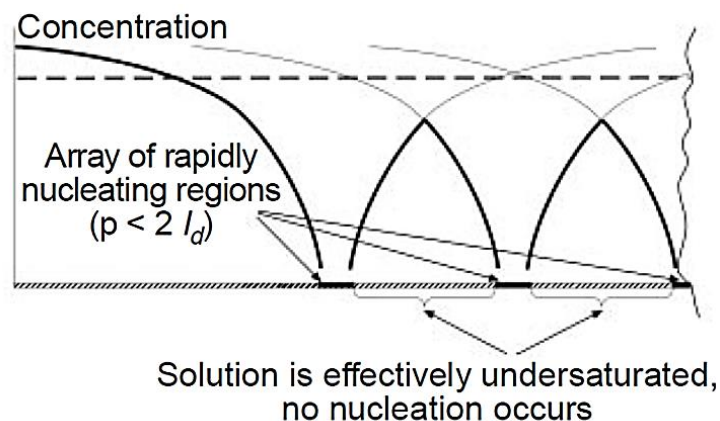
**Figure 1.21.** Scanning electron micrograph (SEM) of the sample patterned surface printed circles of  $\text{HS}(\text{CH}_2)_{15}\text{CO}_2\text{H}$  in a background of  $\text{HS}(\text{CH}_2)_{15}\text{CH}_3$  supported on  $\text{Ag}(111)$  overgrown with calcite crystals. For these experimental conditions  $[\text{Ca}^{2+}] = 25 \text{ mM}$ ,  $\text{pH} = 7$ , crystallization time  $t = 30 \text{ min}$  the nucleation is highly specific to the acid-terminated regions, and the crystals are remarkably uniform in size and nucleation density.<sup>58</sup>

They justified that there is a relationship between the size of the motif printed, its periodicity, with the *depletion zones* ( $l_d$ ) – which are the zones where nucleation does not happens. Once the nucleation starts, on the array of rapidly nucleating regions (Figure 1.22)

<sup>57</sup> G. Di Profio, E. Fontananova, E. Curcio, E. Drioli, *Cryst. Growth Des.*, **2012**, *12*, 3749-3757.

<sup>58</sup> J. Aizenberg, A. J. Black, G. M. Whitesides, *Nature*, **1999**, *398*, 495-498.

the *mass transport* is favoured from the depletion to the nucleating regions. This depletion zone is also influenced by the diffusion and the flux of molecules over the functionalised surface.<sup>58</sup>



**Figure 1.22.** Calculated profiles of the crystallising solution (calcite) in the vicinity of an array of rapidly nucleating regions with periodicity  $p < 2l_d$ . the effective concentration (bold lines) over the entire slowly nucleating region is then below  $c_{\text{sat}}$ . Crystallisation will only take place on the rapidly nucleating regions.<sup>58</sup>

Myerson and co-workers have used micropatterned SAMs to control of crystallization process of organic compounds (such as glycine) from aqueous solution in order to study the surface's influence on growth and have demonstrated the influence that the layers have on the polymorphs that crystallize.<sup>59</sup> Spatial segregation of two types of monolayers, with different polarities, on the same surface makes it possible to induce mass transport that aids the crystallization process.<sup>60</sup>

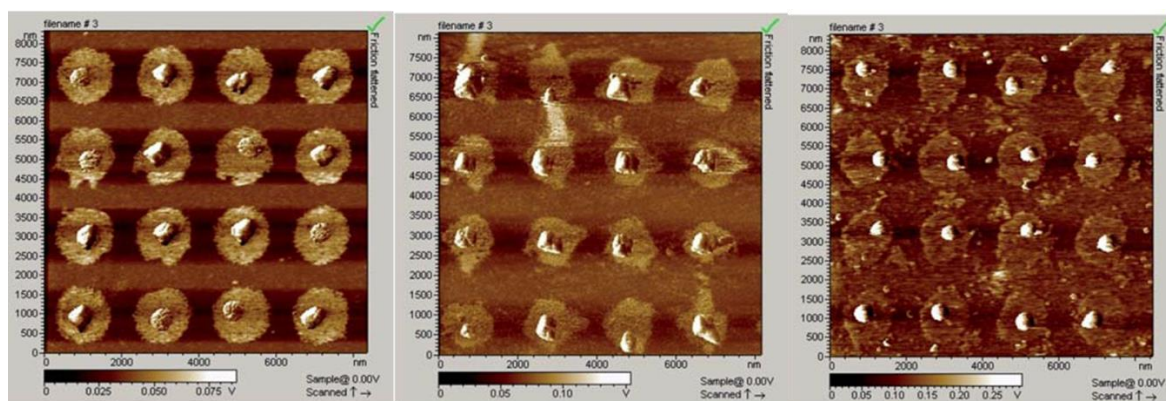
In confined systems such as micropatterned surfaces, formation of crystalline nuclei is influenced by the depletion of a liquid phase due to the phase transition process (nucleation). When the phase transition occurs, a portion of molecules is transferred from the liquid to the newly forming crystalline phase, nuclei.<sup>61</sup>

**A** **B** **C**  
<sup>59</sup> (a) A. Singh, I.S. Lee, A.S. Myerson, *Cryst. Growth Des.*, **2009**, *9*, 1182-1185. (b) K. Kim, A. Centrone, T.A. Hatton, A.S. Myerson, *Cryst. Eng. Comm.*, **2011**, *13*, 1127-1131.

<sup>60</sup> (a) A.Y.Lee, I.S. Lee, S.S. Dettet, J. Boerner, A.S. Myerson, *J. Am. Chem. Soc.*, **2005**, *127*, 14982-14983. (b) K. Kim, I.S. Lee, A. Centrone, T.A. Hatton, A.S. Myerson, *J. Am. Chem. Soc.*, **2009**, *131*, 18212-18213.

<sup>61</sup> Z. Kozisek, *CrystEngComm*, **2013**, *15*, 2269-2274.

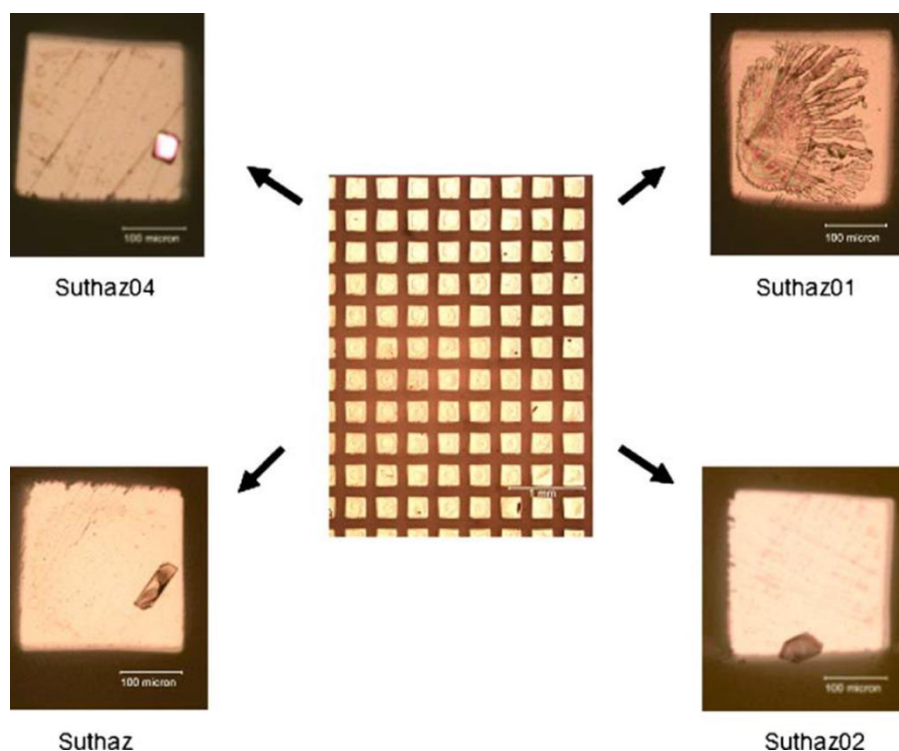




**Figure 1. 23.** AFM images of  $64 \mu\text{m}^2$  of the  $1 \mu\text{m}$  patterned SAM substrate. (a) Glycine crystals were generated by slow cooling at a cooling rate of  $0.1^\circ\text{C min}^{-1}$  (3.0 M); (b)  $0.001^\circ\text{C min}^{-1}$  (3.0 M); and (c) slow evaporation for 100 hours (2.8 M).<sup>60</sup>

The control of the evaporation rate allows remarkable effects to be seen in the growth of the crystals, many polymorphs have been characterised (Figure 1.24). these polymorph obtained on micropatterned surface are far more uniform than those crystals grown over the whole surface.<sup>60a</sup>

Growing crystals on surfaces from volatile organic solvents presents considerable challenges. The wetting behaviour on the surface is completely different to water, because of the high surface tension of the latter. The evaporation rate of a solution has a great influence on the nucleation process and the crystal growth, and so the processes taking place from volatile organics are particularly hard to control.



**Figure 1.24.** Sulfathiazole polymorph crystals nucleated on 250  $\mu\text{m}$  functionalised metallic gold islands supersaturated solution (0.2 M) of formamide/water (4:1, v/v).<sup>60a</sup>

In summary, heterogeneous nucleation should be favoured in any crystallisation where a functionalised surface is present. This is because the energetic barrier for the heterogeneous nucleation ( $\Delta G_{\text{heter}}$ ) is influenced by the wettability, the geometric complementarity SAMs-solution, and for the mass transport that is increased for the combination of SAMs on micropatterned surfaces.

In this Thesis, this hypothesis shall be tested with the aim of separating enantiomers from organic solutions, as detailed in the following section.

# Chapter 2

## Objectives

---

The research presented in this Thesis has as the main objective:

Establish the effect of chiral self-assembled monolayers (SAMs) on the nucleation and the crystal growth of organic compounds, and find conditions which favour heterogeneous nucleation and subsequent growth.

Within this broad objective, the most important specific goals are to:

- Understand the structure and nature of crystals of a family of resolving agents and their diastereomeric salts in order to be able to understand surface-mediated crystallisation.
- Form SAMs on gold with a novel chiral thiol and to establish its potential for nucleating crystal growth.
- Achieve controlled crystallization of organic compounds on functionalized surfaces from organic solutions.
- Determine influence of the evaporation rate and the roughness of the substrate on the crystal growth.
- Investigate the influence of the shape of the motif printed on surface, the incubation time and the chirality of the surface on the crystal growth.
- Explore the possibility of performing Dutch Resolution in a heterogeneously nucleated system.

# Chapter 3

## Crystal Structure analysis

---

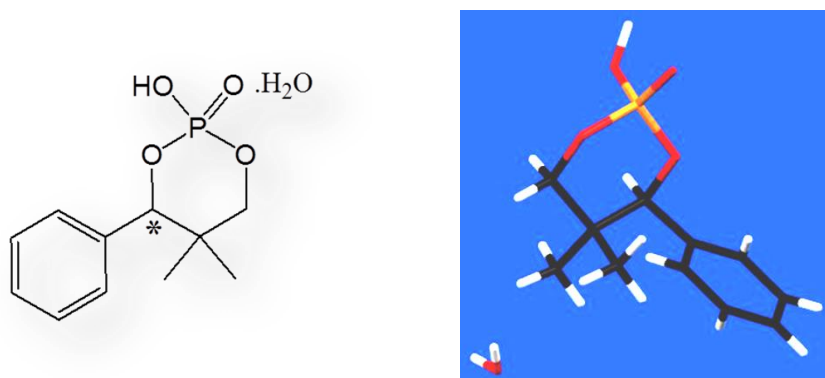
Crystal structures are of upmost importance to understand the nature of crystals and the heterogeneous crystallisation process. Several crystalline structures of derivatives of phencyphos and their diastereomeric salts are explained in details in this Chapter.

### 3.1. Introduction

The formation of crystals on surfaces is driven by the attachment of pre-nuclei at the interface between the solid and the surrounding medium followed by nucleation and growth. On surfaces the growth direction is often in a particular orientation which is associated with a particular arrangement with one of the crystal planes in close contact with the surface on which it grows. For this reason, detailed study of the crystal structures of the compounds selected to crystallise on SAMs is very helpful in order to understand their behaviour during the crystallisation process, which planes might be exposed to the templating surface and which interactions would be stronger and how their arrangement is. According to the geometric complementarity expected at the crystal-SAM interface, we should determine the most polar planes and the direction of the hydrogen bonded networks within each crystal. All structural images for every crystal structure were obtained from the Mercury programme.<sup>1</sup>

### 3.2. Phencyphos derives

Cyclic phosphoric acid groups have been popular in classical chiral resolution (CCR) for several decades<sup>2</sup>. The phencyphos compound (Figure 3.1) is a cyclic phosphoric acid derivative and it has been used in CCR and also in Dutch Resolution<sup>3</sup>.



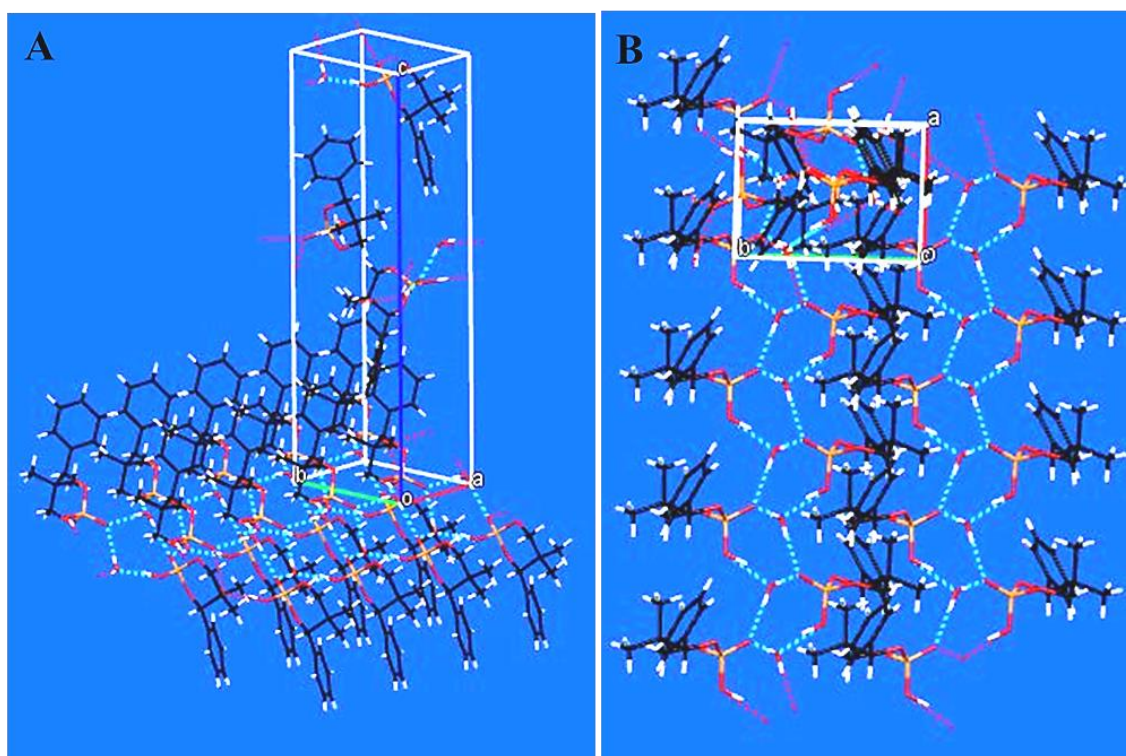
**Figure 3.1.** The chemical structure and crystal structure of phencyphos hydrate.

<sup>1</sup> <http://www.ccdc.cam.ac.uk/Solutions/CSDSystem/Pages/Mercury.aspx>

<sup>2</sup> W. Ten Hoeve, H. Wynberg, *J. Org. Chem.*, **1985**, *50*, 4508–4514.

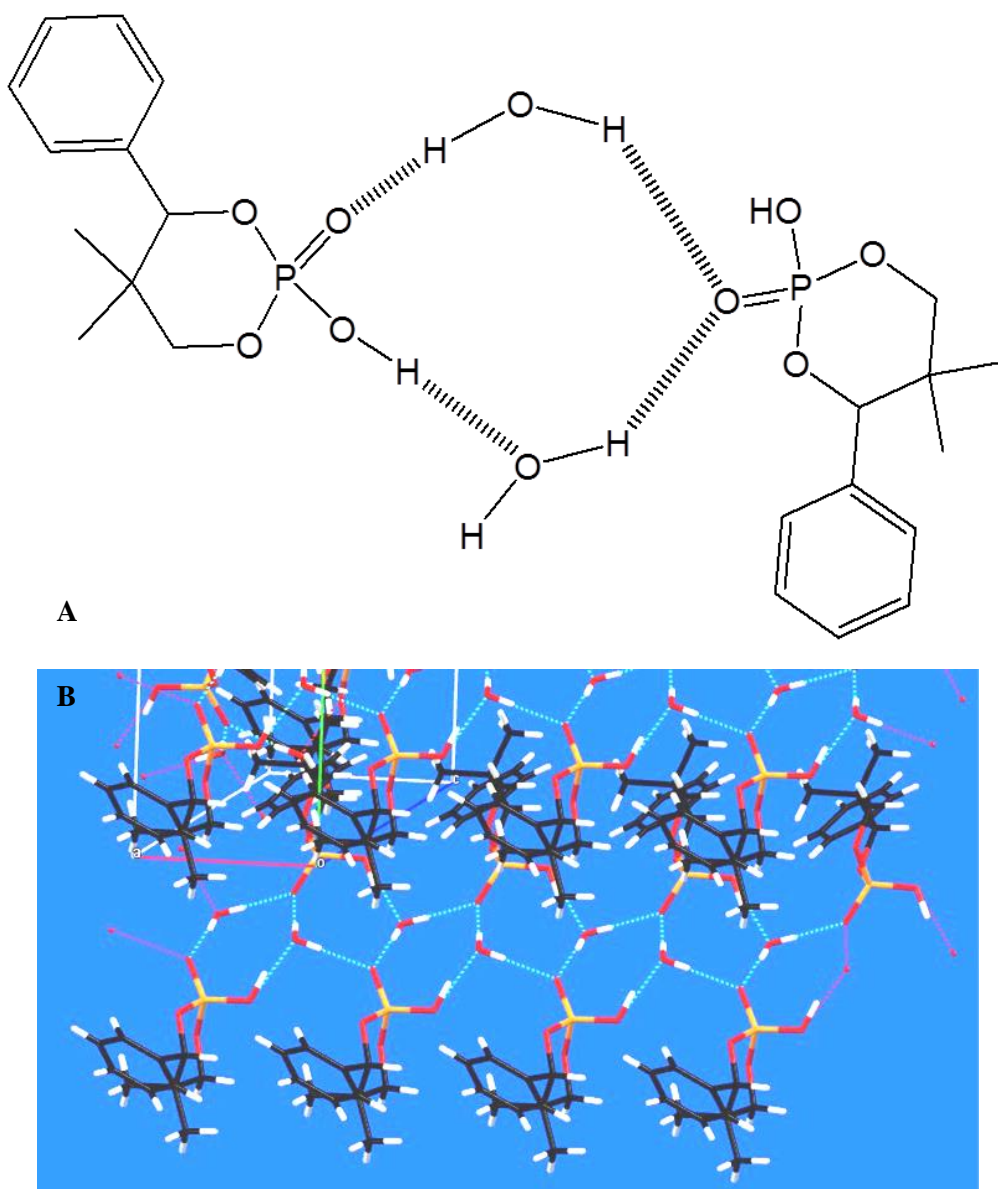
<sup>3</sup> R. M. Kellogg, J. W. Nieuwenhuijzen, K. Pouwer, T. R. Vries, Q. B. Broxterman, R. F. P. Grimbergen, B. Kaptein, R. M. La Crois, E. de Wever, K. Zwaagstra, A. C. van der Laan. *Synthesis*, **2003**, *10*, 1626-1638.

Phencyphos crystallises from a methanol solution (0.05M) when the solvent is allowed to evaporate freely over 24 hours. The compound crystallises in the orthorhombic system in space group  $P2_12_12_1$  ( $a = 6.02$ ,  $b = 8.21$ ,  $c = 25.47$  Å;  $\alpha = \beta = \gamma = 90^\circ$ ). The molecule of phencyphos has two parts which can be distinguished because of their polarity. The polar part – containing the phosphoric acid moiety – interacts with the water molecule of crystallisation through a hydrogen bonded network which grows forming a layer parallel to the  $ab$  plane (Figure 3.2).



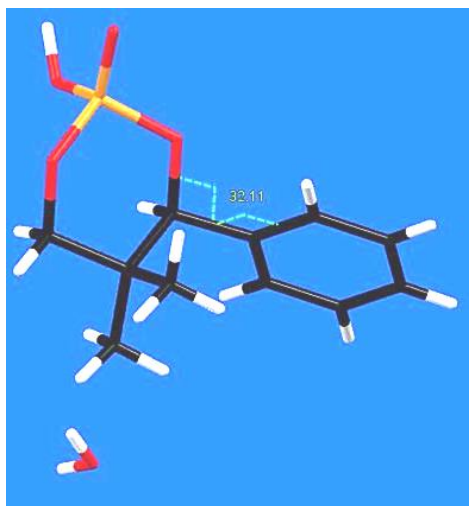
**Figure 3.2.** Phencyphos hydrate hydrogen bond network parallel to  $ab$  plane. (A) Frontal and (B) Top view.

The apolar part formed by the phenyl ring forms a layer, also parallel to both the  $a$  axis and the  $b$  axes. These hydrophobic and hydrophilic layers alternate along the  $c$  axis. The phenyl rings are stacked. The most important close contacts that this compound present an uncommon *10-membered ring* formed by the hydrogen bond between the phosphoric acid group and the water molecules. (Figure 3.3). The torsion angle between the cycles of the polar and apolar part of the phencyphos molecules (Phenyl ring and cyclic phosphoric acid) is of  $32.11^\circ$  (Figure 3.4).



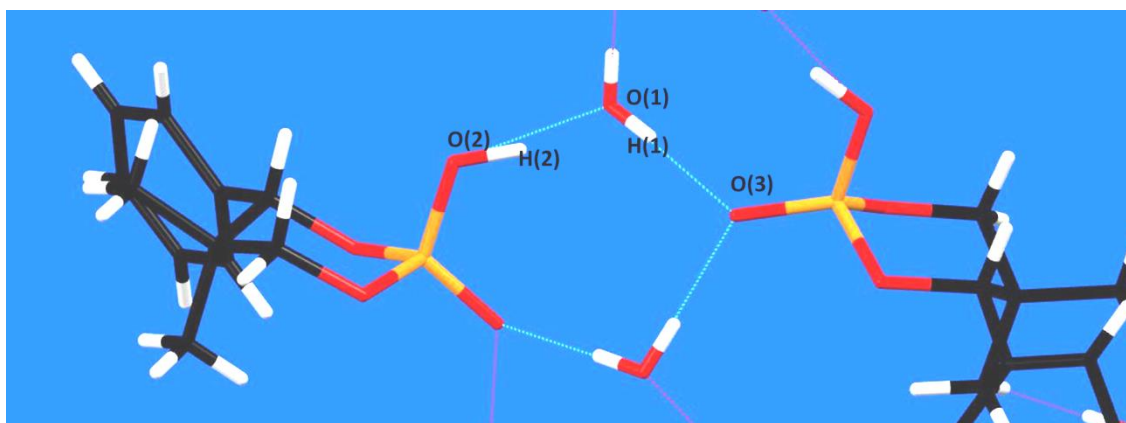
**Figure 3.3.** Hydrogen bonds in the crystals of phencyphos hydrate: (A) 10-membered ring scheme. (B) Graphical representation from the Mercury programme of the 10-membered ring. The hydrogen bond network parallel to  $ab$  plane forming 10-membered rings is shown. The 10-membered rings are formed by two phosphoric acid groups of two molecules of different layers, and two water molecules.





**Figure 3.4.** A view of the phencyphos crystal structure showing the torsion angle between the two rings in the compound.

The hydrogen bonded rings stack back-to-back, forming a puckered ribbon propagating in the direction of both the *b* axis and the *c* axis. Molecules are hydrogen bonded to equivalent molecules generated by the  $2_1$  screw symmetry. The acidic proton of the phosphoric acid group forms a very strong hydrogen bond with the water molecule. All strong donors and acceptors are used in non-covalent interactions in this crystal structure; they form strong hydrogen bonds, which are almost linear (see hydrogen bond geometry in the Table 1.1 and Figure 3.5).

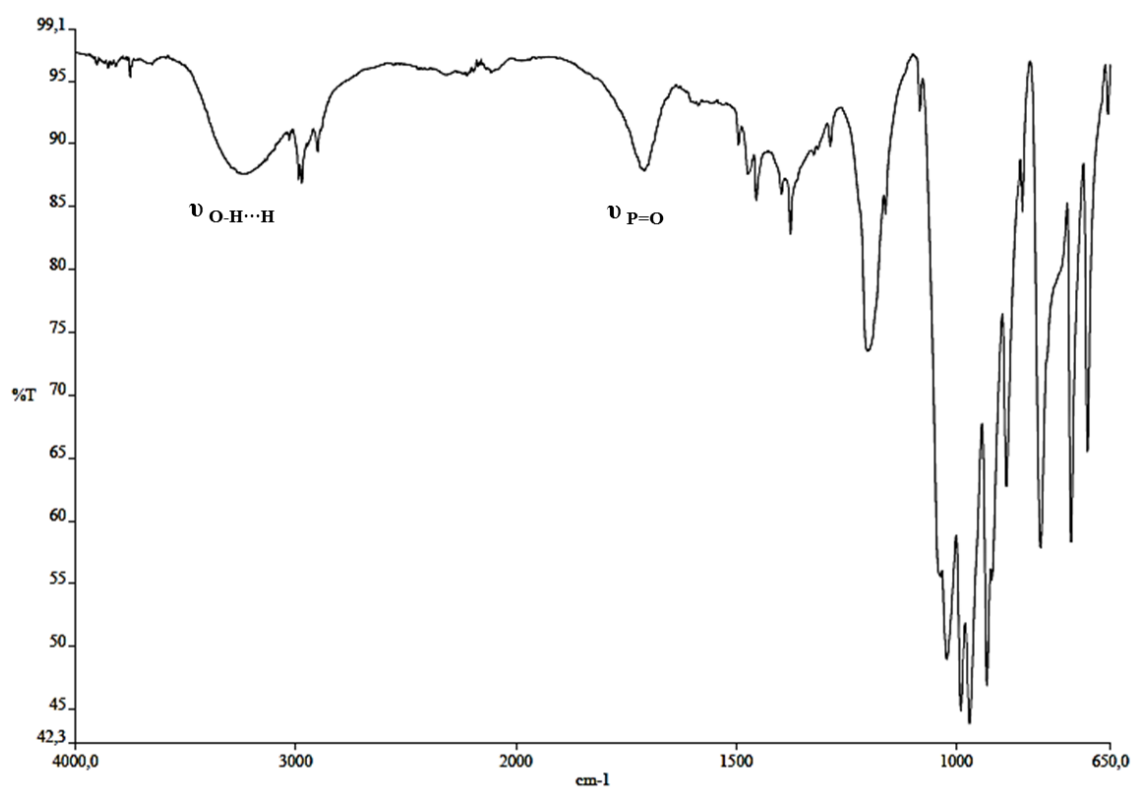


**Figure 3.5.** Hydrogen bond distances in the 10-membered ring.

**Table 1.1.** Hydrogen bond geometry.

Bond O-H...O	$d_{\text{O-H}} (\text{Å})$	$d_{\text{H...O}} (\text{Å})$	$d_{\text{O...O}} (\text{Å})$	$\alpha_{\text{O-H...O}} (^{\circ})$
O(2)-H(2)...O(1)	0.98	1.47	2.44	163.7
O(1)-H(1)...O(3)	0.81	1.91	2.18	176.0

The infrared spectrum shown in the figure 3.6 indicates the existence of the hydrogen bonding judging from the position of the OH group ( $\nu_{\text{OH}}=3250 \text{ cm}^{-1}$ ) forming hydrogen bonds (O-H...H) and the tension of P=O ( $\nu_{\text{P=O}}=1700 \text{ cm}^{-1}$ ) of the -POOH group.<sup>4</sup> These bands indicate what is demonstrated by the X-ray crystal structure, the hydrogen bonds form 10-membered ring.



**Figure 3.6.** Infrared spectra of phencyphos indicate the hydrogen bonds existence in the structure.

<sup>4</sup> A. Herrera Fernández, R. Martínez Álvarez, *Tablas para la determinación estructural por métodos espectroscópicos*, 2000, (ISBN 84-07-00501-0).

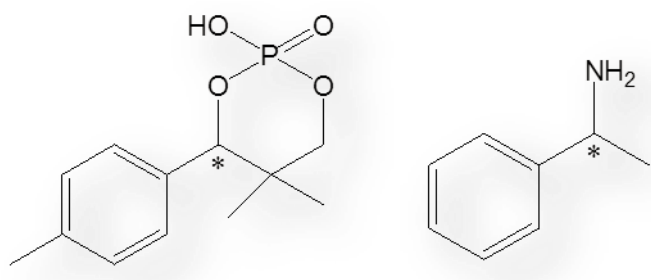
In order to control the crystallisation process of phencyphos on functionalised surface we can predict that the more polar phencyphos crystalline planes—which are run across the to *ab* plane- will interact with a polar area, nucleating faster, since they are kinetically favourable due to the natural growth direction of this crystal and also due to the high affinity for the polar SAMs.

### 3.3. Diastereomeric salts

#### 3.3.1. New structures

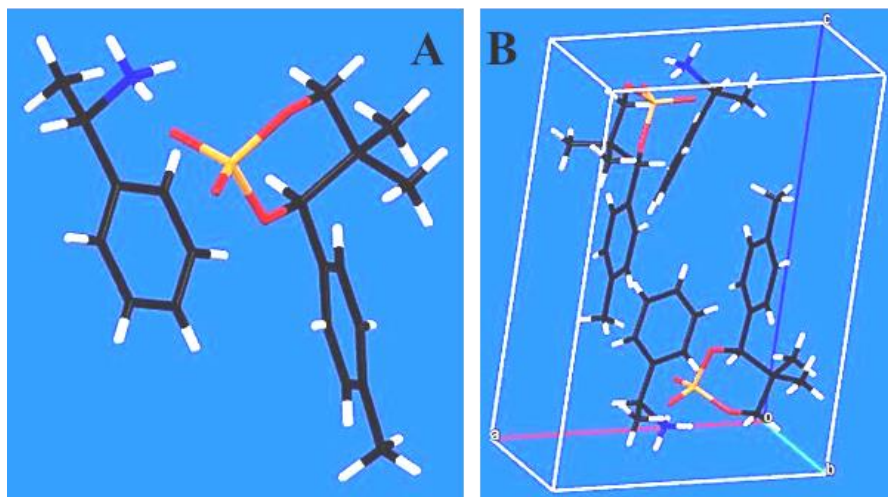
Diastereomeric salts are also interesting in order to study their crystallisation process on functionalised surfaces. Bulk crystallisations of various combinations of phencyphos derivatives with several amines were attempted,<sup>5</sup> and a pair of these combinations produced single crystals suitable for single crystal X-ray diffraction.

✚ (-) *Para-methyl phencyphos (PMPP)* and (-)-*phenylethylamine (PEA)* were dissolved to give a warm ethanolic solution, which was allowed to cool down with the solvent evaporating freely (Figure 3.7). This process afforded needle-like colourless crystals. X-ray single crystal diffraction was made and solved by Dr. K. Wurst (Institut für Anorganische Chemie, University of Innsbruck). (-) *Para-methyl phencyphos (PMPP)* and (-)-*phenylethylamine (PEA)* diastereomeric salts crystallises in the monoclinic system ( $a=10.337$ ,  $b=6.394$ ,  $c=15.197\text{Å}$ ,  $\alpha=90$ ,  $\beta=95.49$ ,  $\gamma=90^\circ$ ), in space group  $P2_1$  (Figure 3.8).



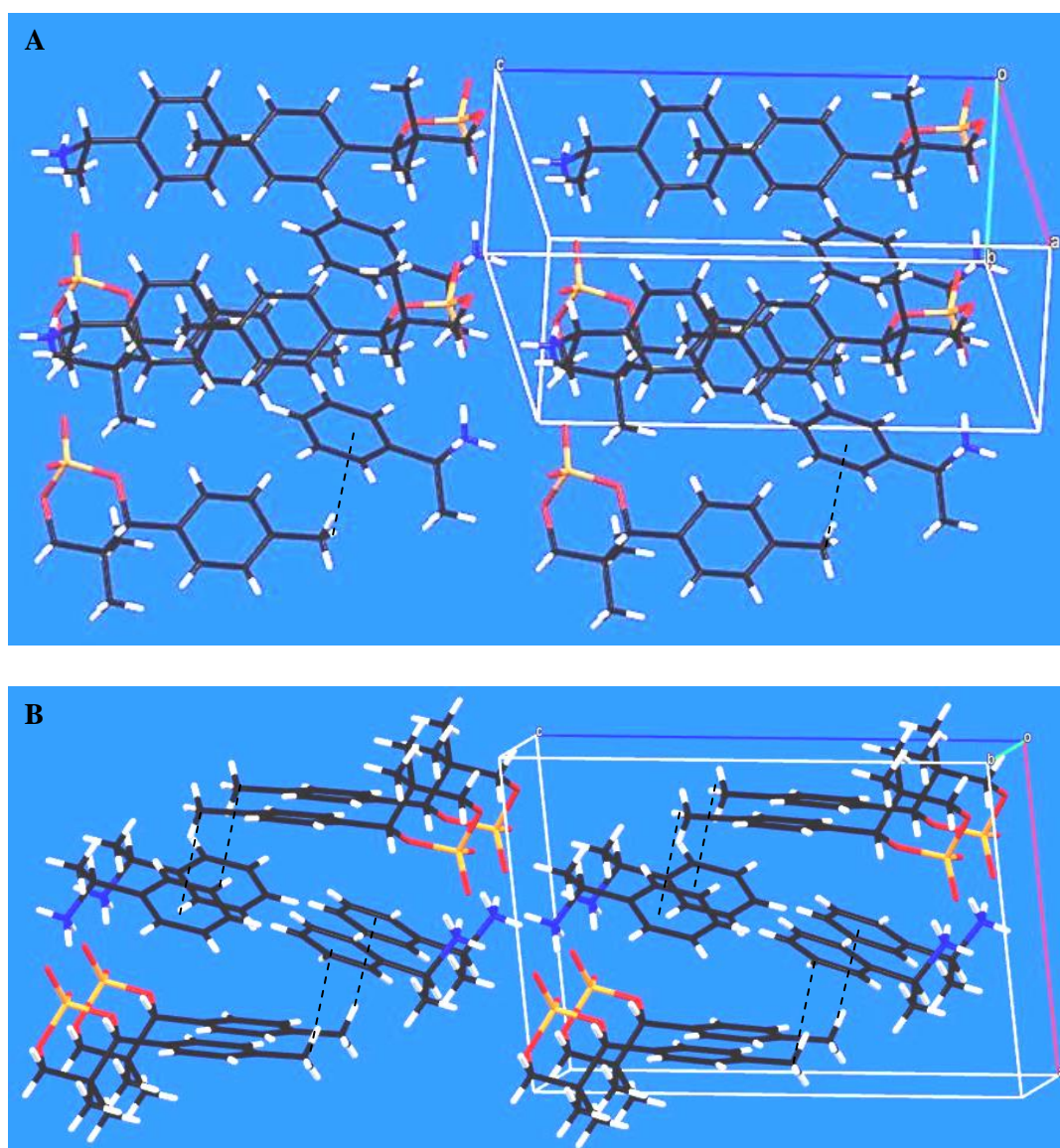
**Figure 3.7.** *p*-Methyl phencyphos and phenylethylamine.

<sup>5</sup> (rac) Phencyphos (PP) + (+) Phenylethylamine (PEA) in ethanol; (rac) PP + (-) PEA in ethanol; (+) PMPP + (rac) PEA in ethanol; (-) PMPP + (rac) PEA in ethanol; (+) P<sub>MIX</sub> + (rac) PEA in ethanol; (-) P<sub>MIX</sub> + (rac) PEA in ethanol; (-)P<sub>MIX</sub> + (+) Ephedrine in isopropanol. (+)P<sub>MIX</sub> + (-) Ephedrine in isopropanol. (+) PMPP + (+) PEA in ethanol; (-) PMPP + (-) PEA in ethanol;



**Figure 3.8.** (A) Independent molecules of (-) PMPP and (-) PEA in the diastereomeric salt and (B) the unit cell of the structure.

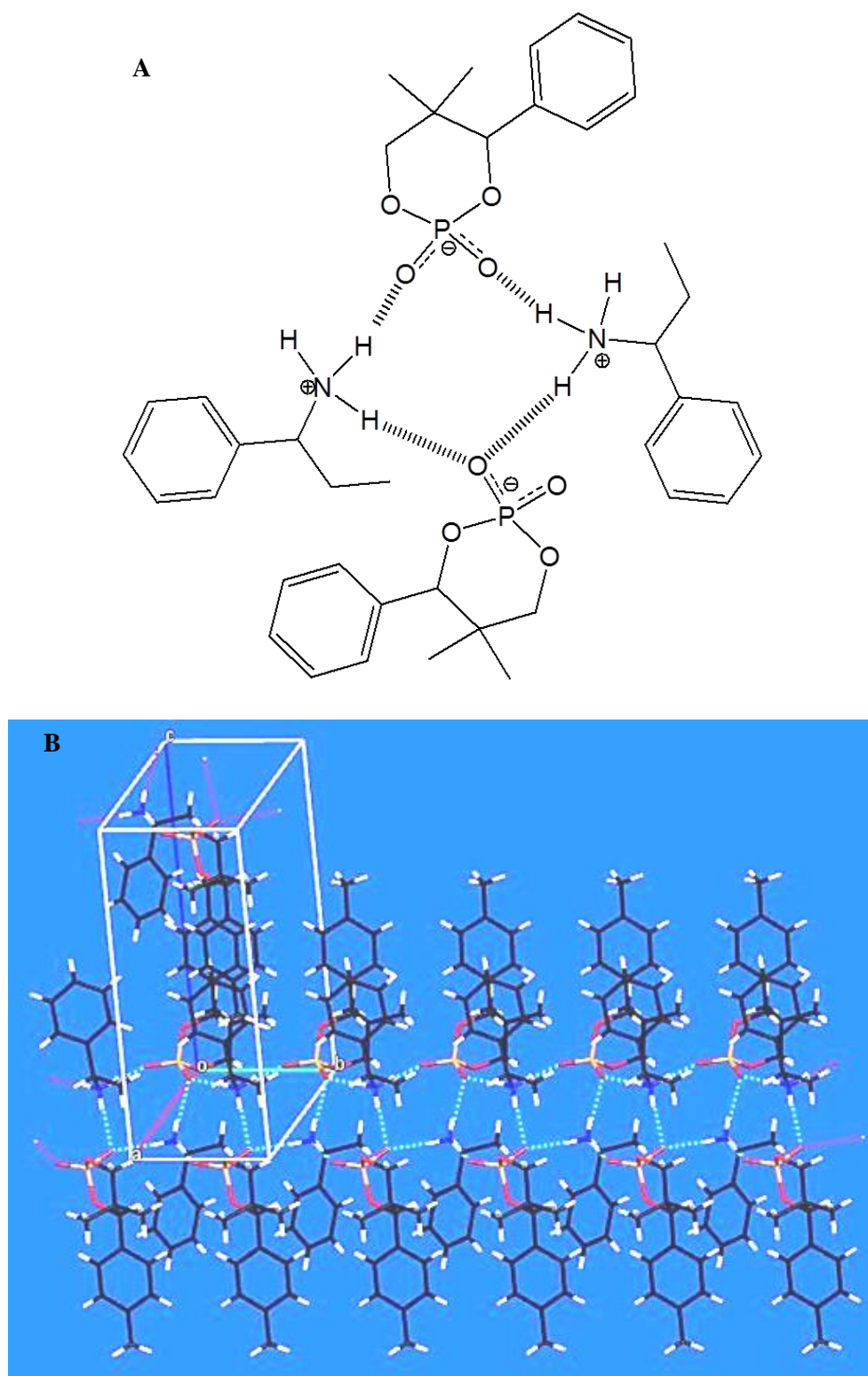
This diastereomeric salt is formed from two neutral compounds, and during the crystallisation from bulk solution there is an acid-base reaction in which the phosphoric acid group passes its acidic hydrogen atom to the amine group, which becomes an ammonium group. Thus, the final product is the diastereomeric salt: *deprotonated (-)-p-Methyl-Phencyphos* + (-) *Phenylethylaminium*. Both molecules have a polar region (the functional groups) and a much more apolar region (phenyl rings). The hydrophobic parts interact through edge-to-face stacking -attractive interaction H-  $\pi$  electrons, by the methyl group of the PMPP to the phenyl ring of the PEA (Figure 3.9).



**Figure 3.9.** H- $\pi$  electrons of the phenyl ring attractive interactions. (A) Top and (B) lateral view.

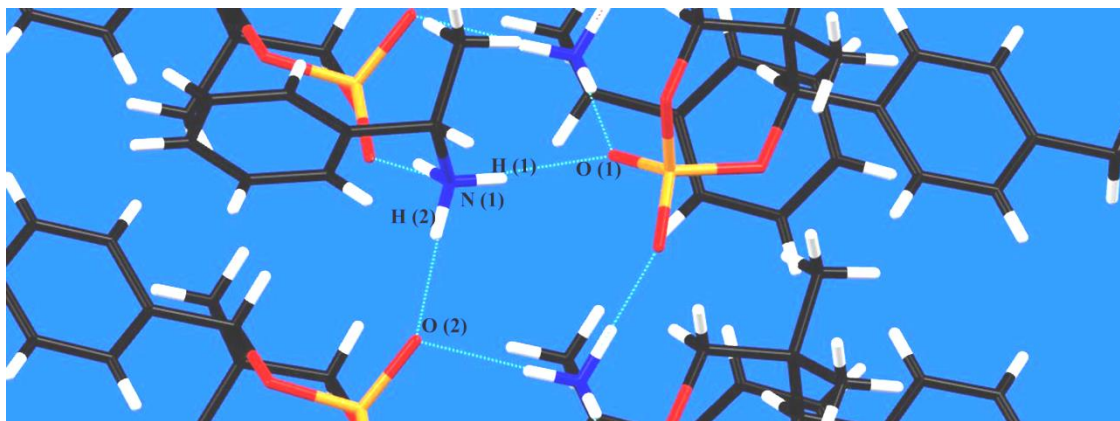
The hydrophobic and hydrophilic layers are alternated along the  $c$  axis. The phenyl rings are stacked and slightly twisted with respect to a normal stacking arrangement due to the phosphate group interaction to the ammonium group. Hydrogen bonds between the ammonium and phosphate groups result in the formation of 10-membered rings in this structure (Figure 3.10). The oxygen atom of the phosphate group that is not involved in the ring forms a hydrogen bond with an ammonium group of a neighbouring ring, and one of the oxygen atoms in the ring forms a bifurcated hydrogen bond (one with the ammonium group in the ring and another with an ammonium group in a neighbouring ring). The hydrogen bond network is thus grown along the  $2_1$  screw axis parallel to the  $b$  axis, forming a ribbon-like topology along this direction in the

crystal. The hydrophobic layers are come together keeping the ribbons joined due to the phenyl ring attractive interaction (Figure 3.9).



**Figure 3.10.** (A) A schematic structure showing the 10- membered rings in the structure of the salt formed by (-) PMPP and (-) PEA. (B) Hydrogen bonded network of the 10-membered ring parallel to *b* axis

All strong donors and acceptors are used in this crystal structure and form strong hydrogen bonds, which are almost linear (see hydrogen bond geometry in the Table 1.2 and Figure 3.11).

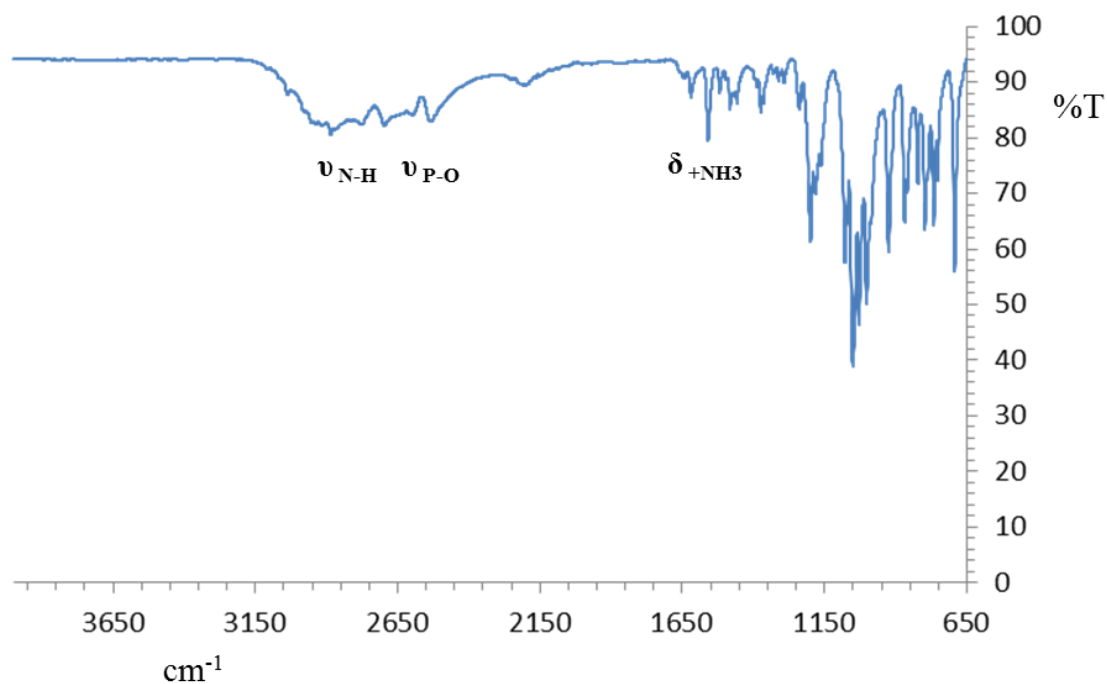


**Figure 3.11.** Hydrogen bonds in the 10-membered ring in the structure of the salt formed by (-)-PMPP and (-)-PEA.

**Table 1.2.** Hydrogen bond geometries in the (-)-PMPP-(-)-PEA salt.

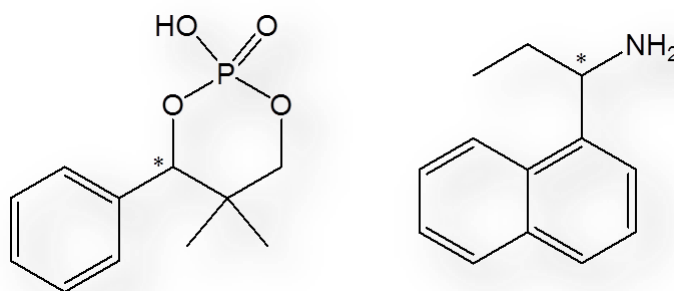
Bond N-H···O	$d_{\text{N-H}}$ (Å)	$d_{\text{H···O}}$ (Å)	$d_{\text{N····O}}$ (Å)	$\alpha_{\text{N-H···O}}$ (°)
N(1)-H(1)···O(1)	0.87	1.97	2.83	171.5
N(1)-H(2)···O(2)	0.92	1.85	2.77	175.4

Analysing the infrared spectra of the (-)-PMPP-(-)-PEA salt (Figure 3.12), we observed several bands which support the presence of the salt and the hydrogen bond formation. They are those corresponding of the stretching of P-O ( $\nu_{\text{P-O}}=2300 \text{ cm}^{-1}$ ) the stretching of N-H ( $\nu_{\text{N-H}}=2700 \text{ cm}^{-1}$ ) and the vibration of the N-H ( $\delta_{\text{N-H}}=1600\text{-}1400 \text{ cm}^{-1}$ )- $\text{NH}_3^+$  group.<sup>5</sup>



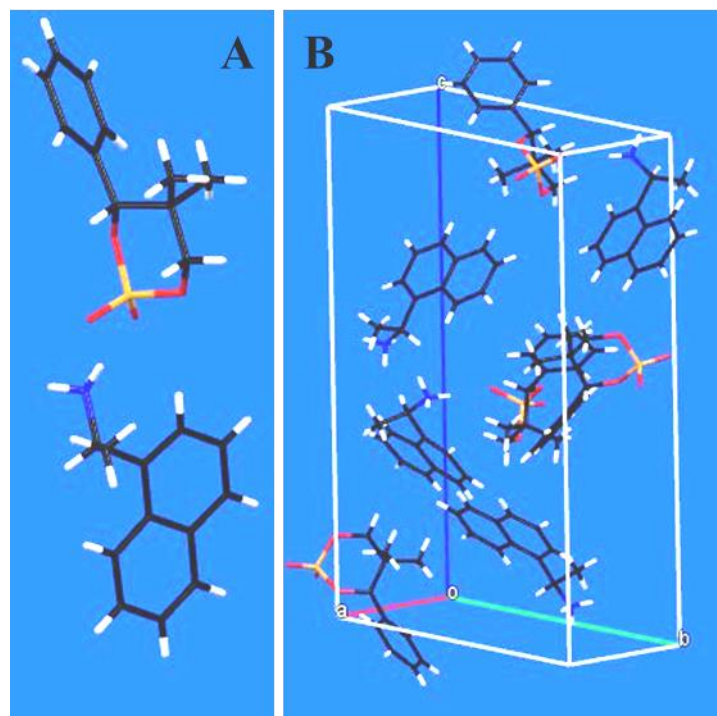
**Figure 3.12.** Infrared spectra of (-)PMPP+(-)PEA.

✚ (-)Phencyphos (PP) and (+)-naphthalenpropylamine (NEA) (Figure 3.13) were combined in ethanol solution and the mixture was warmed and then allowed to cool down while the solvent evaporated freely. This procedure gave needle-like colourless crystals. X-ray single crystal diffraction was made and solved by Dr. K. Wurst. The PP and NEA diastereomeric salt crystallises in the orthorhombic system ( $a=6.24$ ,  $b=15.56$ ,  $c=22.52\text{\AA}$ ,  $\alpha=90$ ,  $\beta=95.49$ ,  $\gamma=90^\circ$ ), (Figure 3.14) in the space group  $P2_12_12_1$ .



**Figure 3. 13.** The chemical structures of (-)-Phencyphos and (+)-(+)-Naphthalenpropylamine.

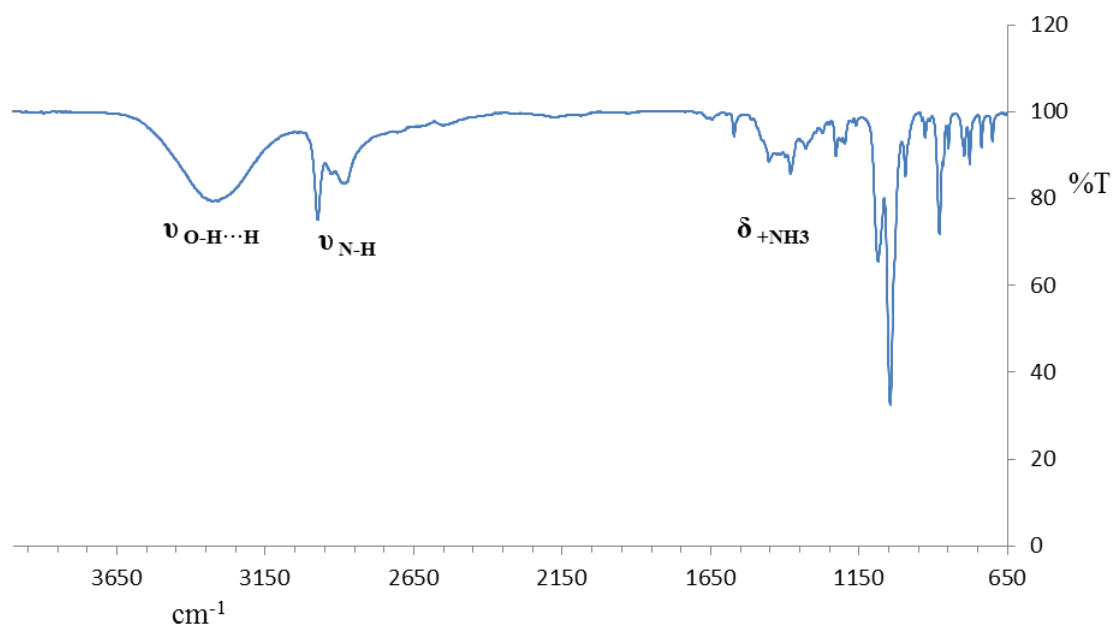




**Figure 3.14.** (A) Independent molecules of (-)-PP and (+)-NEA in the diastereomeric salt and (B) the unit cell of the structure.

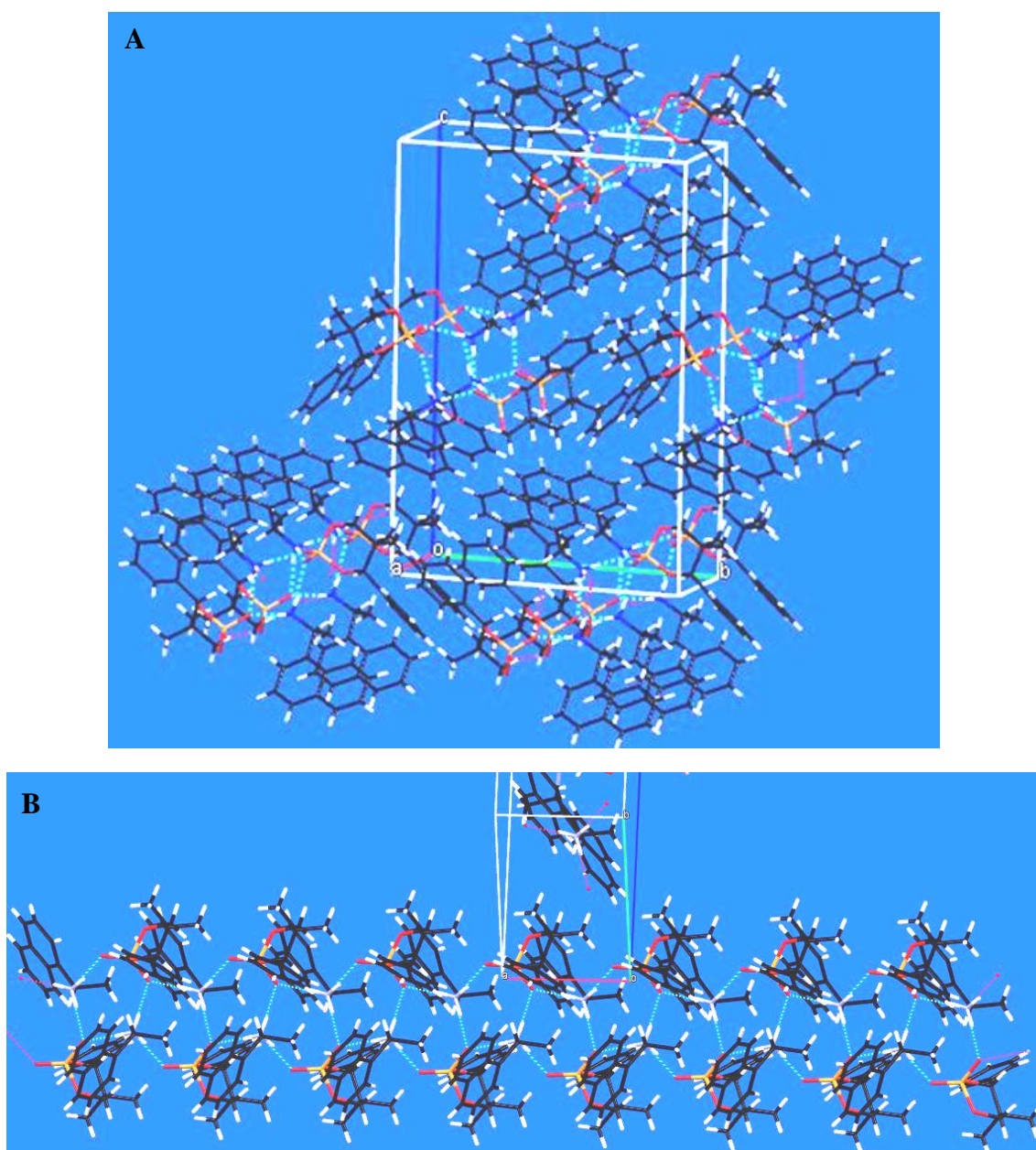
As in the other diastereomeric salt described above, the formation of this ionic compound consists of an acid-base reaction in which the phosphoric acid group passes the hydrogen atom from the acid group to the amine moiety, which becomes an ammonium group. Thus, the final product is the diastereomeric salt: *deprotonated (-)-Phencyphos* + (-) (+)-*naphthalenpropylaminium*. Both molecules have a polar region (where the functional groups are located) and an apolar region (the aromatic rings).

To support the X-ray diffraction data, an infrared spectrum (Figure 3.15) would confirm the existence of the hydrogen bonds in the crystal structure. The stretching of OH group ( $\nu_{\text{OH}}=3300 \text{ cm}^{-1}$ ) forming hydrogen bonds (O-H $\cdots$ H), the stretching of N-H ( $\nu_{\text{N-H}}=2700 \text{ cm}^{-1}$ ) and the vibration of the N-H ( $\delta_{\text{N-H}}=1600\text{-}1400 \text{ cm}^{-1}$ )  $\text{-NH}_3^+$  group.<sup>5</sup> These bands indicate the existence of the hydrogen bonds.



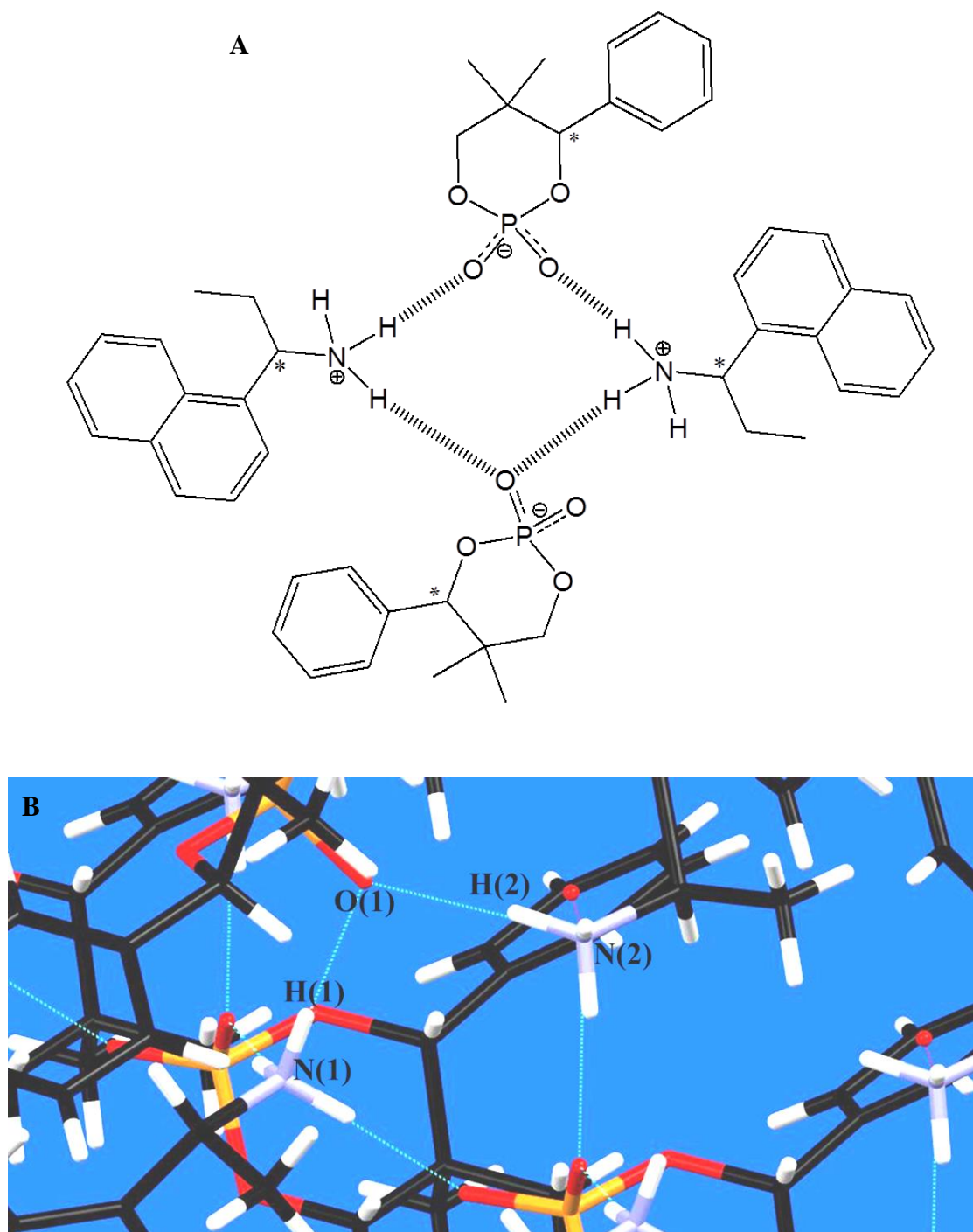
**Figure 3.15.** Infrared spectra of (-)-PP-(+)-NEA salt.

The polar and less polar layers alternate along the  $c$  axis (Figure 3.16 A). The naphthyl rings are stacked and slightly twist. Hydrogen bonds that form a 10-membered ring are also found in this structure, thanks to the hydrogen bond formed by the phosphate group and the ammonium group. The hydrogen bond network growth is governed by the  $2_1$  screw axis parallel to the  $a$  axis, forming a ribbon along this direction of the crystals (Figure 3.16).



**Figure 3.16.** Hydrogen bond network -parallel to the *a* axis and the 10-membered hydrogen bonded rings formed by two phosphate groups and two ammonium groups. (A) Lateral and (B) top view.

According to the geometric described in the Table 1.3 and Figure 3.17, all strong donors and acceptors are used in this crystal structure and form strong hydrogen bonds, which are almost linear with angles closed to  $180^\circ$ .



**Figure 3.17.** (A) A schematic view of the 10-membered hydrogen bonded ring in the salt formed by (-)-PP and (+)-NEA. (B) Part of the crystal structure showing the 10-membered ring.

**Table 1.3.** Hydrogen bond geometry of PP-NEA salt.

Bond N-H $\cdots$ O	$d_{\text{N-H}}$ (Å)	$d_{\text{H}\cdots\text{O}}$ (Å)	$d_{\text{N}\cdots\text{O}}$ (Å)	$\alpha_{\text{N-H}\cdots\text{O}}$ (°)
N(1)-H(1) $\cdots$ O(1)	0.87	1.97	2.83	171.5
N(2)-H(2) $\cdots$ O(1)	0.92	1.85	2.77	175.4

### 3.3.2. Crystalline diastereomeric salt structures retrieved from the CSD

The *Cambridge Structural Database (CSD)*, is a repository for small molecule crystal structures and is compiled and maintained by the *Cambridge Crystallographic Data Centre*. Once a structure of a new compound is solved, the crystallographic information about the structure is saved in a file (CIF format) and deposited in the CSD. This file contains the information of the space group symmetry, its cell parameters, and the coordinates of all atoms in 3D. This information can be exploited using software (such as the freeware Mercury)<sup>6</sup> to visualize the structure and even calculate the powder diffraction pattern of the compound. This option is very important in order to identify the different crystalline phases present in a crystalline powder mixture without the need for growing single crystals. The library of structures is also useful to understand the conformational preferences of molecules and their habitual non-covalent interactions and packing patterns.<sup>7</sup>

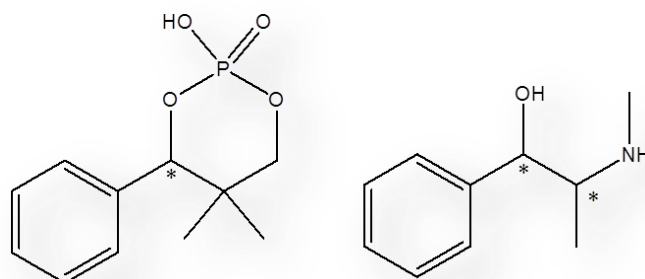
As many of the organic molecules of the sort that could potentially act as medical drugs are archived in the CSD, we did a search in this database in order to analyse which salts containing phencyphos derivatives have already had their structures solved. Phencyphos has several diastereomeric salts already characterised and archived in the CSD, here the most relevant ones will be described.

---

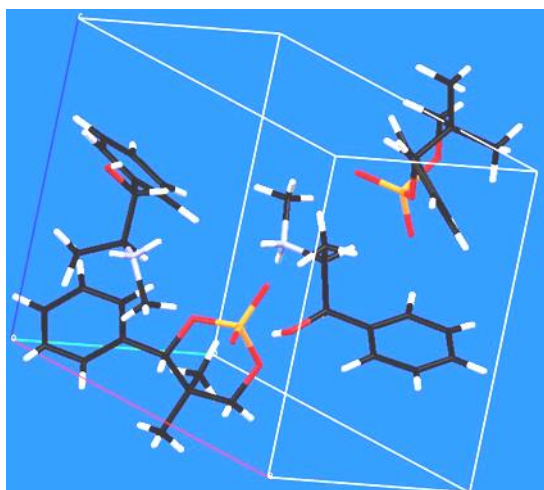
<sup>6</sup> C. F. Macrae, I. J. Bruno, J. A. Chisholm, P. R. Edgington, P. McCabe, E. Pidcock, L. Rodriguez-Monge, R. Taylor, J. van de Streek and P. A. Wood, *J. Appl. Cryst.*, **2008**, *41*, 466-470.

<sup>7</sup> (a) F. H. Allen, W. D. S. Motherwell, *Acta Cryst.*, **2002**, *58*, 407-422. (b) A. D. Bondw, *The Role of the Cambridge Structural Database in Crystal Engineering in Organic Crystal Engineering: Frontiers in Crystal Engineering*, **2010**, (eds E. R. T. Tiekink, J. Vittal and M. Zaworotko), John Wiley & Sons, Ltd, Chichester, UK. doi: 10.1002/9780470681794.ch1

- ✚ One of the diastereomeric salts in the CSD is that formed by (-) phencyphos and (+) ephedrine (Figure 3.18).<sup>8</sup> It crystallises in the monoclinic system ( $a=13.842$ ,  $b=7.804$ ,  $c=10.168\text{\AA}$ ,  $\alpha=90$ ,  $\beta=92.95$ ,  $\gamma=90^\circ$ ) in the space group  $P2_1$  (Figure 3.19).



**Figure 3.18.** Chemical structures of phencyphos and ephedrine.

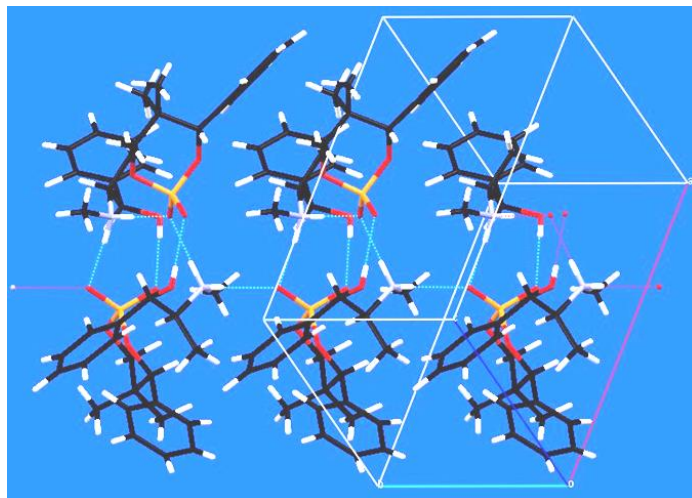


**Figure 3.19.** The unit cell of the salt formed from phencyphos and ephedrine.

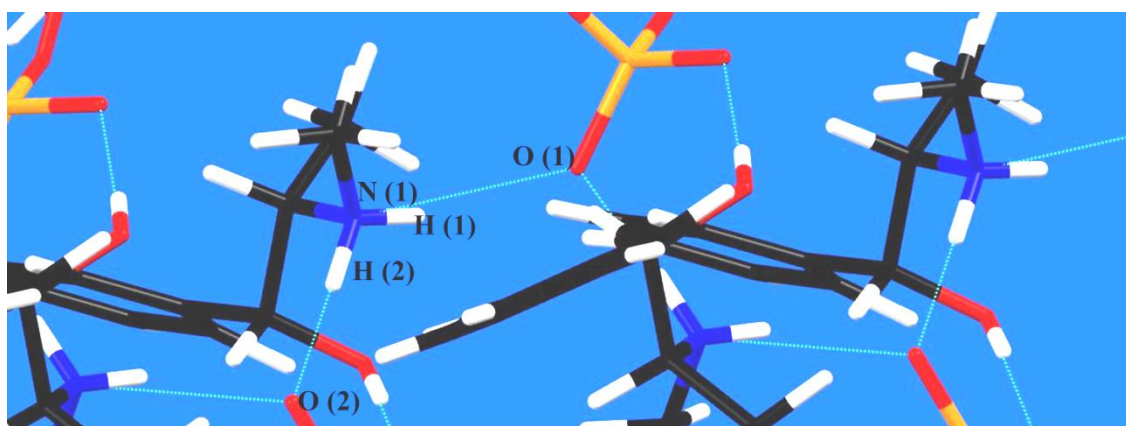
As in other salts of this kind, the polar and apolar regions separate, with the functional groups interacting through strong hydrogen bonds (Table 1.4). A  $2_1$  screw axis runs parallel to  $a$  axis, forming a ribbon along this direction (Figure 3.20). The hydrophobic parts interact by edge-face stacking (attractive H- $\pi$  interactions) between the methyl groups of the phencyphos to the phenyl ring of the ephedrine (Figure 3.22). The diastereomeric salt of (-) Phencyphos + (+) Ephedrine, as the ephedrine has a hydroxyl group, the hydrogen bond 10 membered ring is not present in its crystal

<sup>8</sup> A. M. G. Kok, H. Wynberg, J. M. M. Smits, P. T. Beurskens, V. Parthasarathi, *Acta Crystallogr., Sect. C: Struct. Commun.*, **1987**, 43, 1328.

structure. The OH group is involved in the hydrogen bond network as it is shown in the figure 3.21.



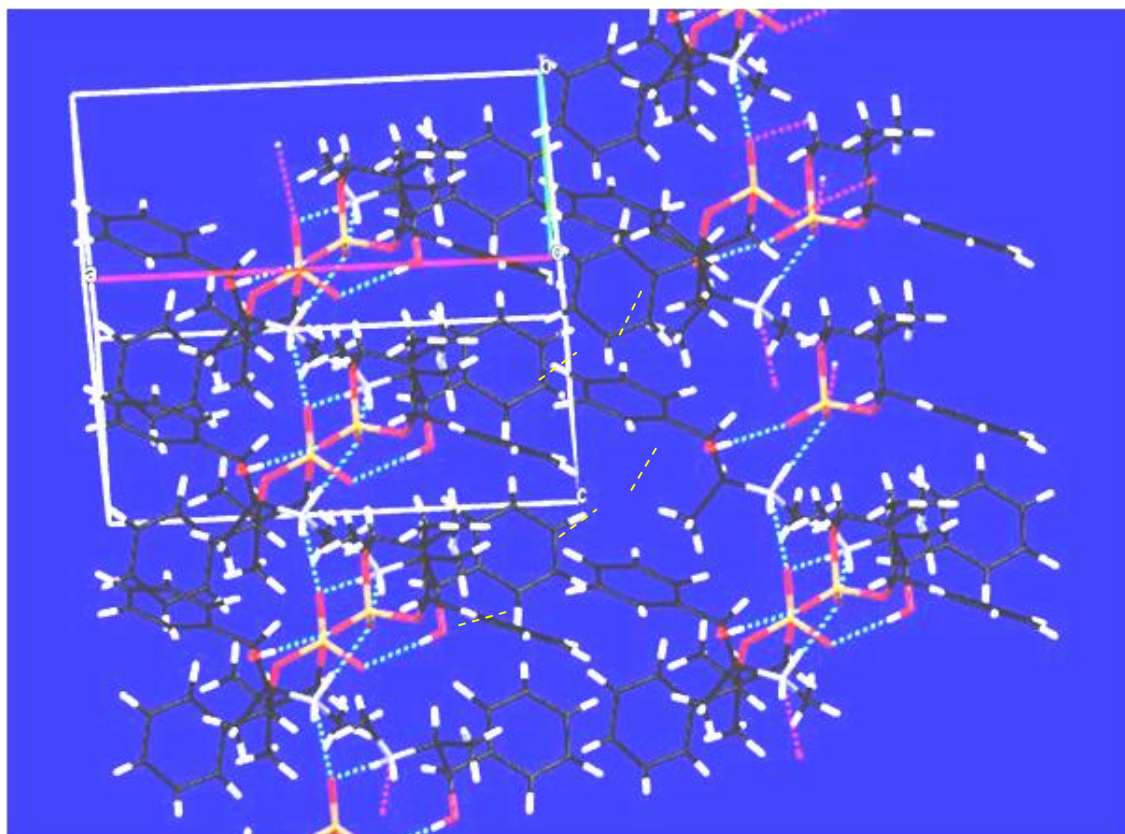
**Figure 3.20.** The hydrogen bonding network in the crystals of the salt formed from phencyphos and ephedrine parallel to *a* axis.



**Figure 3.21.** The hydrogen bond network in the crystals of the salt formed from phencyphos and ephedrine.

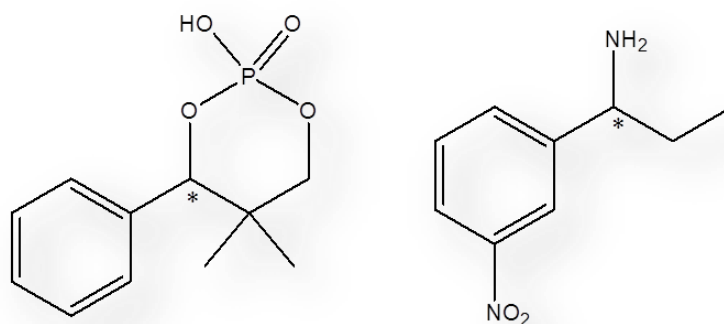
**Table 1.4.** Hydrogen bond geometry of (-) Phencyphos + (+) Ephedrine salt.

Bond N-H $\cdots$ O	$d_{\text{N-H}}$ (Å)	$d_{\text{H}\cdots\text{O}}$ (Å)	$d_{\text{N}\cdots\text{O}}$ (Å)	$\alpha_{\text{N-H}\cdots\text{O}}$ (°)
N(1)-H(1) $\cdots$ O(1)	0.79	2.08	2.82	156.4
N(1)-H(2) $\cdots$ O(2)	0.96	1.85	2.80	173.6



**Figure 3.22.** Hydrophobic parts interactions by edge-face stacking (attractive H- $\pi$  interactions).

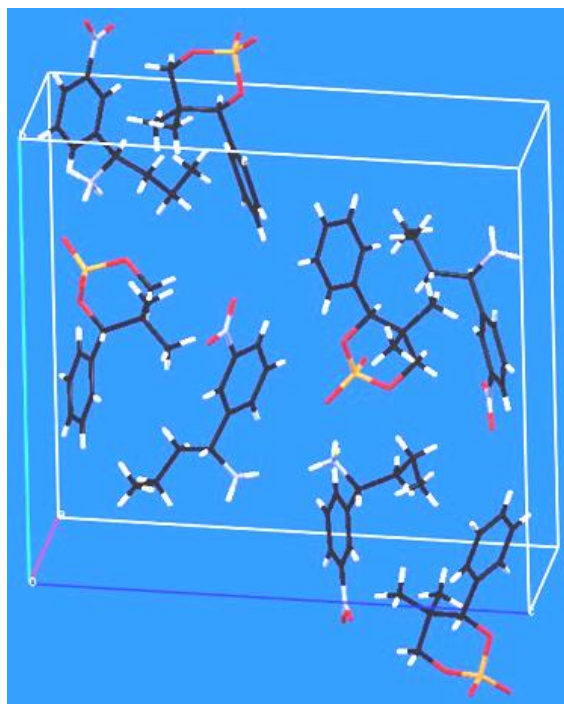
- ✚ The diastereomeric salt formed by (+)-1-(3-nitrophenyl) butylamine (-)-phencyphos<sup>9</sup> (Figure 3.23) crystallises in the orthorhombic system ( $a=6.0128$   $b=18.562$ ,  $c=19.190\text{\AA}$ ,  $\alpha=\beta=\gamma=90^\circ$ ) in the space group  $P2_12_12_1$ . (Figure 3.24).



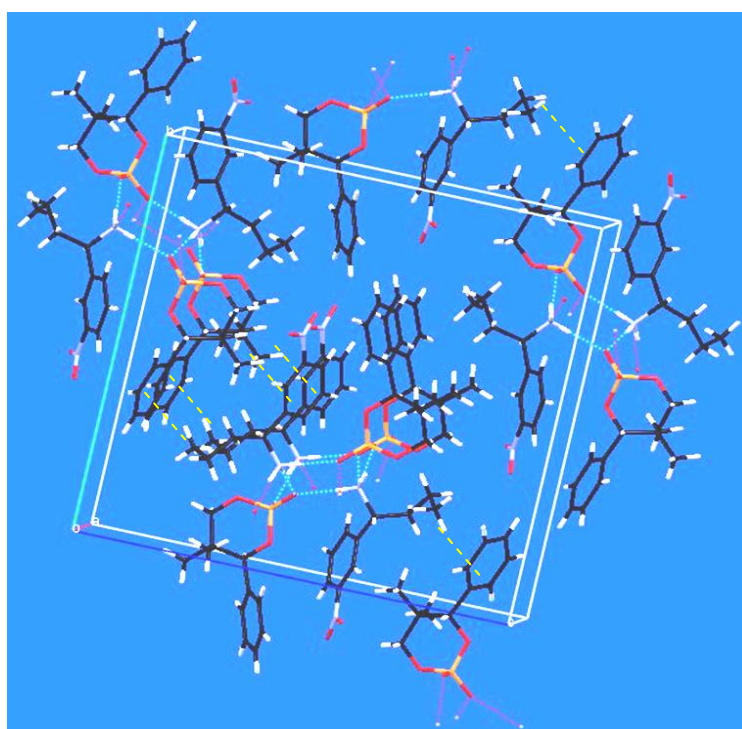
**Figure 3.23.** Chemical structures of phencyphos and 1-(3-nitrophenyl)butylamine .

<sup>9</sup> J. Dalmolen, M. van der Sluis, J.W. Nieuwenhuijzen, B. de Lange, B. Kaptein, R.M. Kellogg, Q.B. Broxterman. *Eur. J. Org. Chem*, **2004**, 1544-1557.





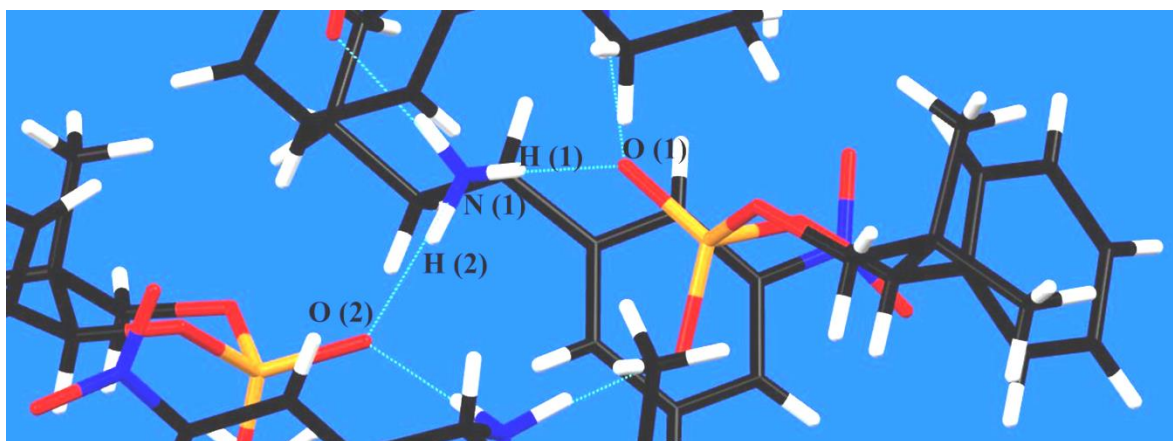
**Figure 3.24.** The unit cell of the salt formed between (+)-1-(3-nitrophenyl)butylamine and (-)-phencyphos.



**Figure 3.25.** Clear blue dashed lines indicate the hydrogen bond network parallel to *b* axis in the salt formed between (+)-1-(3-nitrophenyl) butylamine and (-)-phencyphos. Yellow dashed lines indicate the interaction through the methyl group of the phencyphos to the phenyl ring of the (+)-1-(3-nitrophenyl) butyl amine.

In this structure the functional groups interact through hydrogen bonds, generating a  $2_1$  screw parallel to  $b$  axis, forming a ribbon along this direction (Figure 3.25). The hydrophobic parts of the molecules interact by edge-to-face stacking – interactions, with alternance to the polar layer and parallel to the  $b$  axis through the methyl group of the phencyphos to the phenyl ring of the (+)-1-(3-nitrophenyl)butylamine (Figure 3.26).

Analysing the hydrogen bond geometry, we can conclude that in this structure is significant the 10-membered ring formation, and the strength of them, since their angle of bond are closer to  $180^\circ$ , the hydrogen bond formed is strong (Table 1.5 and Figure 3.26).

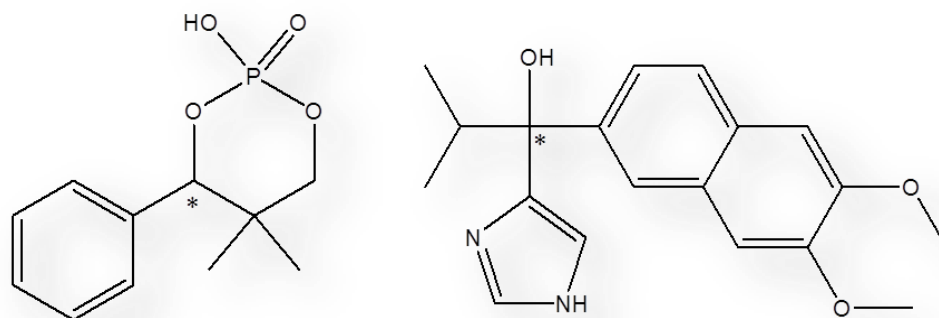


**Figure 3.26.** Hydrogen bond network in the salt formed between (+)-1-(3-nitrophenyl)butylamine and (-)-phencyphos.

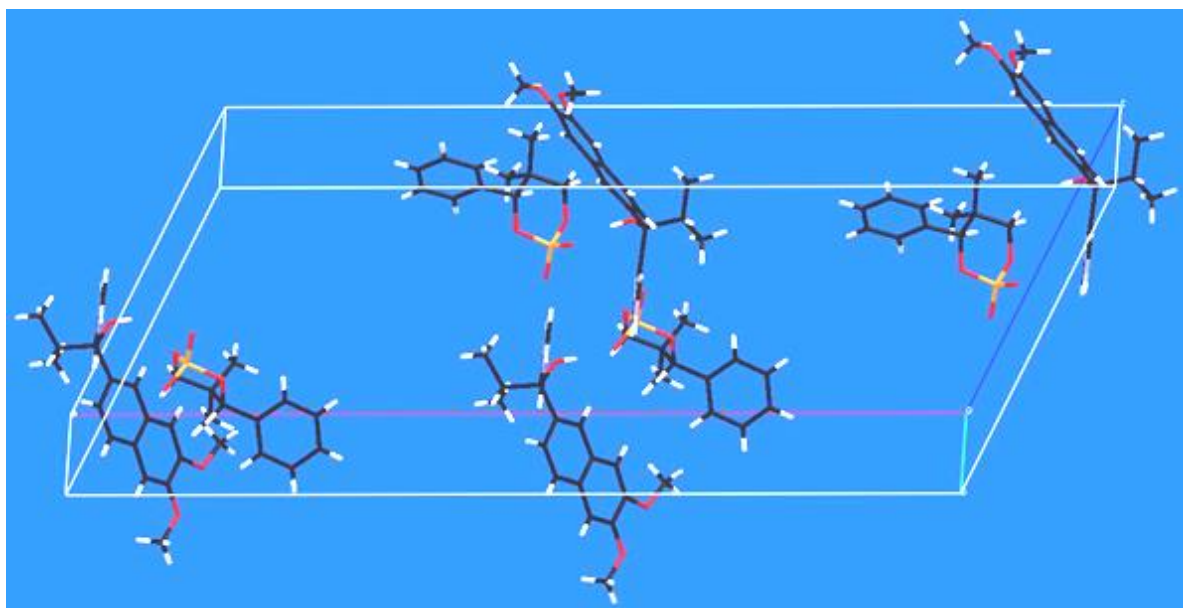
**Table 1.5.** Hydrogen bond geometry of (+)-1-(3-nitrophenyl)butylamine (-)-phencyphos salt.

Bond N-H $\cdots$ O	$d_{N-H}$ (Å)	$d_{H\cdots O}$ (Å)	$d_{N\cdots O}$ (Å)	$\alpha_{N-H\cdots O}$ (°)
N(1)-H(1) $\cdots$ O(1)	0.92	1.86	2.74	160.1
N(1)-H(2) $\cdots$ O(2)	0.90	1.85	2.75	176.6

- ✚ The diastereomeric salt formed by (-) phencyphos and (+)1-(6,7-dimethoxy-2-naphthyl)-1-(1H-imidazol-4-yl)-2-methylpropan-1-ol<sup>10</sup> (Figure 3.27) crystallises in the monoclinic system ( $a=36.232$ ,  $b=6.604$ ,  $c=15.735\text{\AA}$ ,  $\alpha=90$ ,  $\beta=114.6$ ,  $\gamma=90^\circ$ ) in the space group  $C2$ , (Figure 3.28). The polar functional groups interact through hydrogen bonding again, and a 2-fold axis parallel to  $c$  axis is formed. (Figure 3.29).

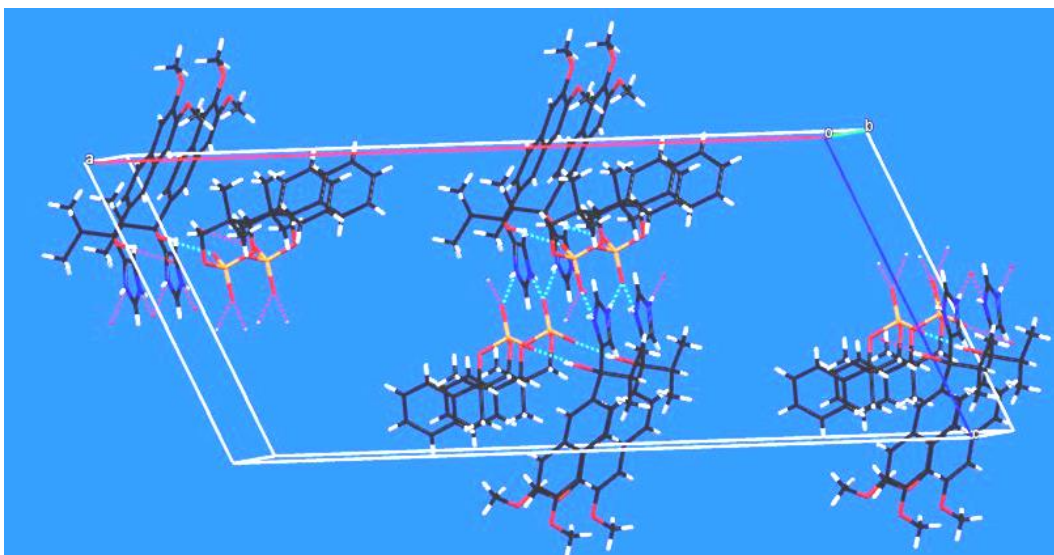


**Figure 3.27.** (-)Phencyphos + (+)1-(6,7-dimethoxy-2-naphthyl)-1-(1H-imidazol-4-yl)-2-methylpropan-1-ol.



**Figure 3.28.** Unit cell of the crystal structure of the salt formed between phencyphos and 1-(6,7-dimethoxy-2-naphthyl)-1-(1H-imidazol-4-yl)-2-methylpropan-1-ol.

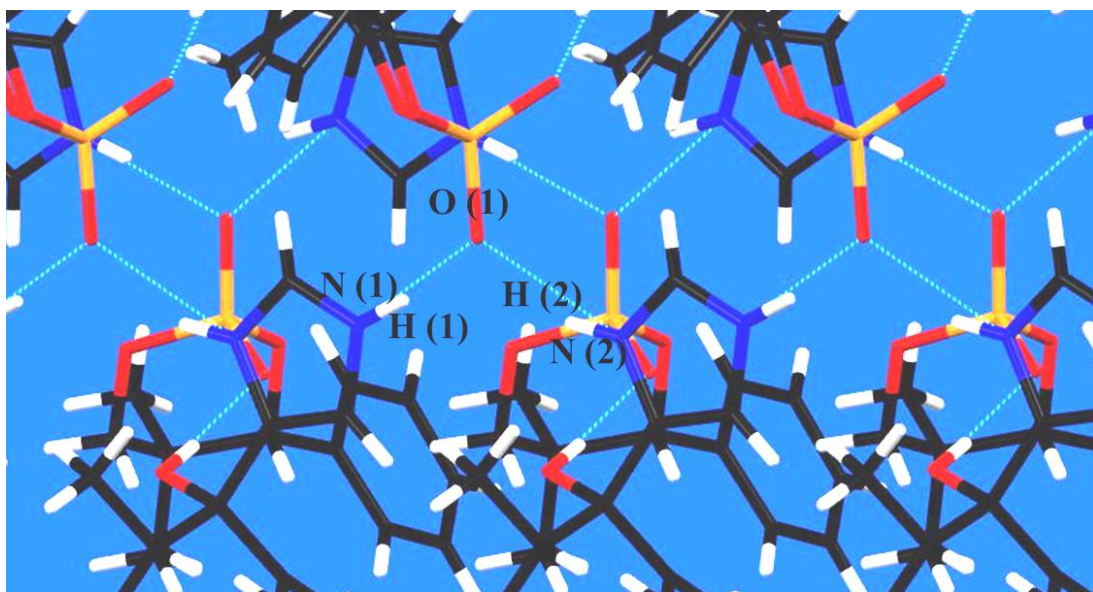
<sup>10</sup> N.Matsunaga, T. Kaku, A. Ojida, T. Tanaka, T. Hara, M. Yamaoka, M. Kusaka, A. Tasaka, *Bioorg. Med. Chem.*, **2004**, *12*, 4313.



**Figure 3.29.** Hydrogen bond network parallel to *c* axis in the salt formed between phencyphos and 1-(6,7-dimethoxy-2-naphthyl)-1-(1H-imidazol-4-yl)-2-methylpropan-1-ol.

The hydrogen bond networks grow along the *c* axis and the interaction between these chains is not very strong as in the figure 3.29 is shown, since the naphthyl rings are far ones to the others to provide the suitable  $\pi$ - $\pi$  stacking.

Nevertheless, hydrogen bond geometry (Table 1.6 and Figure 3.27) describes a relatively strong hydrogen bond interaction. This structure also has the 10-membered ring formation and the angle of these interaction are not so closer to the  $180^\circ$  as the structures described before, thus the intermolecular interactions in this structure are not so strong.

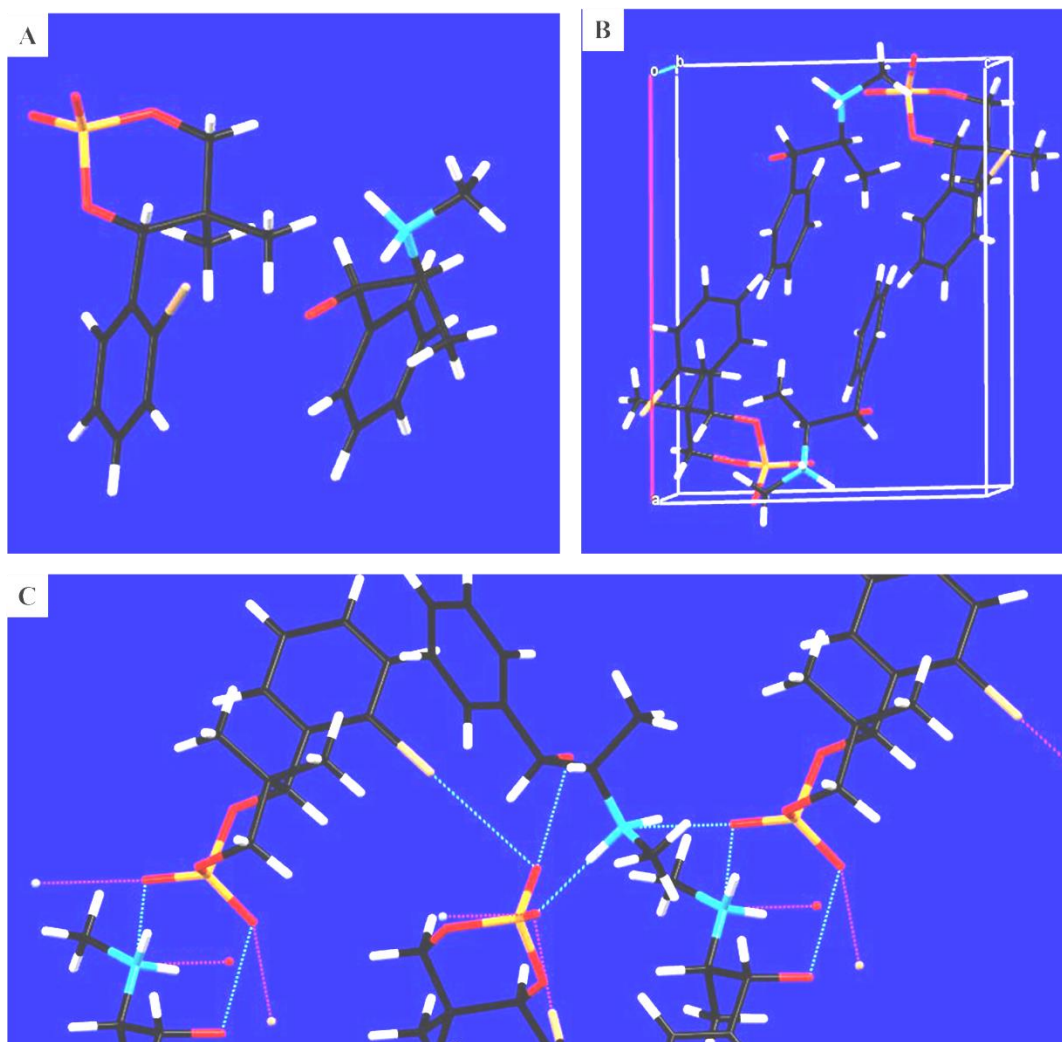


**Figure 3.30.** Hydrogen bond network in the salt formed between phencyphos and 1-(6,7-dimethoxy-2-naphthyl)-1-(1H-imidazol-4-yl)-2-methylpropan-1-ol.

**Table 1.6.** Hydrogen bond geometries in crystals of the salt formed between phencyphos and 1-(6,7-dimethoxy-2-naphthyl)-1-(1H-imidazol-4-yl)-2-methylpropan-1-ol.

Bond N-H $\cdots$ O	$d_{\text{N-H}}$ (Å)	$d_{\text{H}\cdots\text{O}}$ (Å)	$d_{\text{N}\cdots\text{O}}$ (Å)	$\alpha_{\text{N-H}\cdots\text{O}}$ (°)
N(1)-H(1) $\cdots$ O(1)	0.86	1.81	2.66	168.1
N(2)-H(2) $\cdots$ O(1)	0.86	1.90	2.67	148.6

Apart from all the structures described in these chapter, there are a few of them that they are still related to the phencyphos since they are halogen derivates and have specific bonds which do not have much sense to include their description although is deserved to point out. A good example is the diastereomeric salt formed by (R)-(+)-4-o-Bromophenyl-2-hydroxy-5,5-dimethyl-1,3,2- dioxaphosphorinane 2-oxide and (1R,2S)-(-)-a-(1-(methylamino)ethyl)benzyl alcohol, of the monoclinic system with a spacial group  $P 2_1$ , ( $a = 13.35$ ,  $b = 8.16$ ,  $c = 10.48$ ;  $\alpha = 90$ ,  $\beta = 91.33$ ;  $\gamma = 90$ ). The figure 3.31 shows the diastereomeric salt (A), the unit cell (B) and in the (C) shows the intermolecular interactions between the molecules in the crystal structure. There is a bond between the bromo and the oxygen of the phosphate group of the phencyphos compound and notice that the 10-membered ring is not formed



**Figure 3.31.** (A) Independent molecules of (R)-(+)-4-o-Bromophenyl-2-hydroxy-5,5-dimethyl-1,3,2-dioxaphosphorinane 2-oxide and (1R,2S)-(-)-a-(1-(methylamino)ethyl)benzyl alcohol diastereomeric salt, (B) unit cell; (C) bromo-oxygen bond and hydrogen bonds presence in the structure.



A CSD search showed a tendency of the diastereomeric salts - formed from phencyphos derivatives and chiral amines - to crystallise in two crystalline systems: orthorhombic and monoclinic, always with a  $2_1$  axes as. These axes are present in the majority of crystal structures of chiral compounds.<sup>12</sup> The hydrogen bonds are strong in each structure, and also the 10-membered ring is formed due to their directionality.

The CSD search also showed several crystal structures of phencyphos derivatives with chiral amines in which a halogen derivative caused different bonds to be formed in the crystal structure: In these derivatives the 10-membered ring is not formed.

---

<sup>12</sup> H. D. Flack, *Helvet. Chim. Acta*, **2003**, 86, 905- 921.



**Table 1.7.** Crystal data and structure refinement for (-) *p*-methyl Phencyphos-(-)-phenylethylamine.

Empirical formula	C <sub>20</sub> H <sub>28</sub> N O <sub>4</sub> P	
Formula weight	377.40	
Temperature	296(2) K	
Wavelength	0.71073 Å	
Crystal system	Monoclinic	
Space group	P2 <sub>1</sub> (no. 4)	
Unit cell dimensions	a = 10.3374(2) Å	α = 90°.
	b = 6.3947(3) Å	β = 95.495(2)°.
	c = 15.1974(4) Å	γ = 90°.
Volume	1000.00(6) Å <sup>3</sup>	
Z	2	
Density (calculated)	1.253 Mg/m <sup>3</sup>	
Absorption coefficient	0.161 mm <sup>-1</sup>	
F(000)	404	
Crystal size	0.4 x 0.25 x 0.15 mm <sup>3</sup>	
Theta range for data collection	1.98 to 24.99°.	
Index ranges	-12 ≤ h ≤ 12, -7 ≤ k ≤ 7, -18 ≤ l ≤ 17	
Reflections collected	6103	
Independent reflections	3449 [R(int) = 0.0142]	
Reflections [I > 2σ(I)]	3312	
Completeness to theta = 24.99°	98.6 %	
Absorption correction	None	
Refinement method	Full-matrix least-squares on F <sup>2</sup>	
Data / restraints / parameters	3449 / 1 / 249	
Goodness-of-fit on F <sup>2</sup>	1.074	
Final R indices [I > 2σ(I)]	R1 = 0.0267, wR2 = 0.0666	
R indices (all data)	R1 = 0.0284, wR2 = 0.0677	
Absolute structure parameter	-0.02(7)	
Extinction coefficient	0.043(6)	
Largest diff. peak and hole	0.107 and -0.144 e.Å <sup>-3</sup>	

**Table 1.8.** Crystal data and structure refinement for (-)-**phencyphos**-(+)-**naphthalenpropylamine**.

Empirical formula	C <sub>23</sub> H <sub>28</sub> N O <sub>4</sub> P	
Formula weight	413.43	
Temperature	233(2) K	
Wavelength	0.71073 Å	
Crystal system	Orthorhombic	
Space group	P2 <sub>1</sub> 2 <sub>1</sub> 2 <sub>1</sub> (no. 19)	
Unit cell dimensions	a = 6.2453(3) Å	α = 90°.
	b = 15.559(1) Å	β = 90°.
	c = 22.521(2) Å	γ = 90°.
Volume	2188.4(3) Å <sup>3</sup>	
Z	4	
Density (calculated)	1.255 Mg/m <sup>3</sup>	
Absorption coefficient	0.154 mm <sup>-1</sup>	
F(000)	880	
Crystal size	0.21 x 0.06 x 0.04 mm <sup>3</sup>	
Theta range for data collection	1.59 to 21.99°.	
Index ranges	-6 ≤ h ≤ 6, -15 ≤ k ≤ 16, -21 ≤ l ≤ 23	
Reflections collected	9111	
Independent reflections	2691 [R(int) = 0.1086]	
Reflections [I > 2σ(I)]	1976	
Completeness to theta = 21.99°	100.0 %	
Absorption correction	None	
Refinement method	Full-matrix least-squares on F <sup>2</sup>	
Data / restraints / parameters	2691 / 3 / 274	
Goodness-of-fit on F <sup>2</sup>	1.059	
Final R indices [I > 2σ(I)]	R1 = 0.0534, wR2 = 0.0915	
R indices (all data)	R1 = 0.0900, wR2 = 0.1002	
Absolute structure parameter	-0.17(17)	
Largest diff. peak and hole	0.185 and -0.295 e.Å <sup>-3</sup>	

# Chapter 4

## Self-assembled monolayers

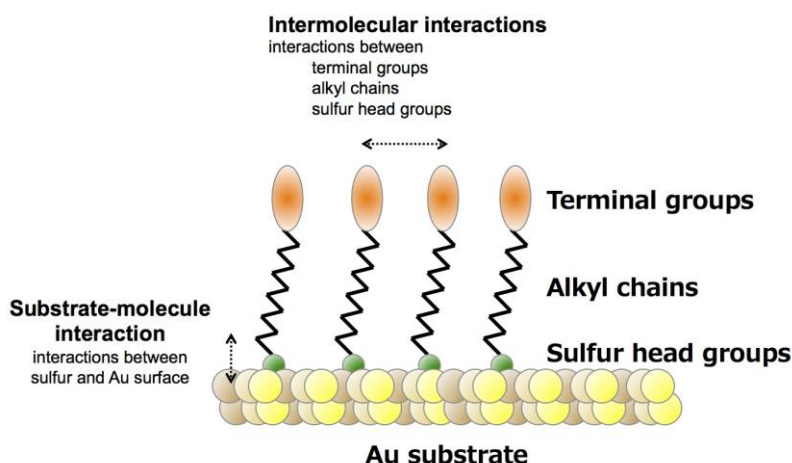
---

This section describes the Self-assembled monolayer basic and the characterization of the Self-assembled monolayers of (+)-phencyphos 4-methylthiol, dodecanethiol and 11-mercaptoundecanoic acid.

## 4.1. Introduction

*Self-assembly* is the property of a disordered system far from equilibrium with similar or disparate components to start to organize itself through local non-covalent chemical interactions between its components without an external influence.<sup>1</sup> Self-assembly is a bottom-up technique that has excited the nanoscience community mainly because it offers a new way to develop products that simply “make themselves” because the structures formed by self-assembly are very difficult to be prepared by the traditional lithographic methods.<sup>2</sup> Moreover it is an interesting process for its biological relevance because it provides a novel approach to complex structures having nanometre-scale dimensions.<sup>3</sup>

*Self-assembled monolayers (SAMs)* (Figure 4.1) are formed when a substrate (metallic, semi-conducting or insulating, single crystal or glass) is placed in contact with a solution of organic molecules, which then spontaneously align themselves with respect to the substrate’s surface. SAMs provide a convenient, flexible and simple system with which to tailor the interfacial properties of metals, semiconductors, ceramics and polymers.<sup>4</sup>



**Figure 4.1** Representation an alkanethiol self-assembled monolayer formed on gold scheme.

<sup>1</sup> V. A. Shchukin, D. Bimberg, *Rev. Mod. Phys.*, **1999**, *71*, 1125-1171.

<sup>2</sup> S. Hecht, *Angew. Chem. Int. Ed.*, **2003**, *42*, 24-26.

<sup>3</sup> X. Li, J. Huskens, D. N. Reinhoudt, *J. Mater. Chem. B*, 2004, 2954-2971.

<sup>4</sup> J. C. Love, L. A. Estroff, J. K. Kriebel, R. G. Nuzzo, G. M. Whitesides, *Chem. Rev.*, **2005**, *105*, 1103-1139.

SAMs of alkanethiols on gold surfaces are the most studied of all this type of layer. The order of alkanethiol is high (depending on the chain length and end functionality) for the quite large domains on surface and this feature permits characterization of alkanethiol SAMs by many techniques with relative ease. In the SAM formation, the strong affinity between the sulphur and the gold, the lateral van der Waals interaction between the alkyl chains and the dipole interaction between polar end groups, drive the alkanethiols order, along with the coincidence of the lattices of the gold surface (generally 111) and the alkyl chains. The structure of 2D SAMs is characterized by positional and orientational order. The first one is due to the headgroup binding at the surface, whether the chain lies flat on the surface or adopts some vertical orientation. Positional order does not imply the existence of orientational order (and vice versa).<sup>5</sup>

SAMs are used for many applications that require a homogeneous surface modification, such as control of wetting, biocompatibility, lubrication, corrosion inhibition, passivation, etc., and the use of SAMs is a result of their properties:<sup>6</sup>

1. They are very easy to prepare and form relatively quickly from immersion into the solution of the assembling molecules.
2. They are molecularly ordered and are robust under many conditions of use.
3. They are thermodynamic minimum structures, thus they form spontaneously and tend to surpass surface defects.
4. They permit strict control of film thickness.
5. They allow surface properties to be controlled through tailoring of the exposed surface functional groups.<sup>1</sup>

In the scope of the research presented in this Thesis, the aim of surface functionalization by SAMs is to favour crystallization on a surface by heterogeneous nucleation and subsequent growth. The structure of the SAMs could have high geometric complementarity with the nucleus of the compound to crystallise,<sup>7</sup> and this

---

<sup>5</sup> A. Badia, R. B. Lenox, L. Reven, *Acc. Chem. Res.* **2000**, *33*, 475-481.

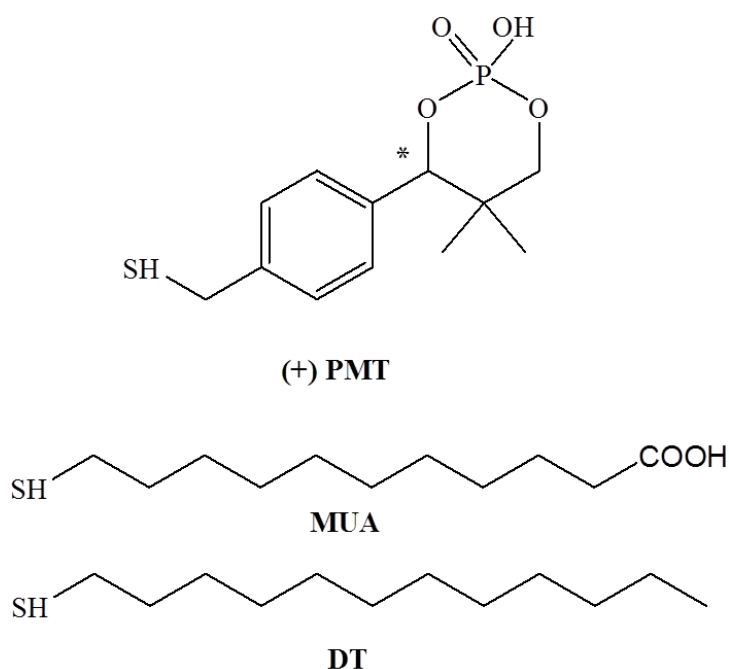
<sup>6</sup> Thin films. Volume 24. J. Tien, Y. Xia, G. M. Whitesides. Department of Chemistry and Chemical Biologym Harvard University, Cambridge, Massachusetts.1998, Academic Press. ISBN 0-12-533024-3.

<sup>7</sup> J. Aizengber, *Bell Labs Technical Journal*, **2005**, *10*, 129-141.

epitaxial model has been invoked to explain crystal orientation on surfaces. The geometric complementarities have been put forward as the driving force to favour the nucleation and the crystal growth on the SAMs rather than the homogeneous nucleation inside the bulk solution. In any case, SAMs are used as controlled heterogeneous nucleation centres,<sup>8</sup> and the objective here is to create chiral polar surfaces which might show diastereoselectivity in this process

## 4.2. SAMs

In this chapter, we explain gold surface functionalization by SAM formation using the thiols shown in Figure 4.2 which show very different characteristics in terms of shape and terminal group polarity. These thiols were chosen because of their varied polarity and chirality. The SAMs were prepared on monocrystalline gold (with the (111) surface exposed) on mica or polycrystalline gold on glass. These surfaces differ significantly not only in their crystallinity but also in the size of the terraces that the gold forms and the overall roughness of the surface. The monocrystalline gold has large, flat terraces with clear evidence of monoatomic steps while the polycrystalline gold has small terraces (sub-200 nm) with large undulations and bumps and crevices over the surface.



**Figure 4.2.** Alkanethiols selected to form the SAMs on gold.

<sup>8</sup> A. Y. Lee, A. Ulman, A. S. Myerson, *Langmuir*, **2002**, *18*, 5886-5898.

Figure 4.2. shows the thiols used to functionalize the gold substrates. The gold substrates were reacted with the thiols by immersing the cleaned metal surfaces in ethanol solutions of the compounds at a concentration of 1 M. The resulting SAMs were characterized by several techniques as X-ray Photoelectron Spectroscopy (XPS), Contact Angle (CA), and Scanning Tunnelling Microscopy (STM).

XPS is a very sensitive spectroscopic technique which gives precise chemical information about which elements are present at a surface and their environment in terms of bonding. Thus, if the functionalization of the gold surface is successful, in the case of alkanethiols, a peak of the S-Au moiety at the surface would appear in the XPS spectrum. Another technique which can give qualitative information concerning the functionalization of the gold substrates is the *contact angle* measurement, which is cheap and fast. The technique – which comprises the observation of the angle formed between a water drop's surface and the surface under study - gives information of the polarity changes at the surface, thus a significant change on the number of the angle means a change in the functional groups which are exposed to the water drop. This technique is very suitable for routine use in the laboratory.

The two dimensional order in SAMs on gold surfaces could be very important from the viewpoint of matching the structure of the nucleus with the monolayer templates so that crystallization on them is favoured. Understanding of this order provides useful information about how the nucleus could interact with the. The technique which gives most precise imaging of the structure of the SAMs on gold is *Scanning Tunnelling Microscopy* (STM). The technique has the advantage over diffraction techniques in that both crystalline and amorphous regions can be imaged, and an averaged view of the surface is not obtained but rather the more realistic situation of defects and local order and disorder. The following subsections explain in detail the study carried out of these SAMs by XPS, CA and STM.

### 4.3. (+) Phencyphos 4-Methylenethiol SAMs on monocrystalline gold.

#### 4.3.1. XPS Analysis

Representative S (2p) and P (2p) spectra of a monolayer of (+) PMT on gold are shown in Figure 4.3 a-b. Spectra 4.3.c-d corresponds to the carbon and oxygen atoms present in the monolayer.

The main binding energy peak observed at 161.80-163.00 eV in the sulphur region of the spectrum (Figure 4.3.a) consists of a spin-orbit-split doublet, corresponding to S ( $2p_{1/2}$ ) and S ( $2p_{3/2}$ ), representing one type of chemical state corresponding to the chemisorbed thiolate group (S-Au), and showing that monolayer formation was successful. The other binding energy peak observed at 164.5 eV in the sulphur region of the spectrum (Figure 4.3.a) consists of a spin-orbit-split doublet, S ( $2p_{1/2}$ ) and S ( $2p_{3/2}$ ), representing one type of chemical state corresponding to the free thiol group (S-H), this peak is commonly found in physisorbed alkylthiols on gold<sup>9</sup>. Fitted S (2p) curve has a spin-orbit-split of 1.2 eV.

The binding energy for a cyclic phosphoric acid group was not found in the literature, thus, the binding energy as reference is the one fitted corresponding to the XPS analysis presented here. The only peak observed in the XPS spectra of P (2p) at 133.7-134.5 eV consists of a spin-orbit-split doublet, P ( $2p_{1/2}$ ) and P ( $2p_{3/2}$ ) (Figure 4.3.b), arising from one type of chemical state corresponding to the cyclic phosphoric acid group (-POOH), similar to a value for a phosphoric acid group.<sup>10</sup> The fitted P (2p) curve has a spin-orbit-split of 0.8 eV.

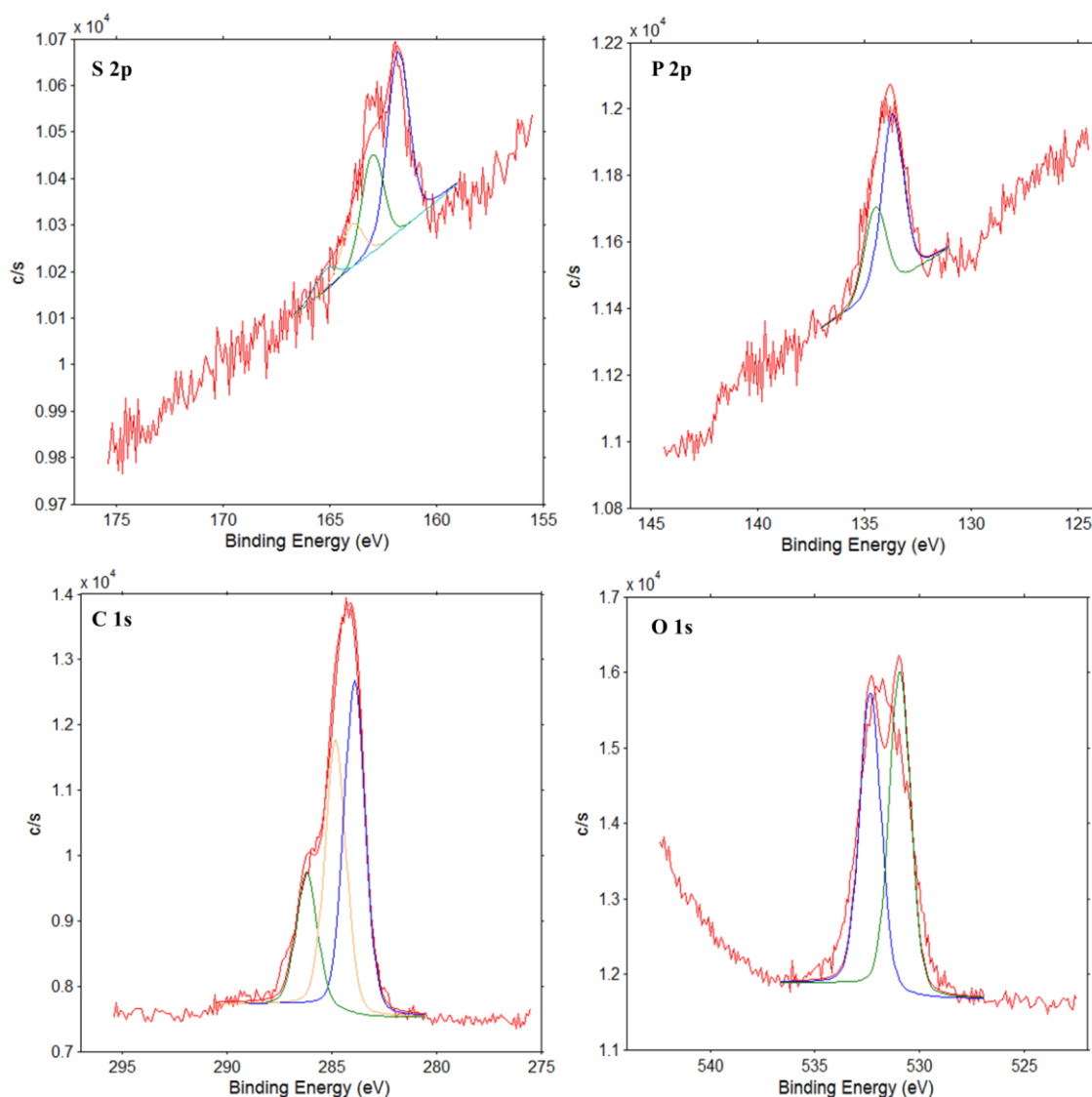
The relatively broad C (1s) main peak at about 283.90 eV is assigned to the C-H of aromatic carbon component of the adsorbed molecule, while the curved-fitted peak at 284.81 eV (Figure 4.2.c) corresponds to the aliphatic carbon atoms. The binding energy peak observed at 286.2 eV corresponds to the carbon bonded with sulphur (C-S). The O (1s) spectra (Figure 4.3.d) shows two binding energy peaks corresponding to the single and double bonds to the phosphorous atom.

---

<sup>9</sup> K. Hinds, D.W. Grainger, *Langmuir* **1996**, *12*, 5083-5086.

<sup>10</sup> R.M.Petoral Jr., F. Björefors, K. Uvdal, *J. Phys. Chem. B*, **2006**, *110*, 23410-23410.





**Figure 4.3.** Selected regions of the core-level XPS data for SAMs of (+)-PMT on gold. (A) S (2p), (B) P (2p), (C) C (1s) and (D) O (1s) XPS core-level spectra.

All this data confirm the presence of the PMT molecule on the surface of the gold. The apparent high proportion of physisorbed thiol is somewhat surprising and could indicate a non-covalent trapping of molecules between chemisorbed materials.

#### 4.3.2. Contact angle measurement

Contact angle measurements on the clean monocrystalline gold and the SAM functionalized metal are consistent with the covalent attachment of the thiol. Water forms a contact angle of  $18^\circ$  on the SAM of (+) PMT on monocrystalline gold while the SAM on polycrystalline gold gives a contact angle of  $53^\circ$ . The bare gold has a contact angle of approximately  $76^\circ$ . The lower value of the monocrystalline gold surface is

because it is much smoother than the polycrystalline gold on glass. The surface roughness, as well as the chemical nature of the surface that is exposed to the drop, has an important influence on the contact angle with higher roughness tending to give higher contact angles because of pinning of the drop. These low contact angles indicate that the phosphoric acid moiety is directed away from the surface mainly (bearing in mind the disorder seen in the STM images, see below) and therefore makes the surface polar and able to interact with polar molecules which would adsorb to it.

### 4.3.3. Scanning Tunnelling Microscopy

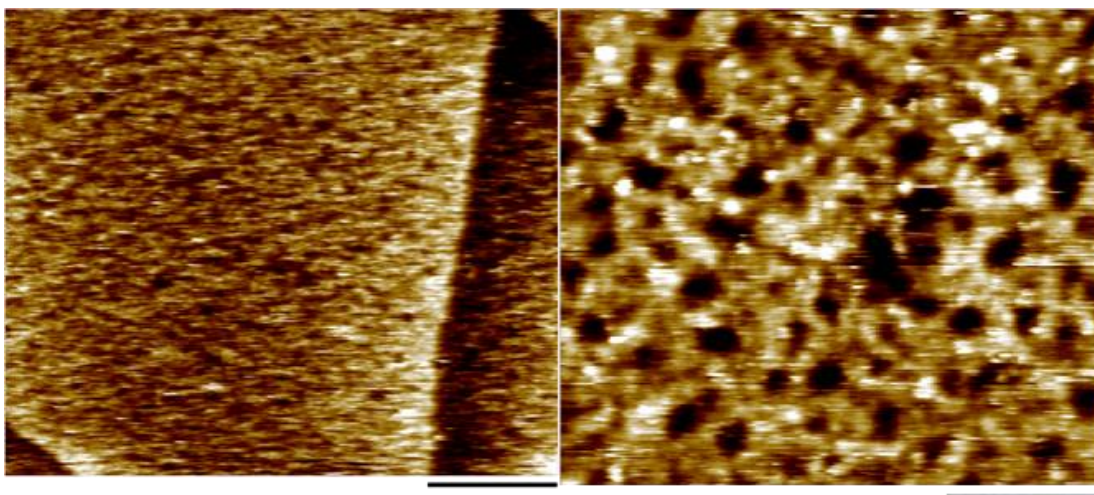
STM images of the monolayer formed on monocrystalline gold on mica under 1-phenyloctane as a covering fluid to aid image resolution show a layer of uniform thickness on the stepped gold surface (Figure 4.4, left), but which at the local level shows no order even at the shortest of scales (Figure 4.4, right). The images show the characteristic gold vacancy islands<sup>11, 12</sup> (which appear as dark areas corresponding to dents in the surface in these topographic images) surrounded by areas of varying contrast where there is no molecular order, but where bright specks appear which intuitively might correspond to the polar groups of the (+) PMT molecule attached to the surface. While layers of alkane thiols on gold can be ordered with crystalline characteristics because of the possibility of uniform packing of the alkyl chains,<sup>13</sup> (+) PMT has a twisted conformation which presumably obviates this possibility. The high torsion angle between the six membered rings in the molecule caused by and the bulk of the cyclic phosphoric acid head group (which we have seen in the X-ray crystal structures of derivatives of these compounds) mean that the layers – where in principle all the acid groups face away from the surface – cannot form an even dense packed arrangement.

---

<sup>11</sup> G.E. Poirier, *Langmuir*, **1997**, *13*, 2019-2026; b) R. Yamada, K. Uosaki, *Langmuir*, **1998**, *14*, 855-861.

<sup>12</sup> E. Torres A.T. Blumenau, P.U. Biedermann, *Phys. Rev. B.*, **2009**, *79*, 075440.

<sup>13</sup> C. Vericat, M.E. Vela. R. C. Salvarezza, *Phys. Chem. Chem. Phys.*, **2005**, *7*, 3258-3268.



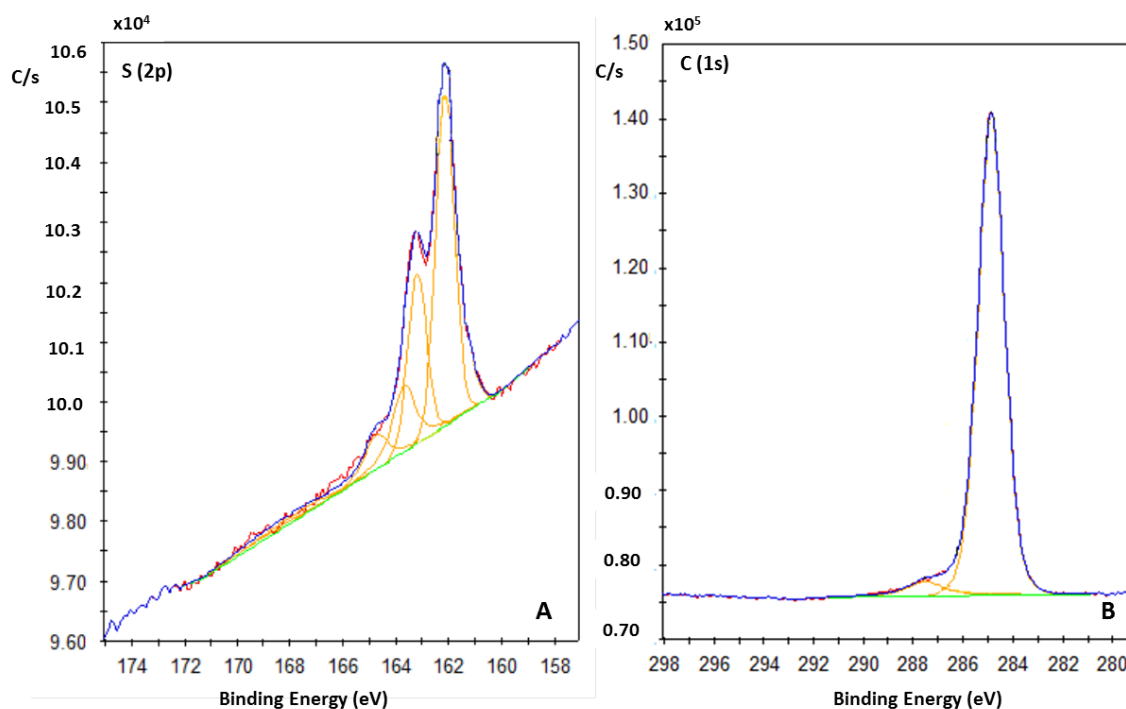
**Figure 4.4.** STM topography images of (+)-PMT on the gold/1-phenyloctane interface ( $I_{\text{set}} = 500$  pA,  $V_{\text{bias}} = 700$  mV). Scale bar top 40 nm, bottom 20 nm.

#### 4.4. Dodecanethiol SAMs on monocrystalline gold.

##### 4.4.1. XPS Analysis

The main binding energy peak observed for the DT monolayer on gold at 163.2 eV in the sulphur region (Figure 4.5.a) consists of a spin-orbit-split doublet, S ( $2p_{1/2}$ ) and S ( $2p_{3/2}$ ), representing one type of chemical state corresponding to the thiol group (-SH), commonly found in physisorbed alkylthiols and also present in the (+) PMT layer.<sup>14</sup> The fitted S (2p) curve has a spin-orbit-split of 1.2 eV. The other binding energy peak observed at 164.5 eV in the sulphur spectra (Figure 4.5.a) consists of a spin-orbit-split doublet, S ( $2p_{1/2}$ ) and S ( $2p_{3/2}$ ), arising from one type of chemical state corresponding to the thiolate group (-S-Au) which is the state usually assumed for this kind of self-assembled monolayer. These peaks are presented in all samples, in every gold surface functionalization by thiols these peaks coexist, even when the surface functionalization is highly success there is a low percentage of free thiol physisorbed.

<sup>14</sup> K. Hinds, D.W. Grainger, *Langmuir* **1996**, *12*, 5083-5086.



**Figure 4.5.** Selected regions of the core-level XPS data for SAMs of 1-dodecanethiol on gold (A) S (2p), (B) C (1s) XPS core-level spectra.

The relatively broad C (1s) main peak at about 285.5 eV is assigned to the aliphatic carbon component (Figure 4.5.b). The binding energy peak observed at 287.5 eV corresponds to the carbon bonded with the sulphur head group of the amphiphile (C-S).

#### 4.4.2. Contact Angle

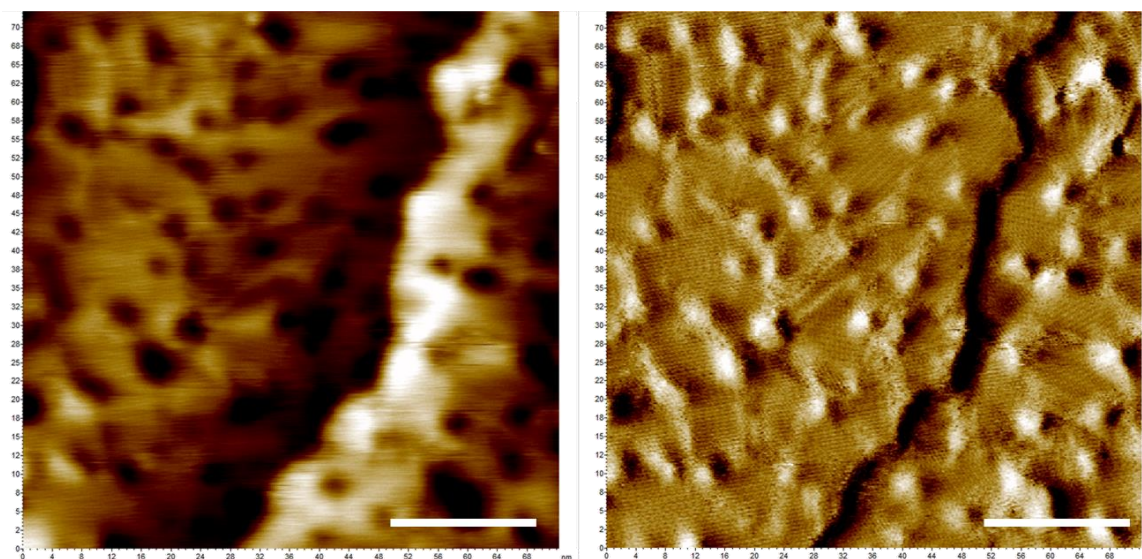
The water contact angle measured of the SAMs of dodecanethiol on monocrystalline gold is  $108^\circ$ . This high contact angle, of the order of values observed for the same SAM reported previously.<sup>15</sup> Thus, the surface is very hydrophobic after its functionalization because of the apolar nature of the dodecanethiol and the high degree of order in the layer which has been noted by others.<sup>16</sup>

<sup>15</sup> H.-S. Ahn., P. D. Cuong, S. Park, Y.-W. Kim, J.-C. Lim, *Wear* 2003, 255, 819-825.

<sup>16</sup> (a) G. E. Poirier, M. J. Tarlov, *Langmuir* 1994, 10, 2853-2856. (b) C. Munuera, E. Barrera, C. Ocal, *J. Phys. Chem. A* 2007, 111, 12721-12726

### 4.4.3. STM

The STM images of 1-dodecanethiol on gold (111) were recorded for direct comparison with the images of the new SAMs reported here, although many studies have reported the STM imaging of this and other related thiols in their layers on gold.<sup>17</sup> The monolayer appears as expected with vacancy islands evident in the topographic image and very well ordered regions – albeit of limited area – apparent in the current image (Figure 4.6). The similarity of these images to those published for this monolayer made in other laboratories around the world show confirm the validity of the images of the other monolayers reported here.



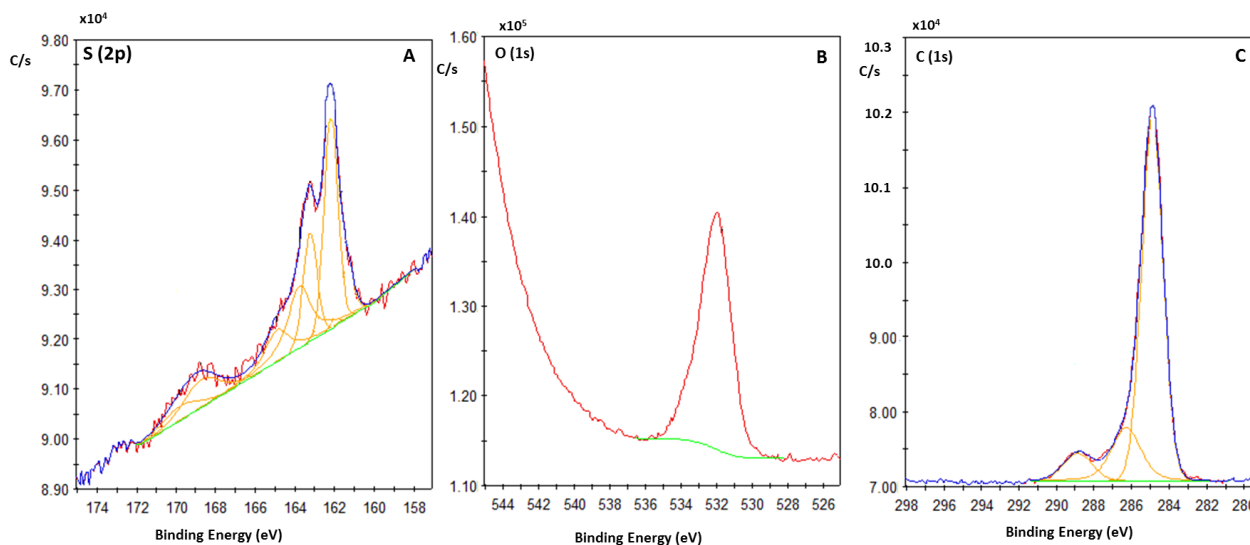
**Figure 4.6.** STM images (left topography, right current map) of a monolayer of 1-dodecanethiol on Au (111) ( $I_{\text{set}} = 0.60$  pA,  $V_{\text{bias}} = 0.85$  V) showing vacancy islands, ordered areas, and a gold step edge.

Scalebar 20 nm.

<sup>17</sup> (a) G. E. Poirier, *Chem. Rev.* **1997**, *97*, 1117-1127. (b) C. Vericat, M.E. Vela, G. Benitez, P. Carro, R.C. Salvarezza, *Chem. Soc. Rev.* **2010**, *39*, 1805-1834. (c) E. Pensa, E. Cortes, G. Corthey, P. Carro, C. Vericat, M.H. Fonticelli, G. Benitez, A.A. Rubert, R.C. Salvarezza, *Acc. Chem. Res.* **2012**, *45*, 1183-1192.

## 4.5. 11-Mercaptoundecanoic acid SAMs on Monocrystalline gold.

### 4.5.1. XPS analysis



**Figure 4.7.** Selected regions of the core-level XPS data for SAMs of **MUA** on gold (A) S (2p), (B) O (1s), (C) C (1s) XPS core-level spectra.

Representative S (2p) spectra of a monolayer of **MUA** on gold are shown in Figure 4.7 a. The main binding energy peak observed at 162.46 eV in the sulphur region (Figure 4.7.a) consists of a spin-orbit-split doublet, S (2p<sub>1/2</sub>) and S (2p<sub>3/2</sub>), representing one type of chemical state corresponding to the thiolate group (-S-Au), commonly found when chemisorbed monolayer formation has been accomplished.<sup>18</sup> The fitted S (2p) curve has a spin-orbit-split of 1.2 eV. The peak at lower binding energy observed at 163.24 eV in the sulphur spectra (Figure 4.7.a) consists of a spin-orbit-split doublet, S (2p<sub>1/2</sub>) and S (2p<sub>3/2</sub>), representing one type of chemical state corresponding to the thiol group (-S-H), commonly found in physisorbed alkylthiols. The other peak corresponds to S-S dimer (164.98 eV) specie.<sup>19</sup>

The binding energy peak observed (Figure 4.7.b) in the XPS spectra of O (1s) at 532.2 eV corresponds to a C-O bond of the carboxylic group. The relatively broad C (1s) main peak at about 284.9 eV is assigned to the aliphatic carbon atoms (CH<sub>2</sub>) while the curved-fitted peak at 286.3 and 288.9 eV (Figure 4.2.c) corresponds to the single bond C-S and the double bond C=O respectively.

<sup>18</sup> K. Hinds, D.W. Grainger, *Langmuir* **1996**, *12*, 5083-5086.

<sup>19</sup> J. Zhou, D. A. Beattie, R. Sedev, J. Ralston, *Langmuir* **2007**, *23*, 9170-9177.

#### 4.5.2. Contact angle

The water contact angle measured over the SAMs of MUA on monocrystalline gold is 61.8°, and is evidence that the functionalisation of the surface, as the bare gold has a contact angle of approximately 76°. The surface is very hydrophilic after its functionalization because MUA is a carboxylic acid and these polar headgroups are presumably directed away from the surface. The contact angle is not as low as the SAMs of PMT because the phosphoric acid group is more polar than the carboxylic group.

#### 4.6. Experimental section

**Self-assembled monolayer formation.** The monolayers were prepared by immersion of the gold substrate into the ethanolic solutions of the thiol solution at a concentration of 1 mM overnight under Argon at ambient temperature. The surfaces were removed, washed with five aliquots of 1 mL HPLC ethanol, and dried with a flow of nitrogen and then in vacuum. The monocrystalline gold on mica substrates were purchased from purchased from George Albert PVD.

**XPS measurements.** XPS experiments were performed in a PHI 5500 Multitechnique System (from Physical Electronics) with a monochromatic X-Ray source (Aluminium K $\alpha$  line of 1486.6 eV energy and 350 W), placed perpendicular to the analyser axis and calibrated using the 3d $_{5/2}$  line of Ag with a full width at half maximum (FWHM) of 0.8 eV. The area analysed was a circle of 0.8 mm diameter, and the selected resolution for the spectra was 187.5 eV of Pass Energy and 0.8 eV /step for the spectra and 23.5 eV of Pass Energy and 0.1 eV/ step for the spectra of the different elements. All measurements were made in ultra-high vacuum (UHV) chamber pressure between  $5 \times 10^{-9}$  and  $2 \times 10^{-8}$  torr. A low energy electron flood gun (0-3 eV) was necessary in order to discharge the sample. The binding energy scale was aligned through the Au (4f) peak at 84 eV. The Multipak data analysis software was used to resolve the signal of each element on the surface.

**Contact angle measurements** were measured using a DSA100 equipment (KRÜSS, GmbH) in a clean room. **STM measurements** were performed using a PicoSPM (Molecular Imaging) with mechanically cut Pt/Ir tips in air; no manipulation of the images has been performed.

# Chapter 5

## Multilayer formation through complementary Interactions on Self- Assembled Monolayers

---

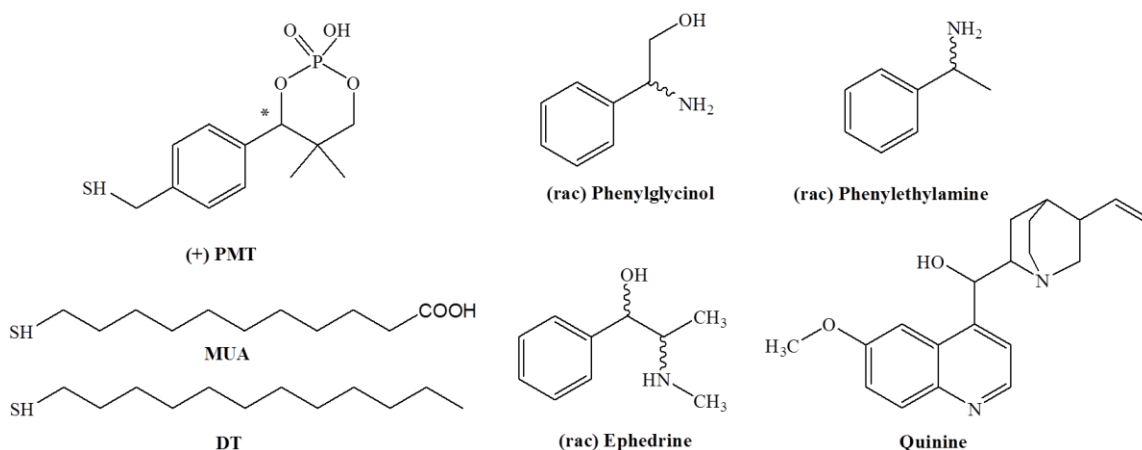
Multilayers formation on SAMs represents the intermediate step to nucleation process on SAMs. The multilayer formation study is described in this chapter deeply in order to understand its behavior.



## 5.1. Introduction

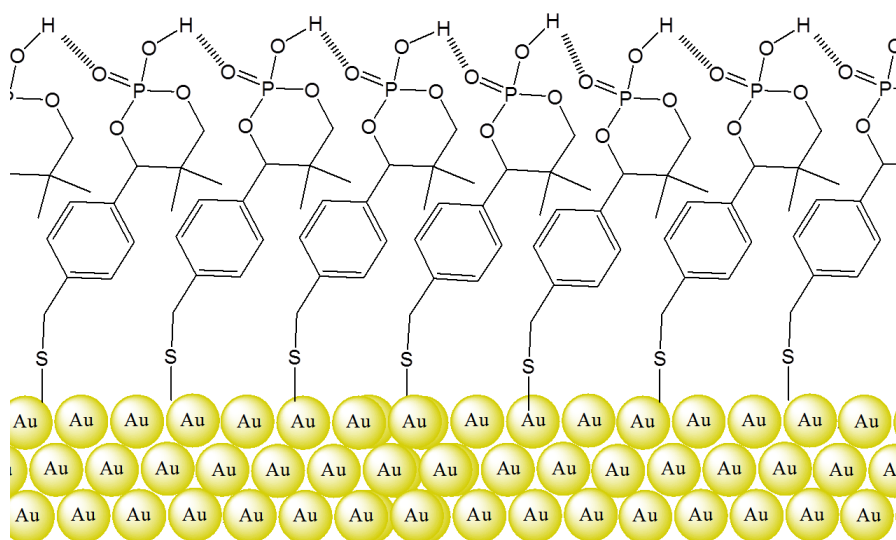
The main objective of the research presented in this Thesis is the study of the nucleation and the crystal growth on chiral SAMs. These chiral SAMs should act as templates in order to favour the crystal growth once a nucleus is formed and the nucleation point attached to the SAMs. The mechanism by which a nucleus may form on a surface could involve either the generation of a critical cluster in solution and its subsequent wetting of a template layer, or the concentration of component molecules on a surface and their condensation to generate the nucleus there. As multilayer growth could conceivably be a previous step to the nucleus formation on the SAM, the study presented in this chapter shows the recognition observed between complementary molecules from solution and the molecules which form part of the SAMs.

The molecules selected for this study are shown in Figure 5.1. For SAM formation the thiols (+) Phencyphos 4-methylthiol ((+) PMT), 11-mercaptopundecanoic acid (MUA) and dodecanethiol (DT) were selected. The acidic moieties in (+) PMT and MUA provide sites for complex formation with complementary groups, especially basic ones, and for this reason chiral amine species were chosen to interact with the SAMs to form eventual multilayers. The amines (*rac*) Phenylglycinol, (*rac*) Phenylethylamine and Quinine which are known to form diastereomeric salts in crystalline solids were considered good candidates.



**Figure 5.1.** Thiols and amines selected to grow multilayers.

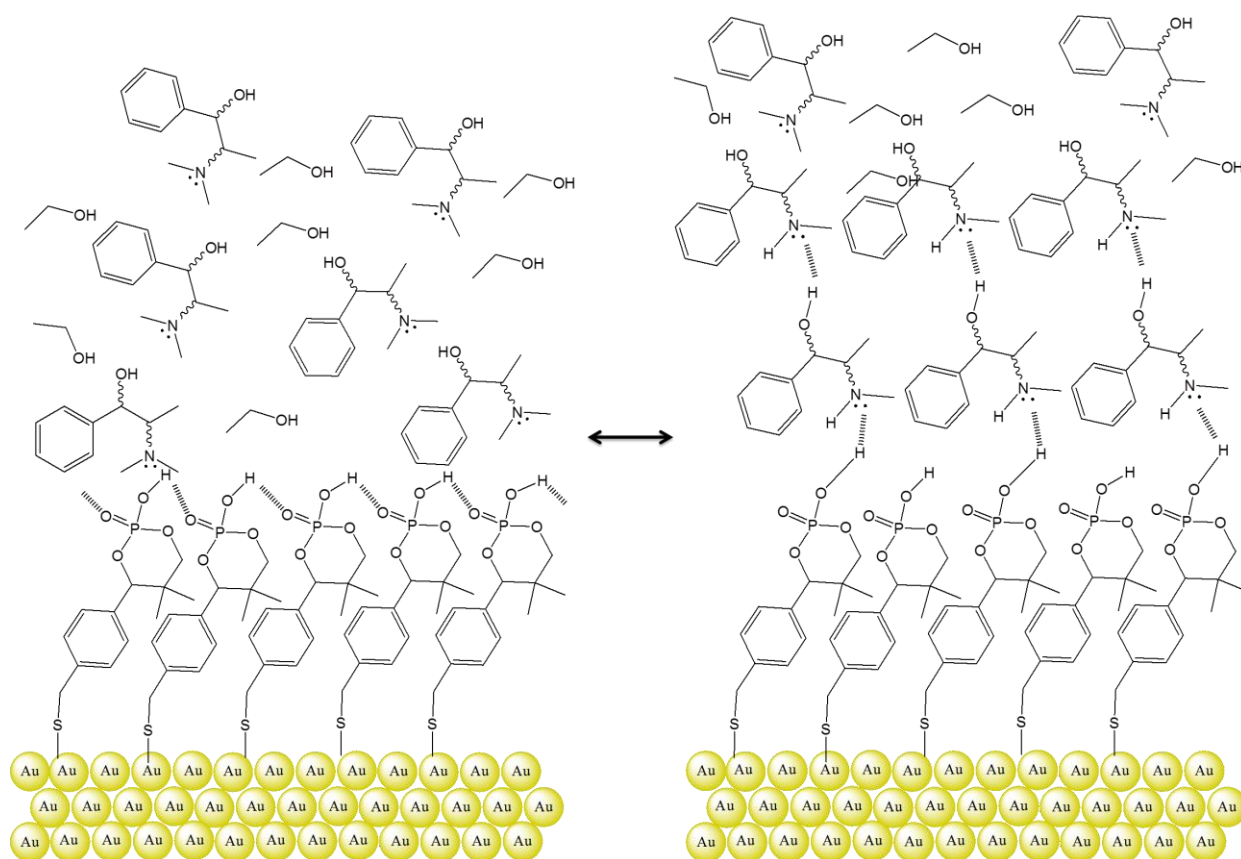
Chiral multilayer formation is a process that is entropically favoured if there is a selective chiral interaction between the layers involved. The monolayer of (+) PTM on gold surfaces is believed to have local structure as depicted in Figure 5.2, where hydrogen bonds between adjacent phosphoric groups are suggested. This hydrogen bond would have to be broken in order to form a hydrogen bond with the amino group in presence of a solution of the amine in contact with the SAM (Figure 5.3), a crucial moment in which the amine layer starts to grow. Hydrogen bond formation would be more or less favoured depending on the chirality of the monolayer and the amine since the diastereomeric relationship between configurational isomers could allow a distinction between enantiomers. These experiments require very low concentrations, otherwise nucleus formation would be unavoidable, and so in these experiments the concentration is of the mM order.



**Figure 5.2.** Hydrogen bonding in the (+) PMT monolayer on gold surfaces.

The  $pK_a$  or  $pK_b$  of the Phencyphos and chiral amines used in these experiments are the following:<sup>1</sup> for the chiral acids *Phencyphos hydrate* is 1.80; for the 1.3 *PMT* and for the *MUA* is 4.8. In the case of the amines is the  $pK_b$ , and they are for each one: *Ephedrine* is 4.4 and *Phenylglycinol* is approx. 5, for *Phenylethylamine* is 4.2, and for *Quinine* is 5.48.

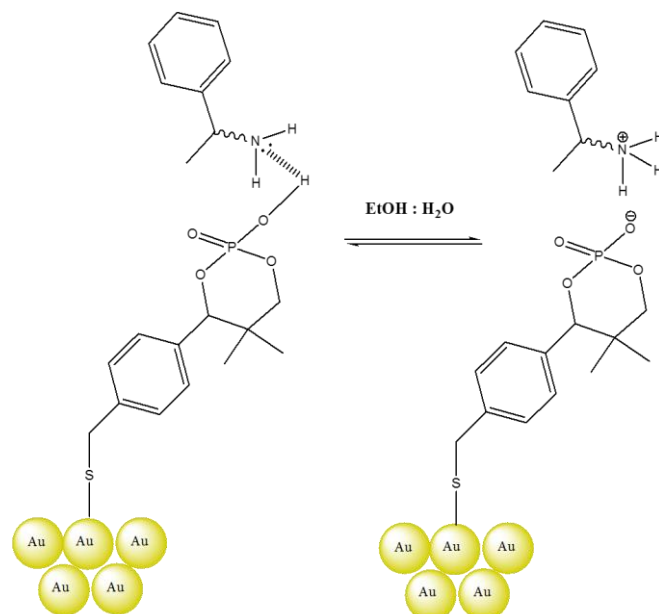
<sup>1</sup> R. William, *pKa Data Compiled*, University of Washington at Seattle.



**Figure 5.3.** A representation of the hypothetical growth of (rac) Phenylglycinol multilayers from solution.

Characterisation of the multilayer formation was done mainly using available surface techniques, such as X-Ray photoelectron spectroscopy (XPS), which is very sensitive to any change in the chemical state – such as valence and/or charge - of the atoms analysed.<sup>2</sup> The formation of a chemical bond would be the best evidence of multilayer by SAM recognition. Although in this system, intermolecular interactions such as hydrogen bonding would correspond to recognition between multilayers and the SAMs. Since hydrogen bonds are formed between functional groups of different molecules which are close enough to allow the interaction of the oxygen atom with the hydrogen atom of the neighbouring molecule, the XPS spectra would show the hydrogen bond at the interface. There is a possible acid-base equilibrium to take into account in the analysis of the XPS spectra. Hydrogen bonds between layers of the amine and phosphoric acid groups could be sufficiently strong that they result in the formation of a diastereomeric salt at the interface. This charged specie will appear at a different binding energy to the complex in the XPS spectrum.

<sup>2</sup> C. S. Fadley, *Nuclear Instrument and Method in Physics Research A*, **2009**, 601, 8-31.



**Figure 5.4.** Schematic representation of an acid-base equilibrium of (*rac*) Phenylglycinol layer on a SAM of (+)-PMT on a gold surface when in solution.

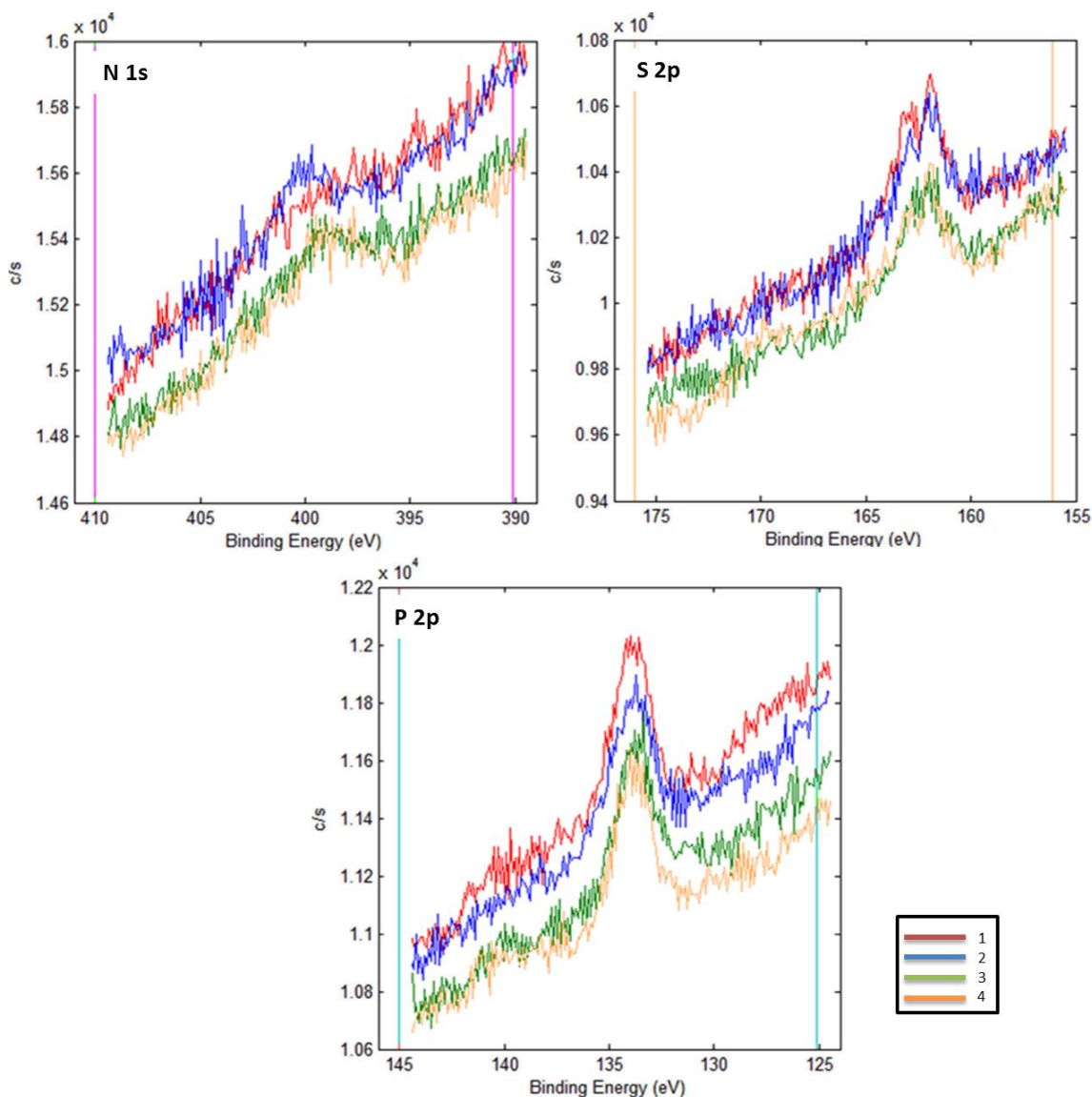
Given the existence of multiple equilibria in the process of formation of adsorbed species on a SAM, the experimental conditions used to prepare the layers were varied, and the trials were done under two different temperatures, room temperature and 40°C.

## 5.2. Room temperature adsorption

### 5.2.1. Neutral multilayer growth on a SAM of (+)-PMT at room temperature.

The chiral (+) PMT monolayer was used in this experiment in order to provide both high diastereoselectivity in binding with the selected chiral amine in solution. The protocol used in this experiment was to prepare the monolayer as before, that is to immerse monocrystalline gold surfaces (111) on mica into an ethanolic solution of (+)-PMT (1 mM) overnight. The resulting SAMs were washed with ethanol of HPLC quality (20 ml) and dried with a flow of nitrogen gas. Each surface was immersed into separate ethanolic solutions of the amines (1mM) overnight at room temperature under an argon atmosphere (to avoid potential oxidation of the amine. Subsequently, each surface was washed as in the step before, and dried with a flow of nitrogen gas and then stored in a vacuum packed box flushed previously with argon. In this experiment, the amine solutions used were: *Quinine*, (*rac*) *Phenylglycinol* and (*rac*) *Phenylethylamine*.

The XPS spectra obtained are shown in Figures 5.5 and 5.6, as a comparison between all samples measured and secondly as independent spectra for each sample measured. These spectra show the regions corresponding to nitrogen, sulphur and phosphorous for the samples analysed since these elements would be those most likely to undergo significant variation caused by binding of the amine to the acid SAM.



**Figure 5.5.** XPS spectra comparison for the samples: (1) (+)-PMT monolayer; (2) (+)-PMT monolayer + (rac) Phenylglycinol; (3) (+)-PMT monolayer + (rac) Phenylethylamine; (4) (+)-PMT monolayer + Quinine.

The most important region in the spectra of the samples resulting from in these experiments is the nitrogen area, where any change in the binding energy would provide information about the presence of new nitrogen-containing species at the surface. The spectrum corresponding to the (+)-PMT monolayer (coloured red in Figure 5.5) shows that (as should be the case) the SAM has not got any absorbed nitrogen, because there is not any peak in this region. Thus, any signal in this area would indicate the presence of amine on the monolayer. The rest of the spectra corresponding to treatment of the SAM with the different amines gave small peaks in the nitrogen region corresponding to two species:  $\text{NH}_2$  or  $\text{NH}$  (binding energy, B.E., 399.5 eV) and  $\text{H}\cdots\text{NH}_2$  (B.E. 401.50 eV)<sup>3</sup>. Although the intensity of the peak is very small, which means there is a low concentration of these nitrogen-containing species on the (+) PMT monolayer, the spectra confirm qualitatively the binding of these amines by the SAMs.

In all cases, the functionalization of the gold surface is demonstrated by the peaks in the sulphur region of the spectra which binding energy of 162.00-163.20 eV that correspond to the thiolate (*S-Au*)<sup>4</sup>. Therefore, the thiol is bound strongly to the gold surface and is not removed upon treatment with the amine. There is a low proportion of the free thiol specie (*-SH*) with the binding energy of approx. 164.00-165.20 eV, which is more evident in the case of the monolayer before amine treatment (therefore the subsequent immersion in the ethanolic amine solution removes this excess). These peaks were present in all the samples that were prepared, on every gold surface functionalized by thiols these peaks coexist, even when the surface functionalization is highly success there is apparently a low percentage of free thiol physisorbed.

The phosphorous region of the XPS spectra present a peak corresponding to the binding energy of phosphoric acid group ( $-\text{POOH}$ ) with a B.E. of 133.60 – 134.40 eV<sup>5</sup>. The binding energy for a cyclic phosphoric acid group was not found in the literature, thus, the binding energy as reference is the one corresponding to the XPS analysis of the monolayer on monocrystalline gold explained in the Chapter 4 of this Thesis. There is no other peak in this region of the spectra, thus the phosphoric group is probably always protonated. If a strong hydrogen bond between the amino groups of any overlayer and the phosphoric acid were formed, there should be a formal hydrogen bond which should

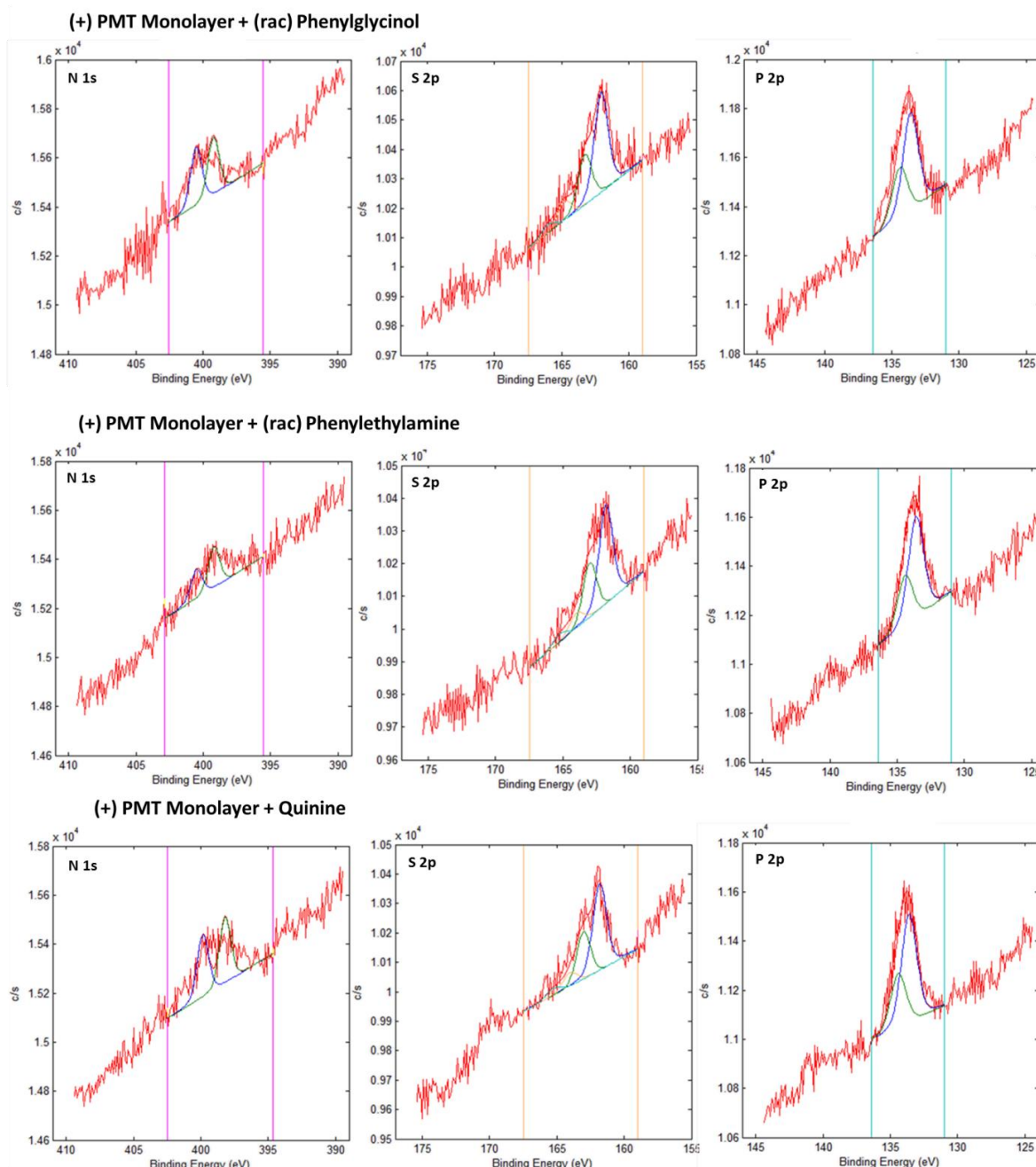
---

<sup>3</sup> P. M. Dietrich, N. Graf, T. Gross, A. Lippitz, S. Krakert, B. Schüpbach, A. Terfortb, W. E. S. Ungera, *Surf. Interface Anal*, **2010**, *42*, 1184–1187.

<sup>4</sup> D. G. Caster, *Langmuir*, **1996**, *12*, 5083-5086.

<sup>5</sup> R. M. Petoral, Jr. F. Björefors, K. Uvdal, *J. Phys. Chem. B*, **2006**, *110*, 23410-23416.

shift the position of the phosphorous peak in the XPS, and therefore it is surmised that any hydrogen bond present is weak. The spectra in Figure 5.6 show peak fitting for each sample and each element. The data are compared in Table 5.1. The peak fitting, of all spectra analysed in this Thesis, was made using the software MultiPak v.9.2.0.5 2010, (Ulvac-phi, Inc.).



**Figure 5.6.** XPS spectra of (+)-PMT Monolayer + (rac)-Phenylglycinol, (+)-PMT Monolayer + (rac)-Phenylethylamine and (+)-PMT Monolayer + Quinine showing the peak fitting using Multipak 9.2 software.

**Table 5.1.** XPS peak fitting of (+) PMT Monolayer + (rac) Phenylglycinol, (+) PMT Monolayer + (rac) Phenylethylamine and (+) PMT Monolayer + Quinine.

<b>(+) PMT Monolayer + (rac) Phenylglycinol</b>				
<b>B. E.(eV)</b>	<b>ΔE (eV)</b>	<b>Area</b>	<b>FWHM</b>	<b>Chemical specie</b>
162.07-163.27	1.2	2:1	1.20	Thiolate (S-Au)
164.80-166.00	1.2	2:1	1.20	Free thiol (-SH)
133.60-134.40	0.8	2:1	1.35	Phosphoric acid (-POOH)
399.13	-	-	1.00	NH <sub>2</sub>
400.5	-	-	1.00	H···NH <sub>2</sub>
<b>(+) PMT Monolayer + (rac) Phenylethylamine</b>				
161.80-163.00	1.2	2:1	1.20	Thiolate (S-Au)
164.00-165.2	1.2	2:1	1.20	Free thiol (-SH)
133.6-134.4	0.8	2:1	1.35	Phosphoric acid (-POOH)
399.2	-	-	1.00	Amine NH <sub>2</sub>
400.5	-	-	1.00	H-bond to amine H···NH <sub>2</sub>
<b>(+) PMT Monolayer + Quinine</b>				
162.07-163.27	1.2	2:1	1.20	Thiolate (S-Au)
164.59-165.79	1.2	2:1	1.20	Free thiol (-SH)
133.60-134.40	0.8	2:1	1.35	Phosphoric acid (-POOH)
399.0	-	-	1.00	Amine NH
400.1	-	-	1.00	H-bond to amine H···NH

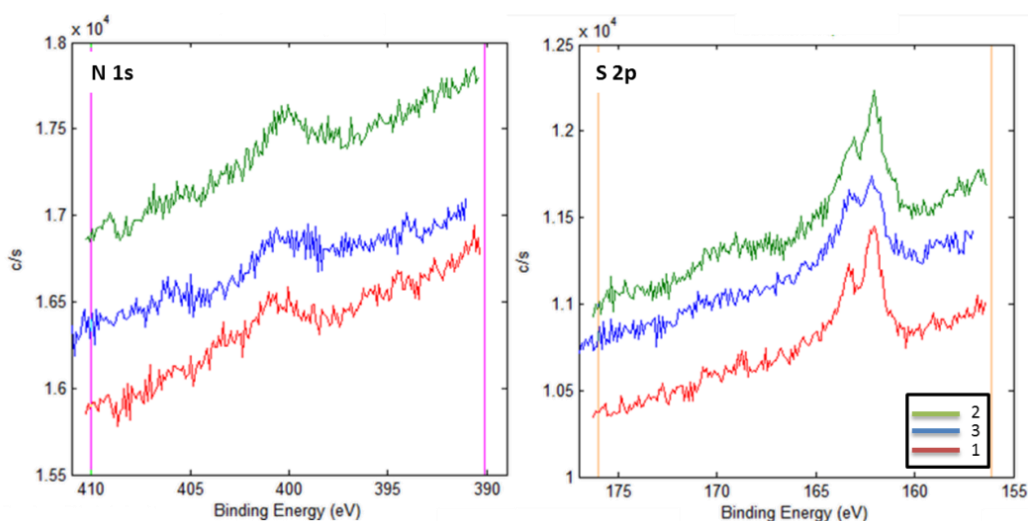
### 5.2.2. Neutral multilayers growth on MUA monolayer at room temperature

In this experiment the monolayer was formed by 11-mercaptoundecanoic acid (MUA), an achiral and polar thiol. This molecule is known to form a well-ordered monolayer on gold surfaces,<sup>6</sup> and would allow a test of whether the chirality or the polarity of the interface between monolayer and solvent would have any influence on the amine binding. The protocol followed was the same as the experiment explained in above: Monocrystalline gold surfaces (111) on mica were immersed into a MUA ethanolic solution 1 mM overnight. They were washed with ethanol of HPLC quality (20 ml) and dried with nitrogen gas. Each surface was immersed into an ethanolic solution of the amine (1mM) in question, and this system was left overnight at room temperature under an atmosphere of argon. Each surface was washed and dried (as in the previous step) before storage in a box which had been flushed with argon and vacuum sealed. Amine solutions used were (*rac*) Ephedrine and (*rac*) Phenylglycinol.

<sup>6</sup> C. Dubois, F. Stellacci, *J. Phys. Chem. C*, **2008**, *112*, 7431-7435.



The XPS spectra obtained from these experiments are shown in Figures 5.7 and 5.8, the former showing a comparison between all the samples measured and the latter as independent spectra for each sample measured. These spectra show the regions corresponding to nitrogen and sulphur for the samples analysed since these elements would be affected by any change in the nature of the layer on the gold during the experiment.



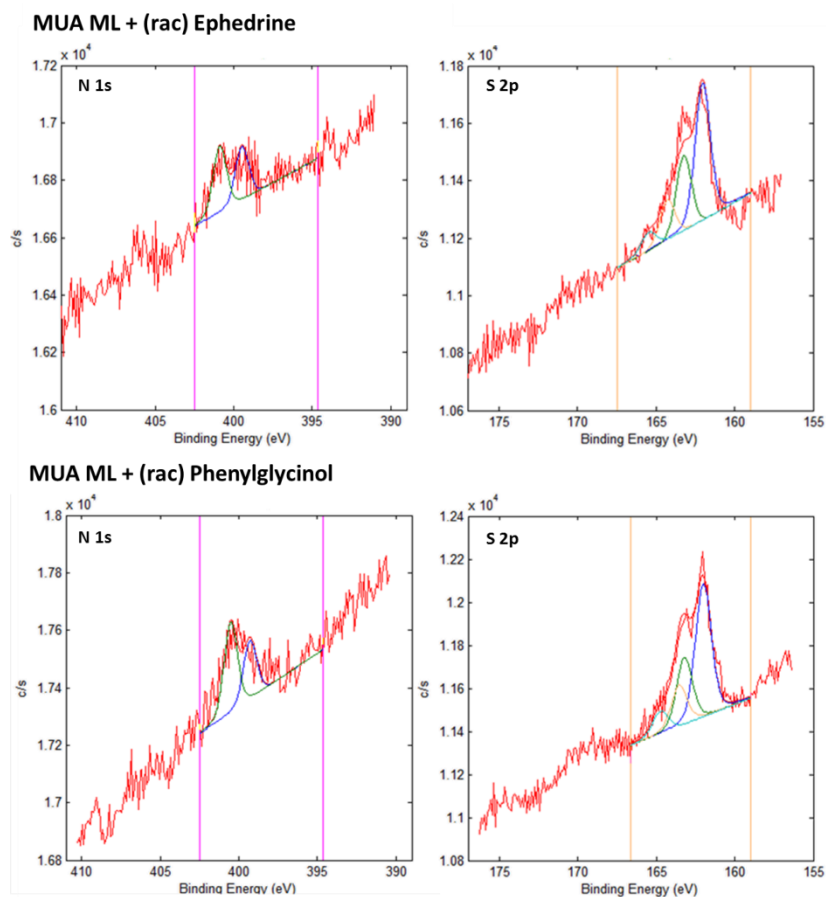
**Figure 5.7.** Comparison of the XPS spectra for the multilayers: (1) MUA Monolayer; (2) MUA + (rac)-Ephedrine; (3) MUA Monolayer + (rac)-Phenylglycinol. The peak fitting was done using Multipak 9.2 software.

As in the experiments on the SAMs formed by PMT presented above, the most indicative region of the XPS spectrum for the study of binding is the nitrogen area. The red curve corresponding to the MUA monolayer (Figure 5.7) has a small peak in this area which could be from residue from the cleaning agent (Hellmanex) used for the glassware in the SAM preparation. The other samples also present small peaks in the nitrogen region corresponding to two species:  $\text{NH}_2$  (B.E. 399.5 eV) and  $\text{H}\cdots\text{NH}_2$  (B.E. 400.80 eV)<sup>7</sup>. However, nitrogen absorbed at the surface<sup>8</sup> has the same binding energy as  $\text{NH}_2$  as witnessed in the MUA monolayer sample. The peaks are very similar in all the samples, and it is likely that the origin of this peak – possibly of absorbed of nitrogen rather than the amine attached through a hydrogen bonding interaction.

<sup>7</sup> P. M. Dietrich, N. Graf, T. Gross, A. Lippitz, S. Krakert, B. Schüpbach, A. Terfortb, W. E. S. Ungera, *Surf. Interface Anal.*, **2010**, 42, 1184–1187.

<sup>8</sup> A. Atrens, A. S. Lim. *Applied Physics A*, **1990**, 51, 411-418.

The successful functionalisation of gold surface is demonstrated by the peaks of the sulphur regions where the binding energy is 162.07-163.27 eV and corresponds to the thiolate ( $S-Au$ )<sup>9</sup>. There is also a low proportion of the free thiol specie ( $-SH$ ) with the binding energy of 164.00-165.20 eV. The following spectra (Figure 5.8 and Table 5.2)) show peak fitting for each sample and each element.



**Figure 5.8.** XPS spectra fitting of the multilayers: (1) MUA Monolayer; (2) MUA + (rac) Ephedrine; (3) MUA Monolayer + (rac) Phenylglycinol. The peak fitting was done using Multipak 9.2 software.

<sup>9</sup> D. G. Caster, *Langmuir*, **1996**, *12*, 5083-5086.

**Table 5.2.** XPS peak fitting of MUA + (*rac*) Ephedrine; MUA Monolayer + (*rac*) Phenylglycinol.

<b>MUA Monolayer + (<i>rac</i>) Phenylglycinol</b>				
B. E.(eV)	$\Delta E$ (eV)	Area	FWHM	Chemical specie
162.00-163.20	1.2	2:1	1.15	Thiolate (S-Au)
163.55-164.75	1.2	2:1	1.15	Free thiol (-SH)
399.29	-	-	1.00	NH <sub>2</sub>
400.51	-	-	1.00	N <sub>2</sub>
<b>MUA Monolayer + (<i>rac</i>) Ephedrine</b>				
B. E.(eV)	$\Delta E$ (eV)	Area	FWHM	Chemical specie
162.03-163.23	1.2	2:1	1.15	Thiolate (S-Au)
164.28-165.48	1.2	2:1	1.15	Free thiol (-SH)
399.48	-	-	1.00	NH <sub>2</sub>
400.88	-	-	1.00	N <sub>2</sub>

### 5.2.3. Charged multilayers for growth on SAM of (+) PMT at room temperature.

As the results presented previously in this Chapter were not conclusive regarding the formation between multilayers through hydrogen bond, we designed this experiment in order to check whether the chemical state of the SAM could affect the recognition in chiral patterns and the amine solutions or not. There is an extra step in this experiment, the ionic species formation to favour the recognition.

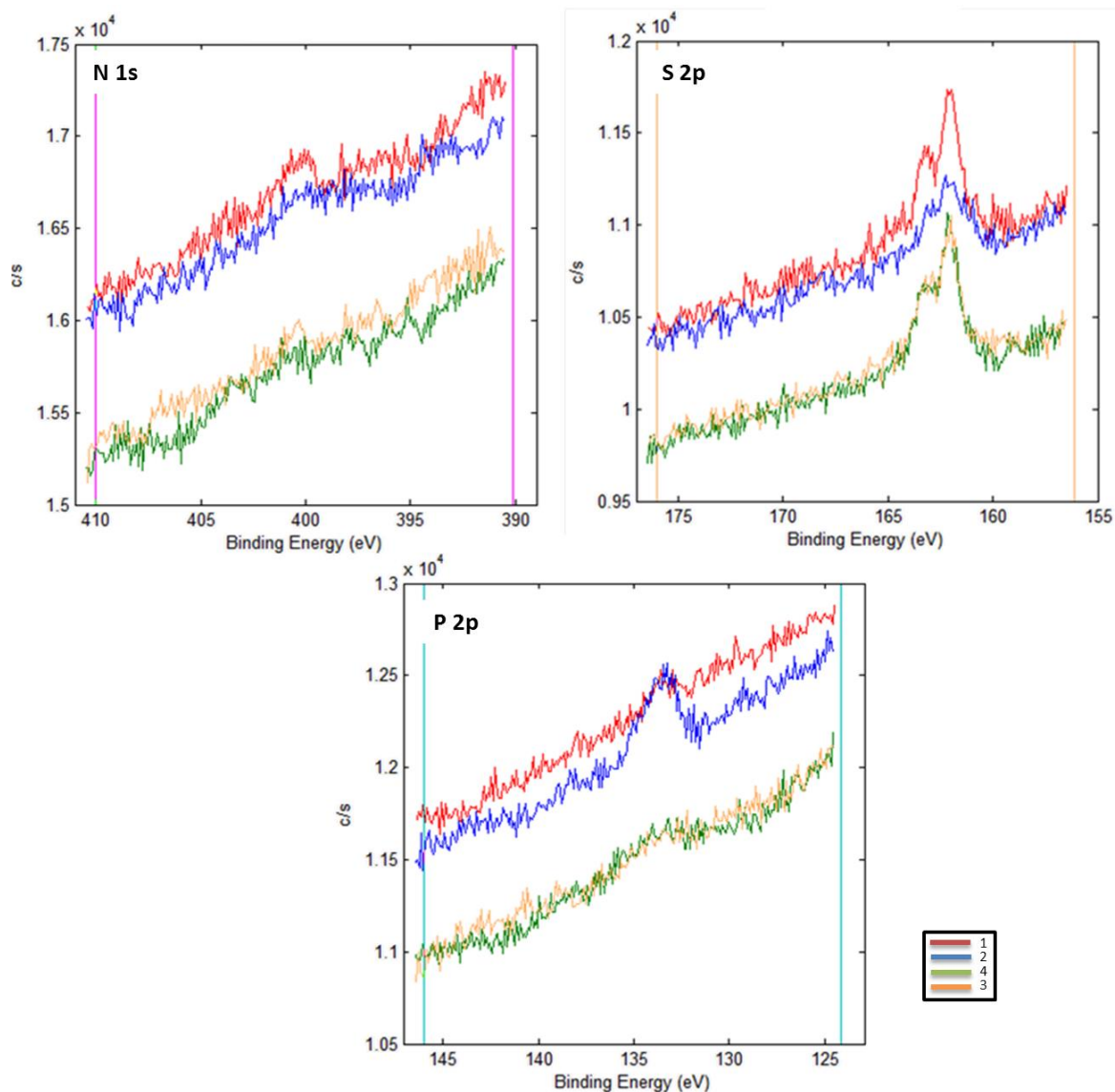
The protocol followed was to use polycrystalline gold surfaces on glass which were functionalised by microcontact printing<sup>10</sup> using stamps of circles or lines of 50 microns of (+)-PMT with a filling layer of dodecanethiol in between the features. After their functionalization, each surface was immersed into a basic solution of NaOH (0.01 M) for 30 seconds<sup>11</sup> in order to form the sodium salt of the phosphonate. The surfaces were washed with water and dried with a flow of nitrogen gas before being immersed into (*rac*)-Ephedrine or (*rac*)-Phenylglycinol as their hydrochloride salts solution (H<sub>2</sub>O), each surface was cleaned with water and dried with nitrogen before being stored in a box that had been flushed with argon and vacuum sealed.

<sup>10</sup> The microcontact printing protocol explained in detail in Chapter 7

<sup>11</sup> Kun-Lin Yang et al. *Adv. Mater.* **2003**, *15*, 1819-1822

The XPS spectra obtained are shown in Figures 5.9 and 5.10 below, as again comparing all samples measured and then as independent spectra for each sample measured. These spectra show the regions corresponding to nitrogen, sulphur and phosphorous for the samples analysed since these elements would be affected by any chemical change experienced by the SAM during the adsorption experiment.

There are two types of samples, both of them are micropatterned surfaces, although they are slightly different. On the one hand, lines were stamped while the others are circles of the same size (50 microns). The curves corresponding to the line micropattern samples are green and yellow in Figure 5.9. The curves corresponding to the circle micropattern are coloured red and blue. Comparing all the samples in the same spectra in the nitrogen region (Figure 5.9), there seem to be peaks in this area. Nevertheless, usually there is a peak which fits under a curve mathematically, even though the intensity of the peak is negligible. In this case no fit could be made. There is apparently no hydrogen bond between the SAM and the solution-borne amine, thus, recognition seems not to take place.



**Figure 5.9.** XPS spectra for the multilayers: Micropatterned gold surfaces of: (1) (+)-PMT 50  $\mu\text{m}$  Lines; (2) Deprotonated (+)-PMT 50  $\mu\text{m}$  Lines; (3) Deprotonated (+)-PMT 50  $\mu\text{m}$  circles + (*rac*)-Ephedrine hydrochloride; (4) Deprotonated (+)-PMT 50  $\mu\text{m}$  circles + (*rac*) Phenylglycinol hydrochloride. The peak fitting was done using Multipak 9.2 software.

The successful functionalisation of the gold surface, following a microcontact printing protocol which implies two thiols to form two monolayers from different preparation steps, is demonstrated by the peaks in the sulphur regions which correspond to a binding energy of 162.00-163.20 eV and can be assigned to the thiolate sulphur atom (S-Au)<sup>12</sup>. There is a low proportion of the free thiol specie (-SH) with the binding

<sup>12</sup> D. G. Caster, *Langmuir*, **1996**, *12*, 5083-5086.

energy of 164.85-166.05 eV. The proportion of free thiol in these micropatterned surfaces is very low because of the dodecanethiol SAM formation which gives a well-ordered monolayer around the motif printed with the (+)-PMT thiol, the combination covering the whole gold surface.

The phosphorous region of the XPS spectra shows a peak corresponding to the binding energy of the phosphoric acid group (B.E.  $-\text{POOH}$  133.50 – 134.30 eV<sup>13</sup>). There are no other peaks in this region, thus the phosphoric group is apparently still protonated, although it should be stated that no data could be found where a clear distinction between organic phosphoric acid and phosphate anion has been made using XPS.

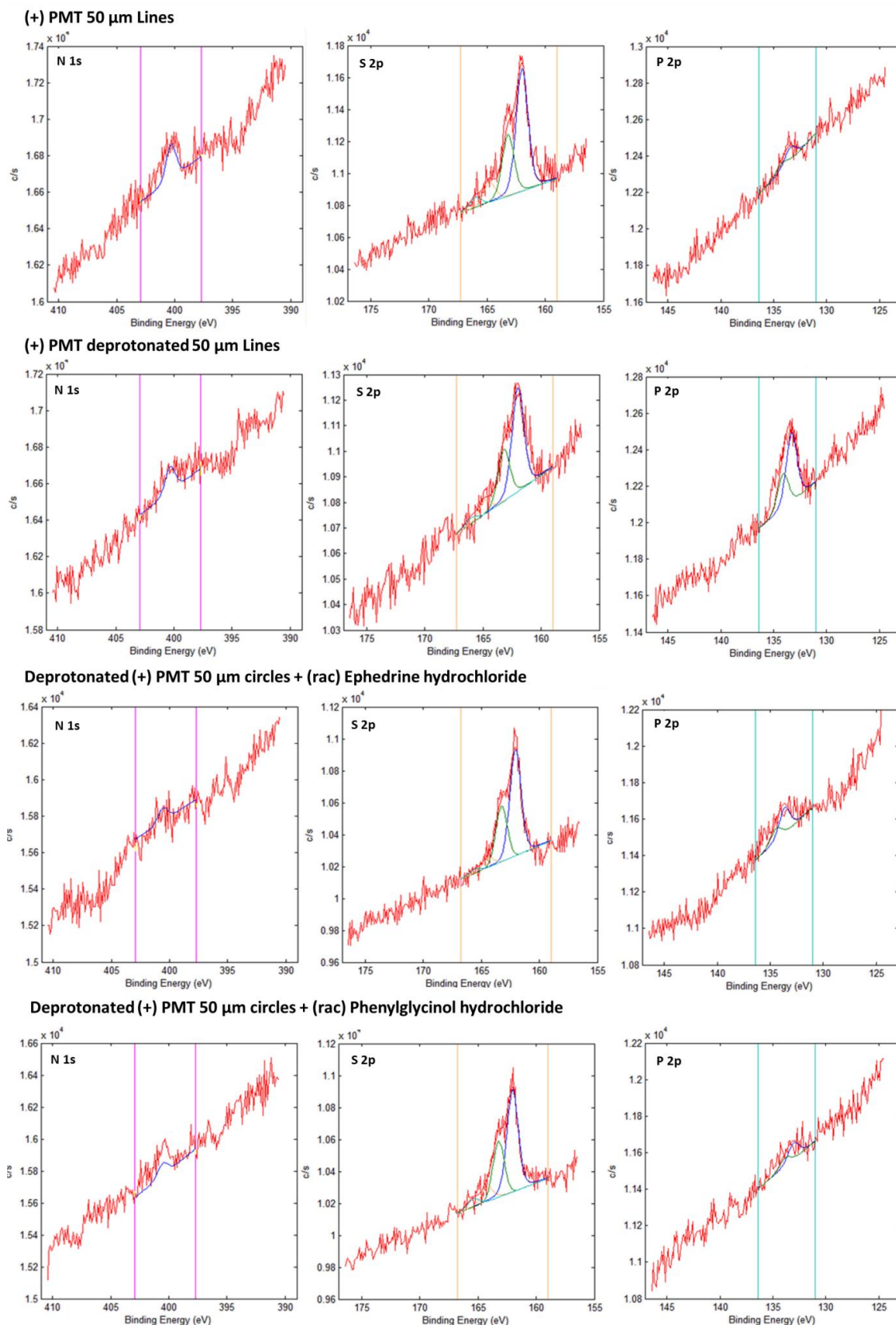
Although, there is different intensity of the same peak in each sample, in three of them the intensity is very low, which means very low concentration of phosphorous on the micropatterned surface. The signal expected for a monolayer sample in a laboratory of XPS is not very high, if the sample is a micropatterned surface and the element of interest is in the micropattern, the signal is even lower. The following spectra show peak fitting for each sample and each element.

---

<sup>13</sup> R. M. Petoral, Jr. F. Björefors, K. Uvdal, *J. Phys. Chem. B*, **2006**, *110*, 23410-23416.

**Table 5.3.** XPS spectra and peak fitting of each sample of charged multilayers experiments.

<b>50<math>\mu</math>m lines of (+) PMT</b>				
<b>B. E.(eV)</b>	<b><math>\Delta E</math> (eV)</b>	<b>Area</b>	<b>FWHM</b>	<b>Chemical specie</b>
162.00-163.20	1.2	2:1	1.14	Thiolate (S-Au)
164.78-165.96	1.2	2:1	1.14	Free thiol (-SH)
133.45-134.25	0.8	2:1	1.20	Phosphoric acid (-POOH)
<b>50<math>\mu</math>m lines of (+) PMT deprotonated</b>				
162.0-163.2	1.2	2:1	1.14	Thiolate (S-Au)
164.85-166.05	1.2	2:1	1.14	Free thiol (-SH)
133.30-134.10	0.8	2:1	1.20	Phosphoric acid (-POOH)
<b>Deprotonated (+) PMT 50 <math>\mu</math>m circles + (rac) Phenylglycinol hydrochloride</b>				
162.06-163.26	1.2	2:1	1.14	Thiolate (S-Au)
164.39-165.59	1.2	2:1	1.14	Free thiol (-SH)
133.65-134.45	0.8	2:1	1.20	Phosphoric acid (-POOH)
400.59	-	-	1.00	NH <sub>3</sub> <sup>+</sup>
<b>Deprotonated (+) PMT 50 <math>\mu</math>m circles + (rac) Ephedrine hydrochloride</b>				
162.03-163.23	1.2	2:1	1.14	Thiolate (S-Au)
164.20-165.40	1.2	2:1	1.14	Free thiol (-SH)
133.05-133.86	0.8	2:1	1.20	Phosphoric acid (-POOH)
400.53	-	-	1.00	NH <sub>3</sub> <sup>+</sup>



**Figure 5.10.** XPS spectra with peak fitting of each sample of the charged multilayers experiments. The peak fitting was done using Multipak 9.2 software.



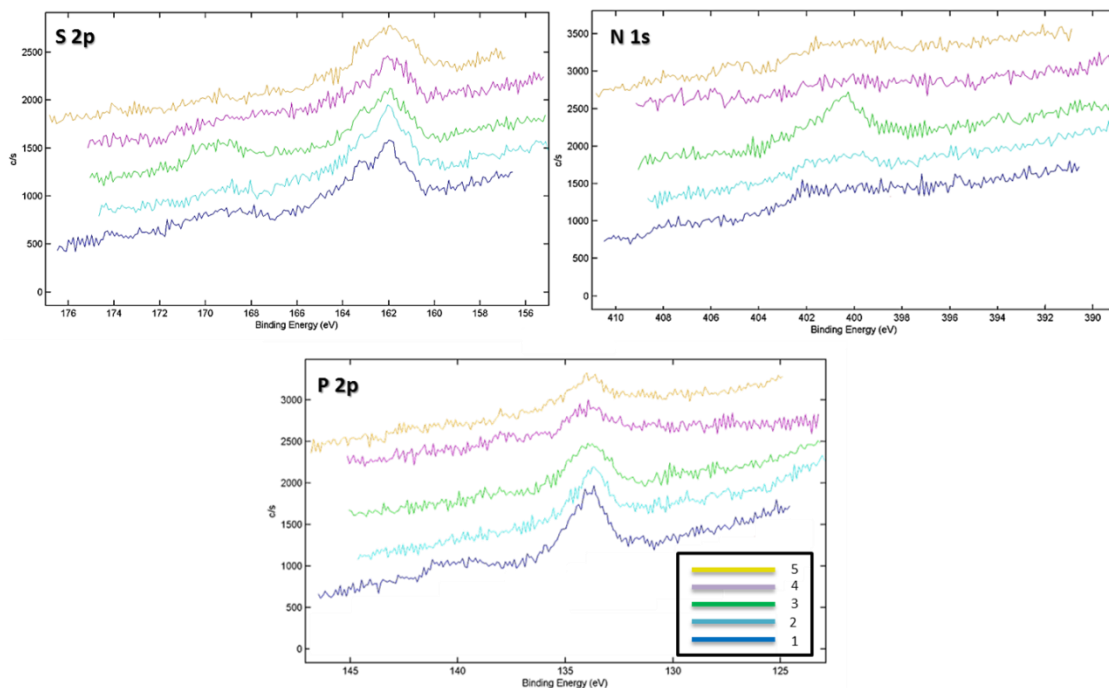
### **5.3. Formation of multilayers at higher temperature**

#### **5.3.1. Neutral multilayer. Monocrystalline gold on mica. (Higher temperature, 40°C)**

Of the methods described thus far in this Chapter, the neutral monolayer at room temperature seems to favour binding of amines the best, even though the nitrogen signal area in the XPS curves are very weak hinting at a process which is rather inefficient. An improvement in the methodology is necessary for any enantioselectivity to be detected or to be able to verify whether nucleation takes place via this initial adsorption. In principle, higher temperatures could favour mass transport and the diffusion over the monolayer, allowing the more efficient recognition between the monolayer and solution, increasing the chance to have an interaction leading to the formation of a layer on the SAM.

In this experiment the protocol followed was: Gold surfaces were immersed into a (+)-PMT ethanolic solution (10 mM) overnight. The plates were washed with ethanol of HPLC quality (20 ml) and dried with a flow of nitrogen gas. The surfaces were immersed into ethanolic solutions of the amine (1mM) overnight in an oil bath at a controlled temperature (40°C). Each surface was cleaned with ethanol and dried with a flow of nitrogen gas before being stored up in an argon flushed box which was vacuum sealed. The amine solutions used were (rac) Ephedrine and (rac) Phenylglycinol.

The XPS spectra obtained from the films are shown below (Figures 5.11 and 5.12), firstly as comparison between all samples measured and secondly as independent spectra for each sample measured. These spectra show the regions corresponding to nitrogen, sulphur and phosphorous.



**Figure 5.11.** XPS spectra for the layers: (1) (+)-PMT Monolayer; (2) (+)-PMT + (*rac*)-Ephedrine (sample A); (3) (+)-PMT + (*rac*)-Ephedrine (sample B); (4) (+)-PMT + (*rac*)-Phenylglycinol (sample A); (5) (+)-PMT + (*rac*)-Phenylglycinol (sample B).

There are two samples with the same characteristics, (A and B), both of which were prepared following the same protocol. The curve corresponding to the (+)-PMT monolayer shown in blue (Figure 5.11) does not present any peak in the nitrogen region, as expected (though not always observed). From the comparison spectra (figure 5.11), focussing on the nitrogen region, all samples present two peaks with significantly intensity. The samples with most intense peaks in this region correspond to the adsorption of (*rac*)-Ephedrine (sample B) and (*rac*)-Phenylglycinol (sample A) on the (+) PMT monolayer.

The successful functionalization of gold surface is demonstrated by the peaks of the sulphur regions in which the binding energy is 162.00-163.20 eV and corresponds to the thiolate group (S-Au)<sup>14</sup>. There is a low proportion of the free thiol specie (-SH) with the binding energy of 164.85-166.05 eV. The phosphorous region presents a peak corresponding to the binding energy of the phosphoric acid group (B.E. -POOH 133.60

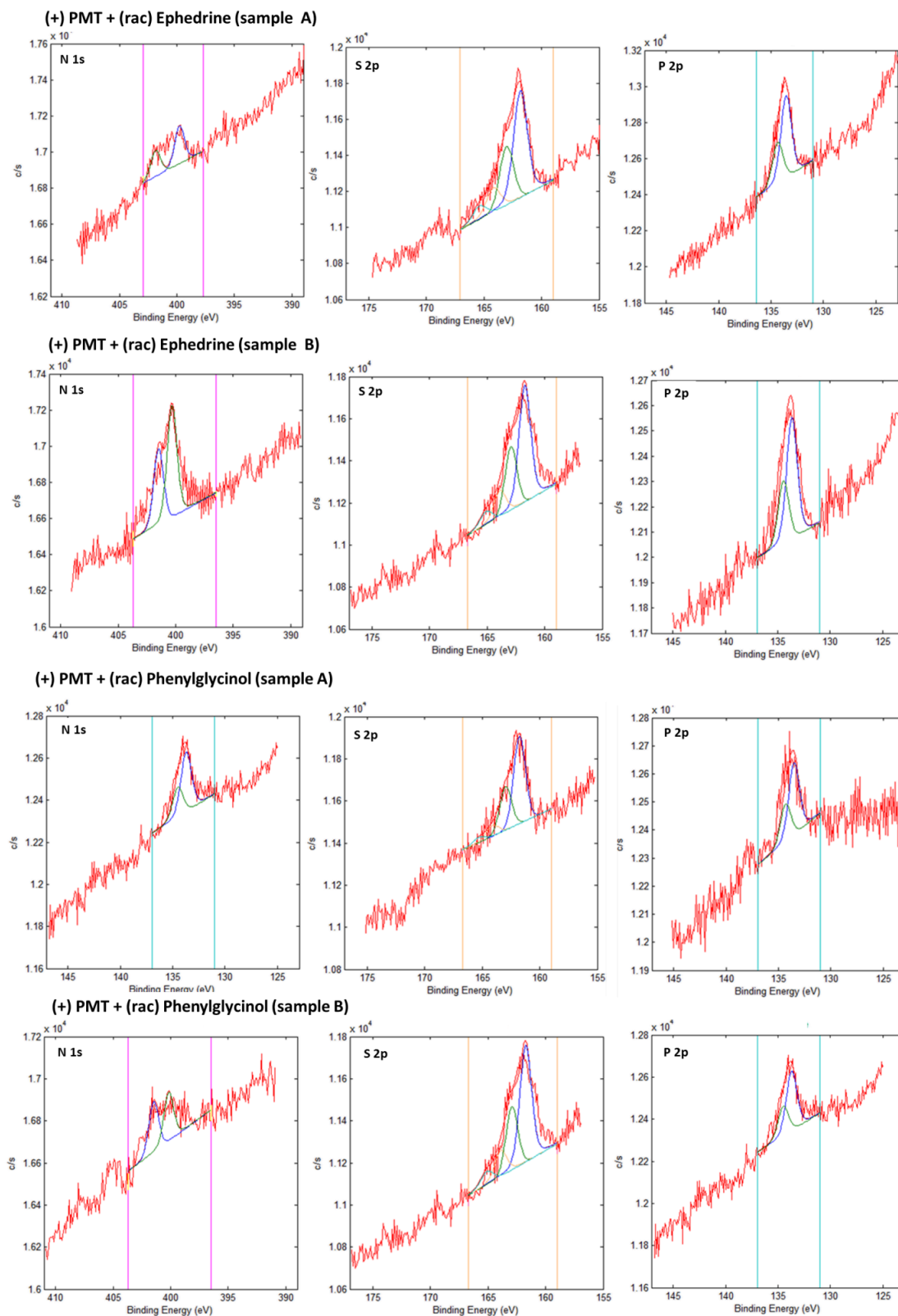
<sup>14</sup> D. G. Caster, *Langmuir*, **1996**, *12*, 5083-5086.

– 134.40 eV<sup>15</sup>). The following spectra (Figure 5.12) show peak fitting for each sample and each element.

**Table 5.4.** XPS peak fitting for the adsorption experiments performed at 40°C.

<b>(+) PMT + (rac)-Ephedrine (sample A)</b>				
<b>B. E.(eV)</b>	<b>ΔE (eV)</b>	<b>Area</b>	<b>FWHM</b>	<b>Chemical specie</b>
161.83-163.03	1.2	2:1	1.20	Thiolate (S-Au)
164.18-165.38	1.2	2:1	1.20	Free thiol (-SH)
133.55-134.35	0.8	2:1	1.20	Phosphoric acid (-POOH)
399.77	-	-	1.00	NH
401.85	-	-	1.00	H···NH
<b>(+) PMT + (rac)-Ephedrine (sample B)</b>				
161.75-162.95	1.2	2:1	1.20	Thiolate (S-Au)
163.87-165.07	1.2	2:1	1.20	Free thiol (-SH)
133.64-134.44	0.8	2:1	1.20	Phosphoric acid (-POOH)
400.32	-	-	1.00	NH
401.48	-	-	1.00	H···NH
<b>(+) PMT + (rac)-Phenylglycinol (sample A)</b>				
161.76-162.96	1.2	2:1	1.20	Thiolate (S-Au)
164.13-165.33	1.2	2:1	1.20	Free thiol (-SH)
133.5-134.31	0.8	2:1	1.20	Phosphoric acid (-POOH)
400.14	-	-	1.00	NH <sub>2</sub>
401.53	-	-	1.00	H···NH <sub>2</sub>
<b>(+) PMT + (rac)-Phenylglycinol (sample B)</b>				
161.73-162.93	1.2	2:1	1.20	Thiolate (S-Au)
163.9-165.10	1.2	2:1	1.20	Free thiol (-SH)
133,7-134,50	0.8	2:1	1.20	Phosphoric acid (-POOH)
400.17	-	-	1.00	NH <sub>2</sub>
401.47	-	-	1.00	H···NH <sub>2</sub>

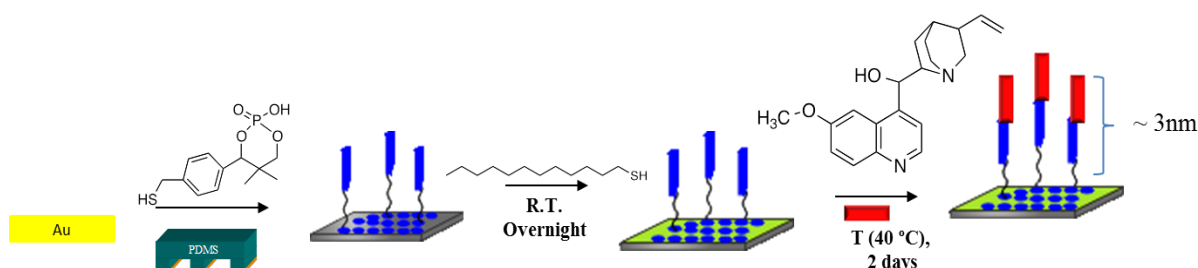
<sup>15</sup> R. M. Petoral, Jr. F. Björefors, K. Uvdal, *J. Phys. Chem. B*, **2006**, *110*, 23410-23416.



**Figure 5.12.** XPS spectra with peak fitting of each sample of the adsorption experiments performed at 40°C. The peak fitting was done using Multipak 9.2 software.

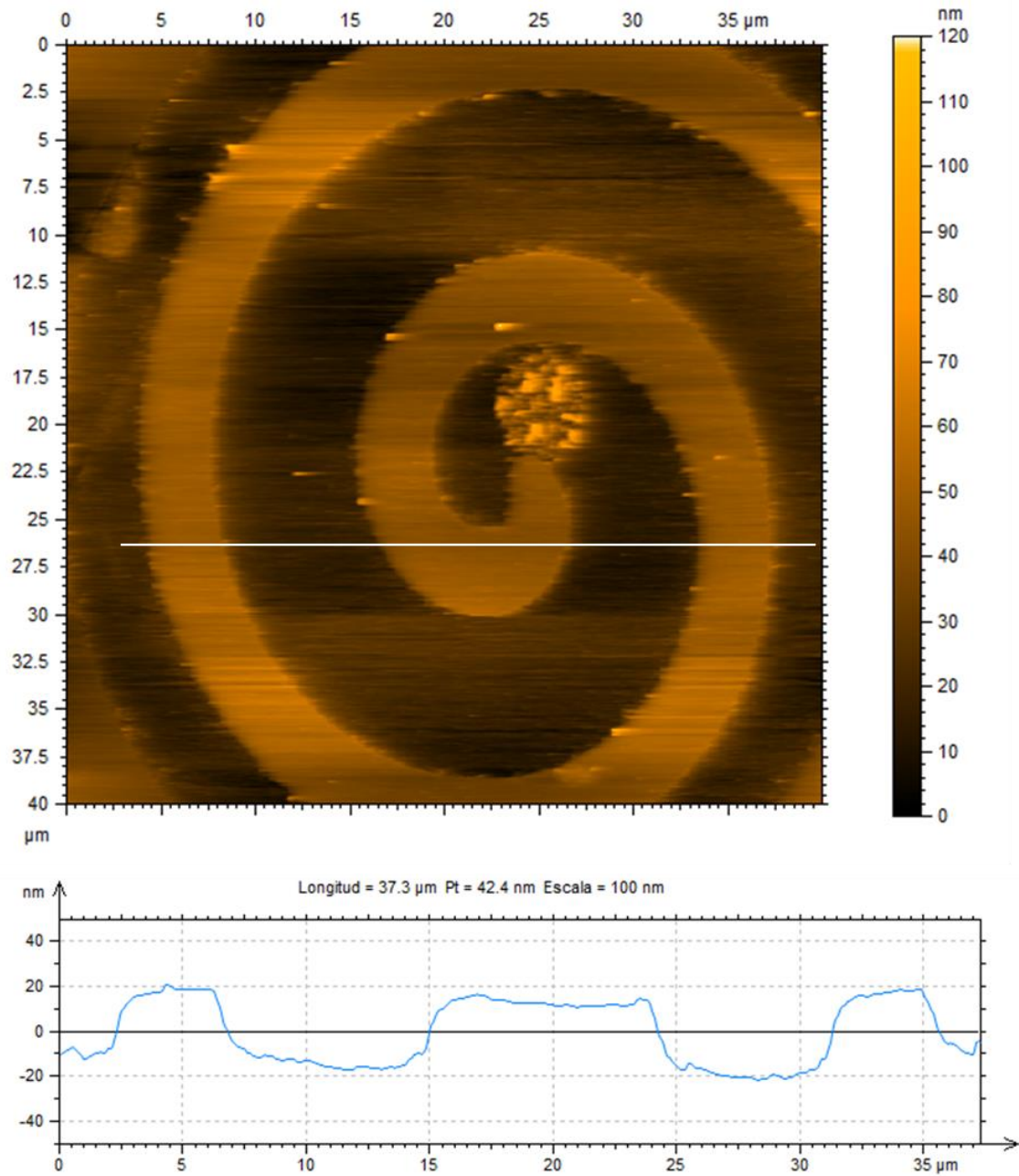
### 5.3.1.1. AFM study

The good results of the adsorption experiment with apparent multilayer growth from the solution of the amines at 40°C proved suitable for an AFM topography study. Multilayers grown on full monolayers are not very suitable to see the film thickness by AFM, so then the samples of this study were carried out on a micropatterned polycrystalline gold surface. Figure 5.12 shows the protocol to functionalise each sample (explained in full in Chapter 7), in which the selected stamp has motif of spirals of 50 x 100 μm. The expected height of the first Quinine layer grown on (+) PMT is 3 nm.



**Figure 5.12.** Microcontact printing protocol and incubation in Quinine solution.

AFM images were made in tapping mode; a representative image is shown below in Figure 5.13. The topographic profile of a Quinine multilayer, grown on spiral micropatterned monolayer of (+)-PMT and the profile graph measured in the selected area (white line on the spiral) clearly evidence multilayer formation. The profile shows several steps which correspond with the spiral shape along a line. Quinine layer grow on (+) PMT and the height of the peaks are related with much more than one layer of quinine. In fact, the height of the features is approximately 30 nm, corresponding to ten layers of the base. Thus, the temperature favours the growth of multilayers on the (+)-PMT monolayers which act as good templates. Not that essentially no adsorption takes place on the dodecanethiol filling layer.



**Figure 5.13.** AFM topography image of multilayers of Quinine on (+)-PMT spirals of 50x100 μm and profile graph below.

## **5.4. Conclusions**

In principle, the adsorption of an amine (a base) to the monolayers of acid-capped thiols should proceed in a spontaneous and rapid manner. However, this study shows that at room temperature the process is slow or even negligible despite the non-covalent interactions that are expected to take place between the acidic protons and the nitrogen atoms of the base. Minimal base is attached at room temperature, and pre-treatment of the monolayer to ensure formation of the anionic form of the layer in contact with ammonium salts does not work.

When an increased thermal energy is supplied to the system diffusion is favoured and interactions apparently take place. The neutral SAM when exposed to the amine at room temperature or at 40°C show a significant increase of the intensity of the XPS peaks in the nitrogen area at higher temperature due to multilayer formation. AFM analysis also confirms the multilayer formation at 40°C, although at this stage the formation of a multilayer cannot be explained easily.

# Chapter 6

## Self-assembled monolayers as templates for crystal nucleation and growth

---

This chapter describes phencyphos crystallisation on functionalised surfaces experiments with very interesting results as branched crystal growth.

Part of this work has been published in:

A. Bejarano-Villafuerte, M. van der Meijden, M. Lingenfelder, K. Wurst, R.M. Kellogg, D.B. Amabilino, *Chem. Eur. J.*, **2012**, *18*, 15984-15993.



## 6.1. SAMs as templates for crystal nucleation and growth

SAMs on surface favours the heterogeneous nucleation<sup>1</sup> at the interface between SAMs-solution inside the homogeneous within the solution (as it was explained in the introduction, Chapter 1).<sup>2</sup> The SAMs described in Chapter 5 were envisaged to favour the heterogeneous nucleation of phencyphos, as shown schematically in figure 6.1. The functionalization of gold substrates (mono and polycrystalline) was designed in order to have a good recognition at the SAM-solution interface between (+)-PMT linked at the surface and the phencyphos in solution.

The decision to crystallise the enantiomers of phencyphos on (+)-PMT was taken first to examine the growth of structurally similar molecules on these SAMs. Phencyphos, which is identical to the SAM molecule except for the methylthiol tail, was an obvious candidate because of the possibility of epitaxial growth, as indicated in the scheme. The similarity comes from both the functional group – the phosphoric acid – and the connectivity of the different moieties, which may allow a truly templated growth where layer and crystal form a continuous contact.<sup>3</sup>

This focus concerning the crystallisation of materials onto self-assembled monolayers (SAMs) is a topic that is receiving increasing attention because it is a way to restrict the crystallisation process so that small monocrystals of different shapes can be prepared, and even influence in the polymorph which is formed.

The true novelty of the approach lies in the use of chiral monolayers which is structurally unique and which in principle should have a different effect on the growth<sup>4</sup> of either enantiomer of the compound whose nucleation is templated.

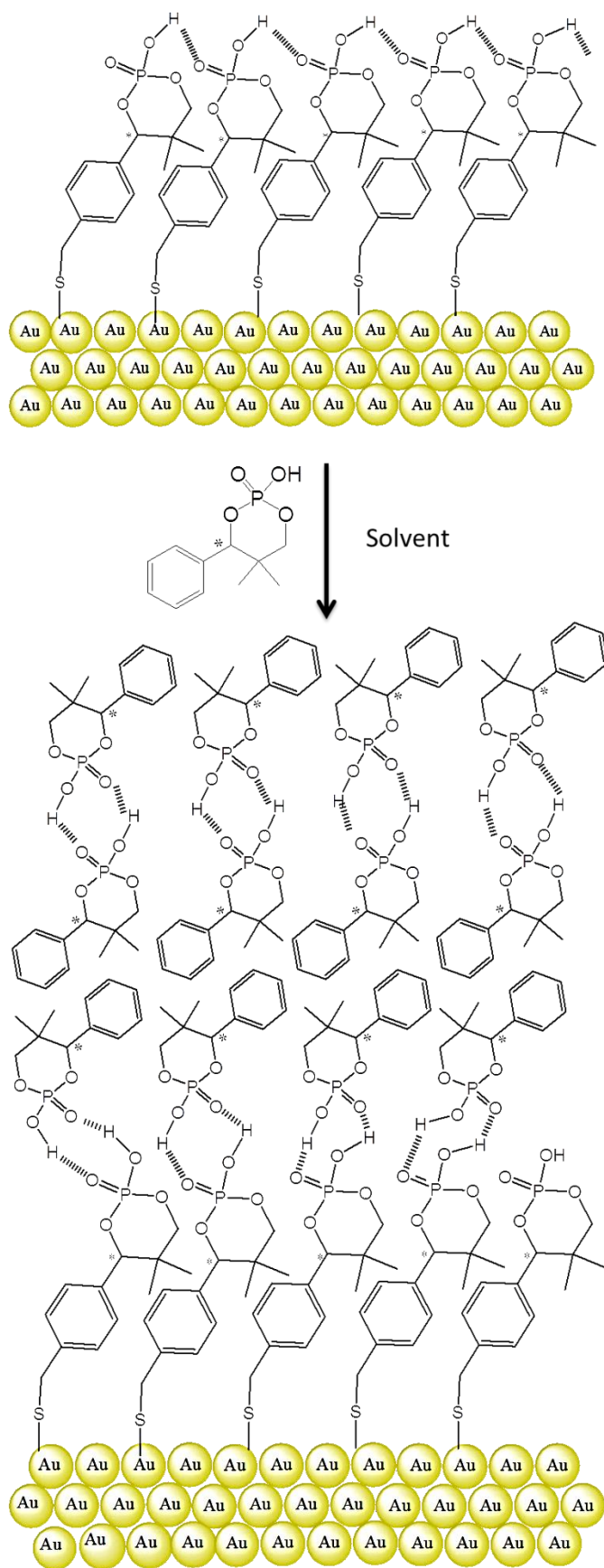
---

<sup>1</sup> R. P. Sear, *J. Phys. Chem. B*, **2006**, *110*, 4985-4989.

<sup>2</sup> B. Pokroy, V. F. Chernow, J. Aizenberg, *Langmuir*, **2009**, *25*, 14002–14006.

<sup>3</sup> Y. J. Han, J. Aizenberg, *Angew. Chem. Int. Ed.*, **2003**, *42*, 3668–3670.

<sup>4</sup> R. Hiremath, J. A. Basile, S. W. Varney, J. Aizenberg. Swift, *J. Am. Chem. Soc.*, **2005**, *127*, 18321-18327.

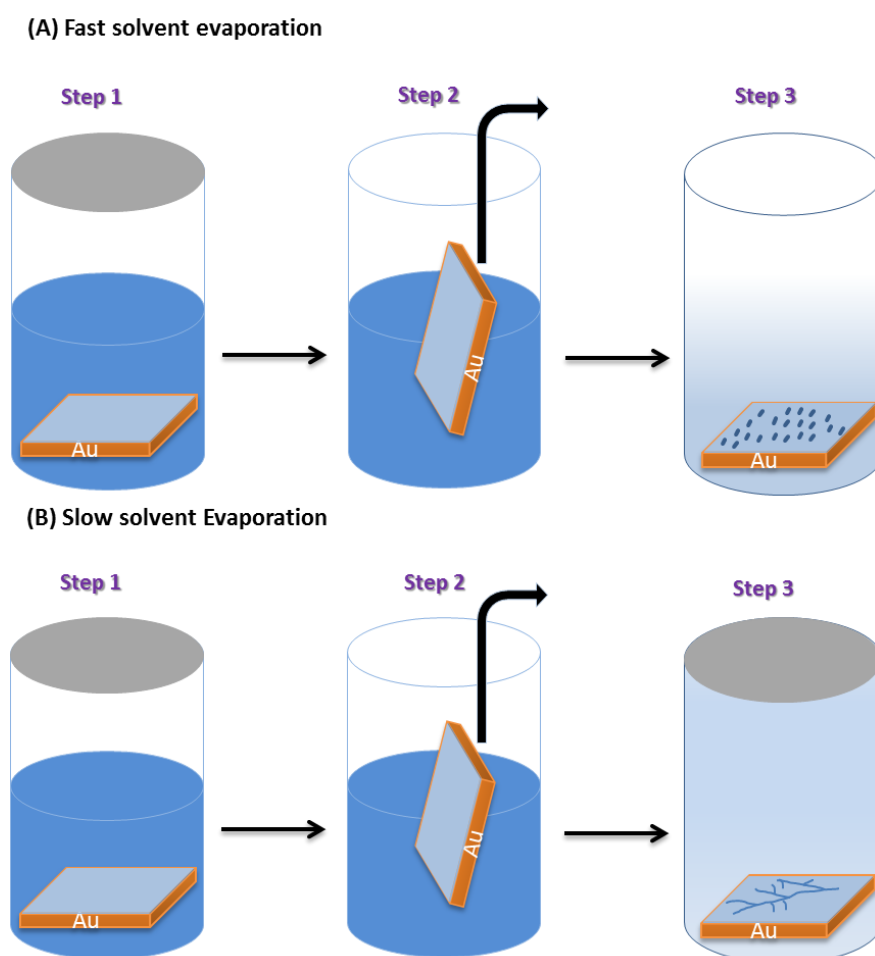


**Figure 6.1.** Molecular level representation of the SAM of PMT and a crystal of phencyphos formed upon it.

## 6.2. Crystallisation of phencyphos on SAMs of (+) PMT.

The method most used for the crystallisation of the organic molecules on the SAMs surfaces was a casting technique, whereby a drop of a solution of the target compound was deposited on the clean SAMs. The reason for this approach is that attempted crystallisation on the surface immersed in a warm supersaturated solution of either enantiomer of phencyphos did not afford reliable crystallisation on the SAM, but rather in the bulk of the solution, meaning that under those conditions homogeneous nucleation is preferred over heterogeneous nucleation.

The evaporation rate has a great influence on the crystallization process. A very fast evaporation of the solvent does not allow the efficient diffusion over the monolayer of the compound from the solution and the crystals obtained should be less ordered than when the solvent evaporation is slow and controlled. To control this aspect, we designed two different crystallization methods, *fast solvent evaporation* and *slow solvent evaporation*. Figure 6.2 shows the two methods.



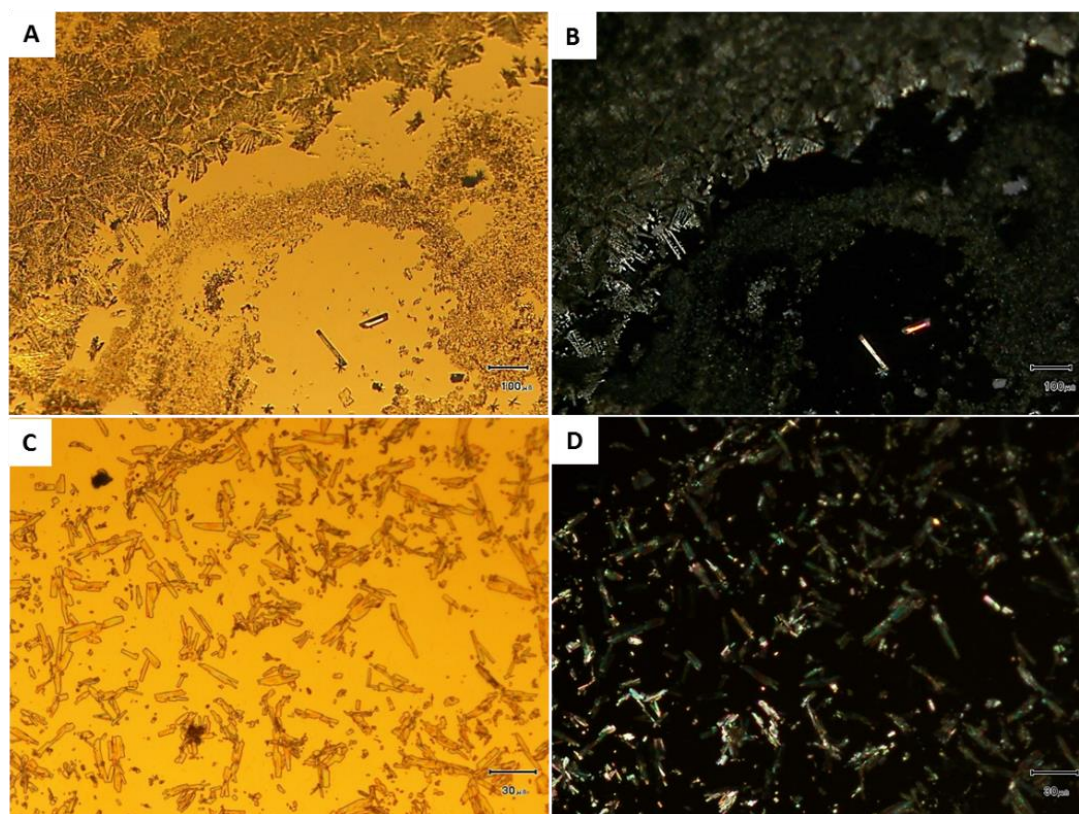
**Figure 6.2.** Crystallization methods employed for solutions of phencyphos on SAMs of PMT.

### 6.2.1. Fast solvent evaporation method

Crystallization of enantiomerically pure phencyphos from solutions on SAMs of (+)-PMT on gold was done following the solvent evaporation out of control method. The same experiments were done in two different solvents: chloroform and isopropanol. Gold substrates used: Monocrystalline gold on mica and polycrystalline gold on glass

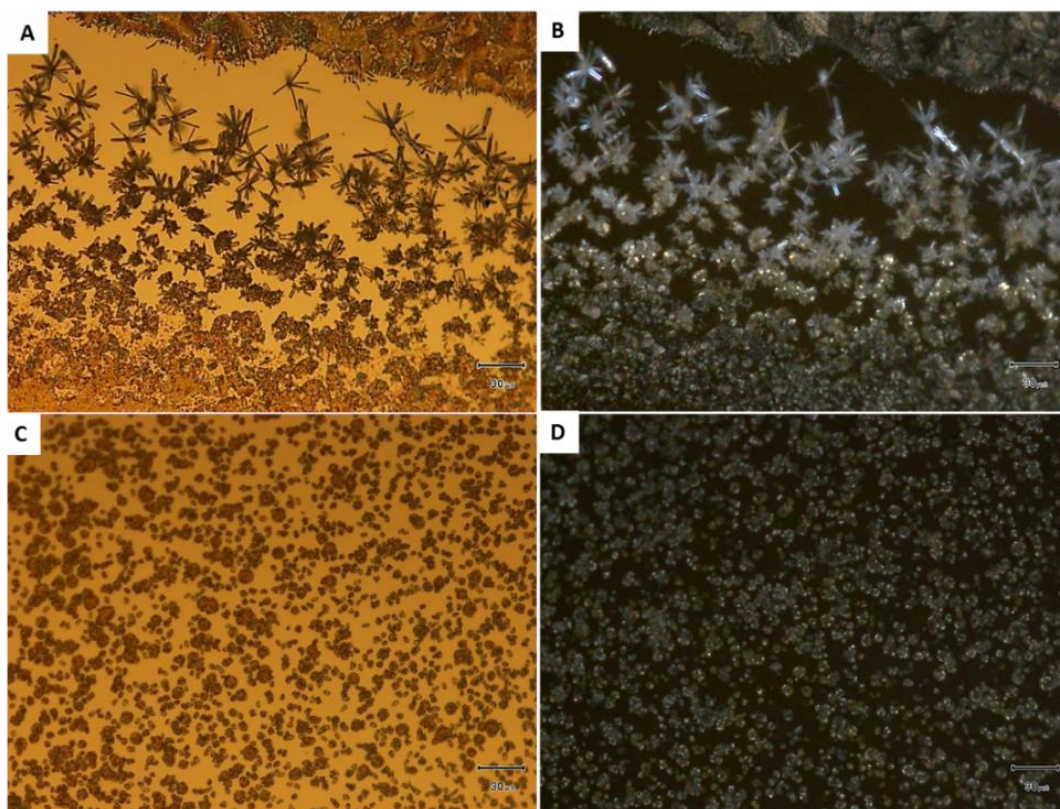
#### 6.2.1.1. Chloroform series

The uncontrolled evaporation of deposited chloroform solutions of either enantiomer of phencyphos on SAMs of (+)-PMT on single crystalline gold on mica gave well-formed rectangular microcrystals lying approximately parallel to the gold surface, as revealed by scanning electron microscopy (Figure 6.5). The size of the crystals ranges from a few to ten microns depending on the area, and the orientation in the plane of the surface is random (Figure 6.3), as is to be expected considering the smoothness of the (111) surface of the metal and the disordered nature of the monolayer of (+)-PMT. Thus, crystal growth is favoured on monocrystalline gold.

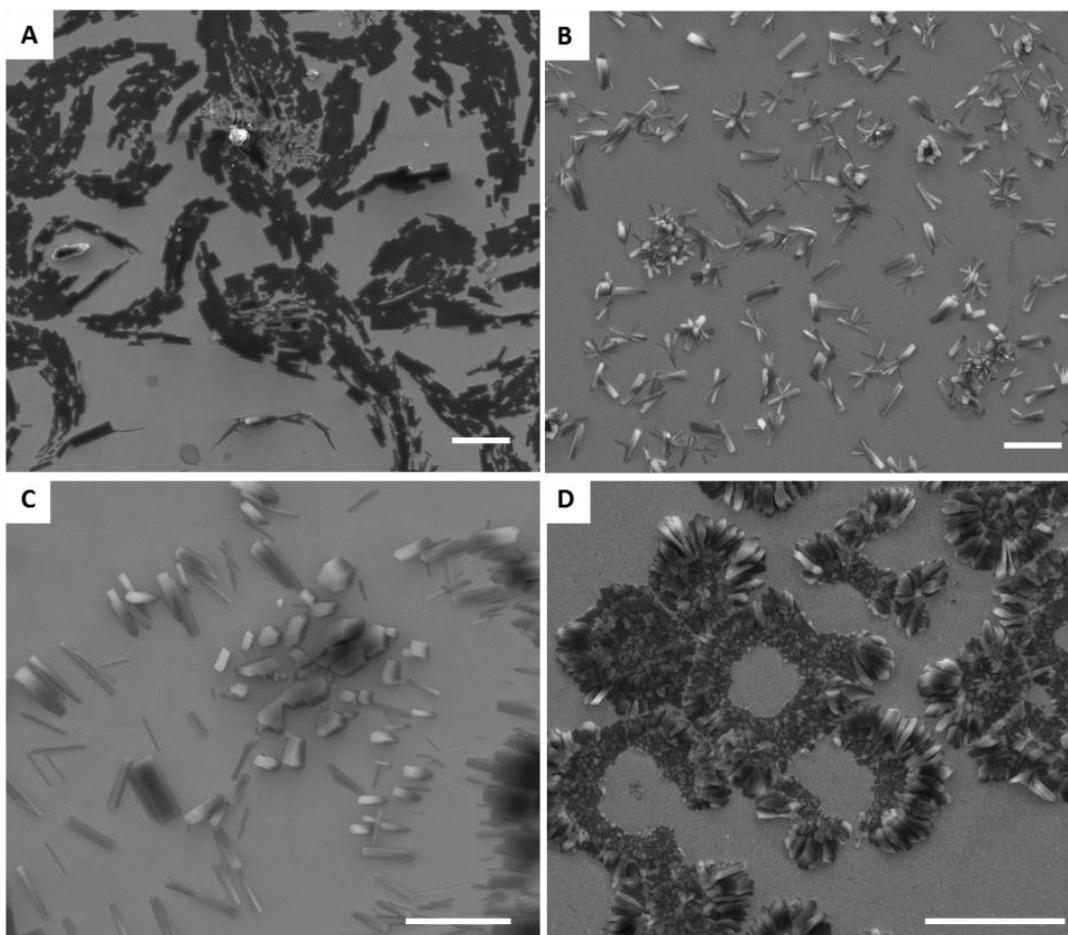


**Figure 6.3.** Optical microscope images of (+) Phencyphos crystals on (+)-PMT monolayer on monocrystalline gold, (A) non-polarized image, (B) polarized image. (-) Phencyphos crystals on (+)-PMT on monocrystalline gold (C) non-polarized image, (D) polarized image.

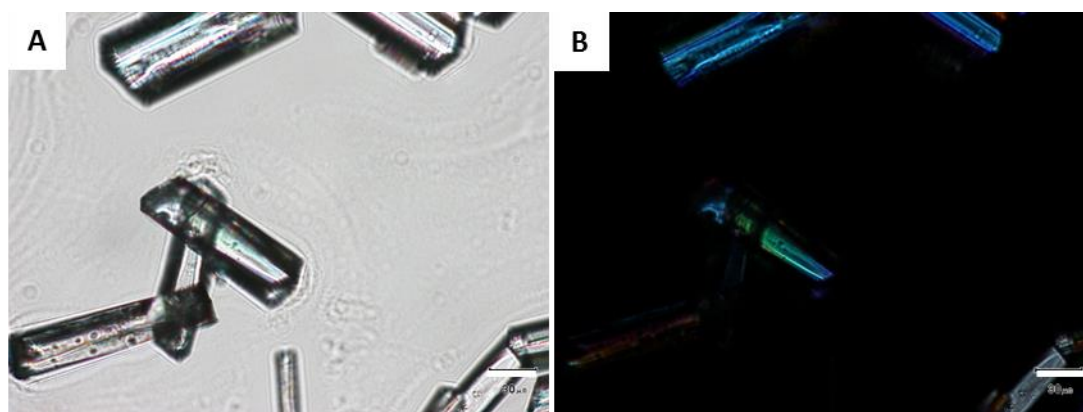
When the same experiment was performed on the SAM of (+)-PMT on polycrystalline gold on glass (Figure 6.4) small needles are the preferential morphology over the surface. This morphology is the same as that of crystals of phencyphos grown from solution, so there is an effect of the surface on the nucleation process, favouring this over the surface. A mixture of morphologies is observed, ranging from closely spaced rectangular crystals similar to those on the flat surface, but also thin needles in some places. The maximum length of the crystals is approximately 1 micron. The much greater number of smaller crystals is an indication of the greater efficiency of the functionalised polycrystalline surface to nucleate phencyphos. Crystals of the compound grown from solution under identical conditions on to glass microscope cover slides had longitudinal dimensions above approximately 50 microns, indicating strongly that the surface plays a determining role in the crystal formation (Figure 6.6).



**Figure 6.4.** Optical micrographs of: (+) Phencyphos crystals on (+)-PMT monolayer on polycrystalline gold, (A) non-polarized image, (B) polarized image. (-) Phencyphos crystals on (+)-PMT on polycrystalline gold (C) non-polarized image, (D) polarized image.

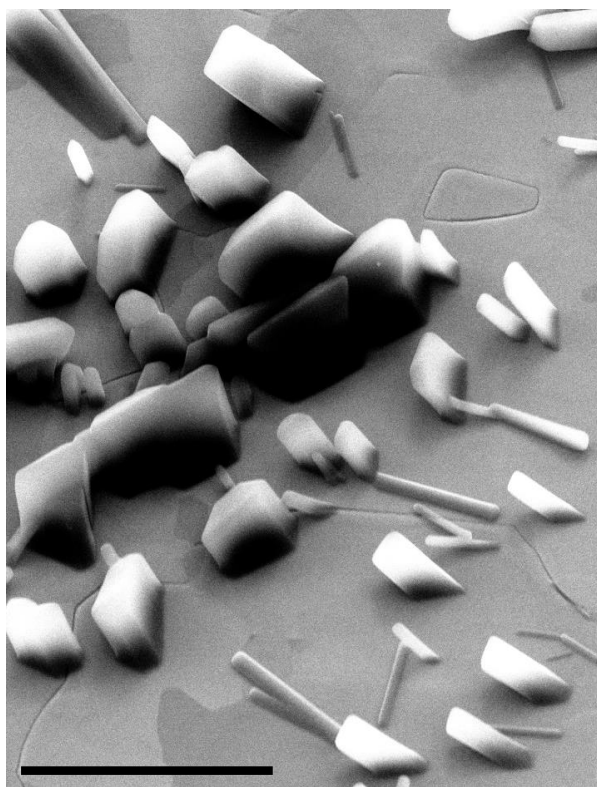


**Figure 6.5.** SEM images: (-) Phencyphos crystals on (+)-PMT monolayer on (A) Monocrystalline gold and (B) Polycrystalline gold. And (+) Phencyphos crystals on (+)-PMT on (C) Monocrystalline gold (D) Polycrystalline gold. Scale bar 10  $\mu\text{m}$ .



**Figure 6.6.** Optical micrographs of: (+) Phencyphos crystals on to glass microscope cover slides (A) non-polarized image, (B) polarized image. Scale bar 30  $\mu\text{m}$ .

The hypothesis that the surface acts as nucleant for the crystals is supported by SEM images recorded at non-perpendicular angles to the surface plane (Figure 6.4). These images reveal that many of the crystals of phencyphos form an angle to the nucleating surface, and that the bases of the crystals are in total contact with it. In addition, identical experiments performed on the gold substrates without the SAM layer produced an amorphous material, indicating the positive role that the monolayer of (+)-PMT has. We hypothesise that this nucleation effect could be a result of the interaction between the acid groups of the surface and those of the crystals being formed, because chains of hydrogen bonds in crystals of these compounds are formed. Figure 6.6 shows how the phencyphos crystals grow off the surface.

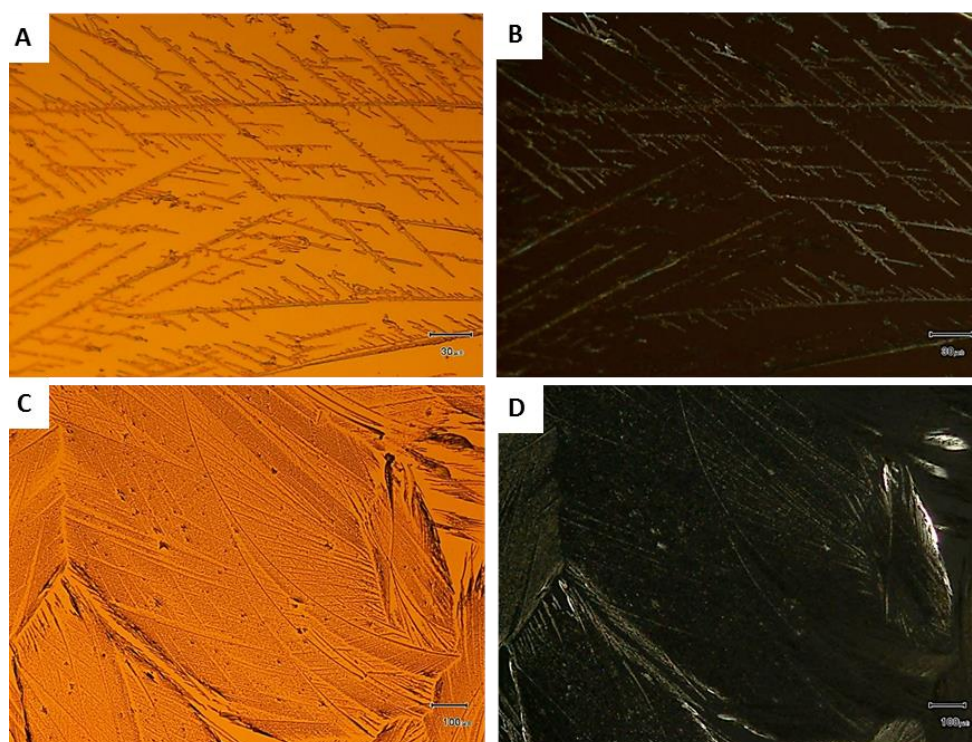


**Figure 6. 7.** SEM image of crystals of (+)-Phencyphos formed on a monolayer of (+)-PMT by fast evaporation of a chloroform solution of the compound on a monocrystalline gold substrate, tilt 30°, scalebar 5 microns taken at an angle to the perpendicular of the surface.

### 6.2.1.2. Isopropanol series

When a solution of either enantiomer of phencyphos was crystallised on a SAM of (+)-PMT on gold from isopropanol (IPA) and the solvent was evaporated with no control, feather-like crystal formations were formed either on the mono- (Figure 6.8) or poly-crystalline metal (Figure 6.9). On a large scale, long objects run along parallel directions over millimetre distances with branching points at certain positions where the direction of crystal growth changes.

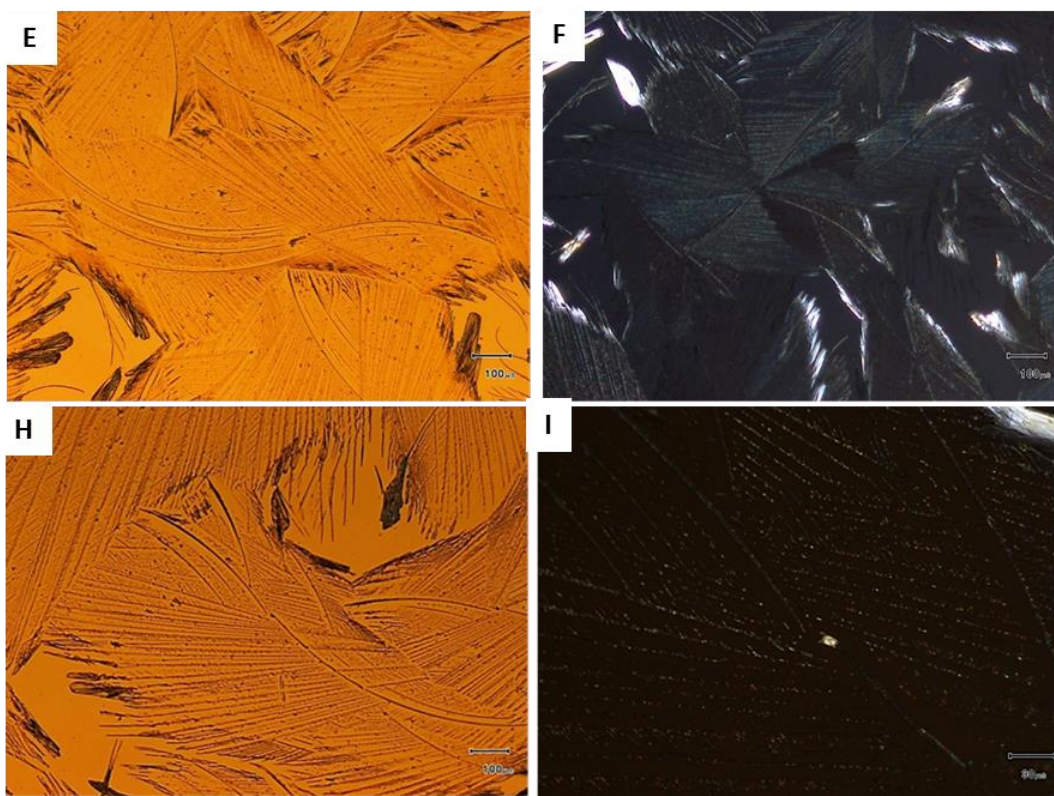
Figure 6.8 shows how the crystals of phencyphos growth in these conditions. They have a particular way to grow, significantly different that from chloroform solution. That means there is a very important effect of the solvent on the crystal growth even though the crystals are formed on the same surfaces. Figure 6.10 shows the same samples as the optical micrographs in figure 6.8, at the same scale, by scanning electron microscopy. There, the special growth is clearer. There is a clear presence of branched crystals.<sup>5</sup>



**Figure 6. 8.** Reflection optical micrographs of crystals of either enantiomers of phencyphos from isopropanol solution on (+)-PMT monolayer on gold substrates: (A) and (B) (+) phencyphos crystals on monocrystalline gold. (C), (D) (-) phencyphos crystals on monocrystalline gold. (A) and (C) non-polarised imaged. (B) and (D) polarised images.

<sup>5</sup> F. Zhang, J. Liu, H. Huang, B. Du, T. He, *Eur. Phys. J. E*, **2002**, 8, 289-297.

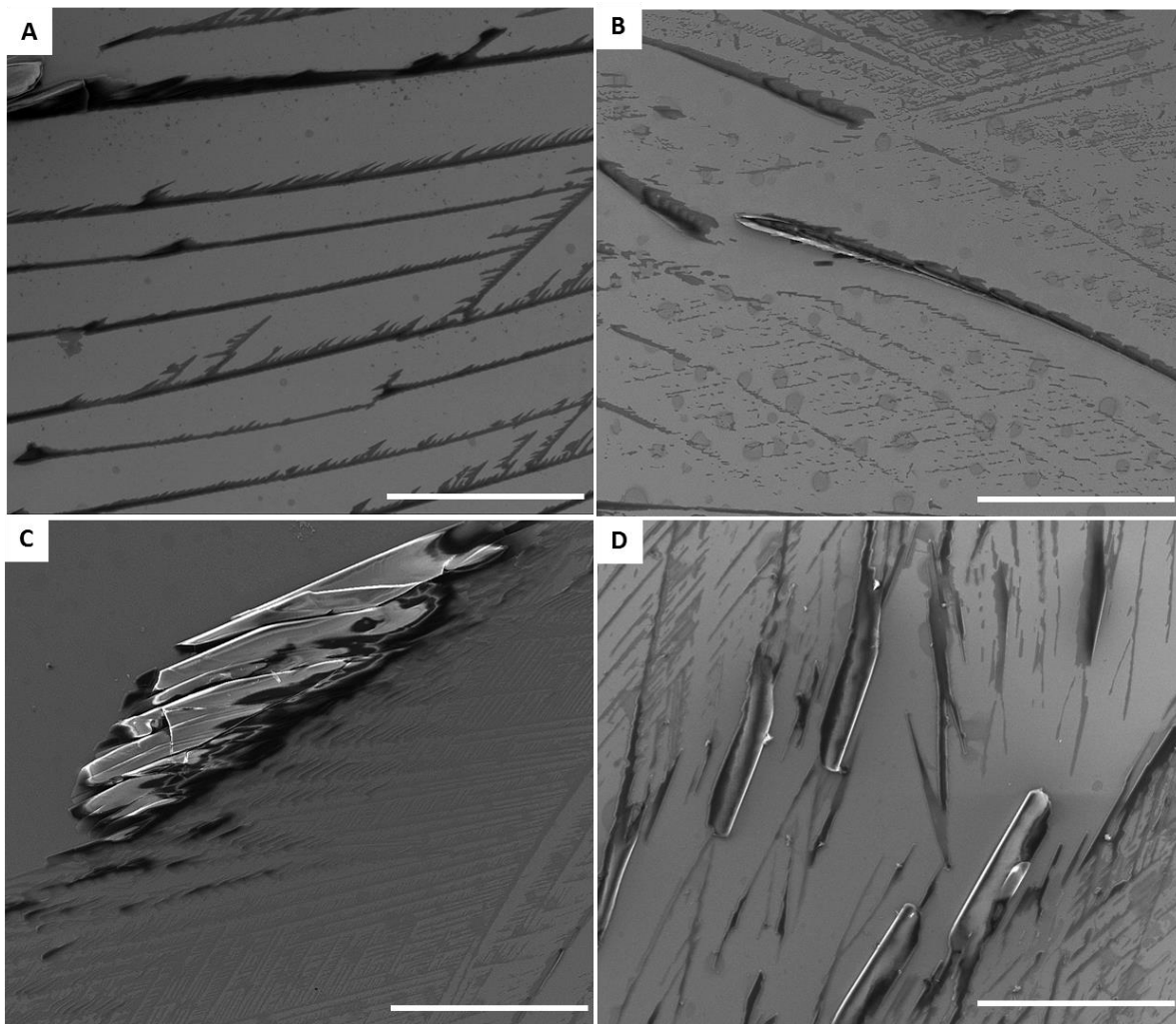




**Figure 6. 9.** Reflection optical micrographs of crystals of either enantiomers of phencyphos from isopropanol solution on (+)-PMT monolayer on gold substrates: (E), (F) (+) phencyphos crystals on polycrystalline gold. (H), (I) (-) phencyphos crystals on polycrystalline. In all samples the solvent evaporation was out of control. (A), (C), (E) and (H) non-polarised imaged. (B), (D), (F) and (I) polarised images.

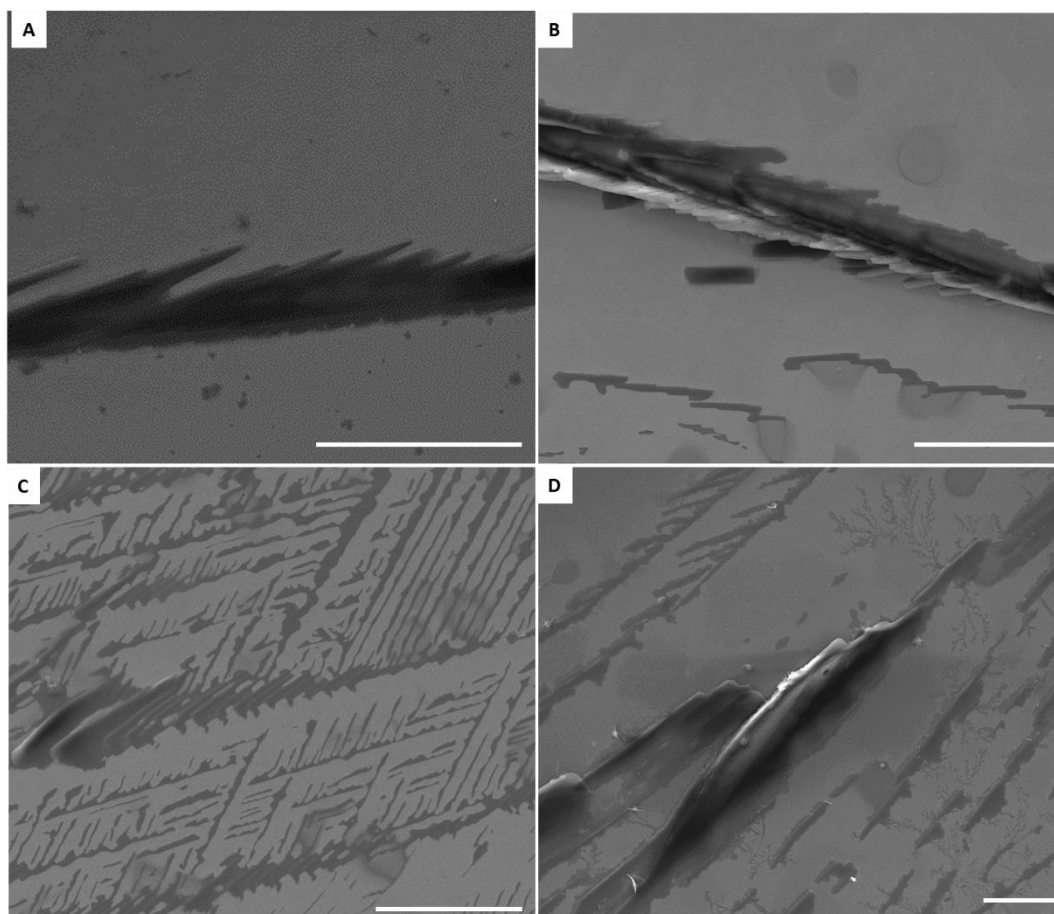
When the features are imaged by SEM on a smaller scale (Figure 6.10), it is clear that the long thin objects are formed from parallel crystallites whose length ranges from a few to tens of microns, and whose width is as little as 0.5 microns. The angle which these crystallites (components of the long crystal) form to the direction of the main object is approximately  $24^\circ$ . The angle which the long crystallites form away from this primary long object is  $47^\circ$ . The growth of the two is always in the same direction, that is locally they have the same chirality (remembering that a given direction on a surface implies homochirality) but the angle is an approximately equal and opposite value in different regions (so globally the sample shows a racemic morphology, despite of the homochirality of the molecular components). Given that in a chosen region the angle has the same sign, it appears that this branching is homochiral, and therefore one might suppose that the chirality of the molecule is passed on to the growth of the

branched crystallites, because when one angle is formed in the long objects the branches have a correlated angle. A similar situation of chiral growth has been observed in the vacuum deposition of 6,13-pentacenequinone.<sup>6</sup> However, in the present case different areas of the sample have angles which are equal and opposite, therefore neither the chirality of the monolayer nor the chirality of the sample influence in the morphology of these surface-grown crystallites. It therefore appears that the crystal growth mechanism dominates any molecular level dissymmetry.



**Figure 6. 10.** SEM images of crystals of phencyphos, from isopropanol solution, on (+)-PMT monolayer on gold substrates. (A) (+) Phencyphos crystals on monocrystalline gold. (B) (-) Phencyphos crystals on monocrystalline gold. (C) (+) Phencyphos crystals on polycrystalline gold. (D) (-) Phencyphos crystals on polycrystalline gold. Scale bar 100  $\mu\text{m}$ .

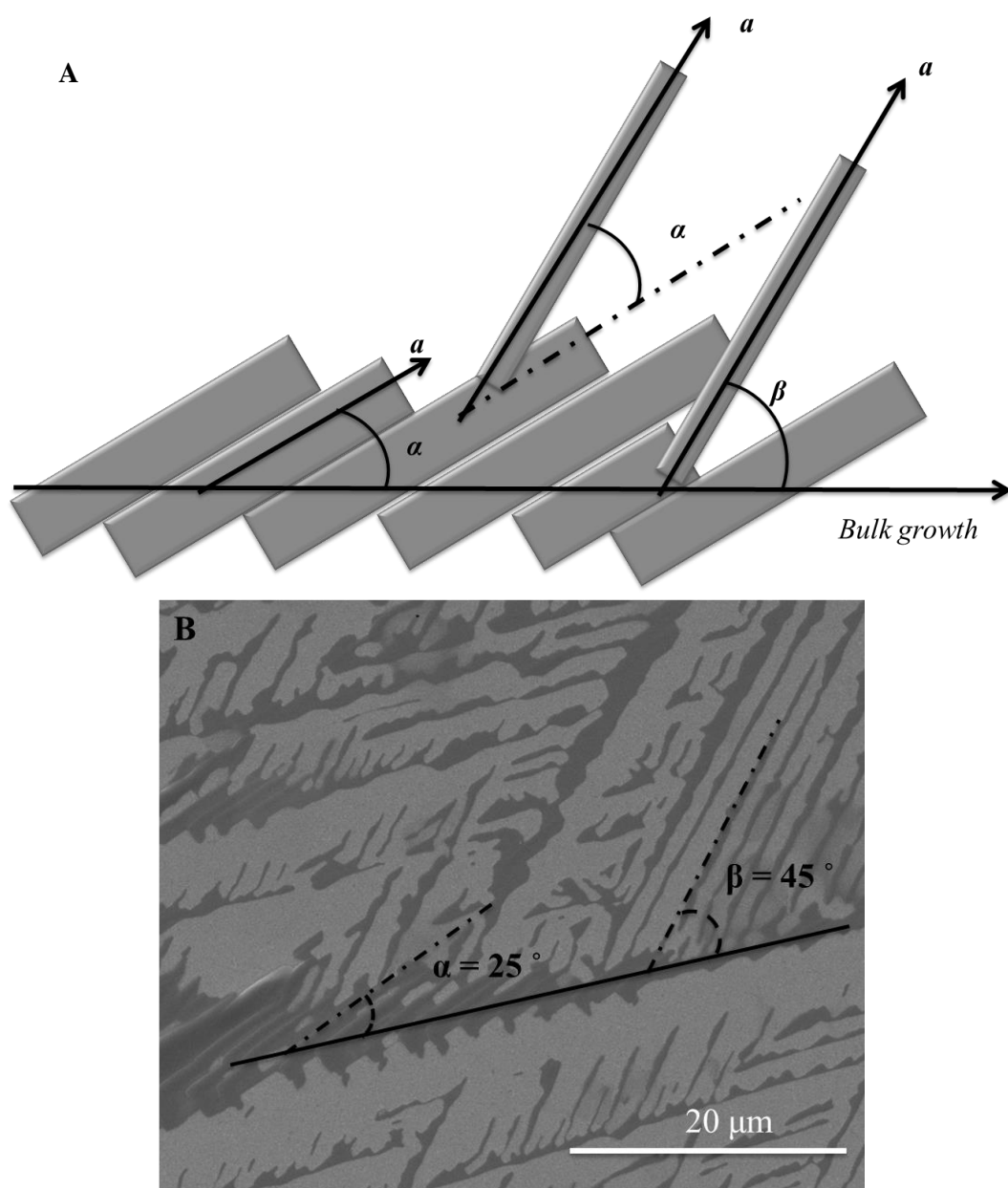
<sup>6</sup> (a) A. Al-Mahboob, J.T. Sadowsk, T. Nishihara, Y. Fujikawa, Q.K. Xu, K. Nakajima, T. Sakurai, *Surf. Sci.*, **2007**, *601*, 1311-1318; (b) P. De Marco, F. Fioriti, F. Bisti, P. Parisse, S. Santucci, L. Ottaviano, *J. Appl. Phys.*, **2011**, *109*, 063508.



**Figure 6. 11.** SEM images of crystals of phencyphos, from isopropanol solution, on (+)-PMT monolayer on gold substrates. (A) (+) Phencyphos crystals on monocrystalline gold. (B) (-) Phencyphos crystals on monocrystalline gold. (C) (+) Phencyphos crystals on polycrystalline gold. (D) (-) Phencyphos crystals on polycrystalline gold. Scale bar 20 μm.

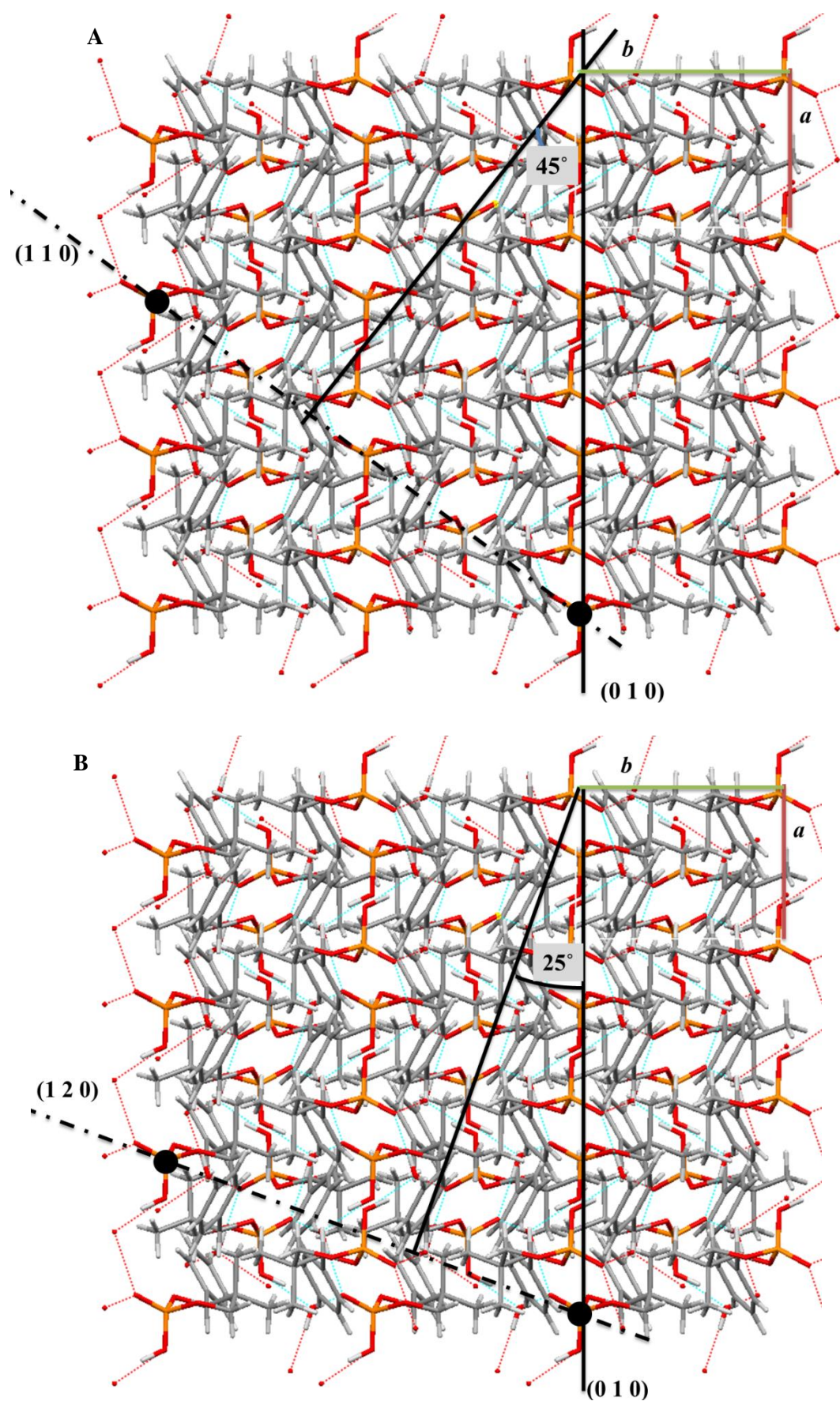
Both phencyphos enantiomer crystallises forming branched crystals (Figure 6.10 and 6.11). The (1 1 0) is the most polar plane of the phencyphos structure since is the hydrogen bond network growth direction and provides the strongest interaction at the interface SAM-crystal<sup>7</sup>, so it should be the plane which govern the main branch of growth (Figure 6.12). Nevertheless, there are other weaker interactions, as phenyl rings  $\pi$ -stacking, that under isopropanol condition can govern the crystal growth since interact at the interface. This type of growth corresponds to the secondary branches (Figure 6.11. A), from the main branch, the secondary branches with a defined angle (Figure 6.12. B, C).

<sup>7</sup> Chapter 3, *Crystal structure analysis*.



**Figure 6. 12.** (A) Branch growth scheme. (B) SEM image of crystals of (+) phencyphos from isopropanol solution, on (+)-PMT monolayer on polycrystalline gold under fast solvent evaporation condition.

The phencyphos space group is  $P2_12_12_1$ , in its structure hydrophilic and hydrophobic layers are alternated due to  $2_1$  axes in the three directions of the unit cell. Thus, from a molecule in the  $ab$  corner to the next in the middle of the  $c$  axis and twisted, the angle formed is approx.  $45^\circ$  (Figure 6.13). The length of the largest objects comprising multiple small crystals is far beyond the size of any gold terrace, and the long range orientation on polycrystalline gold implies a drying effect rather than any directionality induced by the surface, although the surface undeniably plays an important role in the nucleation and growth.



**Figure 6. 13.** Angle of growth relating two crystalline planes (3x3x3 packing) which correspond to two branched in the phencyphos crystal. (A) 45°, (B) 25°. (View along c axis).

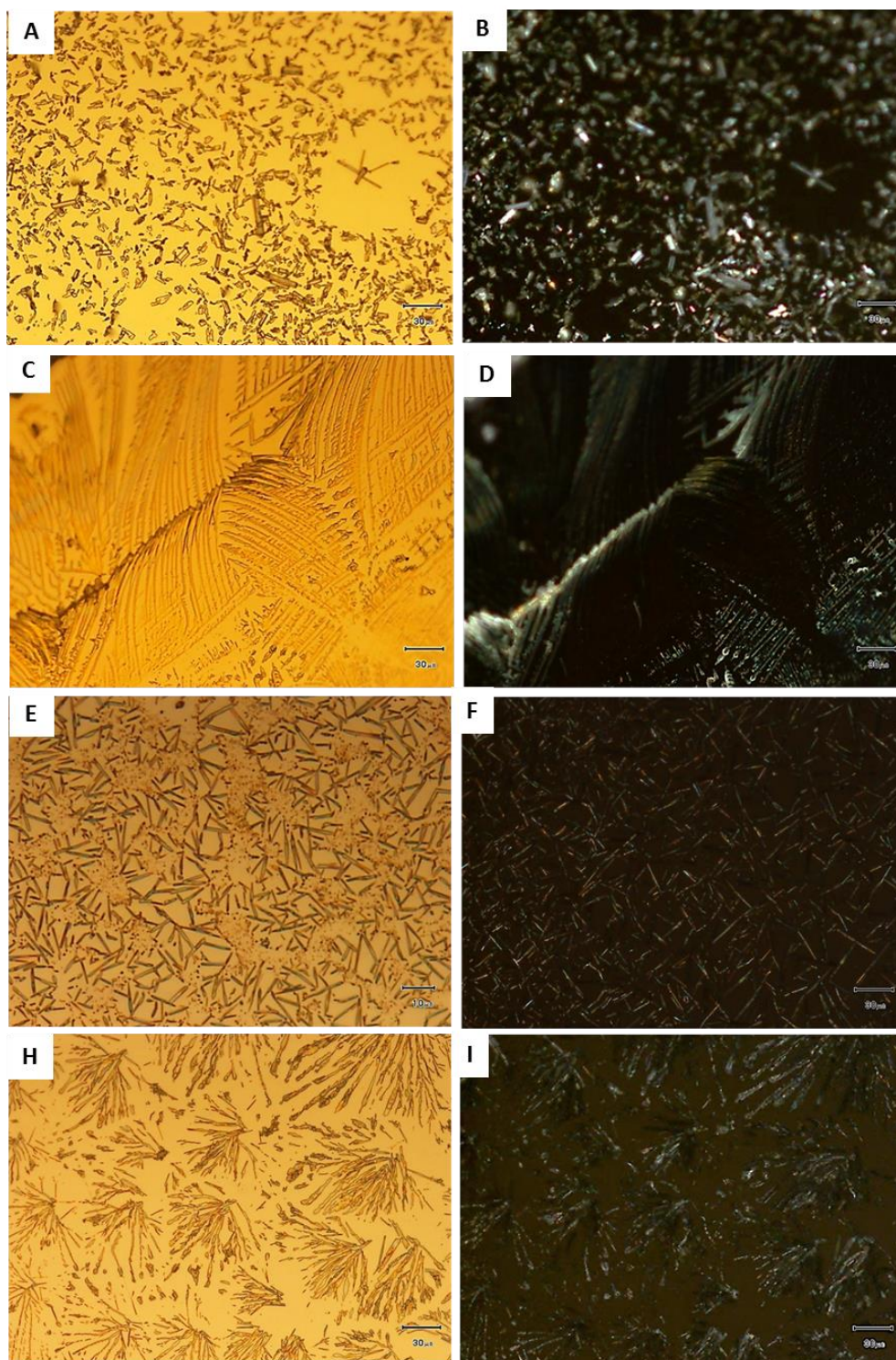
## 6.2.2. Slow solvent (under control) evaporation method

In principle, more controlled crystal growth could be achieved by a slow evaporation of the solution drop on the surfaces. The metastable zone of the crystallisation is approached more slowly and diffusion of the nuclei to the surface should be preferred. Therefore, SAM-functionalised surfaces were incubated in solutions of phencyphos, removed from the solution and immediately transferred to containers with a saturated vapour of the solvent.

### 6.2.2.1. Chloroform series

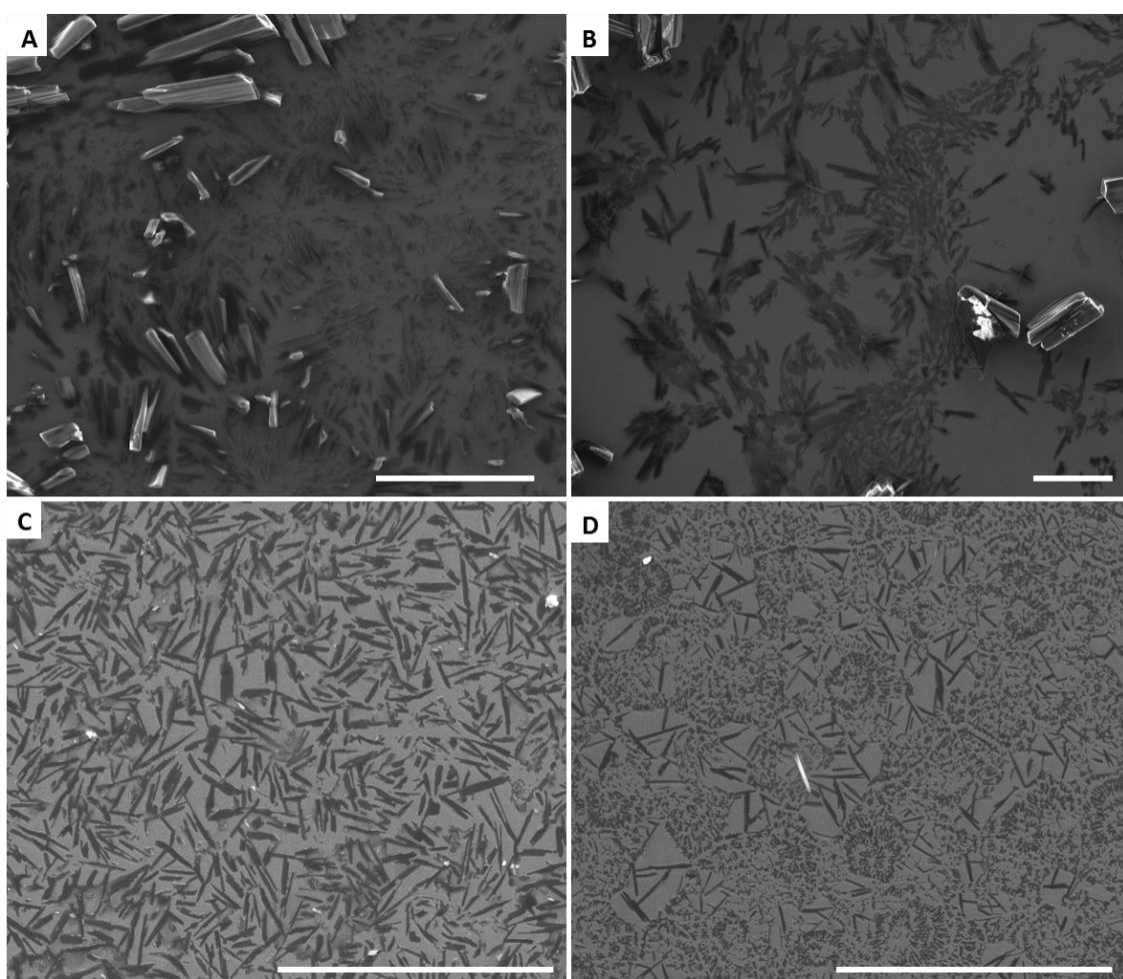
When chloroform was used to crystallise the enantiomers of phencyphos on the same SAMS, crystalline nature of the compound was evident in the polarised reflection optical micrographs of crystals of sufficient size. The images show bright areas wherever the crystals appear on the surface as a result of birefringence, with dark areas in between corresponding to the bare surface (Figure 6.14).

The velocity of evaporation of the chloroform has two main effects. Firstly, on monocrystalline gold the size of the largest crystals is much greater when the evaporation rate is slow, presumably as a result of a slower approach to supersaturation and the low number of nucleation sites on the smooth surface, consequently favouring growth over nucleation. Secondly, for the rougher polycrystalline gold surface, much more uniform crystallisation is seen, giving a collection of surface-nucleated crystals with narrow size distribution.



**Figure 6.14:** . Reflection optical micrographs of crystals of either enantiomer of phencyphos from chloroform solution on (+)-PMT monolayer. Slow solvent evaporation. (A) and (B) (+) phencyphos crystals on monocrystalline gold. (C), (D) (-) phencyphos crystals on monocrystalline gold. (E), (F) (+) phencyphos crystals on polycrystalline gold. (H), (I) (-) phencyphos crystals on polycrystalline. In all samples the solvent evaporation was out of control. (A), (C), (E) and (H) non-polarised imaged. (B), (D), (F) and (I) polarised images. Scale bar 30 µm.

The same procedure gives different crystal growths depending on the surface used. When monocrystalline gold was used as the substrate, SEM showed that crystals of phencyphos similar to those seen using uncontrolled evaporation were formed but in addition much larger crystals – up to 100 microns in length – were formed. In contrast, when the SAM of (+)PMT on polycrystalline gold was used as the substrate a quite uniform array of crystals mainly between 5 and 15 microns in length was formed (Figure 6. 15). The approximate width of the crystallites is 0.5 microns. Some areas like this are seen in the fast evaporation of chloroform, but the sample formed under controlled evaporation is far more homogeneous.



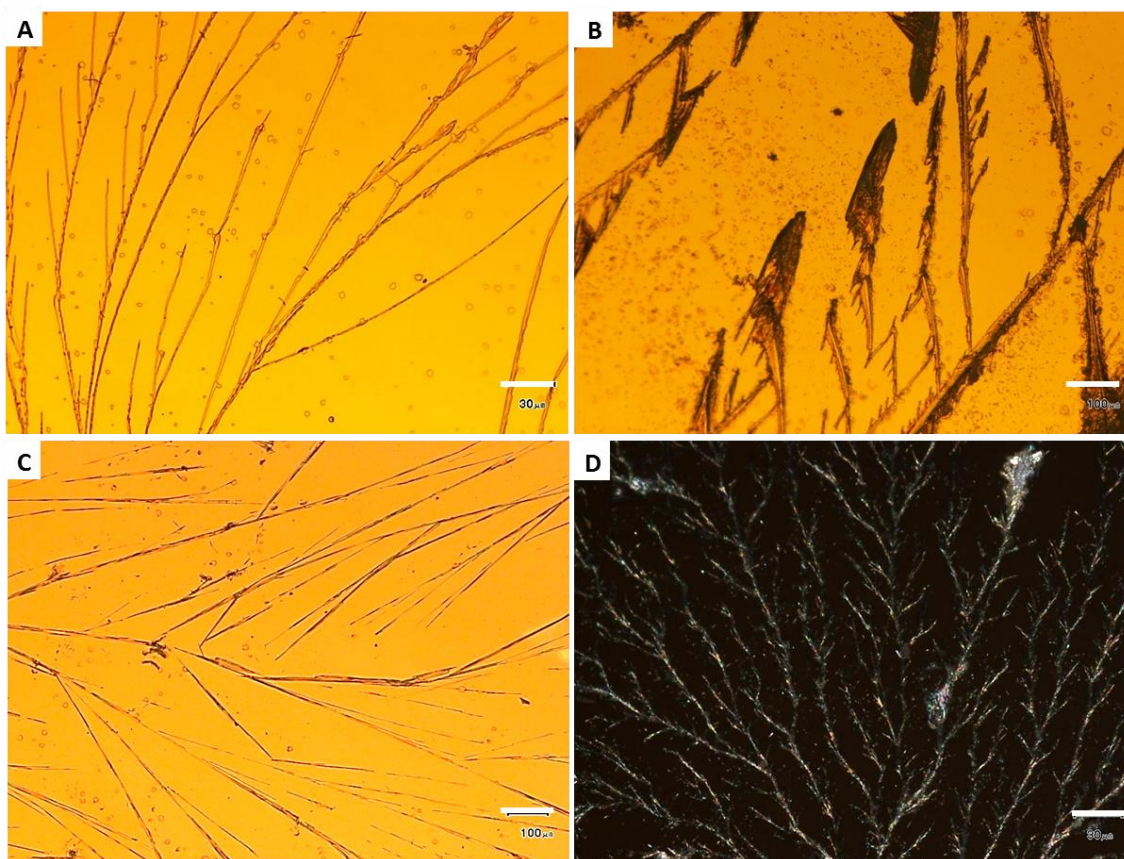
**Figure 6. 15.** SEM images of crystals of either enantiomers of phencyphos from chloroform solution on (+)-PMT monolayer. Slow solvent evaporation. (A) (+) Phencyphos and (B) (-) Phencyphos crystals on monocrystalline gold. (C) (+) Phencyphos and (D) (-) Phencyphos crystals on polycrystalline gold. Scale bar 50  $\mu\text{m}$ .



The velocity of evaporation of the chloroform has two main effects. Firstly, on monocrystalline gold the size of the largest crystals is much greater when the evaporation rate is slow, presumably as a result of a slower approach to supersaturation and the low number of nucleation sites on the smooth surface, consequently favouring growth over nucleation. Secondly, for the rougher polycrystalline gold surface, much more uniform crystallisation is seen, giving a collection of surface-nucleated crystals with narrow size distribution.

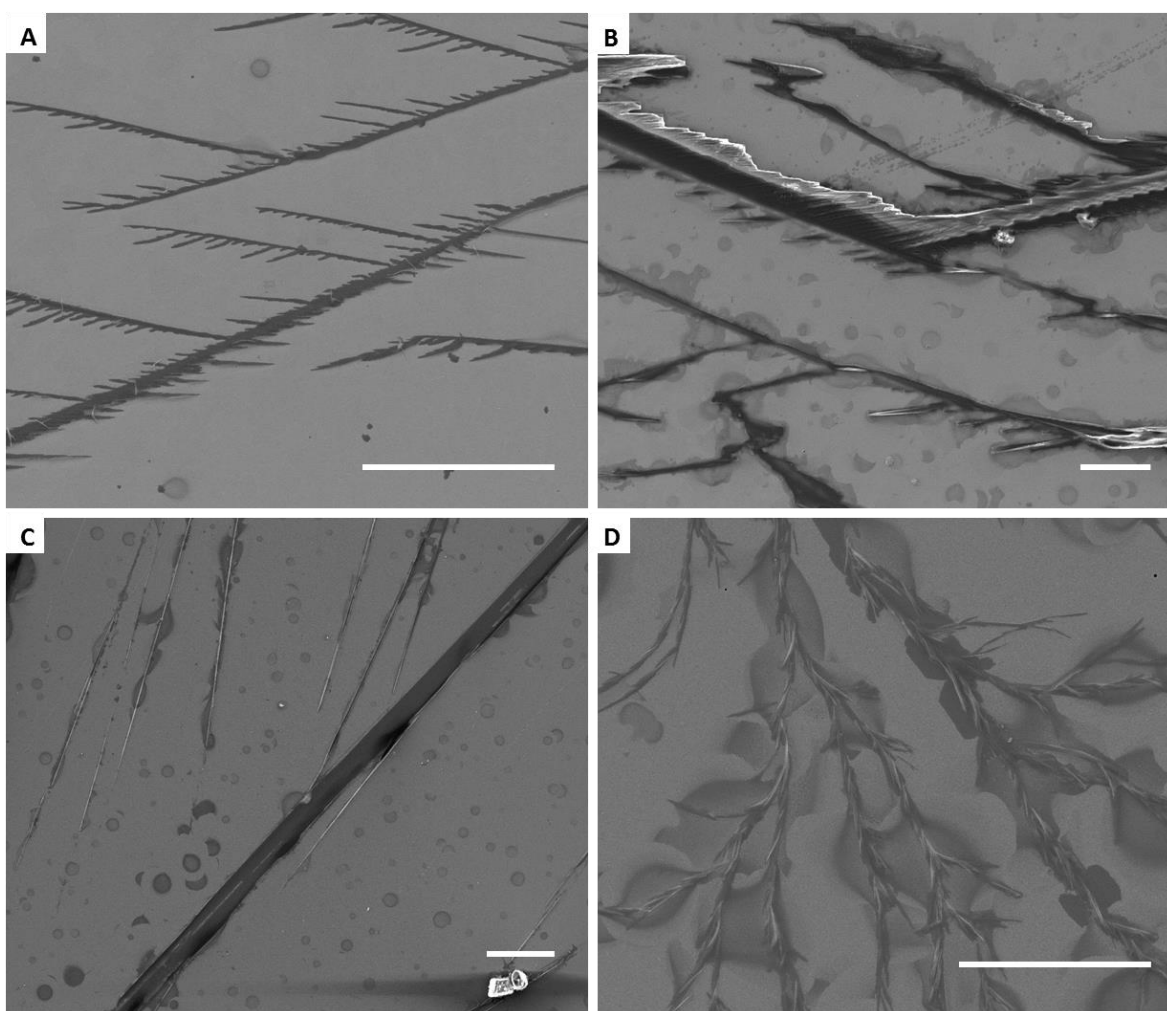
#### **6.2.2.2. Isopropanol series**

When isopropanol was evaporated slowly from solutions of phencyphos on monolayers of (+) PMT larger crystals were formed which appeared differently on the two types of metal substrate used (Figure 6.16).



**Figure 6. 16.** Reflection optical micrographs of crystals of phencyphos from isopropanol solution grown on (+) 4-methylthio-phencyphos monolayer under slow solvent evaporation. (A) (+) Phencyphos and (B) (-) Phencyphos crystals on monocrystalline gold. (C) (+) Phencyphos and (D) (-) Phencyphos crystals on polycrystalline gold.

On the smooth gold surface branched crystals are formed with a morphology and angles between the branches that are similar to those grown by fast evaporation of the same solvent. The crystals grown on the rougher gold are much larger (note the sizes of the scale bars in Figure 6.17), and are more perfect acicular objects with very high aspect ratio which run parallel to the metal surface. These large crystals are almost certainly a result of a very slow evaporation which results in few nucleation centres, a situation which is difficult to attain in the more volatile chloroform where small crystals are formed under otherwise identical conditions. The solvation of the surface could also be a factor, and though we have no direct evidence for this effect presently there is evidence in other systems where the medium interacts with self-assembled monolayers.



**Figure 6. 17.** SEM images of crystals of phencyphos from isopropanol solution grown on (+) PMT monolayer under slow solvent evaporation. (A) (+) phencyphos and (B) (-) phencyphos crystals on monocrystalline gold. (C) (+) phencyphos and (D) (-) phencyphos crystals on polycrystalline gold. Scalebar 30  $\mu\text{m}$ .

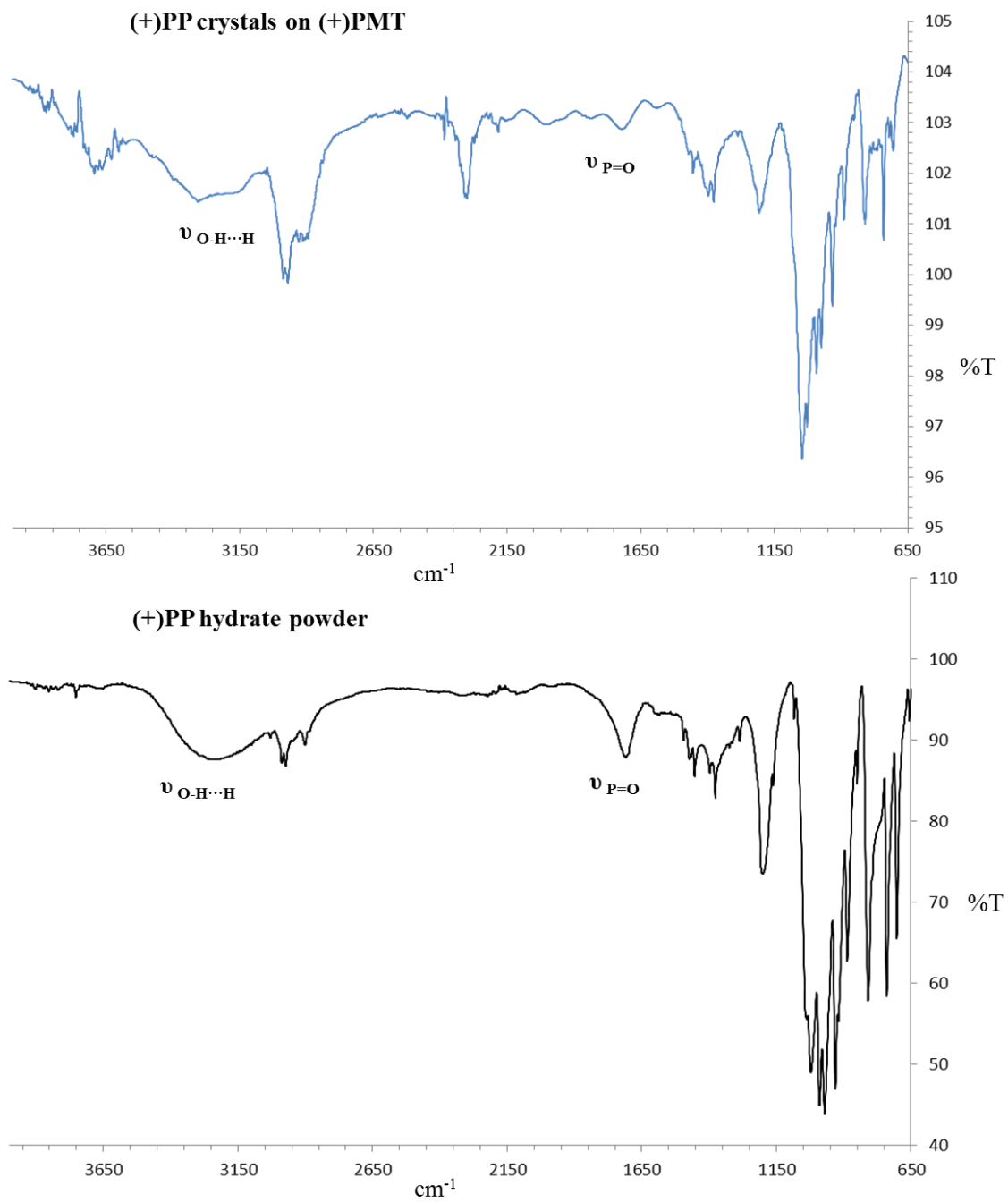
### 6.3. Infrared spectroscopy analysis

Infrared spectroscopy (IR) is a characterization technique chemists use to help determine the molecular structure. IR is based on the concept that functional groups absorb specific frequencies of energy based on their structure. When a functional group absorbs energy, it can vibrate in a bending or stretching mode and the characteristic energy for this vibrational mode is reported in wavenumbers ( $\text{cm}^{-1}$ ). A change in molecular dipole is required for a bending or stretching mode to be visible in by IR.

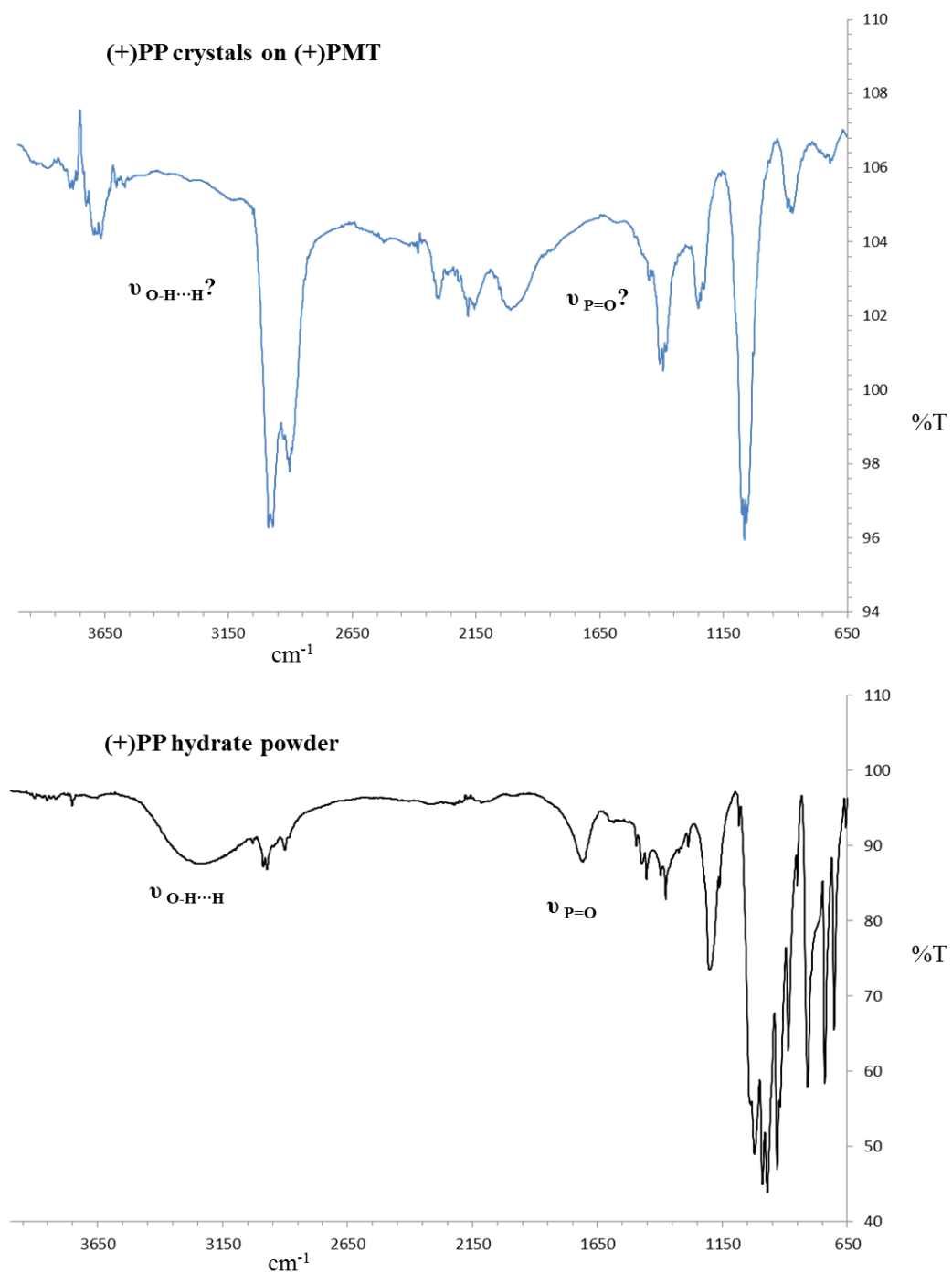
IR is a powerful technique, since it is very sensible to any bond change in the chemical structure of any compound, even can detect changes in the crystalline structures of a compound. IR was used to characterise the phencyphos crystals grown on SAMs presented above comparing them to the phencyphos initial powder.

(+) Phencyphos crystals, grown from chloroform solution on (+)-PMT monolayer on polycrystalline gold under fast solvent evaporation conditions are compared to (+) phencyphos hydrate powder. In the infrared spectra shown in the figure 6.18, both spectra have the tension of P=O ( $\nu_{\text{P=O}}=1700 \text{ cm}^{-1}$ ) of the -POOH group, and the tension of OH group ( $\nu_{\text{OH}}=3250 \text{ cm}^{-1}$ ) forming hydrogen bonds (O-H $\cdots$ H), they are the same compound.

The figure 6.19 compares the IR spectra of (+) Phencyphos crystals -grown from chloroform solution on (+)-PMT monolayer on polycrystalline gold under slow solvent evaporation conditions- to (+) phencyphos hydrate powder. The powder spectra has the tension of P=O ( $\nu_{\text{P=O}}=1700 \text{ cm}^{-1}$ ) of the -POOH group, and the tension of OH group ( $\nu_{\text{OH}}=3250 \text{ cm}^{-1}$ ) forming hydrogen bonds (O-H $\cdots$ H), nevertheless the spectra of crystals grown on SAMs missed these bands. They have mainly the same spectra except a few missed bands. As the crystal orientation could miss the IR bands, (+) phencyphos crystals grown on (+)-PMT SAMs could be highly orientated.



**Figure 6. 18.** (+) Phencyphos IR spectra comparison of crystals grown on SAMs under fast evaporation solvent and powder.



**Figure 6. 19.** (+) Phencyphos IR spectra comparison of crystals grown on SAMs under slow evaporation solvent and powder.

#### 6.4. Experimental section

The Scanning Electron Microscopy (SEM) was performed using FEI QUANTA 220F, voltage used 10kV and high vacuum conditions. The solvents used during the synthesis were purified using standard methods. Optical microscope used was Olympus RXSITRF in reflexion mode.

IR spectra were recorded on a Fourier transform Perkin Elmer, Spectrum One spectrometer. The solvents used were purified using standard methods.

##### **Protocol for crystallisation.**

The functionalised gold surfaces were immersed in solutions of either enantiomer of phencyphos in chloroform (10 mmol) or isopropyl alcohol (10 mmol) for 10 seconds. They were removed from their solution using tweezers and were placed in individual vials so that they lay as flat as possible. The solvent was either allowed to evaporate in a vial with a punctured cap or in a closed vial saturated with the vapour of the solvent used for the dissolution of phencyphos. The surfaces were left until the solvent was completely evaporated (no drops on surface), for the chloroform samples the period was approximately 4 days and 8 days for the isopropyl alcohol samples in the controlled atmosphere.

## 6.5. Conclusions

The successful functionalization of the gold substrate by a chiral thiol with a cyclic phosphate unit containing the stereogenic centre of the molecule provide with a chiral property to the self-assembled monolayer on gold. Chiral self-assembled monolayers on gold which can act as template layers for the heterogeneous nucleation and growth of a structurally related organic molecule from organic solvents. This effect arises despite the intrinsic supramolecular structural disorder and rigidity of the molecule in the monolayer. The nucleation is a result of the interaction between the acid groups of (+) PMT on the surface and those of the crystals of phencyphos being formed: We hypothesise that chains of hydrogen bonds are formed between the phosphoric acid in crystals of these compounds. The nature of the monolayer, coupled with evaporation rate and other solvent characteristics, influences the size distribution and morphology of the organic crystals that are formed.

The homogeneity of crystal size is influenced dramatically by the gold surface being used. The smooth monocrystalline gold surface is no match for the rougher gold on glass in terms of ability for heterogeneous nucleation from chloroform, presumably because it is the defects on the gold surface aided and abetted by the monolayer in that area which favour the nucleation, and the latter produces less polydisperse crystals for this reason.

Epitaxy, the coincidence of crystal surface periodicity with the periodicity of the SAM template, has been used to rationalize the formation of different crystals of varied compounds during crystallizations of this type. However, in the present case the monolayer template is disordered and there is little flexibility in between the anchoring sulphur atom and the phosphate group, and where the orientation of the groups must be understood as being random. All the same, the SAM has a determining influence on the nucleation and growth of the organic crystals formed from the organic solvent. This effect surely has to do with the wettability of the surface by the pre-nucleus, as inferred for the growth of an organic molecule on different polymer substrates. The phosphoric acid derivative used here is likely to improve wetting by polar compounds and is therefore interesting for the exploration of its further use in the heterogeneous nucleation of organic crystals. It is also interesting to speculate as to whether these surfaces might be useful for deracemisation processes.

# Chapter 7: Preparation of Micropatterned Surfaces

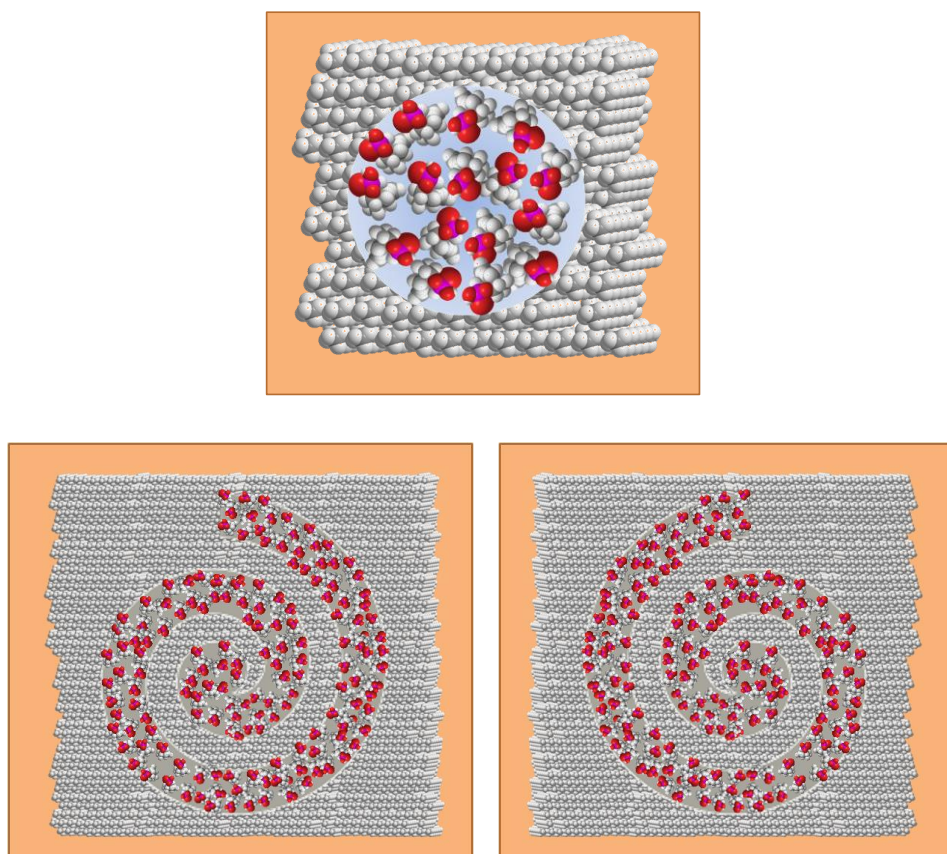
---

Microcontact printing is a powerful method for the preparation of micropatterned surfaces which are very suitable tools in the control of the crystallisation process on surfaces. This section describes this method, its optimisation and the characterisation techniques used.



## 7.1. Introduction

The aim of the research presented in this Chapter is to prepare patterned surfaces which contain chiral surface functionality, chiral surface patterns, and the combination of the two (Figure 7.1). None of these features has been targeted as such in the past, and therefore it is hoped that new effects may be discovered by exploring their properties in terms of ability to act as nucleants for chiral species. Specifically, these patterns will be used for the templating of crystals of chiral compounds (see following chapter), and the influence of the nature of the pattern on the nucleation and growth of the chiral crystals will be studied.



**Figure 7.1.** The three drawings represent a chiral surfactant (PMT) on a circle and on enantiomeric spirals - chiral features - in contrast to the achiral surfactants (grey molecules) around the features on surface (not drawn to scale).

Patterned surfaces are useful in a wide number of applications, including microelectronics where metal patterns are needed to delineate transistors and other electronic components,<sup>1</sup> studies on the assembly of biological materials,<sup>2</sup> and so on.<sup>3</sup> A number of hard lithographic techniques exist for the preparation of patterned surfaces, although these generally require quite aggressive chemical treatments yet with the advantage of chemical robustness. Soft lithographic techniques,<sup>4</sup> on the other hand, are a series of techniques which are particularly suitable for the patterning of molecules on surfaces whereby sensitive polyfunctional materials can be deposited in a relatively straightforward manner. In particular, microcontact printing was born from the need to have SAMs in controlled zones over the surface. It is important to note that this soft lithographic technique requires the use of “traditional” lithographic micropatterning techniques prior to its use.

Microcontact printing ( $\mu$ CP) is a very appropriate soft lithographic technique that can create patterned features of SAMs on both planar and non-planar surfaces.<sup>3</sup> The concept of this technique is very simple. An elastomeric stamp (polymethylsiloxane, PDMS) is fabricated by casting a pre-polymer of PDMS on a master (usually a treated silicon wafer) whose surface has been patterned with a complementary relief structure using photolithography. When carrying out  $\mu$ CP on gold, a PDMS stamp is wetted with an *ink* solution (1-10mM range) containing the thiol that will make up the feature and it is brought into contact with the surface of the gold substrate (Figure 7.2). The patterned gold substrate is immersed into a blocking thiol solution overnight.<sup>5</sup> The blocking region is usually inert to the application which is sought.

---

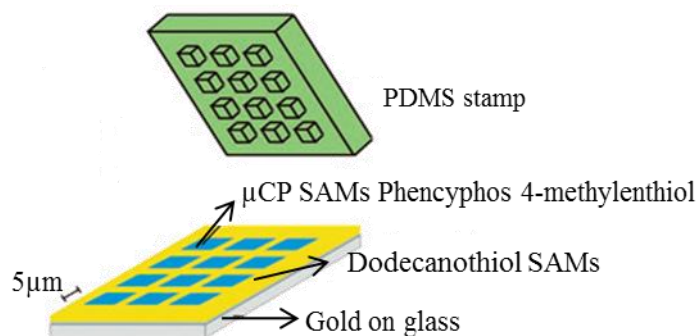
<sup>1</sup> P. Arjan, E. Quist, E. Pavlovic, S. Oscarsson, *Anal. Bioanal. Chem.*, **2005**, *381*, 591–600.

<sup>2</sup> (a) P. Zorlutuna, N. Annabi, G. Camci-Unal, M. Nikkhah, J.M. Cha, J.W. Nichol, A. Manbachi, H.J. Bae, S.C. Chen, A. Khademhosseini, *Adv. Mater.*, **2012**, *24*, 1782-1804. (b) M. Mrksich, G. M. Whitesides, *Trends Biotechnol.*, **1995**, *13*, 228–235.

<sup>3</sup> T. Kaufmann, B. J. Ravoo, *Polym. Chem.*, **2010**, *1*, 371–387.

<sup>4</sup> Y.N. Xia, G.M. Whitesides, *Angew. Chem. Int. Ed.* **1998**, *37*, 551-575.

<sup>5</sup> Y. Xia, G. M. Whitesides, *Langmuir*, **1997**, *13*, 2059-2067.



**Figure 7.2.** Representation of microcontact printing of a surface. Blue squares were printed using a PDMS stamp wetted with the desired ink solution (PMT in our case); yellow zone represent functionalisation with dodecanethiol monolayers (carried out in solution after the printing).

In relation to the wetting of a micropatterned surface by thiols of different nature, the wetting of each area can be different.<sup>6</sup> This feature means that solutions applied to the surface can be localised in certain regions, and molecular recognition processes can be restricted to them provided that the wetting is favoured because of the difference in polarity of the areas. Polar Regions have been mainly achieved through printing carboxylate terminated thiols in gold, amine terminated compounds, or oligoethylene oxide chains to favour wetting by polar solvents. On the other hand, hydrophobicity can be achieved with layers of long chain alkyl- or fluoroalkyl-thiols.

As stated at the start of these introductory comments (see also Figure 7.2), chiral thiols (used for the preparation of the SAMs in the previous chapters) will be patterned, to produce areas of different shapes with locally chiral chemical functionality. On the other hand, chiral patterns will be prepared which may, or not, have chiral chemical functionality upon them. In the case that the chemical functionality is achiral, then the patterns are enantiomeric. In the case that chiral surface modification is achieved, four diastereomeric systems are possible. Here, the formation of these patterns on gold is discussed.

<sup>6</sup> J. Aizenberg, A. J. Black, G. M. Whitesides, *Nature*, **1998**, 394, 868-871.

## 7.2. Optimising a microcontact printing protocol

The  $\mu$ CP method is a multistep process which needs certain tools that allow one to reach the final patterned surface: Firstly, a photo-mask for photolithography is required for the hard lithographic step to make the patterned silicon wafer master. This master is used to mould PDMS, which then peeled off the master and treated is inked and stamped onto a substrate. The final step introduces blocking solutions to fill in the space between features if necessary. The concept of the  $\mu$ CP is very simple; nevertheless, there are many parameters which affect the performance of each step and its reproducibility. They make it very hard to get a reproducible protocol. Many challenges were encountered while establishing the definitive protocol used in this thesis, all of them will be explained in detail in this Chapter, in sequential manner.

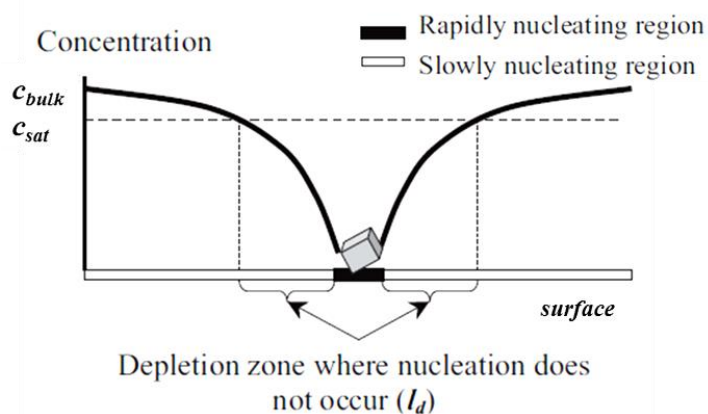
### 7.2.1. Mask design

The first step in the  $\mu$ CP method is the design and realisation of a photo mask, because it is this initial set of shapes which will end up patterned on the surface. The *photo-mask* is made of quartz, coated with a film which absorbs the light where the desired motifs are located. These motifs were designed taking into account a study which showed the importance of the size and the distance in between the motifs to favour the nucleation of inorganic compounds on them.<sup>7</sup> The idea is that the size of the motif and the distance in between should be proportional; the distance between motifs should be double of the diameter of the motif (in the dot case).

In 1999, Aizenberg and Whitesides described a good method to control the nucleation points over a micropatterned surfaces using thiols of different nature, to give polar groups and methyl groups terminating the surface in different regions. These SAMs were used for the crystallisation of Calcite from solution by diffusion of carbon dioxide through a solution of Calcium Chloride. They justified that there is a relationship between the size of the motif printed, its periodicity, with the *depletion zones* ( $l_d$ ) – which are the zones where nucleation does not happen. (Figure 7.3).

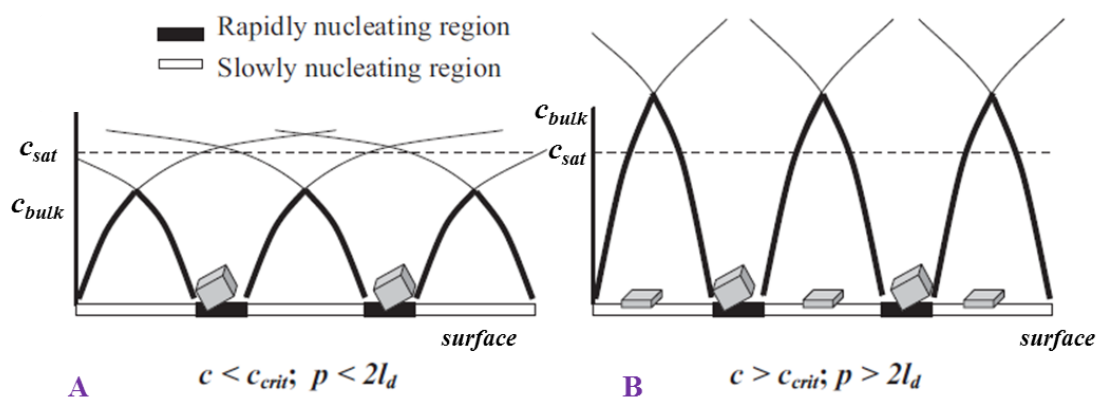
---

<sup>7</sup> J. Aizenberg, A. J. Black, G. M. Whitesides, *Nature*, **1999**, 398, 495-498.



**Figure 7.3.** Depletion zone in the crystallisation process from supersaturated solution on a functionalised surface. Depletion zones (*slowly*) are the double of nucleating zones (*rapidly*).<sup>8</sup>

The depletion zone is influenced by the diffusion and the flux of molecules over the functionalised surface. As soon as crystal growth begins in a polar region, mass transport to the growing crystals depletes over the local methyl-terminated region to the point of under saturation.<sup>8</sup> Thus, a micropatterned surface should be designed in order to have their motifs separated at least  $2l_d$ . In supersaturated conditions, the depletion zones are smaller (Figure 7.4.B) and therefore crystals appear in both slow and rapidly nucleating regions. In the case of under-saturated solution, the depletion zones are slightly bigger, the distance between two rapidly nucleating points is  $2l_d$ . (Figure 7.4 A).



**Figure 7.4.** Mechanism of localized crystal growth in (A) unsaturated solution and (B) highly supersaturated solution conditions.  $c_{sat}$ , saturated concentration (dashed line),  $c_{bulk}$  bulk concentration (bold line),  $p$  periodicity,  $l_d$  depletion zone..<sup>8</sup>

<sup>8</sup> J. Aizenberg, *Adv. Mater.*, **2004**, *16*, 1295-1302.

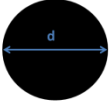
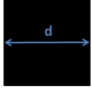

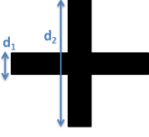
According to the preliminary experimental study in which noticed the best conditions of concentration were solutions close to supersaturation, it would be expected that the slow nucleating region would be the double of the rapidly nucleating region. Therefore, to design the photomask, the distance between the motifs should be double the motif size to obey this relationship.

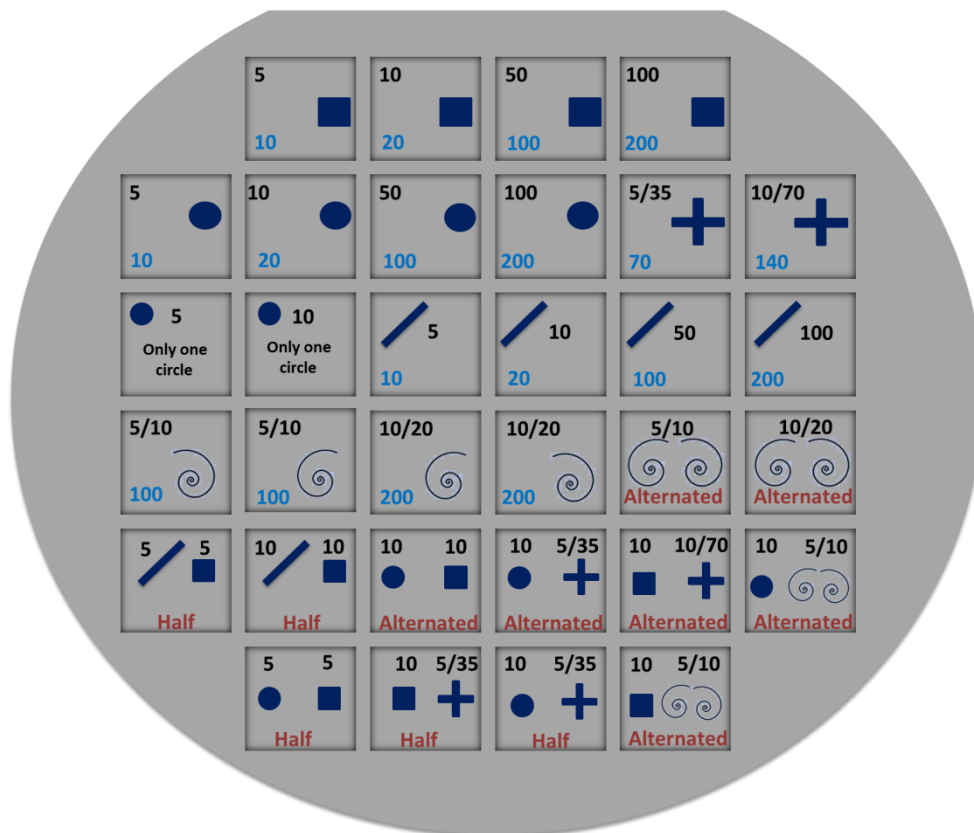
The mask design was done following these criteria and using the software *Clewin version 4.0*.<sup>9</sup> One of the aims of this work was to observe the influence of the motif shape and its size on the ability to template crystallisation, so, the mask design has different motif shapes and sizes in different areas. The varieties of shapes included in the mask are dots, squares, lines, crosses and spirals. The photomask was divided into 32 squares with an area of one square centimetre where the motifs are confined. These areas correspond to the stamps to transfer the design to the surface. Table 7.1 and Figure 7.5 show the motifs designed and their sizes.

---

<sup>9</sup> <http://www.wieweb.com/ns6/index.html>

**Table 7.1.** Sizes and distances of the shapes designed for the photomask.

Motif	D <sub>1</sub> / D <sub>2</sub> (μm)	Distance between motif (μm)
		
		
		
		
<b>Circles</b>	5, 10, 50, 100	10, 20, 100, 200
<b>Squares</b>	5, 10, 50, 100	10, 20, 100, 200
<b>Lines</b>	5, 10, 50, 100	10, 20, 100, 200
<b>Crosses</b>	5 / 35 ; 10 / 70	70, 140
<b>Spirals</b>	5 / 10 ; 10 / 20	100, 200



**Figure 7.5.** Mask design. Numbers in black correspond to the size (see table 7.1) and the numbers in blue the distance in between them. “*Alternated*” means that the repetition of the motifs over the square is alternate in the two perpendicular directions. “*Half*” means each motif fills half of the square.

The size and shape of the motif is very important because it could have a significant influence on the nucleation and the crystal growth processes as was

explained in the context of the depletion zones on a surface. For this reason, we decided to combine different motifs on the same square because it allows a direct comparison between different shaped patterns under identical conditions. Figure 7.6 shows the complete design of the photomask, with all the combinations, where each square of one square centimetre area is represented. The mask was fabricated by Photonics LTD (United Kingdom)<sup>10</sup> made in quartz of 5 inch size.

### ***7.2.2. Photolithography for preparation of Silicon Wafer Master***

The features on the photomask were transferred to a silicon wafer using photolithography. Photolithography is a process used in microfabrication to selectively remove parts of a thin film or the bulk of a substrate. In this method ultraviolet light is used to transfer a design from a photomask to a substrate, usually, silicon wafers. To carry out the process the silicon wafer is firstly covered with a photoresin (or photoresist) - a thin and uniform layer of organic copolymer sensitive to the ultraviolet light used in the process. The ultraviolet light passes through the non-metallised areas of the mask, generating the area-selective polymerisation (or degradation) of the photoresist according to the designed pattern on the mask. After the uncured polymer is removed, the cross-linked photoresist is used as an etch resist in the subsequent etching step of the substrate, yielding a patterned silicon surface.<sup>11,12</sup>

The silicon wafer master was made by the technical service of the Clean Room of the Barcelona Microelectronics Institute - National Centre of Microelectronics (IMB-CNM-CSIC) (Figure 7.6). They used the photomask to transfer the design by photolithography in silicon wafers. In the photolithographic fabrication process of the silicon wafer the first step is deposition of a photoresin on the silicon. In the second step the photomask is placed between a source of ultraviolet light and a thin layer of a photo-reactive polymer (the photoresin, also referred to as a photoresist, type HIPR-6512) that has been coated onto a silicon wafer or glass slide. Exposure to UV light transfers the pattern from the photomask to the polymer; the exposed photoresist is removed using an organic solvent, leaving behind the holes in the layer corresponding to the pattern. These holes are etched with reactive ion etching to create indents in the silicon and the

---

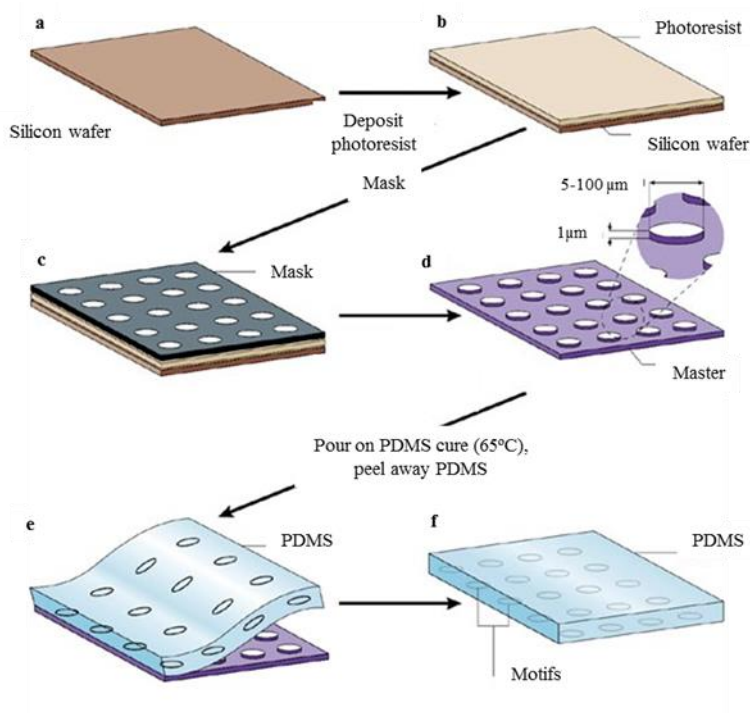
<sup>10</sup> <http://www.photonics.com/plab/photonics/>

<sup>11</sup> A. Perl, D. N. Reinhoudt, J. Huskens, *Adv. Mater.*, **2009**, *21*, 2257-2268.

<sup>12</sup> G. M. Wallraff, W. D. Hinsberg, *Chem. Rev.*, **1999**, *99*, 1801-1821.



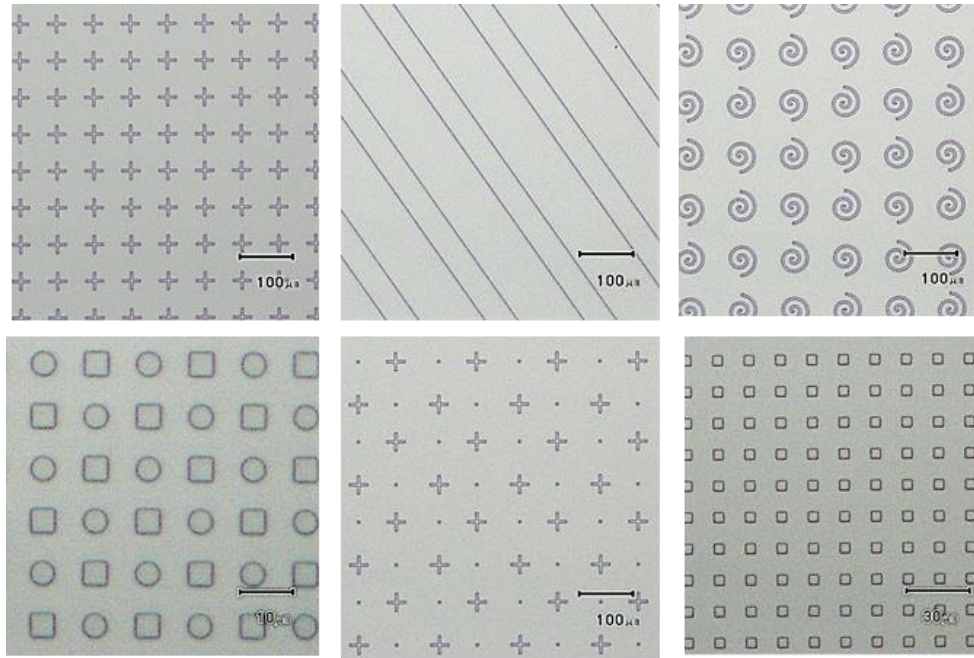
remaining resin is stripped. Figure 7.7 shows some of the different motifs formed on the silicon wafer after the photolithography treatment.



**Figure 7.6.** PDMS stamp preparation. Steps from a to d correspond to silicon wafer treatment to get the master for the PDMS stamp, the size of the motif in the combination on the master are from 5 to 100  $\mu\text{m}$ . Steps from d to f describe the PDMS preparation.<sup>13</sup>

Before the masters could be used, an anti-sticking layer had to be applied to prevent the strong adhesion of the PDMS to them. Thus, the masters were treated with 1H, 1H, 2H, 2H-perfluorooctyltrichlorosilane (PFOTS) 100  $\mu\text{l}$ , overnight by vapour deposition, which forms a siloxane based SAM on the oxide coat of the silicon. This lowered the adhesion of the wafer, and prevented the PDMS sticking to it. After the application of PFOTS, the wafers were cleaned by sonication in ethanol for 15 minutes. Once this process was done, it is necessary to prepare a first PDMS stamp to be discarded because the cured PDMS will remove the excess of the PFOTS that the ethanol could not dissolve. Finally, the master is ready to use.

<sup>13</sup> D. B. Weibel, W. R. DiLuzio, G. M. Whitesides, *Nature Reviews Microbiology*, **2007**, 5, 209–218.



**Figure 7.7.** Optical micrographs of several combinations of motifs on the silicon wafer after photolithography treatment.

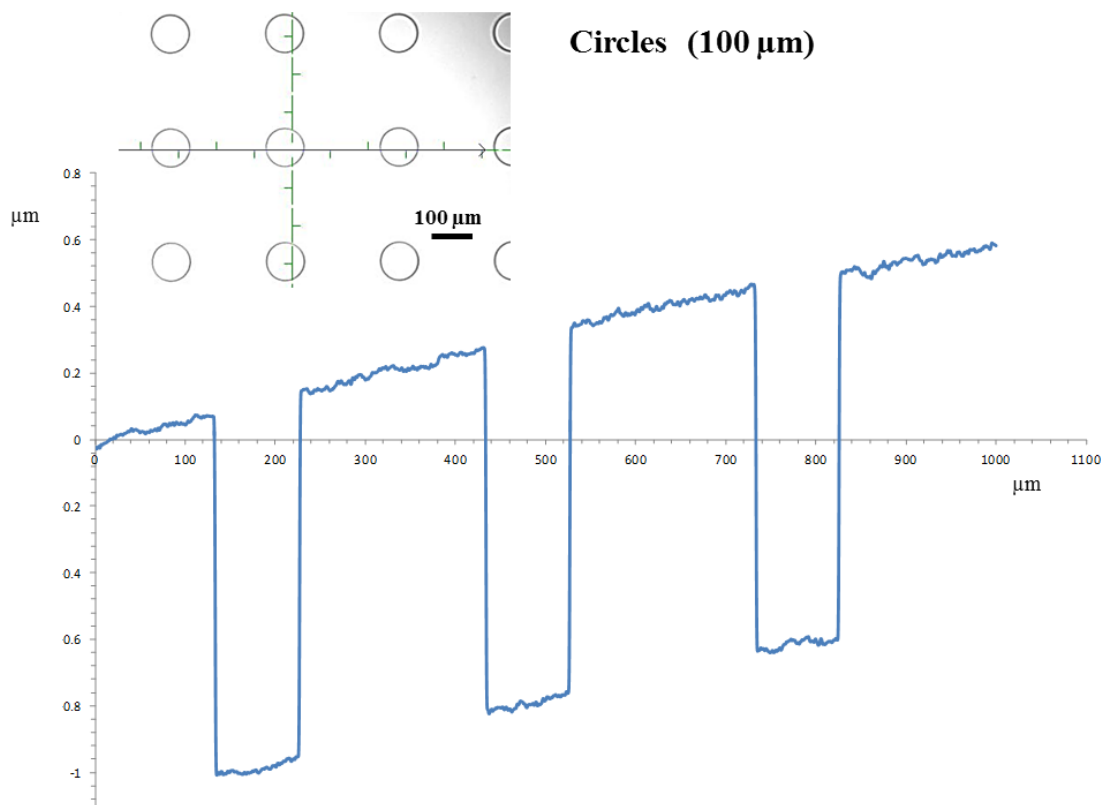


**Figure 7.8.** Photograph of a patterned silicon wafer.

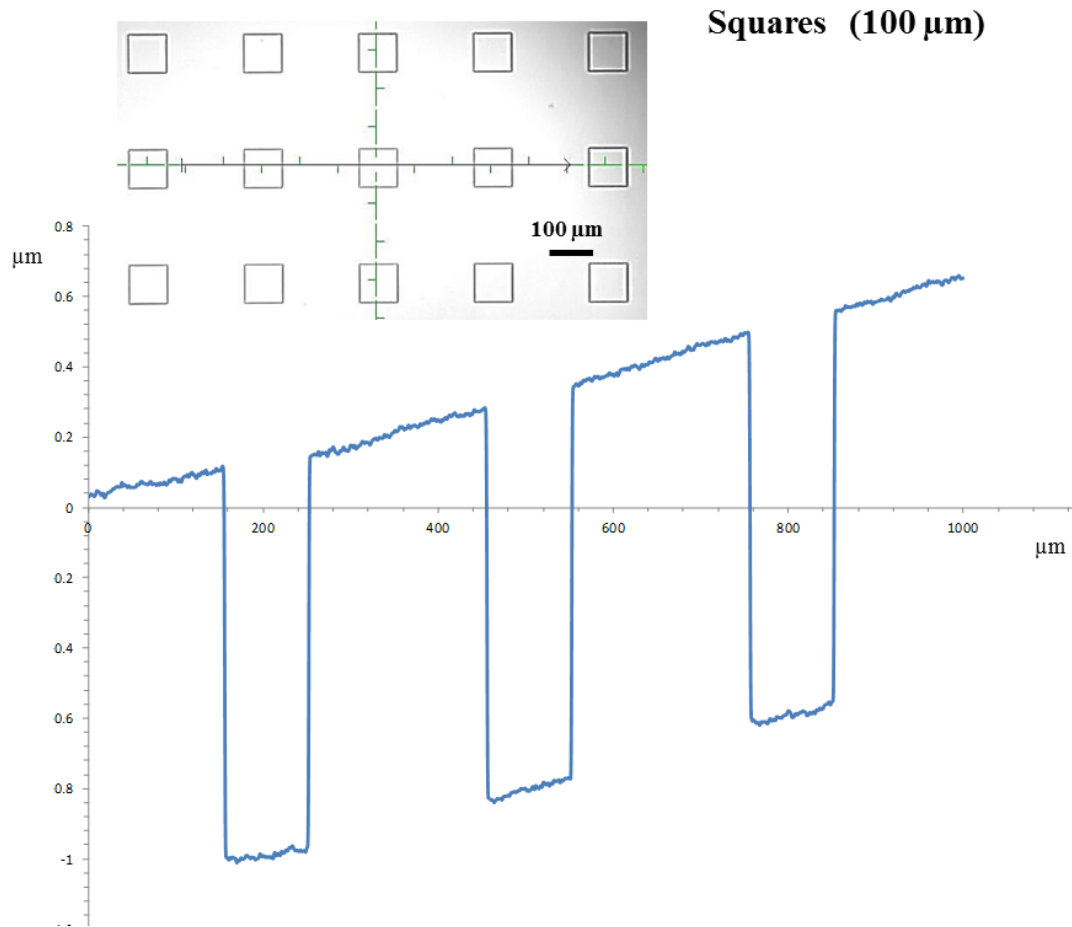
### 7.2.3. Profilometry

A profilometer is equipment designed to measure a surface's profile in order to quantify its roughness. The technique is similar to AFM (Atomic force microscopy) however a profilometer measurement is usually in contact along a line and over larger areas than those measured by AFM.

The profilometer used was P-16+ stylus profiler in the Clean Room of the Material Science Institute of Barcelona (ICMAB-CSIC). The profilometry study was carried out for the most representative motifs of the wafer designed in order to determine their roughness. These motifs are circles, squares, crosses and spirals. In the crosses case, the profilometry was done in two directions to measure the distances  $D_1$  and  $D_2$  (Table 7.1 and Figure 7.5).

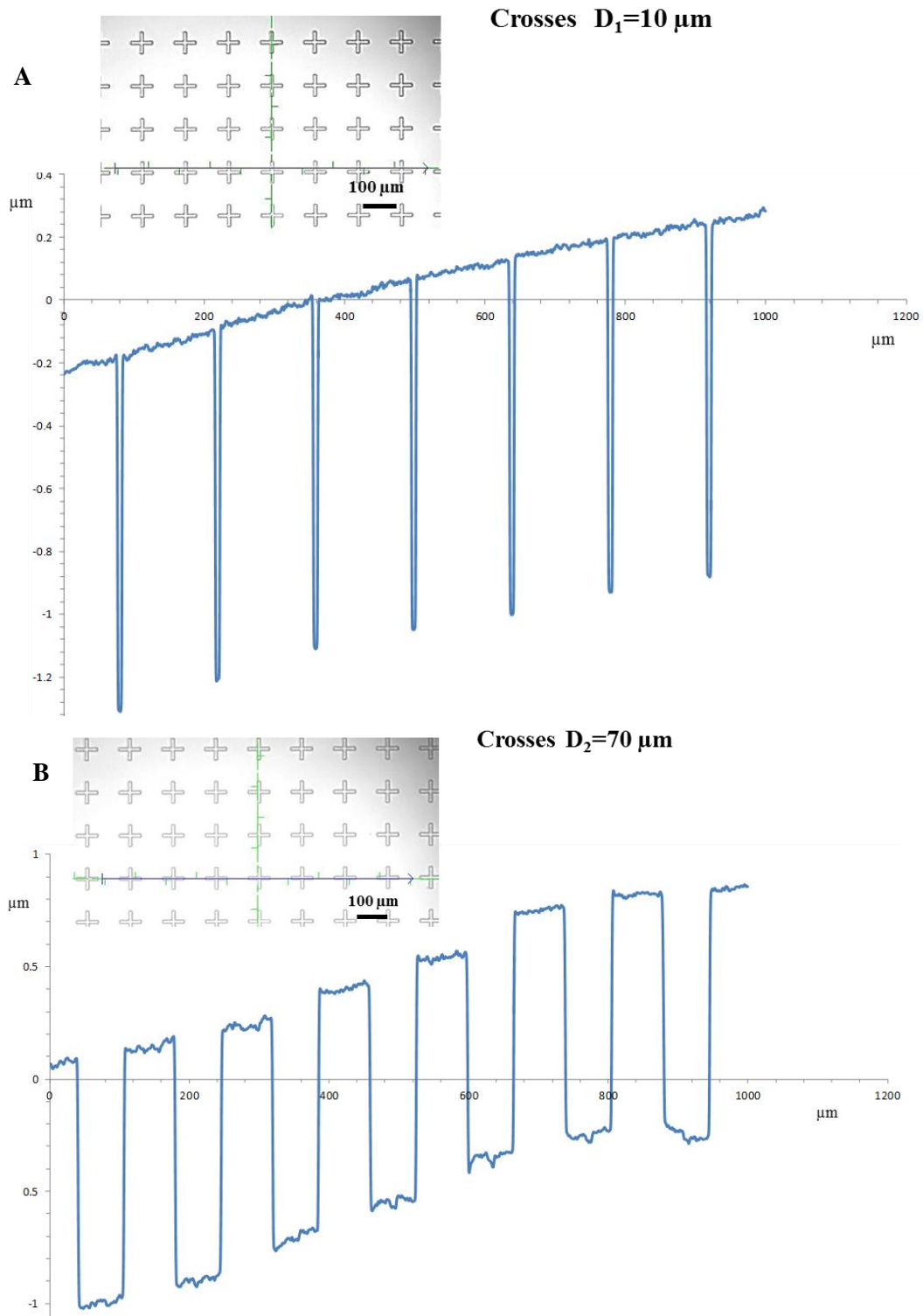


**Figure 7.9.** Profilometry of 100  $\mu\text{m}$  circles pattern spaced 200  $\mu\text{m}$  on silicon wafer. The depth of the motifs on silicon wafer is of 1  $\mu\text{m}$ .

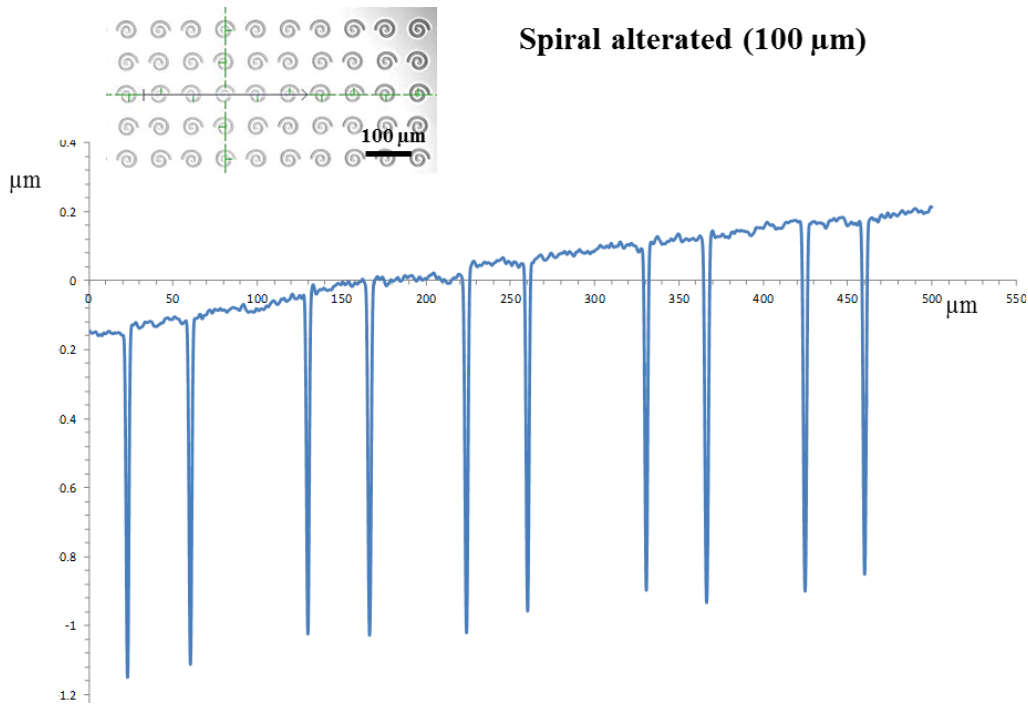


**Figure 7.10.** Profilometry of 100 $\mu\text{m}$  square pattern spaced by 200  $\mu\text{m}$  on silicon wafer. The depth of the motif on silicon wafer is of 1  $\mu\text{m}$ .

All the profile measurements have been represented as graphic relating topography and distances in  $\mu\text{m}$  (Figure 7.9, 7.10, 7.11 and 7.12). Every graph has this shape due to an intrinsic drift of the equipment.



**Figure 7.11.** Profilometry of 70µm cross pattern with spacing of 140 µm between centres on silicon wafer. (A) Measured along  $D_1=10\mu\text{m}$  width. (B) Measured along  $D_2=70\mu\text{m}$  long. The depth of the motif on the silicon wafer is of 1 µm.



**Figure 7.12.** Profilometry of 10 µm width spirals pattern with 100 µm between centres on a silicon wafer. The depth of the motif on silicon wafer is of 1 µm.

The profilometry study reveals the surface's topography of each motif measured. In the circle's case (Figure 7.9), the circle's diameter is 100 µm, and the distance between them is 200 µm, as in the photomask. For the square (Figure 7.10), the is 100 µm and the distance between them is 200 µm, as in the photomask.

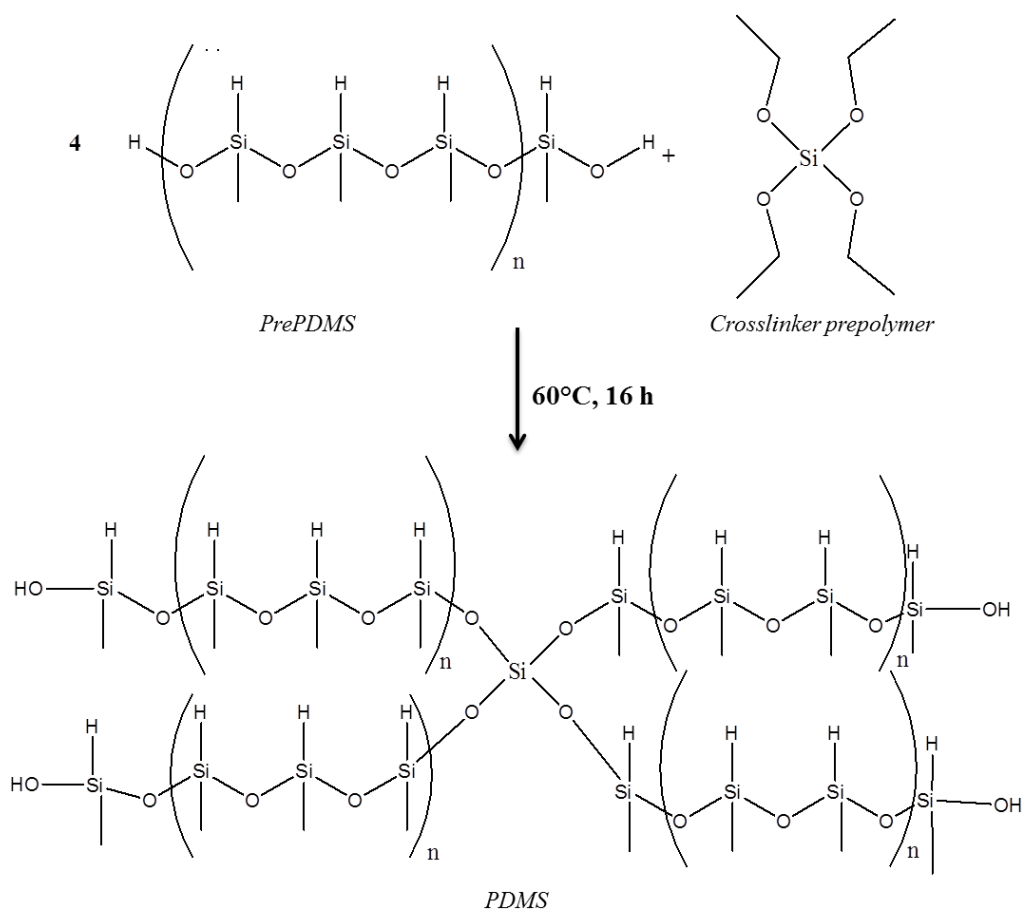
The cross' profile (Figure 7.11) has to be characterised in two directions; one measured along its small side ( $D_1$ ) and the other one along its long side ( $D_2$ ). Both graphics show the correct relationship designed in the photomask,  $D_1$  is 10 µm and the distance between is approximately 140 µm, while  $D_2$  is 70 µm and the distance between them is less than 140 µm, this is because 140 µm is from the motif geometrical centre to other motif geometrical centre.

The spiral profile (Figure 7.12) was characterised for the alternate spiral on the silicon wafer (see Figure 7.5, *Mask design*). The profile reveals the spiral's arcs (2 closer peaks), their width is of 10 µm and the distance between spirals is of 100 µm

(this distance is between the geometrical centres, in the middle of these two closer peaks). In all cases, the depth of the motif in the silicon wafer is of 1  $\mu\text{m}$ .

#### 7.2.4. Preparation of PDMS Stamps

Microcontact printing requires a patterned silicon wafer as template for the preparation of the stamps, made of a polymeric elastomer. The elastomer most widely used to transfer the design of the master to the substrate – and the one employed in this work – is poly(dimethylsiloxane) (PDMS). PDMS is a silicon-based crosslinked organic polymer, containing the  $-\text{Si}(\text{CH}_3)_2-\text{O}-$  structural unit.<sup>14,15</sup> It is a very flexible – the Young's modulus of a PDMS stamp is typically around 1.5 MPa – and weakly adherent material. The PDMS preparation follows the reaction scheme shown in Figure 7.13.



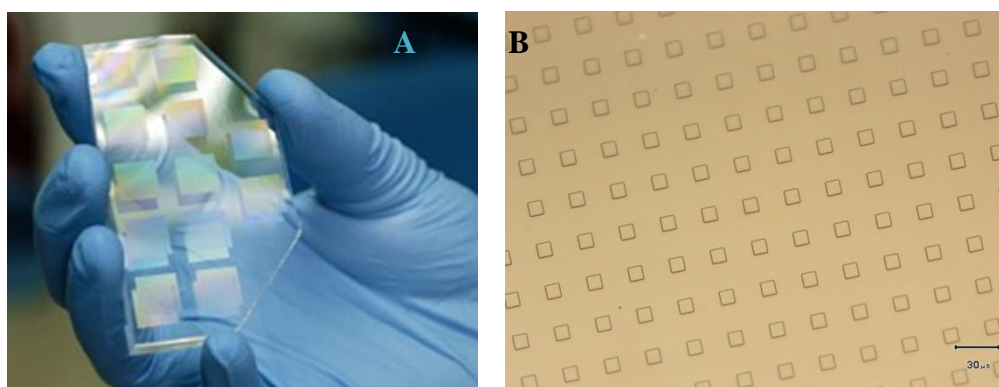
**Figure 7.13.** PDMS formation from precursors.<sup>16</sup>

<sup>14</sup> A. Perl, D. N. Reinhoudt, J. Huskens, *Adv. Mater.*, **2009**, *21*, 2257-2268.

<sup>15</sup> H. Schmid, B. Michel, *Macromolecules*, **2000**, *33*, 3042-3049.

<sup>16</sup> E. E. Hamurcu, B. M. Baysal, *Polymer*, **1993**, *34*, 5163-5167.

The PDMS stamps were made using a standard recipe. First, a 10:1 ratio of elastomer and curing agent (the commercially available two-component siloxane polymer Sylgard 184<sup>17</sup>, from Dow Corning) was mixed together. In the stamp preparation step, the liquid vinyl-terminated pre-polymer and the curing agent, which consists of a short hydrosilane crosslinker containing a platinum complex as a catalyst, were mixed and the mixture was poured onto the patterned silicon master template. The mixture was degassed in a vacuum dessicator for 30 to 40 minutes. When all bubbles were removed, the mixture was left in an oven at 60°C for 16 hours to cure the polymer, leaving a transparent solid but elastomeric material. The slab of PDMS could then be pulled off of the wafer, cut into pieces, oxidised using an UV-Ozone lamp, to obtain a more hydrophilic surface, and used for stamping. Once the PDMS is cured, the surface is hydrophobic; and polar ink solution would be repelled from it. Thus, oxidation of the stamp using a UV-O<sub>3</sub> lamp for 30-45 minutes yielding a hydrophilic surface which proved perfect for the polar ink solutions used. All functionalised gold surfaces were storage under an Argon atmosphere in a closed box.



**Figure 7.14.** (A) PDMS stamp photograph. (B) Optical micrograph of a PDMS stamp of 10  $\mu\text{m}$  squares pattern with spaces between them of 20  $\mu\text{m}$ .

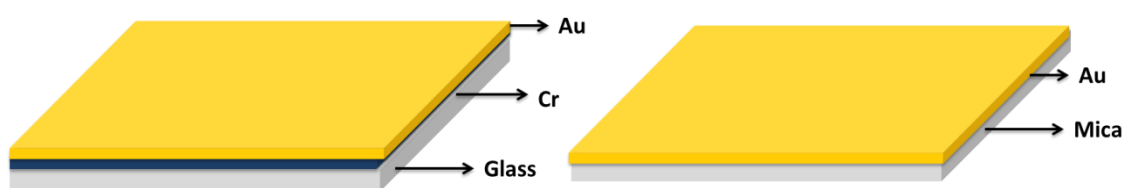
### **7.2.5. Substrates**

The substrates used in  $\mu\text{CP}$  should be mechanically robust to bear all the steps needed for the method and also chemically stable towards them. Polycrystalline gold on glass is a substrate which is mechanically robust because there is a Chromium layer between the gold and the glass which aides adherence of the noble metal (Figure 7.15): The metallic interlayer bonds the two materials very well. Contrarily, monocrystalline gold on mica substrate is less mechanically robust and stable towards  $\mu\text{CP}$  method. The

<sup>17</sup> <http://www.dowcorning.com>



problem with this substrate is in the layers of gold and mica, which do not bind very strongly together. Thus, in the step in which the PDMS stamp is removed from the substrate after the printing the gold is often detached from the substrate, yielding a substrate with an irregular monocrystalline gold layer patterned with monolayer. Thus the best substrate for the  $\mu$ CP method for our purpose is the polycrystalline gold on glass.

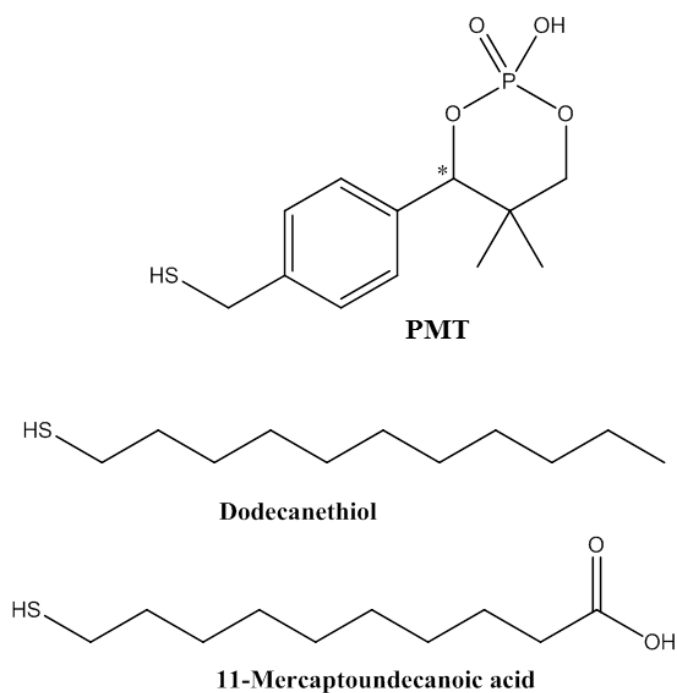


**Figure 7.15.** Polycrystalline gold on glass substrate (left) and monocrystalline gold on mica substrate (right).

### 7.3. Chemical Patterning with Thiols

The inking solutions for the stamps must contain chemicals which will not react with the stamp and which will bind well with the surface being patterned. Also, the solvent used to dissolve the surfactant should not deform or otherwise affect the elastomeric stamp. As the substrate used is gold, the ink solutions are of thiols in ethanol. Ethanol does not have a significant swelling effect on the PDMS<sup>18</sup> and wets well the activated surface. The thiols used for the microcontact printing are the shown in Figure 7.16.

<sup>18</sup> J.N. Lee, C. Park, G.M. Whitesides, *Anal. Chem.*, **2003**, 75, 6544-6554.

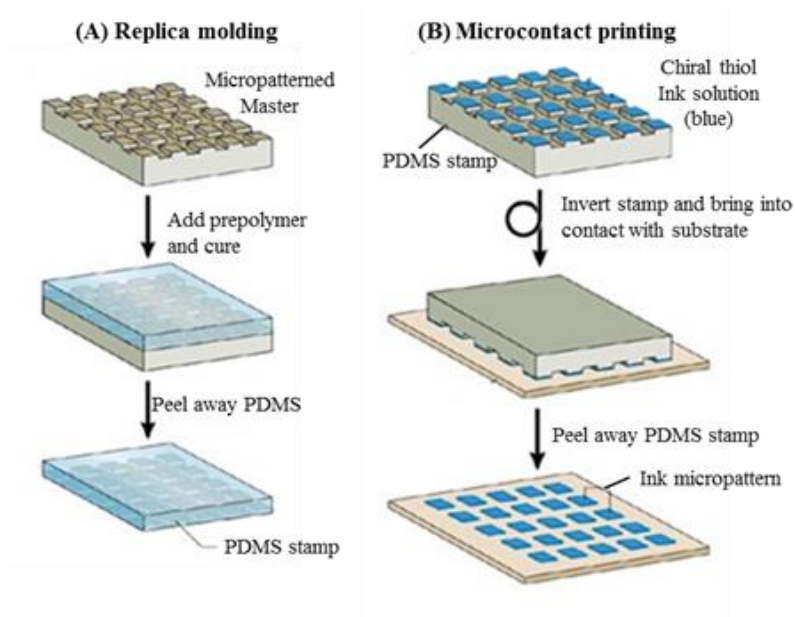


**Figure 7.16.** Selected thiol molecules used to functionalise the gold surface by microcontact printing method.

The solutions most used in this project were 4-methylthiophencyphos as inking solution and dodecanethiol as blocking solution. The principal reasons for using 4-methylthiophencyphos are its chiral nature, the expected chemical and geometric complementarity with the compound to crystallise onto it, favouring the heterogeneous nucleation.

#### 7.4. Microcontact printing Stamping Protocol and Patterning

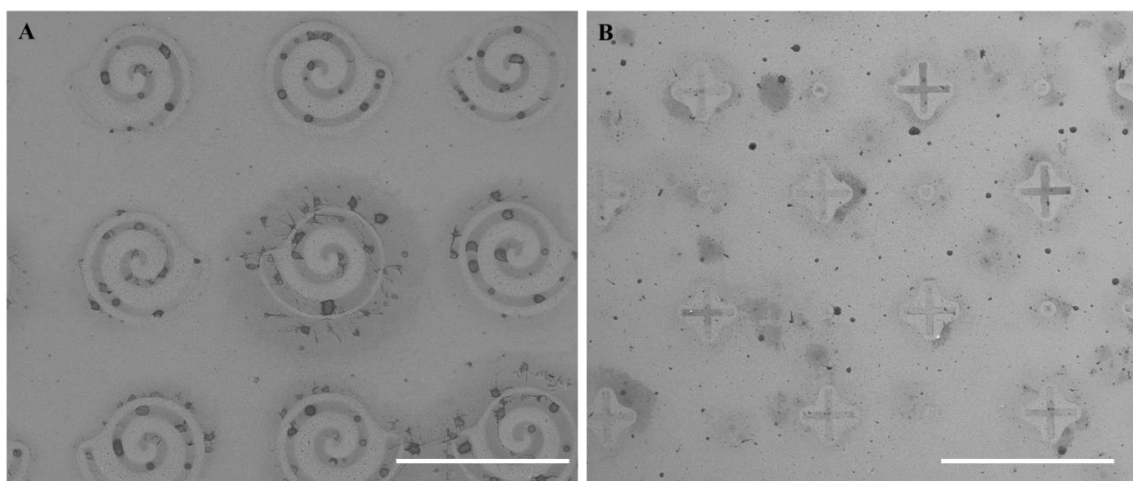
The  $\mu$ CP stamping method comprises a few crucial steps with several parameters that are very sensitive to small changes in terms of the quality of the final pattern. Firstly, the inking of the stamp is important, and printing can be performed with damp or dry inked elastomer. The time in contact with the ink solution used here varied from a few minutes (2-3 minutes) until 5 minutes, the amount used in every experiment was 50  $\mu$ l. The best time for most ink solutions proved to be 5 minutes. The concentration of the ink solution was varied from 0.1 up to 10 mM. The best concentration for most experiments was 1 mM.



**Figure 7.17.** (A) PDMS stamp preparation (B) Microcontact printing method.<sup>7</sup>

The drying of the stamp was achieved with spurts of nitrogen from a compressed gas pistol. It is preferable to keep the stamp slightly wet to make the transfer from the PDMS to the gold surface easy.

In the printing step, the amount of pressure applied to the object is also very important. In preliminary experiments, this step was performed using pressure, although, depending on the shape of the pattern to print, this pressure affects more or less the result. Thus, for circles and squares it is possible to use pressure in this step. However, for crosses and spirals the use of pressure has a detrimental effect on the pattern (Figure 7.18). The printing step should be quick and in one movement, otherwise the pattern will be doubled on surface, due to the chemisorption taking place very fast. The optimal time for this step is 10 minutes.



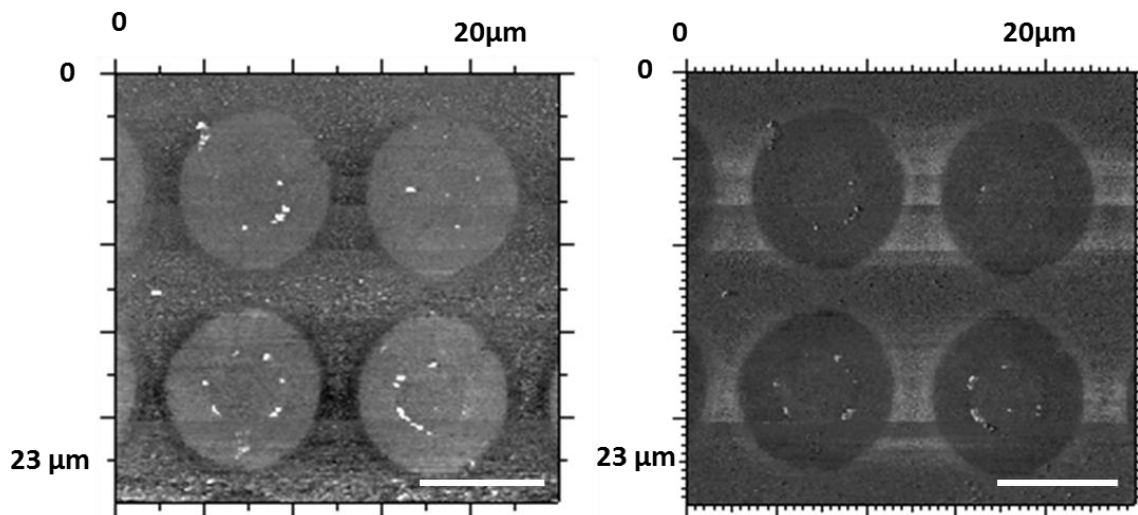
**Figure 7.18.** (A) Spiral 50x100  $\mu\text{m}$  pattern (PMT) on polycrystalline gold surface. (B) Crosses 35x70  $\mu\text{m}$  pattern (PMT) on polycrystalline gold surface, both after a Phencyphos crystallisation experiment (Chapter 8.1). Scale bar 100  $\mu\text{m}$ .

After these steps, the substrate should be washed with ethanol and dried using the nitrogen gun. Every patterned surface was then immersed into the blocking or filling solution (in that it can either be viewed as a SAM which blocks the underlying gold, or merely fills in the space) overnight under argon, to avoid the oxidation of the thiol by atmospheric oxygen during the formation of the SAM. It is important to note that this final step produces a SAM around a printed region, and that the result of performing the printing is not necessarily the same as the formation of a SAM, the density of functional groups can be different in each case.

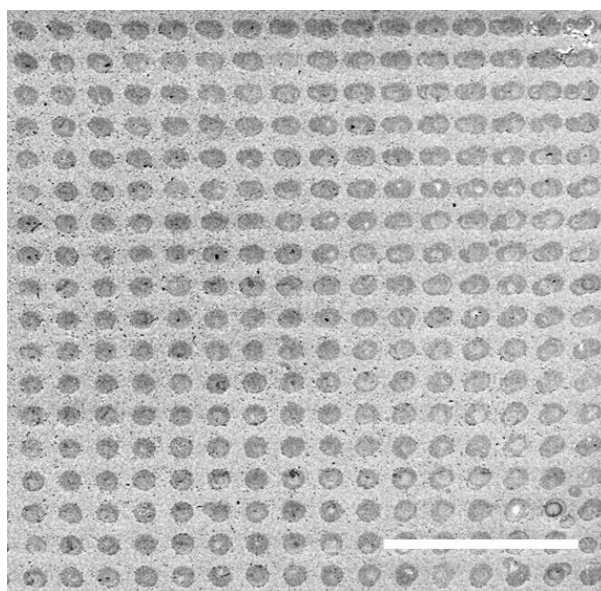
In summary, the protocol followed in all the experiments presented in this work was the following.

1. PDMS oxidation using an UV-O<sub>3</sub> lamp, 30-45 minutes.
2. 50  $\mu\text{l}$  of ink solution 5 minutes on the PDMS stamp.
3. Dry PDMS stamp using 3-4 shoots with a nitrogen gun.
4. Printing step: PDMS stamp in contact with the substrate, 10 minutes. (extra pressure was no added)
5. Wash the substrate and time in the blocking/filling ethanolic solution overnight under argon.

Once the gold surface was functionalised, characterisation of the patterns was achieved by Atomic Force Microscopy (AFM) and Scanning Electron Microscopy (SEM). The micrographs obtained using these microscopes are shown in Figures 7.19 and 7.20.



**Figure 7.19.** AFM images of a micropatterned surface by dots of 5  $\mu\text{m}$  of (+)-4-methylthiophenylphosphine and dodecanethiol around. Topography (left) and phase (right). Scale bar 5  $\mu\text{m}$ .



**Figure 7.20.** SEM micrographs of a micropatterned surface by circles of 5  $\mu\text{m}$  of (+)-4-methylthiophenylphosphine and dodecanethiol around. Scale bar 50  $\mu\text{m}$ .

The AFM micrographs show the different nature of the two thiols terminal groups on surface. The phase image shows this difference more clearly, and the topography one shows the difference between heights. The two thiols are very similar in height, although they have very different structure. This feature is because the alkanethiol (dodecanethiol) molecules pack adopting linear arrangements of the chain (all *trans* conformation) with an angle of 30° to the gold surface. This inclination means that it has a similar height to an “upright” (+)-4-methylthiohencyphos.

SEM microscopy is a useful method for observing patterned surfaces with areas of different polarity. The alkylthiols terminated areas have lighter contrast than those formed by the (+)-4-methylthiohencyphos, presumably because the charge is dissipated more easily in the latter areas. The SEM micrograph for one dot patterned surface sample (Figure 7.7) shows a zone where there are two circles superimposed, where there should be just one. This phenomenon happens when the stamp is moved during the printing step.

In the laboratory, a way to check whether the  $\mu$ CP had proceeded correctly or not was to add a drop of water over the surface and observe it using the optical microscope. If the meniscuses shape change, usually adopting the shape of the pattern, so, if the pattern is circles, the meniscus would change from a one curve (typical shape of the drop) to smaller curves along the drop. Following this simple experiment, we can be sure about the functionalization of the surface without using AFM or SEM microscopes for each substrate functionalised.

## **7.5. Conclusions**

Micropatterned gold surfaces combining thiols provide a very suitable method to achieve controlled crystallisation process. In contrast to the SAMs on whole surface, this method favours the mass transport to the desired thiol, minimizing evaporation effect at small scale. The surface combination of PMT and dodecanethiol has been the key for the development of surfaces which can induce the nucleation process on surface.

A profilometry study revealed the correct relationship conservation in the silicon wafer motifs designed in the photomask. In all cases, the deep of the motif in the silicon wafer is of 1  $\mu$ m.

The gold substrate more suitable for the microcontact printing process is the polycrystalline sample due to present high resistance in the handling steps (washing, etc.).

Microcontact printing is a very simple method to prepare a combined functionalised surface; nevertheless, the optimization of each step in the protocol is very sensible to any effect. This is the main experimental part which has to be very well optimized. Once it is optimized, the microcontact printing becomes a routine method. The more complicated pattern types (cross and spiral) may require further etching in order to produce a cleanly patterned surface. The dots and squares of the same height transfer the inking solution very well to the gold surface.

# Chapter 8:

## Micropatterned surfaces as templates for crystal growth

---

Micropatterned surfaces are used to favour heterogeneous nucleation of organic compounds. This chapter describes the study of three main crystallisation systems, two of them in which the controlled crystallisation has been achieved (Phencyphos and diastereomeric salt) and another one where homogeneous nucleation interferes negating the heterogeneous nucleation.

Part of this work has been submitted to:

A. Bejarano-Villafuerte<sup>a</sup>, M. Lingenfelder<sup>a</sup>, M. van der Meijden, R.M. Kellogg, D.B. Amabilino, *Chemical European Journal*.



## Introduction

The controlled growth of crystals of organic compounds on surfaces is an area of increasing interest because of the many fundamental questions it may answer as well as for the many applications it may have.<sup>1</sup> The possibility to control crystallization processes using self-assembled monolayers (SAMs) is an increasingly interesting and promising approach for the selective growth of ordered organic materials.<sup>2</sup> This control has been achieved to some degree by the use of inorganic crystalline substrates where nucleation is induced via epitaxy, although organic single crystals and SAMs have been used to control the polymorphic<sup>3</sup> selectivity of the compound to crystallize, which is apparently based on the lattice match between the molecular cluster and crystalline substrate terraces.<sup>4</sup>

The control of homogeneous nucleation is difficult on a small scale, as it is a stochastic process requiring high supersaturation and the activation energy barrier for the nucleation event is relatively high.<sup>5</sup> In principle, it is possible to reduce this energetic barrier and to favour nucleation using substances or surfaces where the growing nucleus can be anchored and act as a point of growth for the nascent crystal.<sup>6</sup> Indeed, SAMs have proven their ability to act as nucleation points in a number of chemical systems, both inorganic<sup>7</sup> and organic.<sup>8</sup>

Myerson and co-worker have used SAMs to control of crystallization process of organic compounds from aqueous solution in order to study the surface's influence on growth and have demonstrated the influence that the layers have on the polymorphs which crystallize.<sup>9</sup> Spatial segregation of two types of monolayers, with different polarities, on the same surface makes it possible to induce mass transport which aids the crystallization process.<sup>10</sup> The microcontact printing method is a suitable way to control

<sup>1</sup> D. H. Dressler, Y. Mastai, *Chirality*, **2007**, *19*, 358-365.

<sup>2</sup> K. Kim, A. Centrone, T. A. Hatton, A. S. Myerson, *Cryst. Eng. Comm.*, **2010**.

<sup>3</sup> R. Hiremath, J. A. Basile, S. W. Varney, J. A. Swift, *J. Am. Chem. Soc.*, **2005**, *127*, 18322- 18327.

<sup>4</sup> (a) C. J. Stephens, Y. Kim, S. D. Evans, F. C. Meldrum, H. K. Christenson, *J. Am. Chem. Soc.*, **2011**, *133*, 5210–5213. (b) J. Aizenberg, *Bell Labs Technical Journal*, **2005**, *10*, 129–141.

<sup>5</sup> N. Erdemir, A. Y. Lee, A. S. Myerson, *Acc. Chem. Res.*, **2009**, *42*, 621-629.

<sup>6</sup> (a) A. Y. Lee, A. Ulman, A. S. Myerson. *Langmuir*, **2002**, *18*, 5886-5898. (b) D. J. Turnbull, *Chem. Phys.* **1949**, *18*, 198.

<sup>7</sup> J. Aizenberg, A. J. Black ; G. M. *Nature*, **1999**, *398*, 495-498.

<sup>8</sup> A. Y. Lee, I. S. Lee, A. S. Myerson, *Chem. Eng. Technol.* **2006**, *29*, 281-285.

<sup>9</sup> K. Kim, A. Centrone, T. A. Hatton, A. S. Myerson, *Cryst. Eng. Comm.*, **2011**, *13*, 1127.

<sup>10</sup> R. B. A Sharpe, *Controlling mass transport in microcontact printing*, **2005**, University of Twente, the Netherlands (ISBN: 90-356-2320-6).

the patterning of these different areas.<sup>11</sup> This method has been used successfully to generate layers upon which the crystallization of inorganic substances, such as the calcite,<sup>5</sup> and organic substances, such as glycine<sup>7</sup> and amino acids<sup>4</sup> can be achieved.

Mastai and co-workers<sup>12</sup> and Nakanishi et al.<sup>13</sup> have shown the separation of enantiomers from aqueous solutions on SAMs, although the generality of the approach is not evident. For example, Myerson's group showed that for valine crystallization at equilibrium on SAMs the enantiomer formed at the monolayer surface depended on the one that was in excess in the crystallizing system,<sup>14</sup> although separation was achieved with reversal with respect to the monolayer from racemic mixtures in line with observations in conceptually similar systems.<sup>15</sup> Be that as it may, in the long term, it should be possible that a surface functionalized with a resolving agent could provide a preferential template to get chiral recognition and favour the nucleation on it of one enantiomer in a conglomerate.<sup>16</sup>

Growing crystals on surfaces from volatile organic solvents presents considerable challenges. The wetting behaviour on the surface is completely different to water, because of the high surface tension of the latter. The evaporation rate of a solution has a great influence on the nucleation process and the crystal growth, and so the phenomena taking place during the evaporation of volatile organics are particularly hard to control.

Here, we show the heterogeneous nucleation and the crystal growth of enantiomerically pure compounds and diastereomeric salts from solutions in different solvents upon patterned SAMs. The control of the evaporation rate allows remarkable effects to be seen in the growth of the crystals, which are far more monodisperse than those grown in uniform monolayer systems.<sup>17</sup>

---

<sup>11</sup> Y. Xia, G. M. Whitesides, *Angew. Chem.*, **1998**, *37*, 550-575.

<sup>12</sup> D. H. Dressler, Y. Mastai, *J. Colloid Interface Sci.* **2007**, *310*, 653-660.

<sup>13</sup> J. Nakanishi, T.; Bannob, N.; Matsunaga M.; Asahi, T.; Osaka, T. *Colloids Surf. A: Physicochem. Eng. Aspects* **2006**, *284-285*, 270-275.

<sup>14</sup> A. Singh, A.S Myerson, *J. Pharm. Sci.* **2010**, *99*, 3931-3940.

<sup>15</sup> (a) L. Addadi, J. Vanmil, M. Lahav, *J. Am. Chem. Soc.* **1981**, *103*, 1249-1251. (b) L. Addadi, S. Weinstein, E. Gati, I. Weissbuch, M. Lahav, *J. Am. Chem. Soc.* **1982**, *104*, 4610-4617.

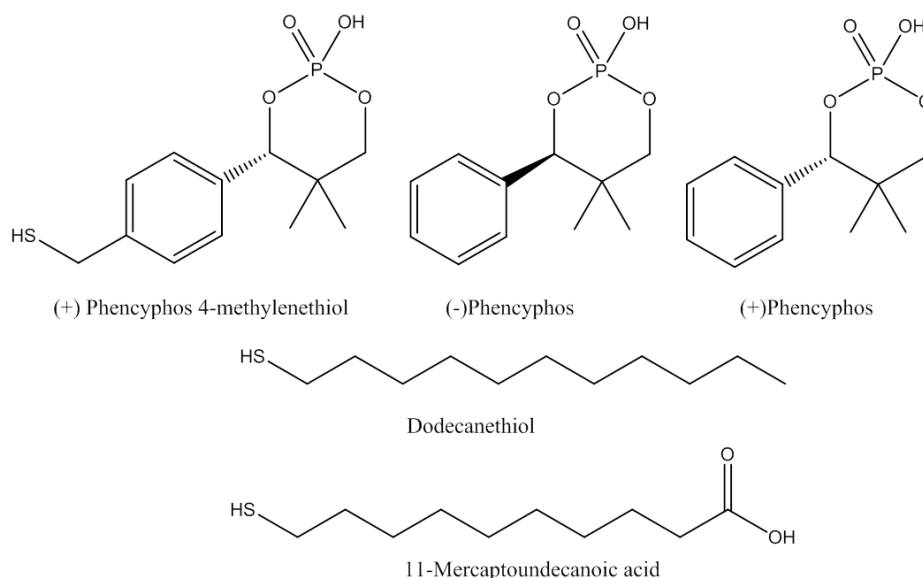
<sup>16</sup> M. Ejgenberg, Y. Mastai, *Chem. Commun.*, **2011**, *47*, 12161-12163.

<sup>17</sup> A. Bejarano-Villafuerte, M. van der Meijden, M. Lingfelder, K. Wurst, R.M. Kellogg, D. B. Amabilino, *Chem. Eur. J.*, 2012, *18*, 15984-15993.

## 8.1. Preferential phencyphos crystallisation on micropatterned surfaces

### 8.1.1. Introduction

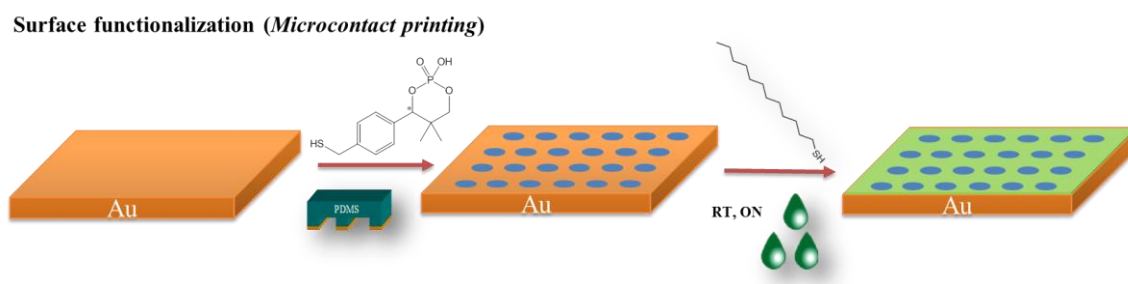
In this section the crystallization of enantiopure phencyphos compounds on micropatterned gold surfaces is described. We chose the chiral enantiopure thiol (+) phencyphos-4-methylenethiol ((+)-PMT) for the polar region, in which the phosphoric group should be directed away from the surface mainly because of the attachment of the thiol group to the underlying metal. We selected phencyphos – a compound with chemical similarity to (+)-PMT and which is a resolving agent for chiral amines<sup>18</sup> – to grow on the monolayer of (+)-PMT because one might expect the formation of non-covalent bond formation between the acid moieties. This hypothesis seems valid, because crystal growth is shown to follow the template pattern of the full monolayer. The compounds used are shown in the following Figure 8.1.1:



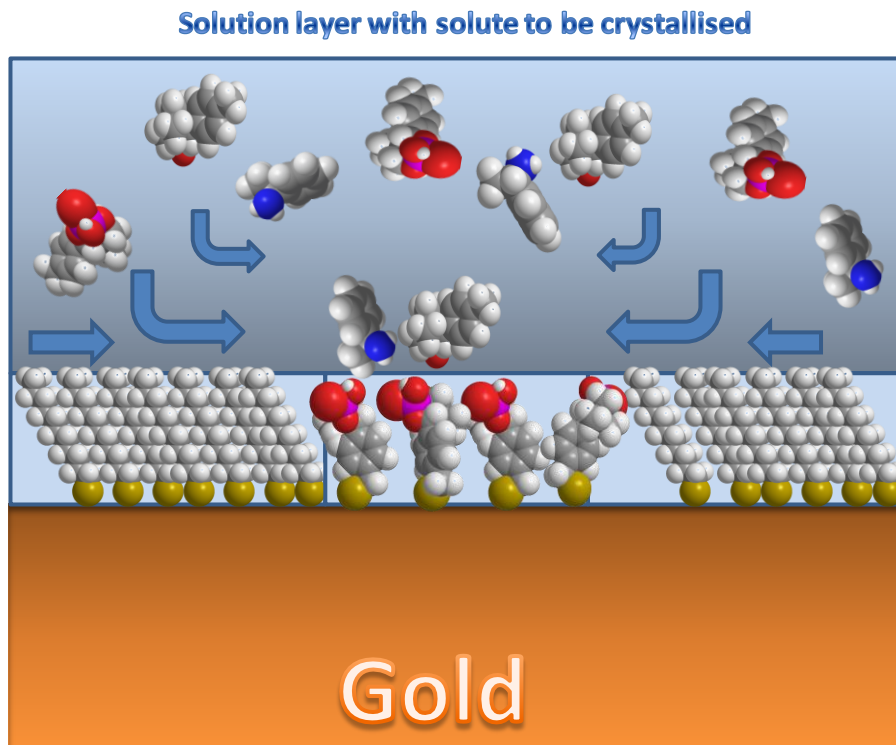
**Figure 8.1.1.** Compounds to crystallise and thiols selected to functionalise the gold surface.

<sup>18</sup> (a) Leeman, M.; Querniard, F.; Vries, T.R.; Kaptein, B.; Kellogg, R.M. *Org. Proc. Res. Dev.* **2009**, *13*, 1379-1381. (b) Nieuwenhuijzen, J.W.; Grimbergen, R.F.P.; Koopman, C.; Kellogg, R.M.; Vries, T.R.; Pouwer, K.; van Echten, E.; Kaptein, B.; Hulshof, L.A.; Broxterman, Q.B.; *Angew. Chem. Int. Ed.* **2002**, *41*, 4281-4286.

This study is focussed on crystallisation at the interface between a solution and a monolayer. In the case of micropatterned surfaces there are two monolayers in contact with the solution; they are (+)-PMT or 11-mercaptopundecanoic acid (MUA) and dodecanethiol in the experiments performed here. The nature of the surface contrasts in that there are very polar and non-polar regions. The surface functionalization was explained in detail in the Chapter 7, the process is reviewed in Figure 8.1.2. The micropatterned surface with these thiols should induce mass transport to the desired regions as is shown in Figure 8.1.3.



**Figure 8.1.2.** Microcontact printing protocol for the preparation of patterned surfaces. Each arrow includes a washing step using ethanol.



**Figure 8.1.3.** A representation of mass transport from a solution of components of the diastereoisomeric salt to be crystallised on micropatterned regions of PMT and the blocking monolayer of alkane thiol around, where nucleation cannot take place because of poor wetting.

The study of the crystallization of enantiopure phencyphos on the micropatterned surfaces involved several crystallization protocols. Each crystallization method was designed in order to probe different effects with the objective of achieving a better understanding of the crystallization process on the surface. Figure 8.1.4 shows the different crystallization methods. These crystallization protocols are explained in detail subsequently in this section.

### 8.1.2. Crystallization methods

Each crystallization method was designed in order to evaluate the importance of the different effects at play during the nucleation and growth processes and to achieve a better understanding of the diastereomeric salt crystallization process on a surface. As stated previously, the parameters studied have been done following a slow solvent evaporation method in order to control the approach to supersaturation thereby allowing mass transport.

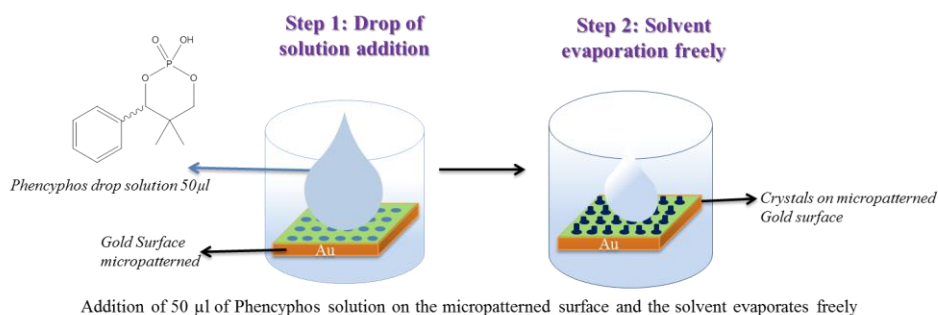
Ostwald's step rule implies that the control the evaporation rate is essential in order to reach the most thermodynamically stable crystal of any compound, fast evaporation under these irreversible thermodynamic conditions could lead to the formation of polymorphs.<sup>19</sup> According to this condition, and to test its importance in the heterogeneous process taking place in the experiments, we started following the most typical and simple technique for crystallisation on a surface that is *Drop casting* (Figure. 8.1.4. A). In order to improve this technique and allow the mass transport to the micropatterned areas we tested two different protocols: *fast solvent evaporation* (Figure. 8.1.4. B) and *slow solvent evaporation* (Figure. 8.1.4. C). The diffusion of the molecules of phencyphos over the surface is probably not very fast and it is extremely challenging to see what happens exactly at the surface, as will be appreciated from the results of the experiments. After performing many experiments in which we could observe a particular effect of the diffusion<sup>20</sup> over the surface we designed an alternative method that could show the diffusion effect: *Prolonged periods in solution with stirring* (Figure. 8.1.4. D). There are two main effects which have a dominant influence on the crystallization process on the surface, the solvent evaporation rate and the diffusion over the surface. All the methods used are described in the following Figure 8.1.4.

---

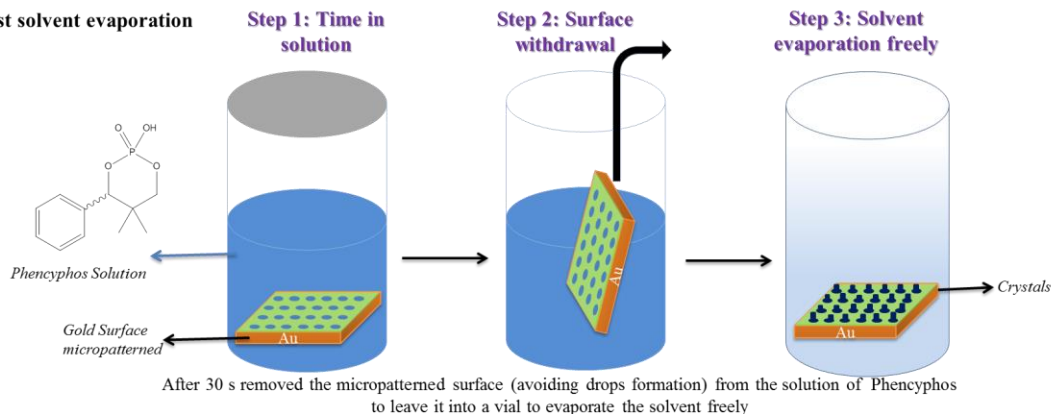
<sup>19</sup> Singh, A.; Lee, I.S.; Myerson, A.S. *Cryst. Growth Des.* **2009**, 9, 1182-1185.

<sup>20</sup> **Chapter 1**, *Introduction*.

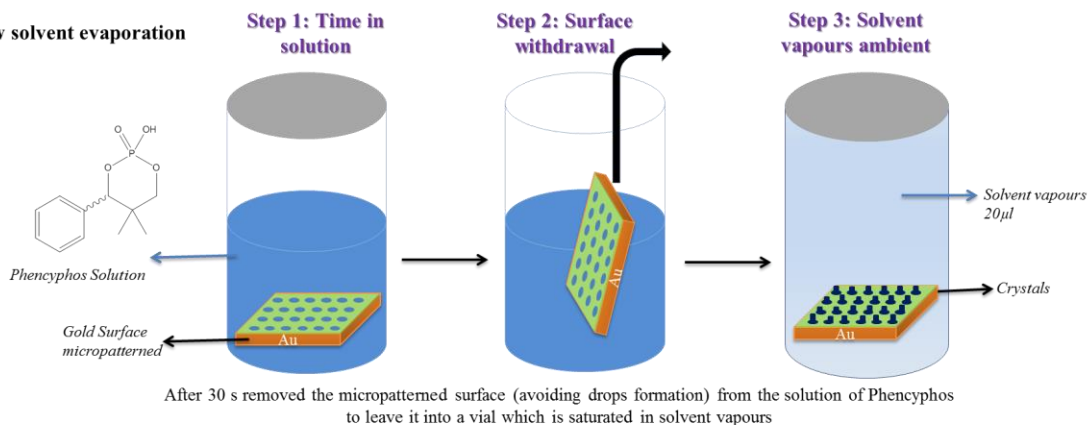
(A) Drop Casting



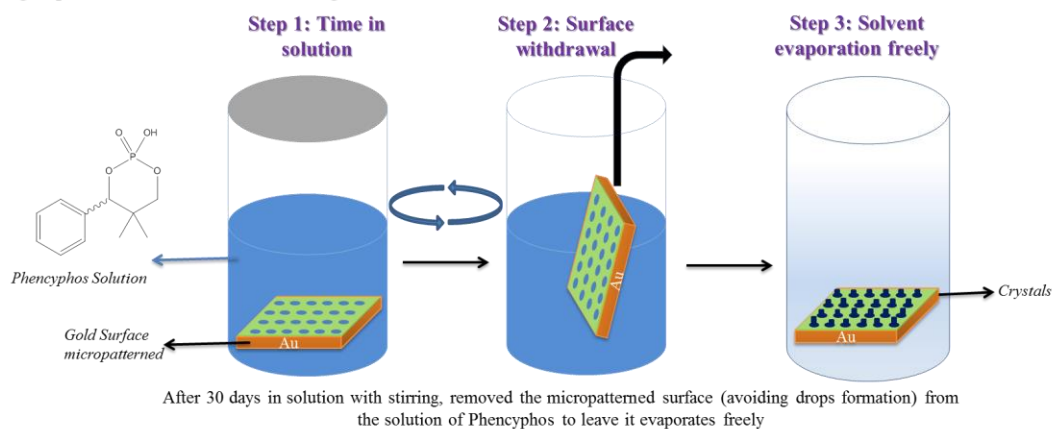
(B) Fast solvent evaporation



(C) Slow solvent evaporation



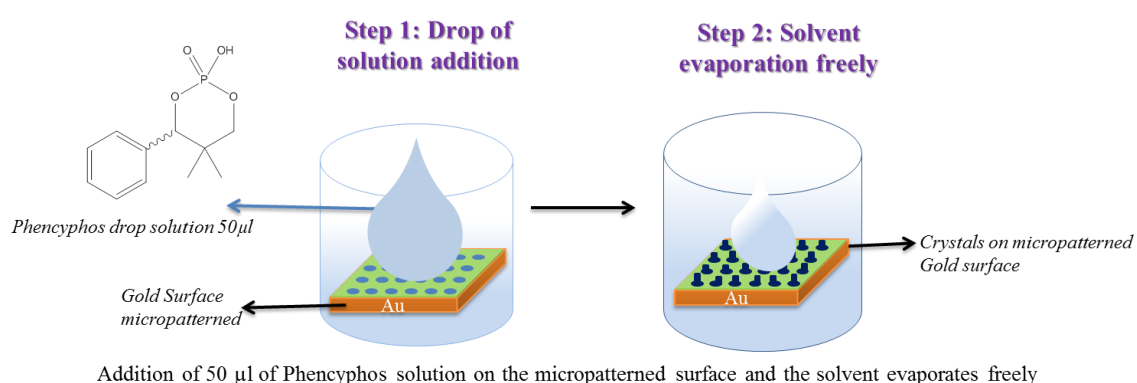
(D) Prolonged periods in solution with stirring



**Figure 8.1.4.** Crystallization methods used in the phencyphos crystallisation on micropatterned surfaces study.

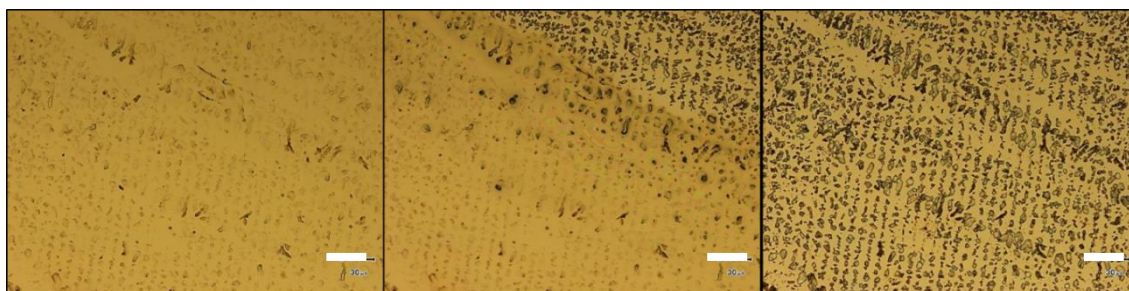
### 8.1.2.1. Drop casting

The simplest method for the deposition of a solid on a surface is by drop casting, where a solution of the compound is dropped onto the substrate in question and is allowed to evaporate. The technique was tried with the aim of observing how the solvent was evaporating on the patterned surfaces. At this moment, it should have been possible to see how crystals formed, or when, because one can see by reflection optical microscopy the crystals when the solvent is evaporated (though visualisation is difficult prior to that because of reflection of light by the drop). The method employed to crystallize the compound (Figure 8.1.5) consists of the addition of a drop solution onto the micropatterned surface and leaving the solvent to evaporate freely while this phenomenon is observed with the optical microscope.



**Figure 8.1.5.** Drop casting crystallisation method

The sample used to check this phenomenon is shown in the Figure 8.1.6 and comprises crystals of (-)-phencyphos formed from a saturated chloroform solution grown over micropatterned substrates as prepared in Figure 8.1.2 under fast evaporation conditions. The optical micrographs describe how a (-)-phencyphos drop solution evaporates freely on already dried micropatterned surface. This drop evaporation increases the material on the micropattern, forming bigger crystals.



**Figure 8.1.6.** Optical micrographs of (-)-phencyphos crystals on a micropatterned gold surfaces 5 x 10  $\mu\text{m}$  dots of (+)-PMT and DT surrounded, crystallized from saturated chloroform solution.

The scale bar corresponds to 30  $\mu\text{m}$  in all cases.

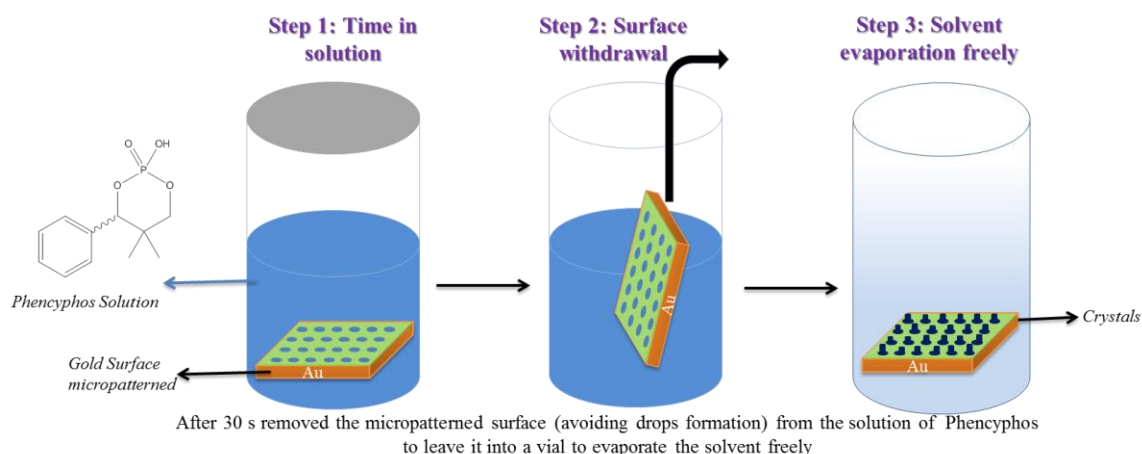
Crystals appear clearly when the solvent has evaporated completely, although it is possible to see crystals under the solvent film. Thus, crystals are formed before solvent evaporates, and they are visible clearly without solvent.

This experiment shows that crystal formation takes place prior to any dewetting phenomenon taking place on the patterned surface: In other words, the crystals are not formed because of the formation of microdroplets on the pattern, but rather because of the specific positive templating effect of the PMT in the polar regions.

#### **8.1.2.2. *Fast solvent evaporation method.***

Under fast evaporation conditions on micropatterned surfaces, an uncontrolled diffusion rate is achieved over the surface and the mass transport between polar and non-polar regions is spontaneous and takes place aided by convective flow to promote crystallization. The fast solvent evaporation method employed to crystallize the compound (Figure 8.1.7) consists of the same immersion time in the phencyphos solution for each surface, withdrawal, and unhindered solvent evaporation, to give a result which in principle is similar to casting with the exception of the incubation time in the solution of the compound.





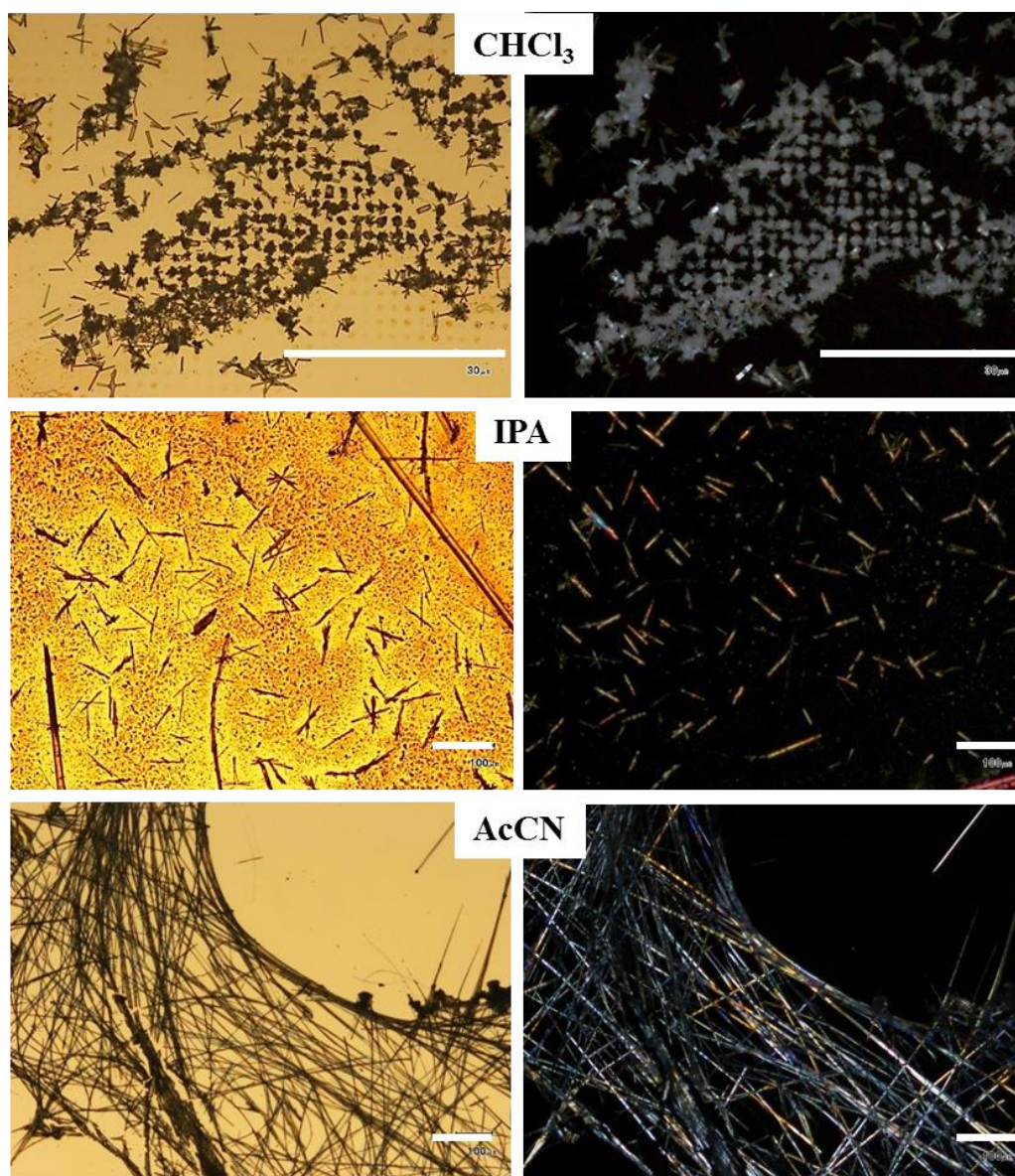
**Figure 8.1.7.** Fast solvent evaporation crystallisation method

Specifically, the functionalized gold surfaces were immersed into a fresh solution of phencyphos at different concentrations: 96 mM and 64 mM solutions, in chloroform, isopropanol and acetonitrile. In the second step, the functionalized surface was removed from the solution carefully (ensuring a uniform film and avoiding drop formation). Finally, the wet functionalized surface (with solution film) was placed in an open vial. This vial was not saturated in the vapour of the solvent of the solution, so there is not a liquid-vapour equilibrium established inside the vial. The solvent evaporates freely depending on environmental conditions (temperature, humidity).

The first experiments carried out following this method were performed with supersaturated solutions of phencyphos in different solvents: isopropanol, chloroform and acetonitrile. The gold substrates used in these experiments were functionalized by the  $\mu$ CP method using a stamp of dots of 5  $\mu$ m to print the (+) PMT and filling with a dodecanethiol monolayer around them.

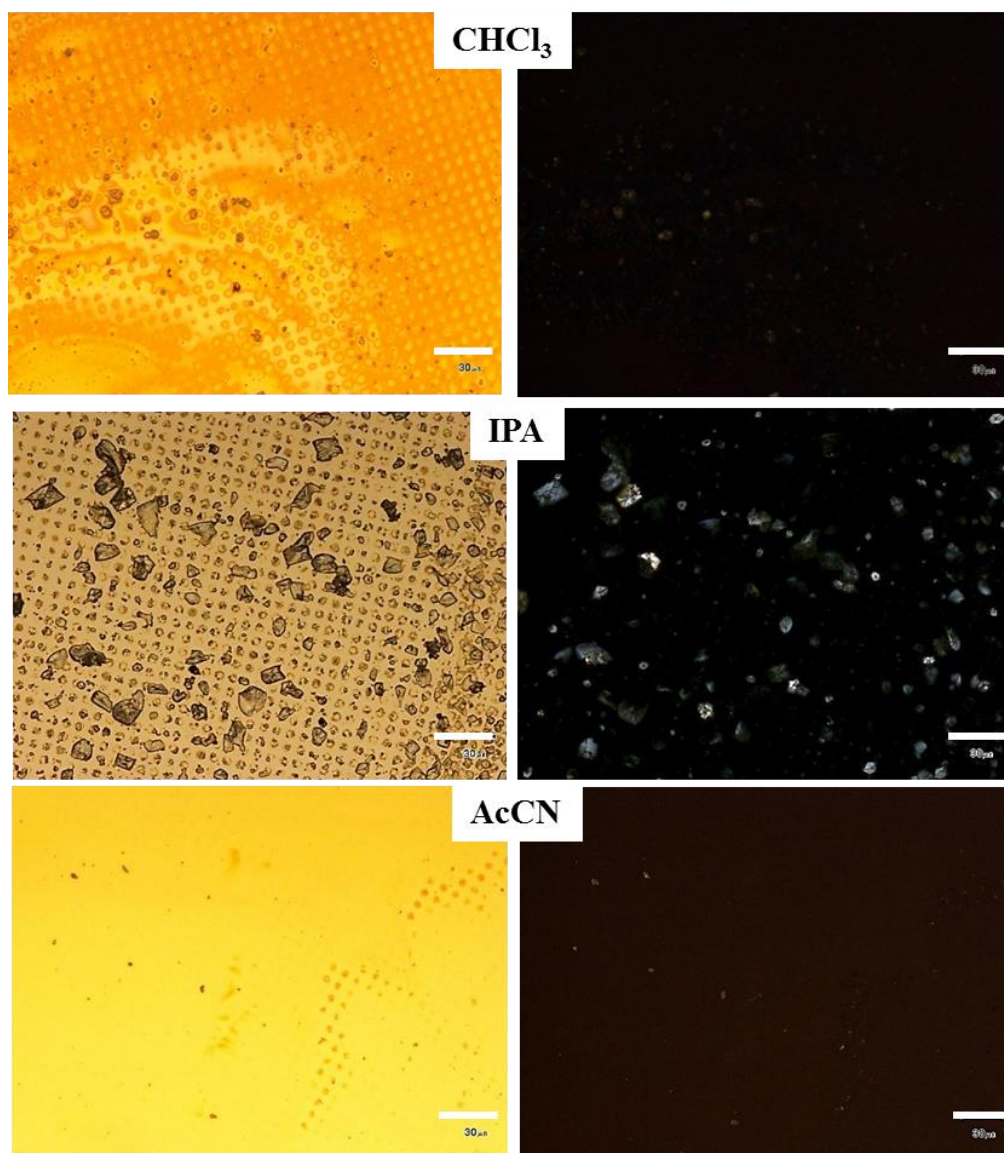
When phencyphos crystallization on the micropatterned surfaces was performed from the more concentrated solution under fast solvent evaporation conditions a dramatic difference between the different solvents was observed, as shown in Figures 8.1.8 and 8.1.9 where the crystals formed under these conditions are visualized in an optical microscope.

Figure 8.1.8 shows the (+)-phencyphos crystallisation from solutions of different solvents (chloroform, isopropanol and acetonitrile) on surfaces micropatterned with (+)-PMT. Only in the case of the crystallisation from chloroform did crystals grow on the micropatterned regions. In the case of crystals from isopropanol solution, the heterogeneous nucleation has been completely uncontrolled over the whole micropatterned surface with no distinction. Homogeneous nucleation has been completely favoured in the case of the crystals from acetonitrile solution under this crystallisation method conditions.



**Figure 8.1.8.** Optical micrographs of (+)-phencyphos crystals on micropatterned gold surfaces of dots of 5  $\mu\text{m}$  separated 10  $\mu\text{m}$  (5 x 10  $\mu\text{m}$ ), crystallized from 96 mM solution in different solvents, chloroform ( $\text{CHCl}_3$ ), isopropanol (IPA), acetonitrile ( $\text{CH}_3\text{CN}$ ). Scale bar corresponds to 100  $\mu\text{m}$  for  $\text{CHCl}_3$  images and 100  $\mu\text{m}$  for IPA and AcCN.

Figure 8.1.9 shows the (-) phencyphos crystallisation from solutions of different solvents (chloroform, isopropanol and acetonitrile) on micropatterned surfaces by (+)-PMT. Only in the case of the crystallisation from isopropanol did crystals grow on the micropatterned regions. In the case of chloroform and acetonitrile, there is material on the micropatterned regions which appears to have been formed by dewetting from the apolar region. In the (-) phencyphos crystallisation under this crystallisation method conditions the heterogeneous nucleation was favoured only for IPA as the solvent.



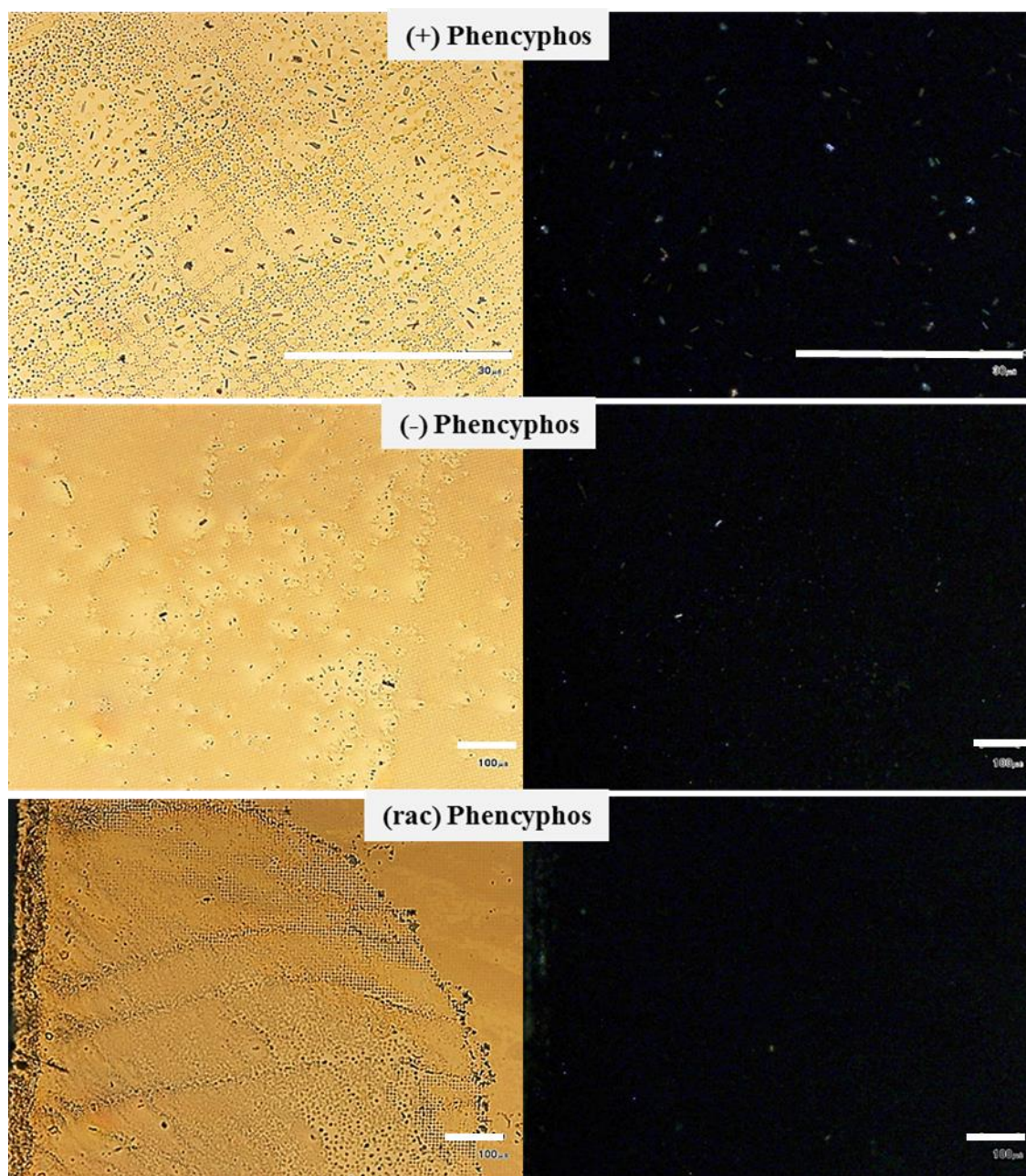
**Figure 8.1.9.** Optical micrographs of (-)-phencyphos crystals on micropatterned 5 x 10  $\mu\text{m}$  gold surfaces crystallized from 96 mM solution in different solvents under fast solvent evaporation conditions. Chloroform ( $\text{CHCl}_3$ ), isopropanol (IPA), acetonitrile ( $\text{CH}_3\text{CN}$ ). Scale bar corresponds to 30  $\mu\text{m}$  in all images.

The nature of each solvent matters greatly in the crystallization process on the patterned surface under fast evaporation. There are two fundamental properties of the solvents involved in the crystallization process on the surfaces: The solvation or affinity between monolayer and solvent and the wettability of this solution-solid interface by the pre-nucleus which may affect the relative rates of homogeneous or heterogeneous nucleation processes. The solvent volatility plays a more important role on the crystal growth rather than possibility of heterogeneous nucleation; a lower volatility should favour the growth of larger crystals because supersaturation is approached more slowly, thus favouring growth over nucleation. On the other hand, a volatile solution enters supersaturation rapidly and many nuclei are formed per unit time. The mass transport under these conditions will also be influenced by the rate of evaporation and the nature of the wetting of the surface, since convective flow towards the edge of the evaporating solvent as well as recirculatory flow will be affected.<sup>21</sup> After many experiments under these conditions we observed a dependence of both solvation and evaporation rate effects.

Phencyphos crystallization on micropatterned surfaces from 64 mM solutions under fast solvent evaporation was done from isopropanol, chloroform and Acetone-water (1:1) solvents. The following Figure (8.1.10) shows the micropatterned surfaces after the crystallisation experiment under fast solvent evaporation crystallisation method. (+)-Phencyphos crystals follow an inversed micropattern to crystallize while (-)-phencyphos follows no pattern and (*rac*) Phencyphos seems crystallize on the micropattern and around.

---

<sup>21</sup> (a) G. Berteloot, A. Hoanga, A. Daerr, H. P. Kavehpour, F. Lequeux, L. Limat, *J. Colloid Interf. Scie*, **2012**, 370, 155–161. (b) H. Y. Erbil, *Adv. Colloid Interf. Scie*, **2012**, 170, 67–86.



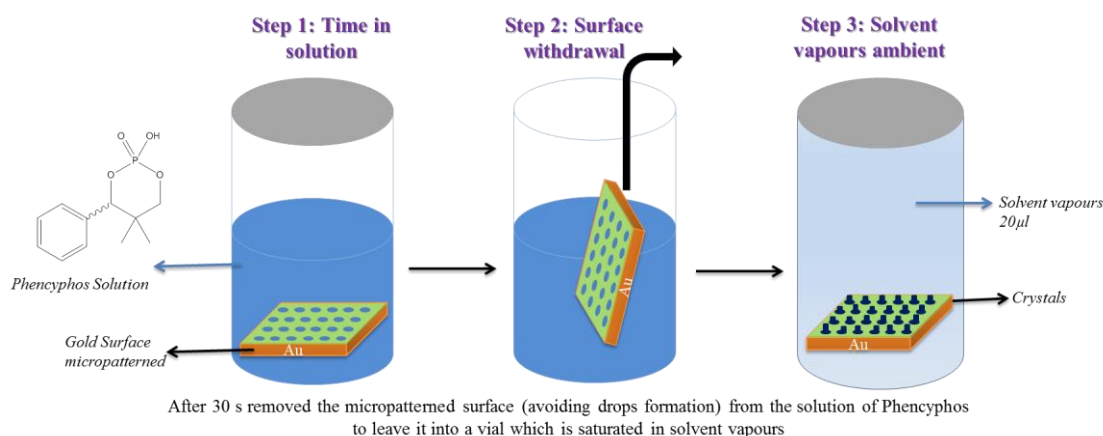
**Figure 8.1.10.** Optical micrographs of (+), (-) and (*rac*) Phencyphos crystals on micropatterned of 5 x 10 μm gold surfaces crystallized from 64 mM solutions in chloroform under fast solvent evaporation conditions. Scale bar corresponds to 100 μm.

Thus, the recognition between nucleus and pattern is not evident: As we shall see, the micropatterned surfaces need to be closer to thermodynamic equilibrium to favour the chiral recognition. To favour this recognition it is necessary to reduce the solvent evaporation rate; otherwise crystals could appear over the whole surface as a result of homogeneous nucleation. Moreover, the racemic phencyphos presents a different

behaviour to the pure enantiomers, which crystallize as hydrates. Both parameters make it hard to control the chiral recognition and subsequent crystallization process on these micropatterned surfaces. From these experiments it was realized that a more controlled method (explained below) which has slower solvent evaporation is necessary in order to favour crystal nucleation and growth on the pattern.

### 8.1.2.3. Slow solvent evaporation

Under slow solvent evaporation conditions on the micropatterned surfaces the lengthy timescale allows a uniform diffusion rate to be achieved over the surface and the most favourable mass transport between polar and non-polar regions takes place to promote crystallization (Figure 8.1.11). The method employed to control the solvent evaporation is based on the liquid-vapour equilibrium inside a closed vial where the surface was placed after a given time in solution of the compound phencyphos. The high vapour content in the vial ensures slow evaporation of the thin layer of solution in contact with the surface. These conditions allow the liquid-vapour solvent equilibrium to be reached from the instant the surface is placed inside the vial.

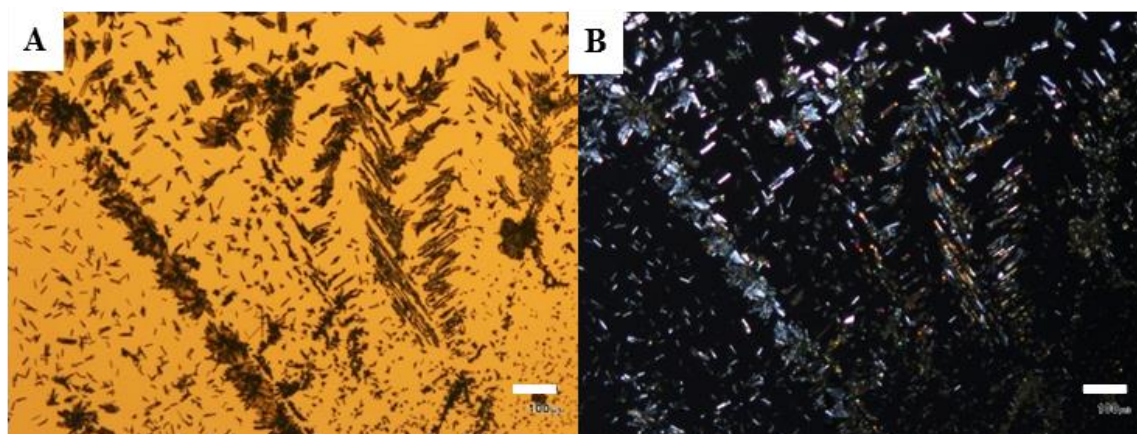


**Figure 8.1.11.** Slow solvent evaporation crystallisation method.

Specifically, the functionalized gold surfaces were immersed into a fresh solution of phencyphos for under-saturated solution in chloroform and isopropanol. In the second step, the functionalized surface was removed from the solution carefully (ensuring a uniform film and avoiding drop formation). Finally, the wet functionalized surface (with

solution film) was quickly but carefully placed in a vial which was immediately sealed. This vial was previously saturated in the vapour of the solvent of the solvent. Using this method, it was possible to control the solvent evaporation rate even for the chloroform solutions, which evaporate within minutes when open to the air. The solvent loss from the vial led to complete evaporation of chloroform samples within 5 days, for the mixture acetone, water samples 6 days, and for the isopropanol samples, at least 7 days.

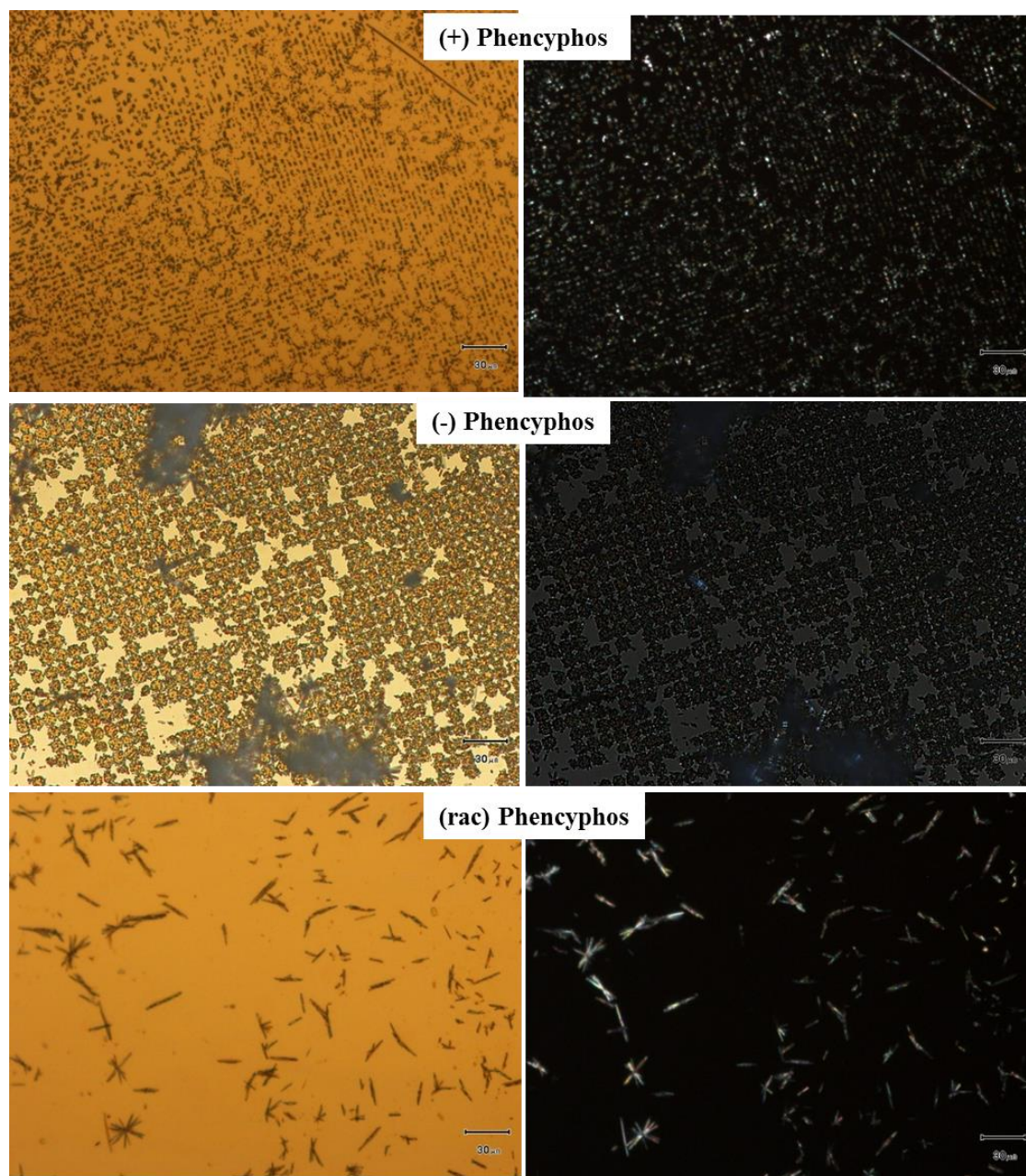
Under-saturated solutions were used in all these experiments after performing many crystallisation attempts using near saturated or supersaturated solutions and observing how crystals appeared over whole surface. Figure 8.1.12 shows the (-) phencyphos crystals grown on micropatterned surface under slow solvent evaporation method from supersaturated (64 mM) chloroform solution.



**Figure 8.1.12.** Optical micrographs of (-)-phencyphos crystals grown on micropatterned surface (+)-PMT dots of 5 x 10  $\mu\text{m}$  and DT surround under slow solvent evaporation method. (A) non-polarised image; (B) polarised image. Scale bar 100  $\mu\text{m}$ .

The dependency between concentration and solvent evaporation rate must be optimised, to favour the desired diffusion and nucleation on the micropattern. The concentration should not be very high and the solvent evaporation rate has to be slow and under control to reach near-thermodynamic conditions. The following figures show the results of this crystallization method with varying solvents having different volatility; chloroform, isopropanol and a mixture of acetone-water (1:1).

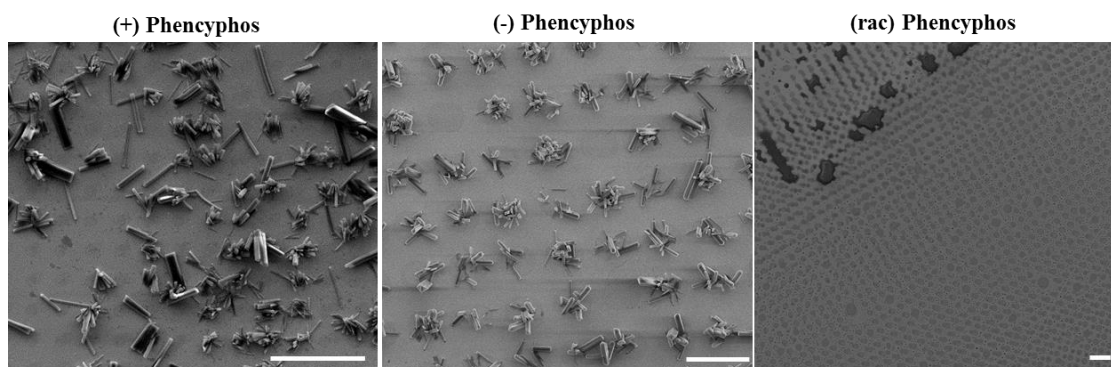
The phencyphos crystallisation from chloroform solution is shown in Figure 8.1.13. Both enantiomers crystallise on the micropatterned regions while the racemate crystallises with no distinction. Enantiomerically pure phencyphos crystals mainly grow on the (+)-PMT region, thus a controlled crystallisation on these regions has been achieved.



**Figure 8.1.13.** Optical micrographs of (+), (-) and (*rac*) Phencyphos crystals on micropatterned of  $5 \times 10 \mu\text{m}$  of (+)-PMT and DT gold surfaces crystallized from undersaturated solution in chloroform solvent under slow solvent evaporation conditions. Scale bar corresponds to  $30 \mu\text{m}$ .

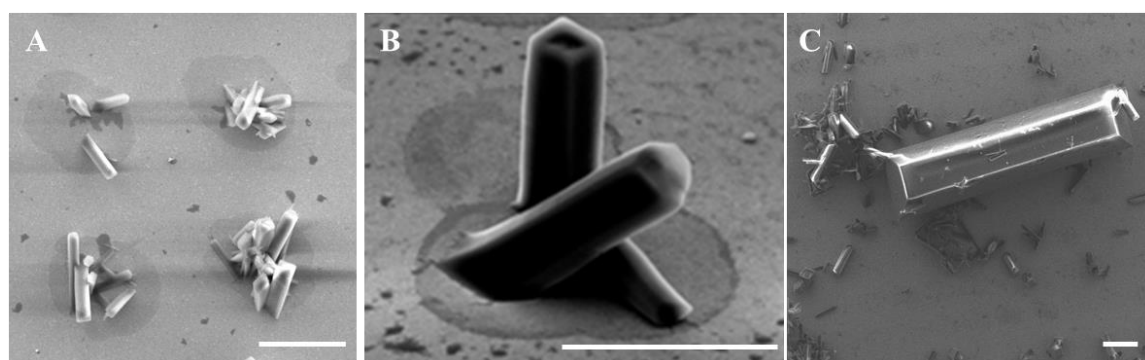


SEM micrographs confirm what is shown by the optical micrographs in the figure above, enantiomerically pure phencyphos crystals grow off the micropatterned regions while in the case of the racemate of phencyphos there is amorphous material over the micropatterned surface.



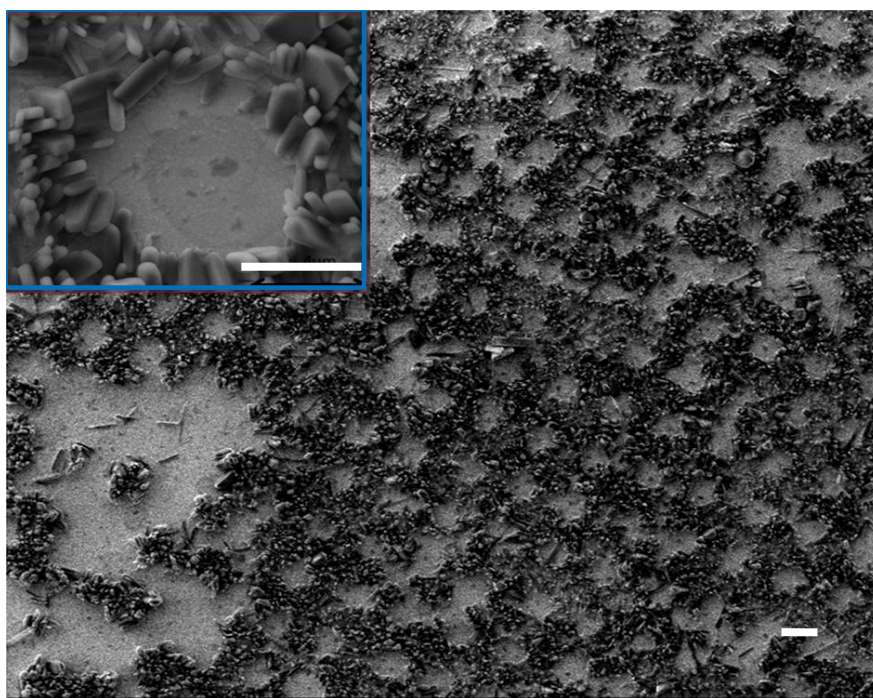
**Figure 8.1.14.** SEM micrographs of (+), (-) and (*rac*) phencyphos crystals on of 5 x 10  $\mu\text{m}$  of (+)-PMT and DT gold surfaces crystallized from undersaturated solution in chloroform solvent under slow solvent evaporation conditions. Scale bar corresponds to 20  $\mu\text{m}$  in all images.

Enantiopure phencyphos crystals grow off the micropatterned region as is shown in Figure 8.1.15-B. This SEM micrograph shows two (-)-phencyphos crystals grown off a dot of (+)-PMT. The nucleation was dramatically influenced by the micropatterned region. The figure 8.1.15-C shows a (-)-phencyphos crystal formed from the bulk solution (homogeneous nucleation), its size is almost 10 times bigger than the same crystals grown on the micropatterned surface.



**Figure 8.1.15.** SEM micrographs (A) Top view, (B) tilt 45° of (-)-phencyphos crystals on micropatterns of dots (5 x 10  $\mu\text{m}$ ) of (+)-PMT and DT surround on gold surfaces from 64 mM solution in chloroform under slow solvent evaporation conditions. (C) (-) Phencyphos crystal from bulk solution. Scale bar corresponds to 5  $\mu\text{m}$ .

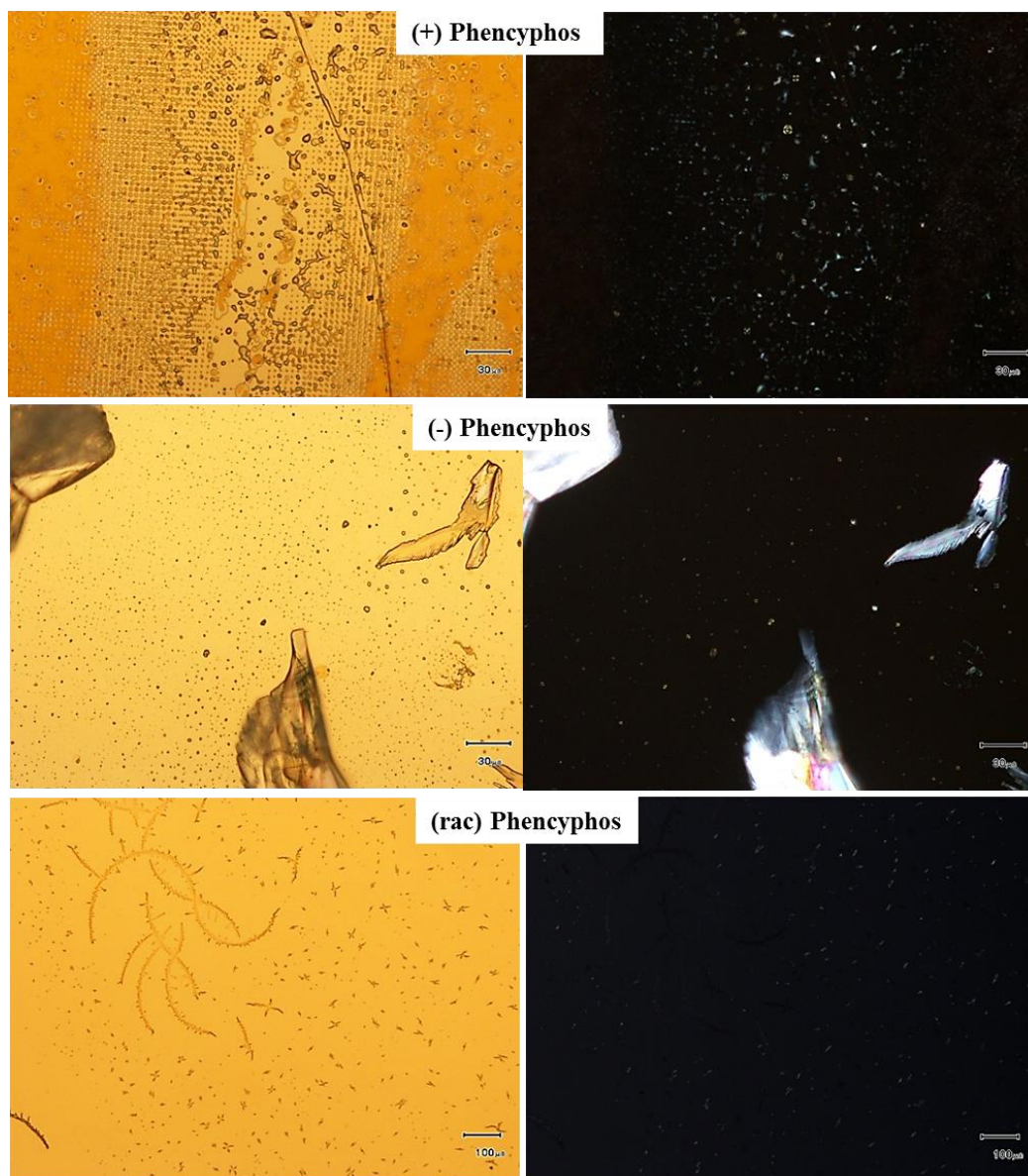
In order to probe the recognition of the micropatterned surface as nucleation point, we designed a micropatterned surface in which the micropattern was done following the protocol described in Figure 8.1.2 but the ink solution was DT and the blocking solution was (+)-PMT. Thus, the SEM micrograph in Figure 8.1.16 confirms the recognition of the (+)-PMT as nucleating zones which favours, in a controlled way, the heterogeneous nucleation on them.



**Figure 8.1.16.** SEM micrographs of (-) Phencyphos on an inversed pattern of 5 x 10  $\mu\text{m}$  of DT and (+)-PMT around gold surfaces crystallized from undersaturated solution in chloroform solvent under slow solvent evaporation conditions. Scale bar corresponds to 5  $\mu\text{m}$ .

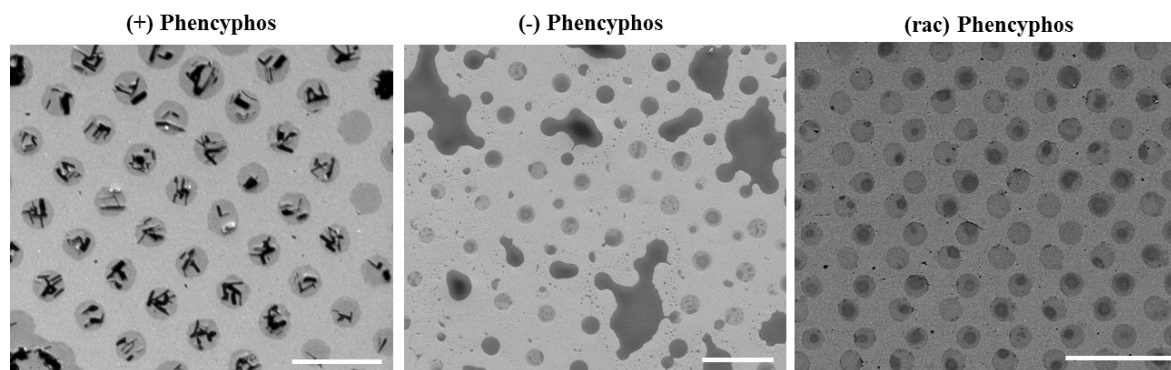
Phencyphos crystallization from isopropanol solutions was already probed in the previous method from supersaturated and saturated solutions. Under-saturated solutions were used with controlled evaporation with promising results. Optical micrographs show controlled crystallisation for (+)-phencyphos on micropatterned surfaces by (+)-PMT and DT, however for the (-) and (*rac*) phencyphos the crystallisation did not proceed through a clean heterogeneous nucleation from the pattern (Figure 8.1.18). During the (-)-phencyphos crystallisation on the micropatterned surface, large crystals grow on either from the homogeneous nucleation or due to the heterogeneous nucleation from a big drop of solution on the surface, forming this crystal.

Nevertheless, SEM micrographs (Figure 8.1.19) confirm the controlled crystallisation on micropatterned surfaces only in the case of (+)-phencyphos. For the other phencyphos forms, that do not crystallize, there is a film on the micropattern selectively over the (+)-PMT region of the monolayer presumably as a result of selective wetting. These results could be promising in order to prove the influence of the chirality of the micropatterned region by (+)-PMT. This effect will be described more in details in the section *Chirality and Polarity on surface* of this chapter.



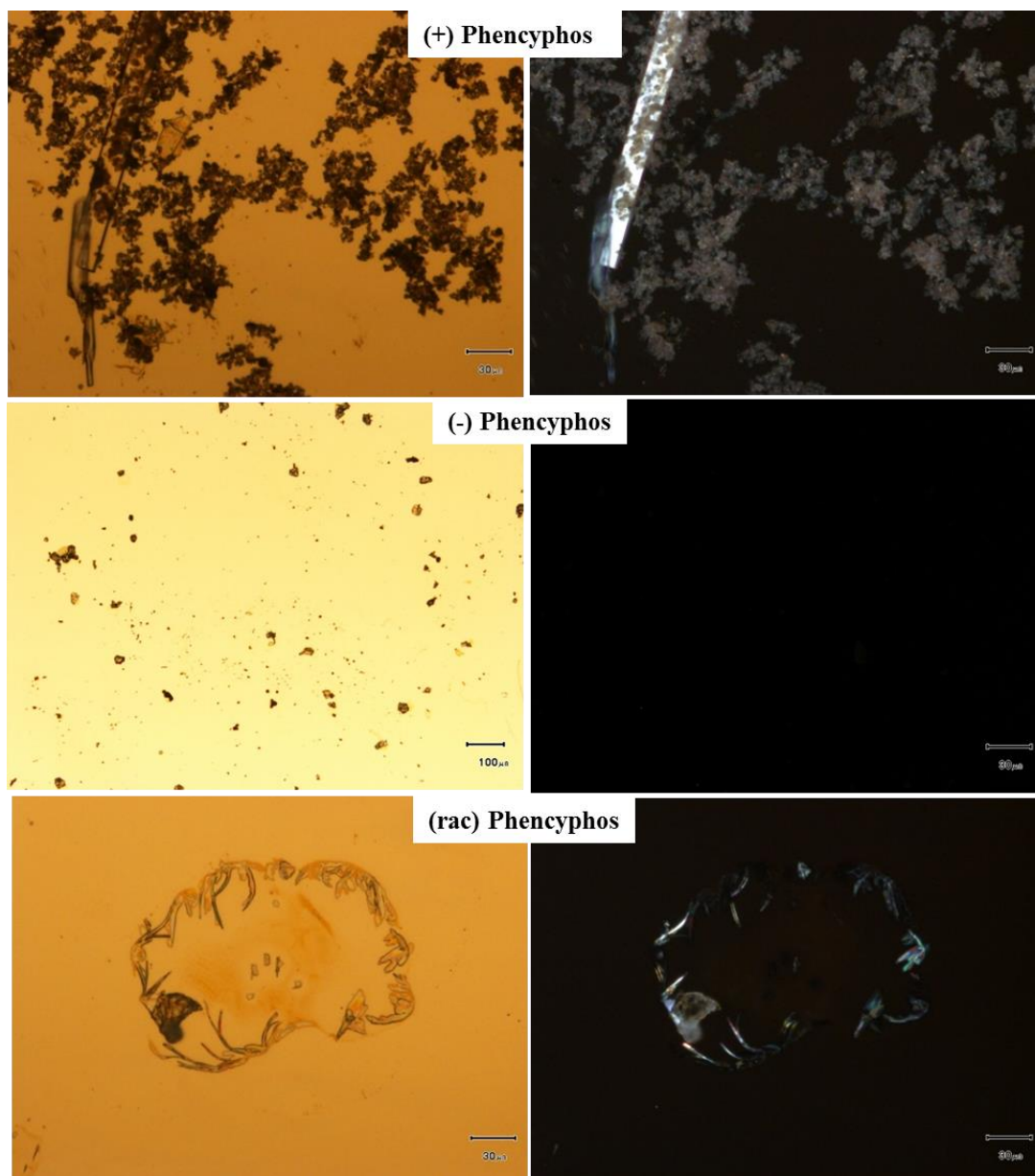
**Figure 8.1.18.** Optical micrographs of (+), (-) and (*rac*) Phencyphos crystals on micropatterned of 5 x 10 μm of (+)-PMT and DT gold surfaces crystallized from undersaturated solution in isopropanol solvent under slow solvent evaporation conditions. Scale bar corresponds to 30 μm, racemic 100 μm.

The optical micrographs shown in the Figure 8.1.18 indicate the controlled crystallisation has not been achieved in this system. Crystals grow on these micropatterned surface are from either homogeneous nucleation in the bulk solution which fell down on the surface or from a heterogeneous nucleation which was not induced by the micropatterned surfaces.



**Figure 8.1.19.** SEM micrographs of (+), (-) and (*rac*) Phencyphos crystals on micropatterned of 5 x 10  $\mu\text{m}$  of (+)-PMT and DT gold surfaces from undersaturated solution in isopropanol solvent under slow solvent evaporation conditions. Scale bar corresponds to 20  $\mu\text{m}$ .

The idea of using the mixture of acetone and water was based on the crystal structure of the pure enantiomers, which are hydrated. If there is water in the solution the crystallization of pure enantiomers would be favoured, as the compound forms a conglomerate as a hydrate. In practice, after many repetitions we observed the crystals do not crystallize on the desired zone of the micropatterned surface, since it is very soluble in water but the proportion 1:1 acetone and water keeps the phencyphos in solution. Figure 8.1.20 shows that crystals do form on the surface, but they do not coincide with the patterned regions for reasons that are enigmatic at the present. The result shows that water is not necessarily beneficial to the crystallisation of phencyphos on this kind of pattern, possibly because of solvation of the patterned region.



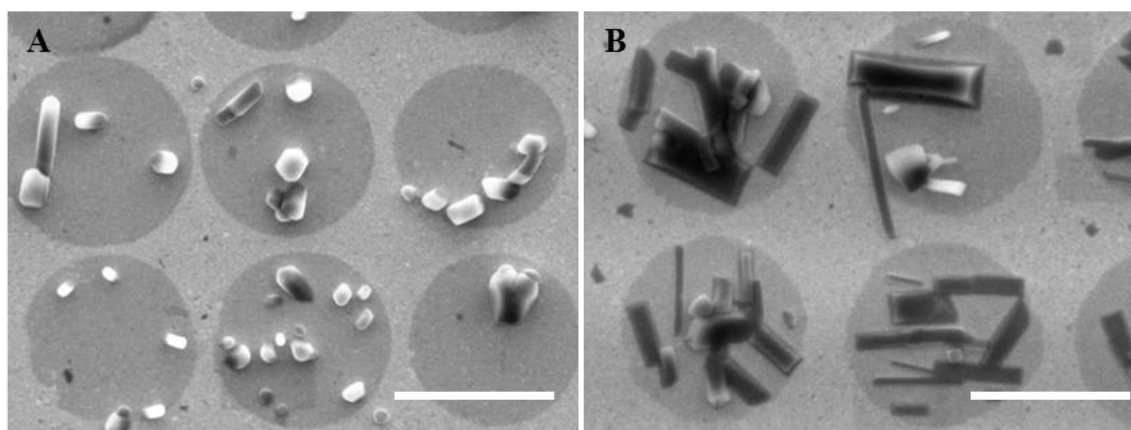
**Figure 8.1.20.** Optical micrographs of (+), (-) and (*rac*) Phencyphos crystals on micropatterned of 5 x 10 μm of (+)-PMT and DT gold surfaces crystallized from undersaturated solution in mixture of solvents (Acetone-water 1:1) under slow solvent evaporation conditions. Scale bar corresponds to 30 μm.

Phencyphos crystallization from undersaturated chloroform solutions under slow solvent evaporation conditions is the best system for the formation of crystals on the patterned surfaces. Figures 8.1.13 and 14 show phencyphos crystals on the micropatterned gold surfaces; both enantiomers crystallize on the (+)-PMT micropattern. The (*rac*) phencyphos does not crystallize, although there is a film on the micropattern selectively over the (+)-PMT region of the monolayer. The crystallization of the racemic phencyphos on micropatterned surfaces from organic solutions is very difficult to control; understanding what happens at the surface is enigmatic. There is no apparent segregation of enantiomers in the sample, as the film in the patterned region is essentially homogeneous.

#### 8.1.2.3.1. Powder X-ray microdiffraction characterisation

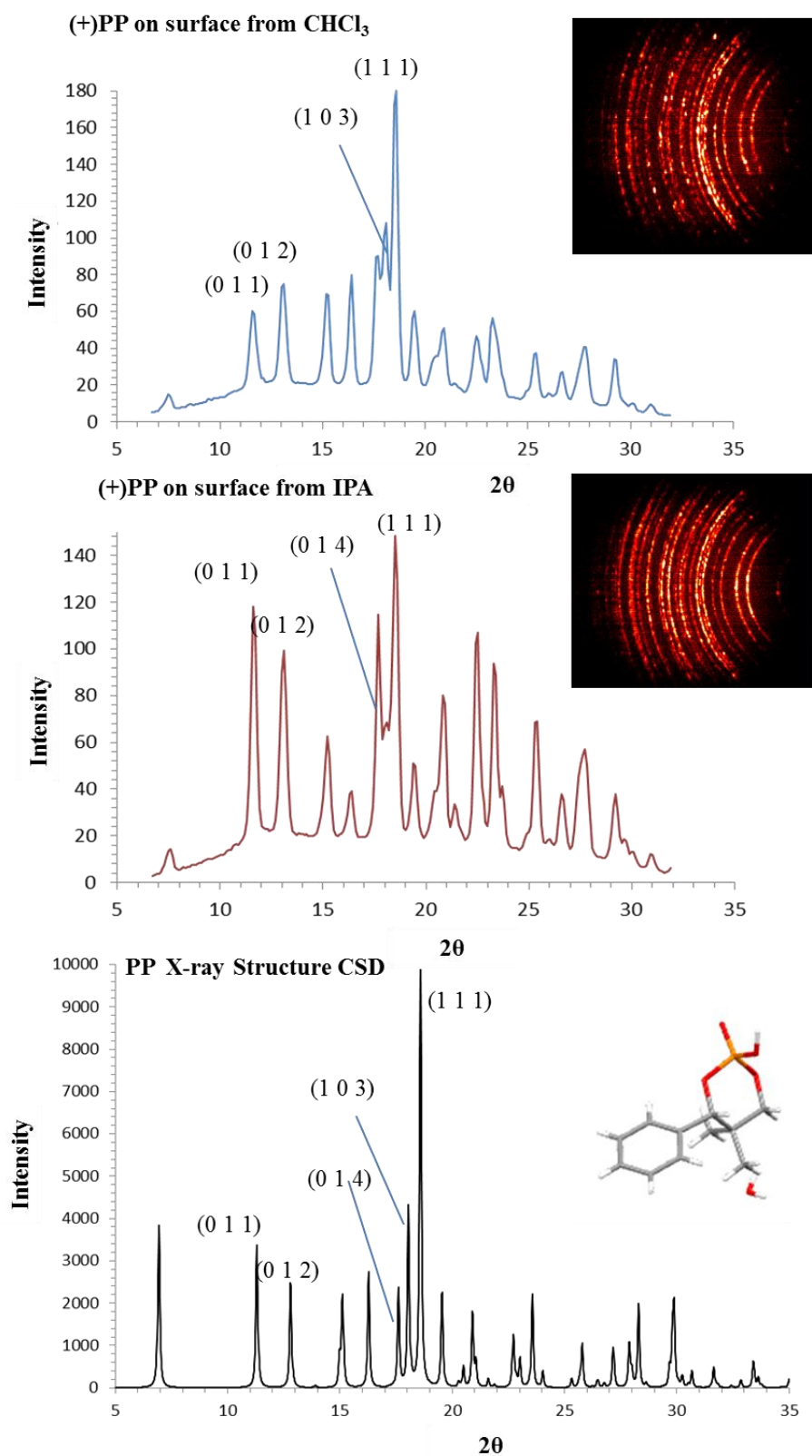
Powder X-ray microdiffraction is a characterisation technique in which a general area detector diffraction system (GADDS) is used in reflection geometry to analyse very small areas of any surface. Powder X-Ray microdiffraction measurements were measured using a Bruker-AXS diffractometer, model D8 advance (GADDS), using an X-Ray tube of Cu ( $\lambda$  (Cu  $K\alpha$ ) = 1.54 Å) at the X-ray diffraction service in the ICMAB-CSIC.

As the solvent used in the crystallization process might have a dramatic influence on packing, we performed powder X-ray micro-diffraction on two samples (previously characterised by SEM, see Figure 8.1.21) of the same enantiomer of phencyphos crystallized from different solutions on the same micropatterned surface, a 5 x 10  $\mu\text{m}$  dot pattern of (+)-PMT with a DT monolayer surround. The results are shown in Figure 8.1.22 where some differences in the relative intensities are observed, but both diffractograms show the same diffraction peak positions and therefore correspond to the same crystal structure (the compound (+)-phencyphos). Thus, there is an influence of the solvent on the crystallization process, but it is upon the nature of the crystal growth process and it does not change the crystalline structure. Therefore, the nucleation step in both solvent systems is essentially the same in terms of formation of the same periodic structure. Nevertheless, there is a difference between the two diffractograms. In the one of the (+)-phencyphos crystals grown on the patterns from isopropanol solution there is a preferential growth along one direction, which is the direction of the *c* axis of the crystal structure that coincides with the hydrogen bonded network.



**Figure 8.1.21.** Samples used for X-ray microdiffraction: SEM micrographs of (+)-phencyphos from (A) chloroform and (B) isopropanol solutions on micropatterned surfaces of dots of  $5 \times 10 \mu\text{m}$  under slow solvent evaporation crystallisation method. Scale bar corresponds to  $5 \mu\text{m}$ .

This hypothesis can be rationalized because the crystals of (+)-phencyphos grow over a monolayer of (+)-PMT where there are many phosphoric acid groups and these groups would form the hydrogen bonded network with the phosphoric acid groups of (+)-phencyphos. This phenomenon could also happen from chloroform solution, but it seems that because of specific solvation of the monolayer and the growing crystal, the growth direction is away from the surface. The isopropanol is less volatile than the chloroform and they are also different in their wetting ability towards the surface. Thus, the crystal growth from isopropanol is along the  $c$  axis supported by the hydrogen bond network between monolayer of (+)-PMT and (+)-phencyphos while in from chloroform the crystal growth is along the  $c$  axis, in this case, where the hydrogen bond network of the crystal grows quasi-perpendicularly to the nucleating surface.

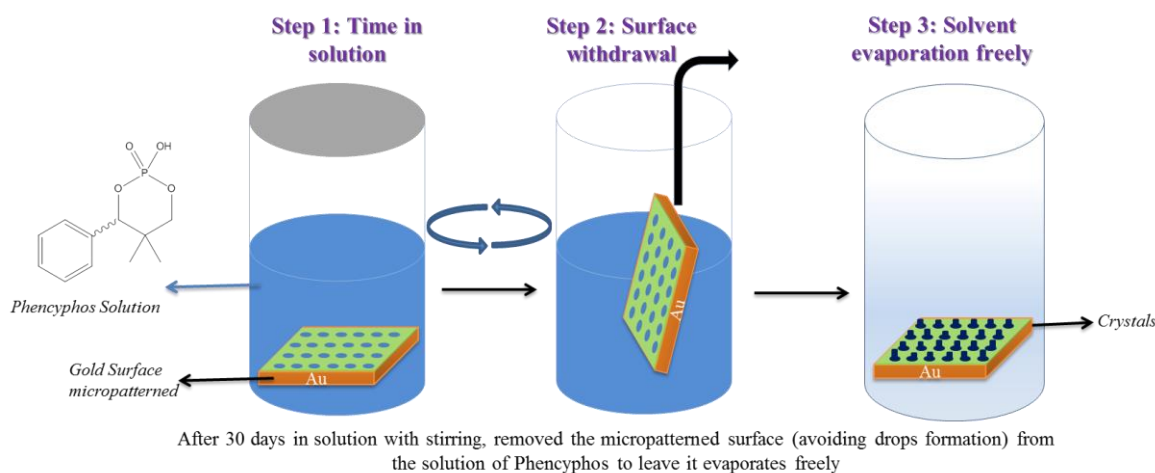


**Figure 8.1.21.** GADDs diffractograms of (+) phencyphos crystallised from  $\text{CHCl}_3$  or IPA solution on micropatterned surfaces of (+)-PMT dots  $5 \times 10 \mu\text{m}$  under slow solvent evaporation from conditions, compared to the calculated powder diffractograms from the X-ray structure of the Cambridge Structural Database (CSD).



#### 8.1.2.4. Micropatterned surface for a prolonged time the in solution with stirring.

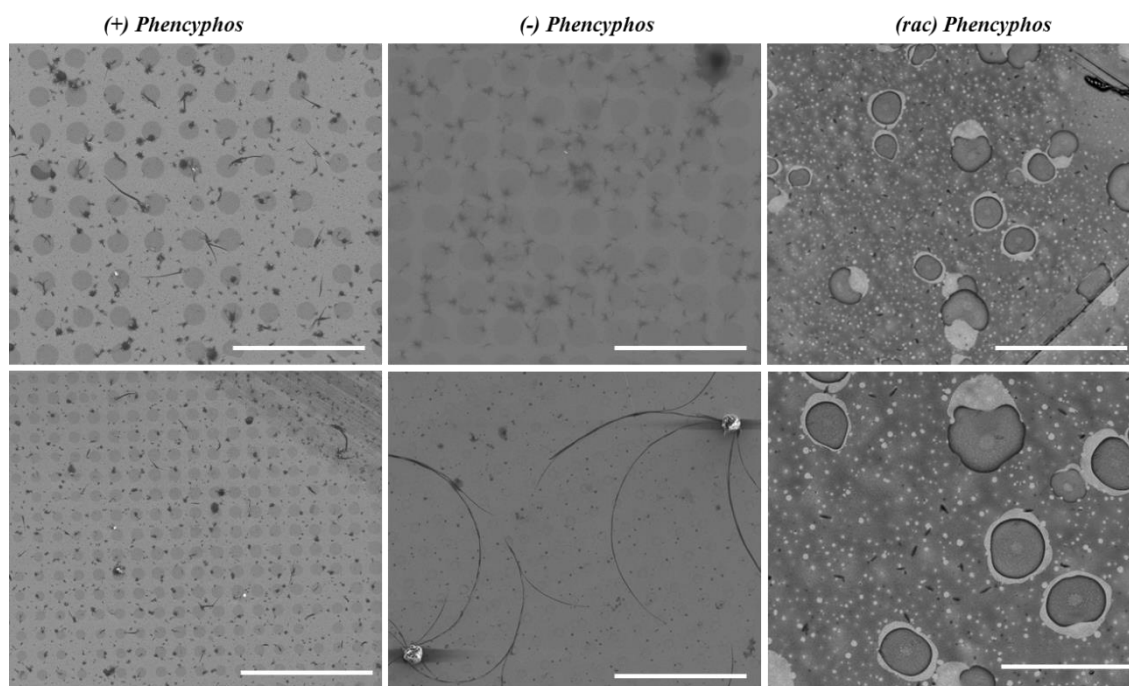
This method was designed in order to test the principle that a stirred solution guarantees diffusion of the crystallizing molecule (mass transport) and uniform growth of a nucleus, avoiding homogeneous nucleation from the surface. The stirring is the most important part of this method when compared with the other samples. The micropatterned surfaces were immersed into phencyphos solutions in different solvents in closed vials which were stirred for 30 days favouring the diffusion and the mass transport between polar and non-polar regions over the micropatterned surface. After this period the micropatterned surfaces were removed and left in a vial in which the solvent evaporated quickly. In these experiments the crystallization of (+), (-) and racemic phencyphos was studied from chloroform and isopropanol solutions.



**Figure 8.1.23.** Micropatterned surface for a prolonged time the in solution with stirring method.

##### 8.1.2.4.1. Chloroform series

The crystallization of (+), (-) and racemic phencyphos from chloroform solutions were done over a micropatterned surface in which half was printed using (-)-PMT and the other half was printed using (+)-PMT with a dodecanethiol monolayer covering the surrounding surface. Both surfaces were micropatterned with  $5 \times 10 \mu\text{m}$  features. The micropatterned surfaces after this crystallisation experiments are shown in the following Figure 8.1.24.

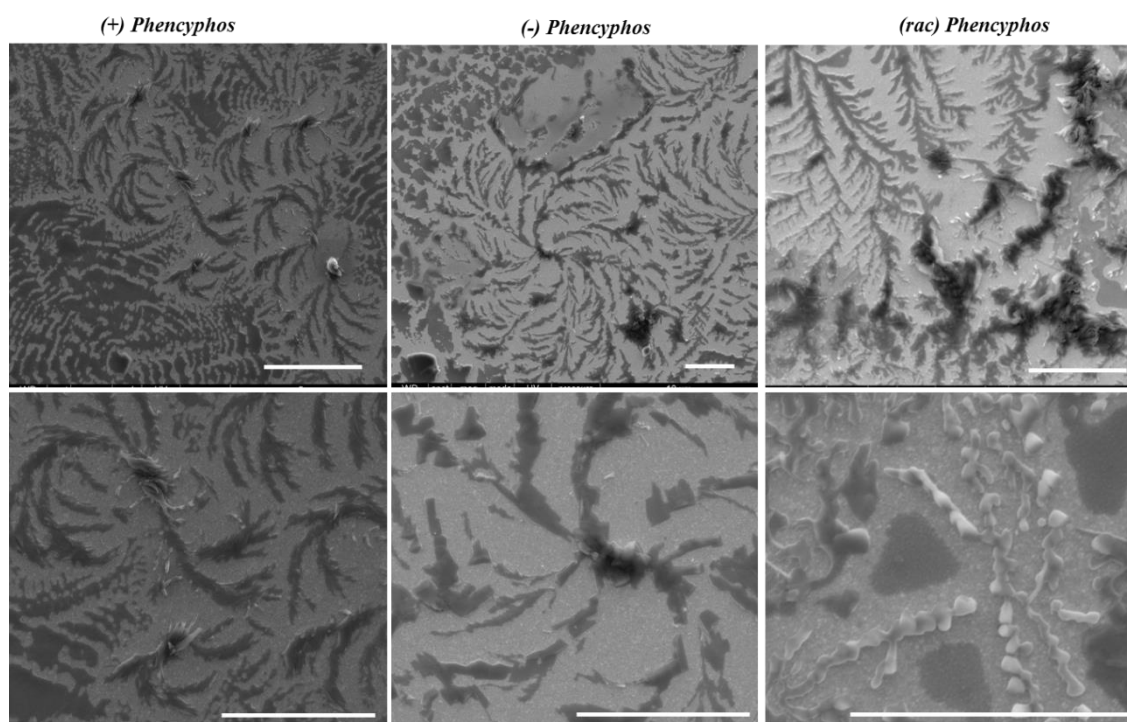


**Figure 8.1.24.** SEM micrographs of micropatterned 5 x 10  $\mu\text{m}$  gold substrates after 30 days in solution with stirring. (+), (-) and (*rac*) Phencyphos in chloroform undersaturated solutions and fast solvent evaporation. Scale bar 40  $\mu\text{m}$  in all images. The images in the lower part are enlarged zones of the images above.

As can be appreciated in Figure 8.1.24, 30 days in solution with stirring was too much time for this solvent because the chloroform evaporated completely even in a closed vial. Thus the concentration was increasing during the stirring and the movement presumably removed the phencyphos from the surface by centrifugal force. Crystals of phencyphos appeared in the bottom of the vial and nothing crystalline on the micropatterned surface. The combination of the low surface tension of the chloroform solvent with the stirring make uncontrolled the diffusion of the phencyphos compounds over the micropatterned surface, forming amorphous solids or layers on surface with no micropatterned regions distinction. Therefore, under these conditions, the chloroform is a bad solvent to use. Nevertheless, the experiment does prove that the dewetting phenomenon is not a dominant factor in the formation of the crystals, as presumably a very thin film is formed prior to evaporation in this experiment.

#### 8.1.2.4.2. Isopropanol series

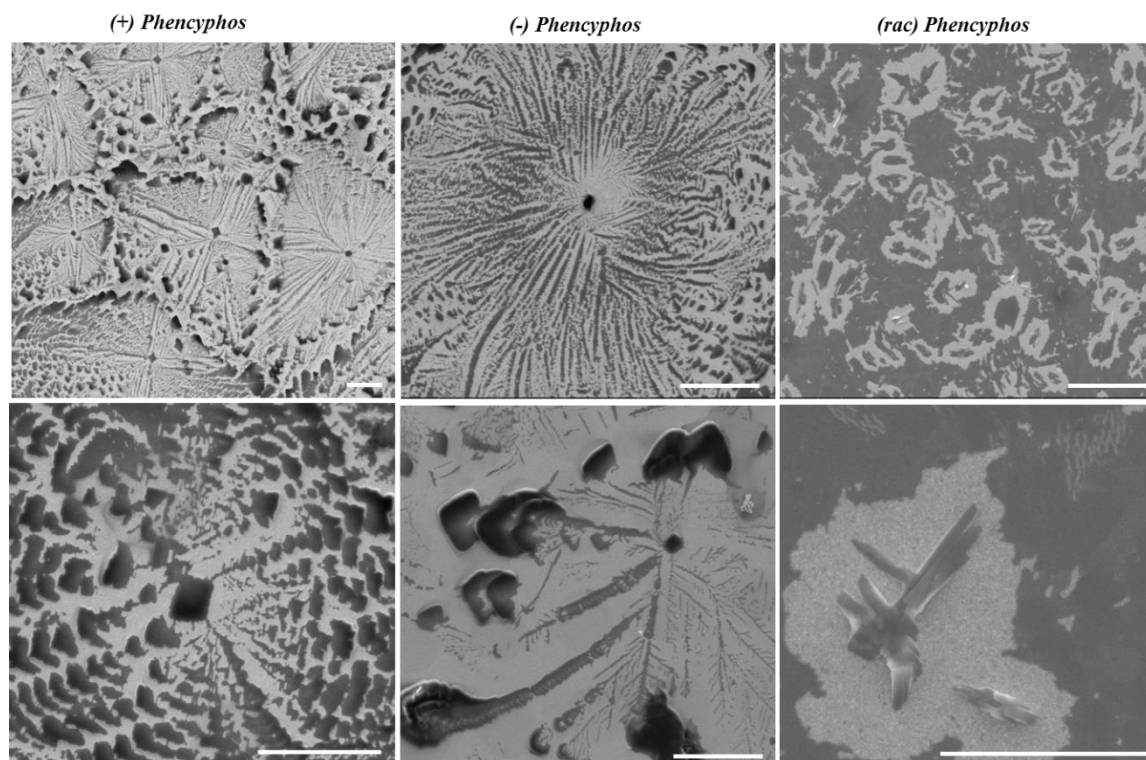
The crystallization of (+), (-) and racemic phencyphos from isopropanol solutions were done over a micropatterned surface with a micropattern of 5 x 10  $\mu\text{m}$  dots of (-)-PMT (Figure 8.1.25) or MUA (Figure 8.1.26) (in separate surfaces) and a DT monolayer surrounding them. The use of thiols of different chirality but similar polarity was performed to check the most favourable interaction, by polarity or chirality, to promote the nucleation on the monolayer of these thiols.



**Figure 8.1.25.** SEM micrographs of a micropatterned gold surface with 5 x 10  $\mu\text{m}$  dots (-)-PMT and DT on gold substrates after 30 days in solution with stirring. (+), (-) and racemic Phencyphos in isopropanol undersaturated solutions and fast solvent evaporation. Scale bar 5  $\mu\text{m}$ . The images in the lower part are enlarged zones of the images above.

In both systems, the crystallization took place over the whole surface, in a similar crystal growth morphology to that observed for crystallisation from sessile drops on full monolayers. The crystal growth clearly starts from a nucleus, in the middle of each domain, to outside forming dendritic-like patterns. These nuclei should be on the micropattern where the interaction is more favourable, although the pattern is not visible with the SEM through the organic material which has grown on the surface. The dark

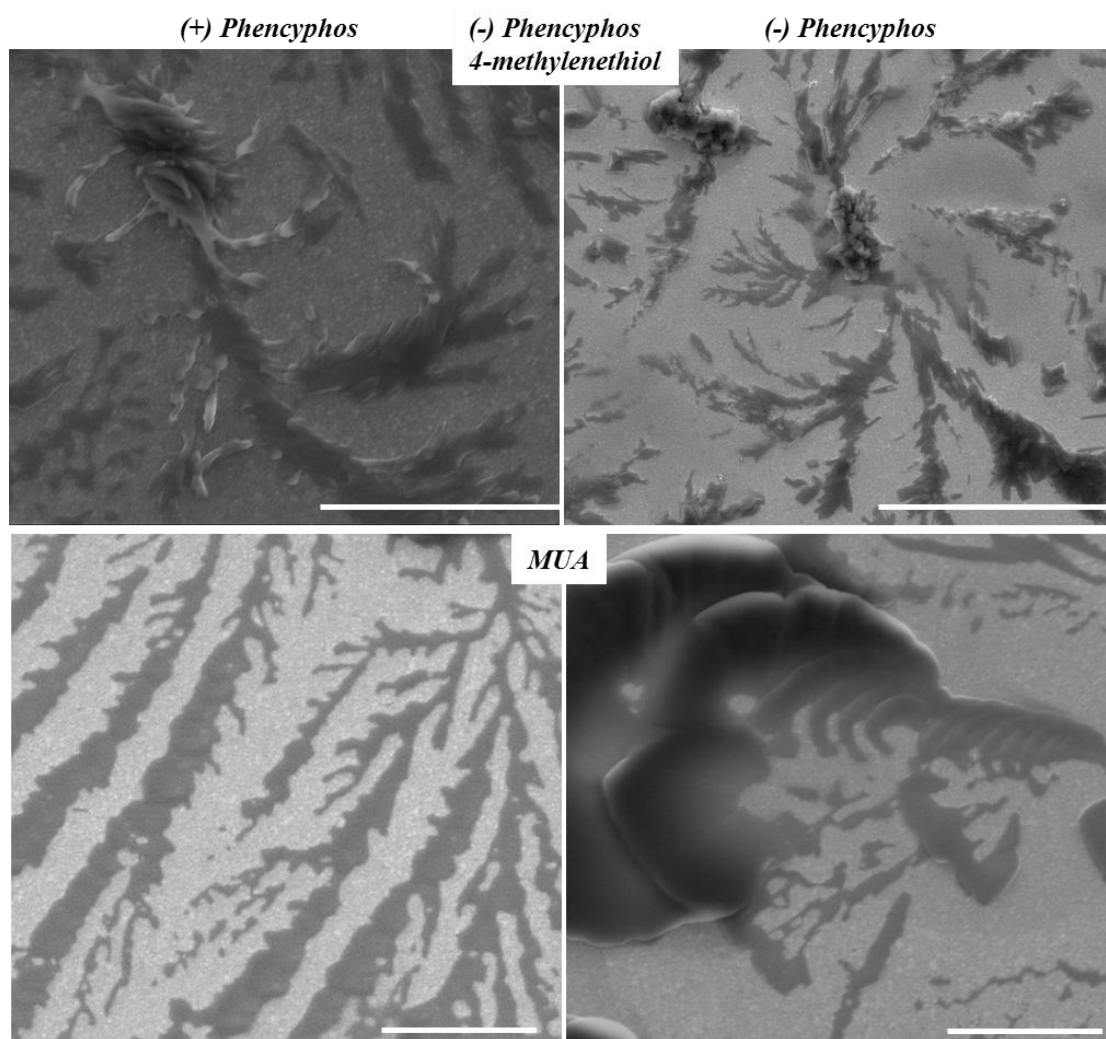
contrast in the SEM images implies that the material is in intimate contact with the underlying gold through the monolayer. Therefore, the long-time in solution with stirring favoured the diffusion over the micropatterned surface.



**Figure 8.1.26.** SEM micrographs of micropatterned  $5 \times 10 \mu\text{m}$  dots of MUA and dodecanethiol on gold substrates after 30 days in solution with stirring. (+), (-) and (*rac*) Phencyphos in isopropanol undersaturated solution. Scale bar  $10 \mu\text{m}$  in all images. The images in the lower part are enlarged zones of the images above.

The only difference between the two systems is the thiol printed on surface, all other materials and conditions were identical. The results of the crystallisations are similar although they present a big difference which is not evident on rapid inspection. The (*rac*) phencyphos crystals on the MUA micropatterned surfaces present an irregular growth while on (-)-PMT micropatterned surfaces their growth is dendritic. There is dramatic difference between in the case of the pure enantiomer crystals on MUA or (-)-PMT micropatterned surfaces, them.

Figure 8.1.27 shows the comparison between the two pure enantiomer crystals on both micropatterned surfaces. Observing the solid on (-)-PMT micropatterned surfaces, the chiral one, there is a particular twist on the growth of each collection of crystallites. They grow following a spiral pattern, and have opposite twist corresponding with their chirality. The individual crystals are not obviously chiral, but have a rectangular shape and are quasi-planar to the surface (as indicated by their contrast, the crystallites appear bright when growing away from the surface). This chiral effect could arise from; (i) induction by the (-)-PMT monolayer on the micropatterned surfaces, or (ii) be inherent to the chirality of each enantiomer at molecular level which is expressed in the crystal. In the case of option (i), it should be recalled that this kind of spiral growth was not observed on the SAMs of PMT without patterning or on the patterned surfaces where evaporation is relatively fast. If this characteristic growth is induced by the chirality of the molecules of each pure enantiomer, they would crystallize on the same growth over any chiral or achiral micropatterned surface. The growth of both pure enantiomers on MUA micropatterned surface do not present any twist, is an epitaxial growth according with the interaction between MUA monolayer and nuclei. A possible effect of the long period in liquid is the formation of mixed SAMs of (-)-PMT and DT. In any case, it appears that there is an influence from the monolayer patterned on surfaces which induces the emergence of chiral morphologies on the surface during the crystallization process.



**Figure 8.1.27.** SEM micrographs of (+) and (-) Phencyphos crystals on (-)-PMT and MUA micropatterned 5 x 10  $\mu\text{m}$  dots surfaces. Scale bar 5  $\mu\text{m}$  in all images.

Enantiomerically pure phencyphos crystallises under these conditions as twinned twisted crystals, due to a possible effect of the long period in liquid is the formation of mixed SAMs of (-)-PMT and DT. In a recent study done by Imai and Oaki,<sup>22</sup> the helical morphologies of amino acids (D- and L-aspartic acids (Asp)) have been observed. The importance of this morphology lies in that usually the D- and L-aspartic acids formed plate-like crystals from aqueous solution, while helical morphologies have been observed on the branches of a spherulitic morphology grown from the precursor solution including an agarose molecule with the evaporation of water (Figure 8.1.28 C-D).<sup>23</sup> The helical Asp

<sup>22</sup> H. Imai, Y. Oaki, *Angew. Chem. Int. Ed.*, **2004**, 43, 1363–1368.

<sup>23</sup> H. Imai, Y. Oaki, *CrystEngComm*, **2010**, 12, 1679–1687.

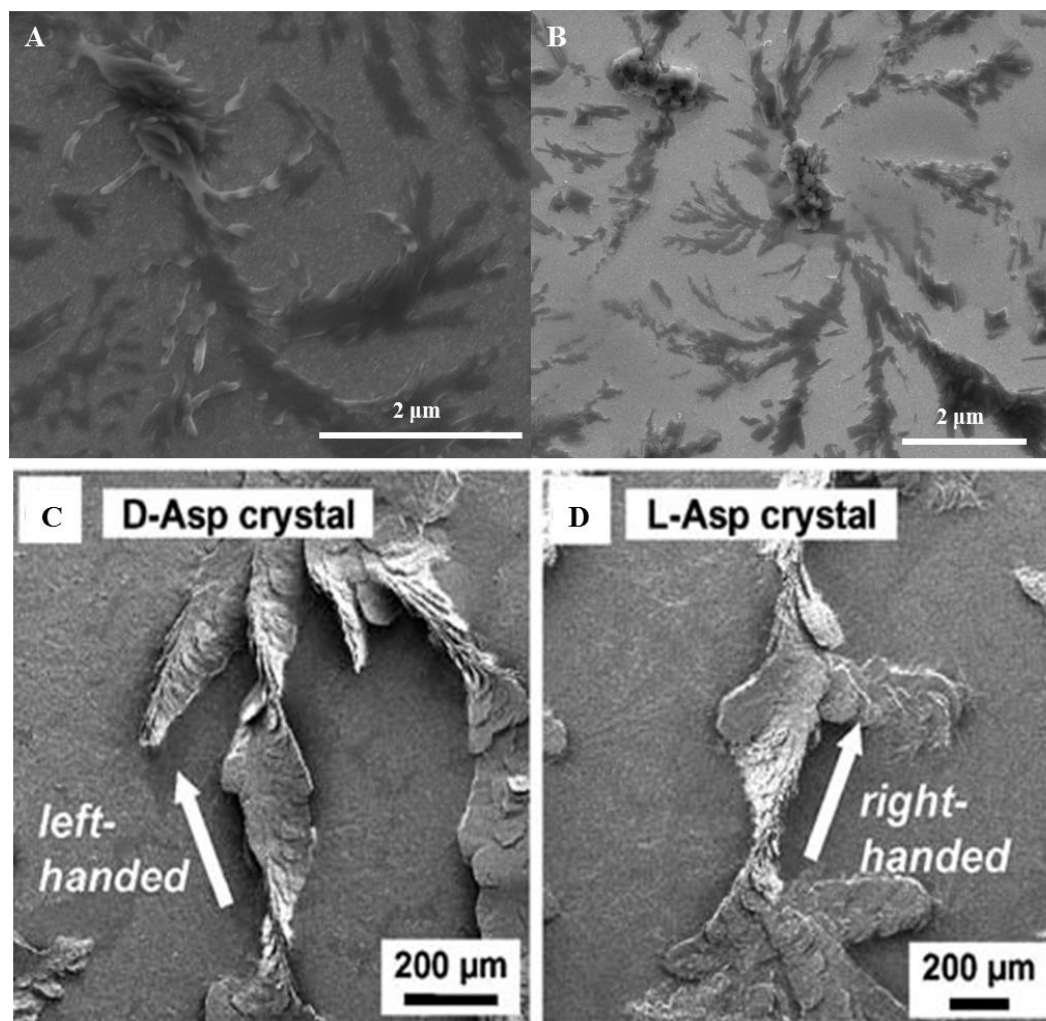
crystals have a backbone structure which consists in tilted units due to twinned connections.

Figure 8.1.29 describes a three-dimensional growth model and formation mechanism of the helical morphology in a diffusion field. This model applied to describe the crystal growth of the Asp helices conclude that the units were regularly accumulated in the backbone structure. The growth of the tilted units (Asp) proceeded in the [010] direction with a rotation of *ca.* 3.0° on the (110) faces as the twin plane.<sup>23</sup> The helical backbone structure of the Asp unit crystals is regarded as twisted twins. The rotated angles may be determined by the coincident lattice on the twin plane, and the local growth condition around the tilted unit crystals contributes to the variation of the helical pitches.<sup>22, 23</sup>

The main difference between enantiopure Phencyphos crystals on (-)-PMT micropatterned surface and the described enantiopure helices of Asp is, apart from the size (100 times bigger the aspartic acids helices than Phencyphos ones), the influence of the micropatterned surface. As it is explained in the figure 8.1.29, the helicoidal crystal growth is due to twin twisted crystals formation. In the Asp case, the size of the crystals allows define the crystal shape in order to translate in subunits, while in the Phencyphos helices on (-)-PMT are tiny defined. Nevertheless, this morphology for the Phencyphos crystals on micropatterned surfaces is uncommon. The reason which has more sense is that under these crystallisation method condition, the long-time in solution, form mixed SAMs of (-)-PMT and DT. The mixed SAMs<sup>24</sup> of (-)-PMT and DT provides an irregular interface, allowing twin twisted formation as it shown in the figure 8.1.28 A-B. The Phencyphos helicoidal crystal growth on (-)-PMT have different twisted, for the (+) Phencyphos is right-handed while for the (-) Phencyphos is left-handed.

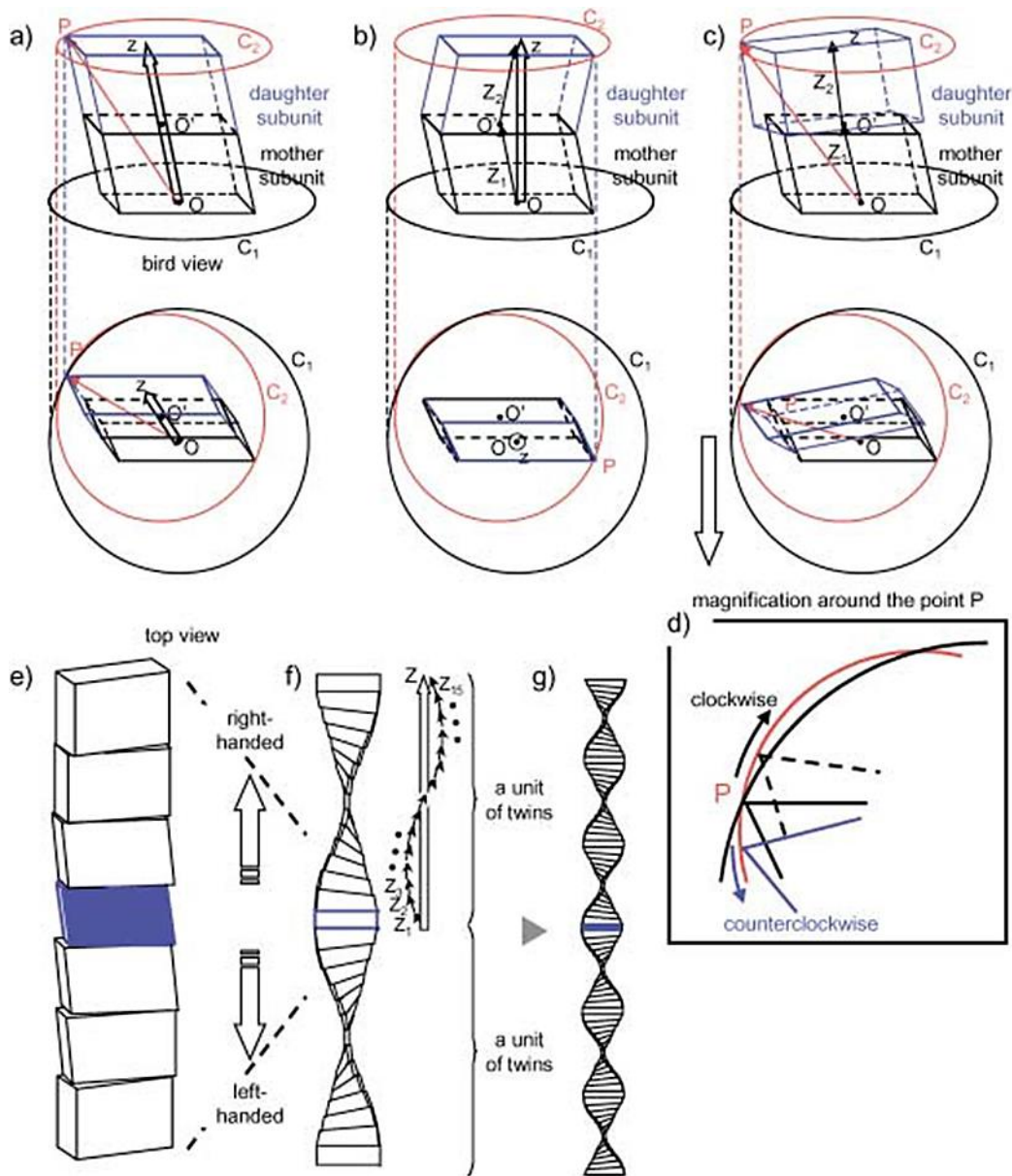
---

<sup>24</sup> J. C. Love, L. A. Estroff, J. K. Kriebel, R. G. Nuzzo, G. M. Whitesides, *Chem. Rev.*, **2005**, *105*, 1103-1169.



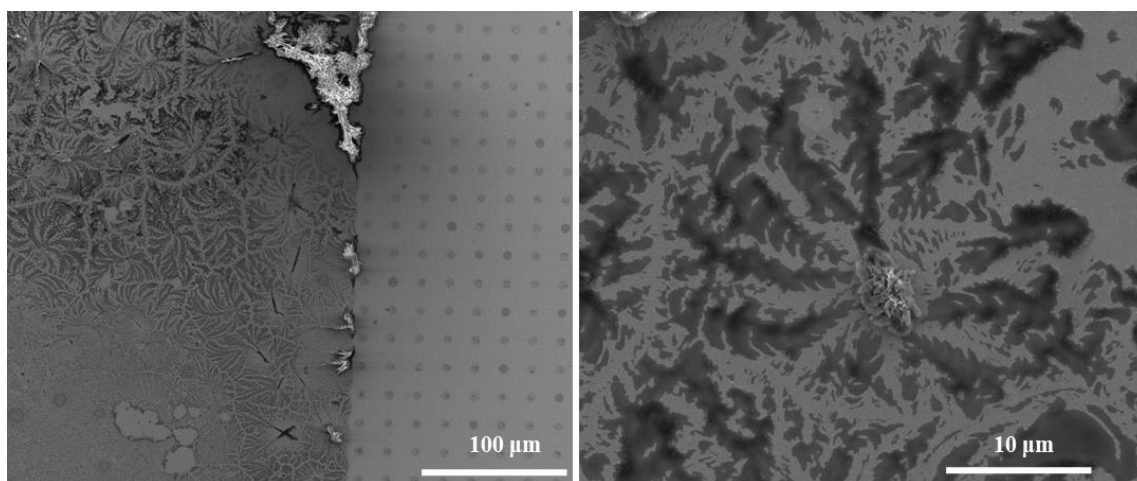
**Figure 8.1.28.** SEM micrographs of (A) (+) and (B) (-) Phencyphos crystals on (-)-PMT micropatterned  $5 \times 10 \mu\text{m}$  dots surfaces. FESEM images of the right- and left-handed helical morphologies generated from (C) D- and (D) L-Asp crystals grew from the precursor solution including an agarose molecule with the evaporation of water.<sup>23</sup>





**Figure 8.1.29.** A three-dimensional growth model and formation mechanism of the helical morphology in a diffusion field. a) The growth subunit is tilted. b) The reverse twin could be formed to achieve the faster growth as seen in the two-dimensional model. c) In three dimensions, the formation of slightly rotated twin nuclei is more probable than that of reversed nuclei. d) Magnification of the region around point P, the twisted direction is determined by the variation of the O–P distance. In this case, counter clockwise rotation viewed from the upper sides is preferable to the clockwise rotation. e) According to this model, the upward and downward accumulations induce the right- and left-handed twists, respectively. f) Right- and left-handed units of twins are produced from the nucleation point. The growth direction ( $Z_1, Z_2, Z_3$  to  $Z_{15}$ ) is finally adjusted to  $Z$ . g) A pile of units forms helices; the specified direction of twist does not change during growth. (O point is the origin growth point).<sup>22</sup>

We also observed the similar crystal growth in the crystallisation of (+)-phencyphos on micropatterned surface by dots  $5 \times 10 \mu\text{m}$  of (+)-PMT and DT (Figure 8.1.30), the helicoidal crystal growth observed in this case is right-handed. When the stamp used to microcontact printing method is smaller than the substrate to functionalise, outside the micropatterned area, mixed SAMs would be formed, providing the similar interface allowing the twin twisted formation. This experiment confirms the influence of the mixed SAMs formation onto the crystal growth of the enantiopure Phencyphos, notice that (rac) Phencyphos under the same crystallisation condition, even on mixed SAMs (-)-PMT and DT, has a spherulitic crystal growth without any twist.



**Figure 8.1.30.** SEM micrographs of (+) Phencyphos crystals outside the pattern of (+)-PMT micropatterned  $5 \times 10 \mu\text{m}$  dots surfaces in dichloromethane undersaturated solutions and slow solvent evaporation. The image on the right part is enlarged zone of the image on the left.

### 8.1.3. Pattern shape and size influence

The influence of the shape of the microcontact pattern motif and its size has an important effect onto the crystal growth at the surface. The use of different motifs to create micropatterns on surface provides a new way to prepare chiral surfaces because of the possibility of changing the size and shapes of the patterns. The study of Phencyphos crystallization on the surfaces implies a several experiments in order to test the diverse effects which have high influence on it.

Phencyphos crystallisation on micropatterned surfaces of different motifs of (+)-PMT with DT surround monolayer was done under slow solvent evaporation conditions (Figure 8.1.27.B). Motifs printed on the surface in these experiments were: squares and dots of 5 x 10  $\mu\text{m}$ , crosses of 35 x 70  $\mu\text{m}$  and spirals of different orientation of 50 x 100.

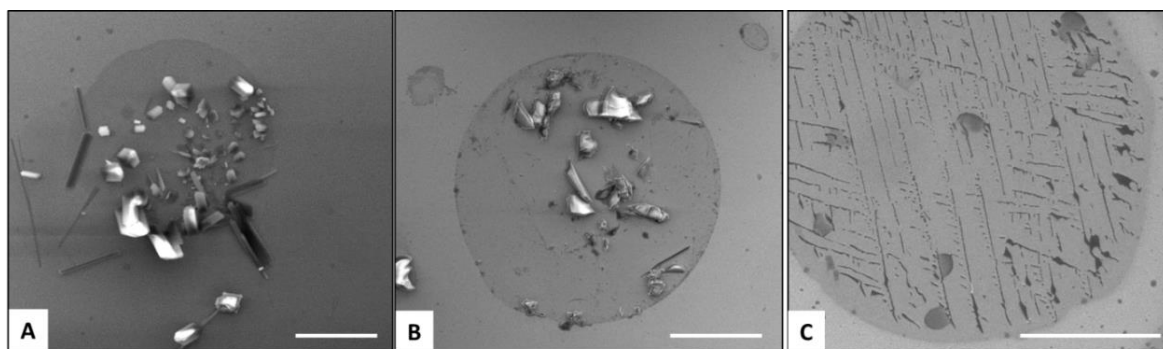
The size of the printed motif on the surface also influences dramatically the outcome of the crystallization process (Figure 8.1.31). When a dot motif of (+)-PMT with 50  $\mu\text{m}$  diameter was used, employing the same protocol to functionalize the gold surface and an identical crystallization method, the crystals formed were more similar to those formed during the crystallization of the compound on monolayers of (+)-PMT. Crystals from chloroform solution are localized in small islands inside the dot of 50  $\mu\text{m}$ , whereas crystals from isopropanol solution grow in the plane of the dot. This growth mode was already seen in previous experiments using full monolayers of (+)-PMT and the same crystallization method.<sup>25</sup> In this case, (+)-Phencyphos from isopropanol solution on a full monolayer, branched crystals grow, and thus, as the size of the printed motif was increased, the drop of the solution was localized over the motif which led to this type of crystal growth. From chloroform solution both enantiomers present similar behaviour, while from isopropanol solution the only one which crystallizes is (+)-Phencyphos, so again there is a qualitative change of chiral recognition depending of the solvent used.

In the case of the cross motifs, (+) Phencyphos crystallizes better than the (-) Phencyphos, the nucleus was formed in the middle of the cross, and many crystals grown around it (Figure 8.1.32.D). Perhaps the most stunning samples correspond to those where

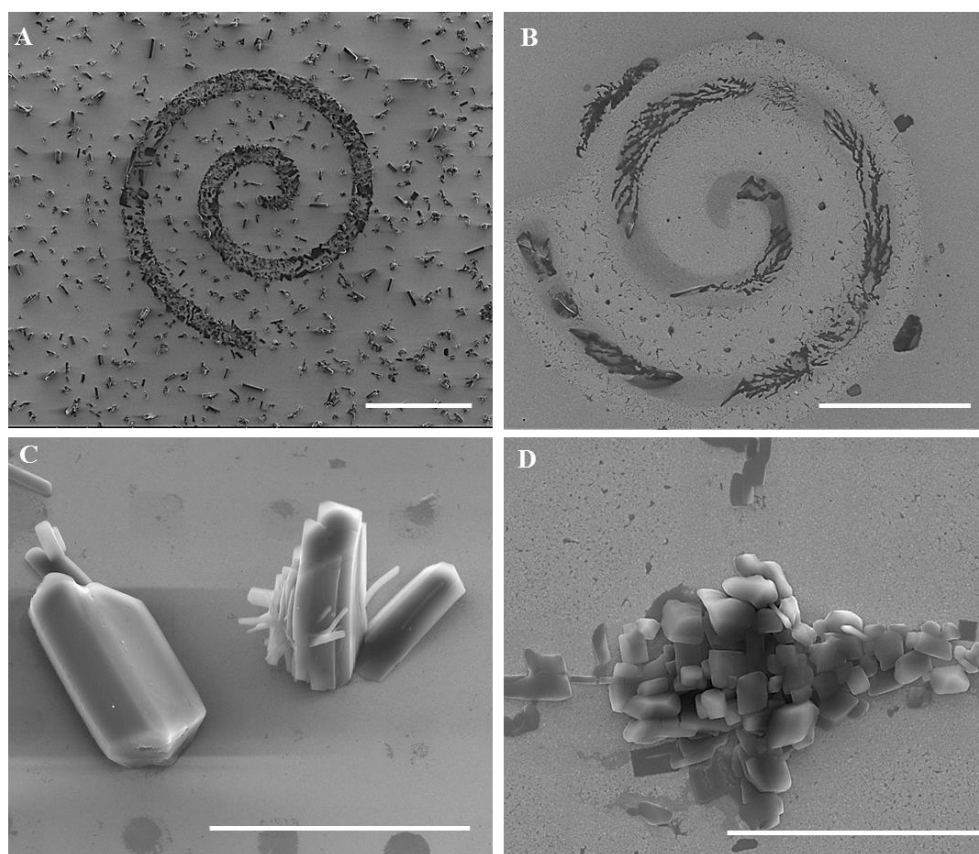
---

<sup>25</sup> A. Bejarano-Villafuerte, M. van der Meijden, M. Lingenfelder, K. Wurst, R.M. Kellogg, D.B. Amabilino, *Chem. Eur. J.*, 2012, **18**, 15984-15993.

the crystals are grown on spirals patterns. There is preferential crystallization over the spirals motif, and on some occasions a twisted propagation of the growth of the crystals, as is shown in the micrographs of (+) Phencyphos on R spirals (Figure 8.1.32.A).



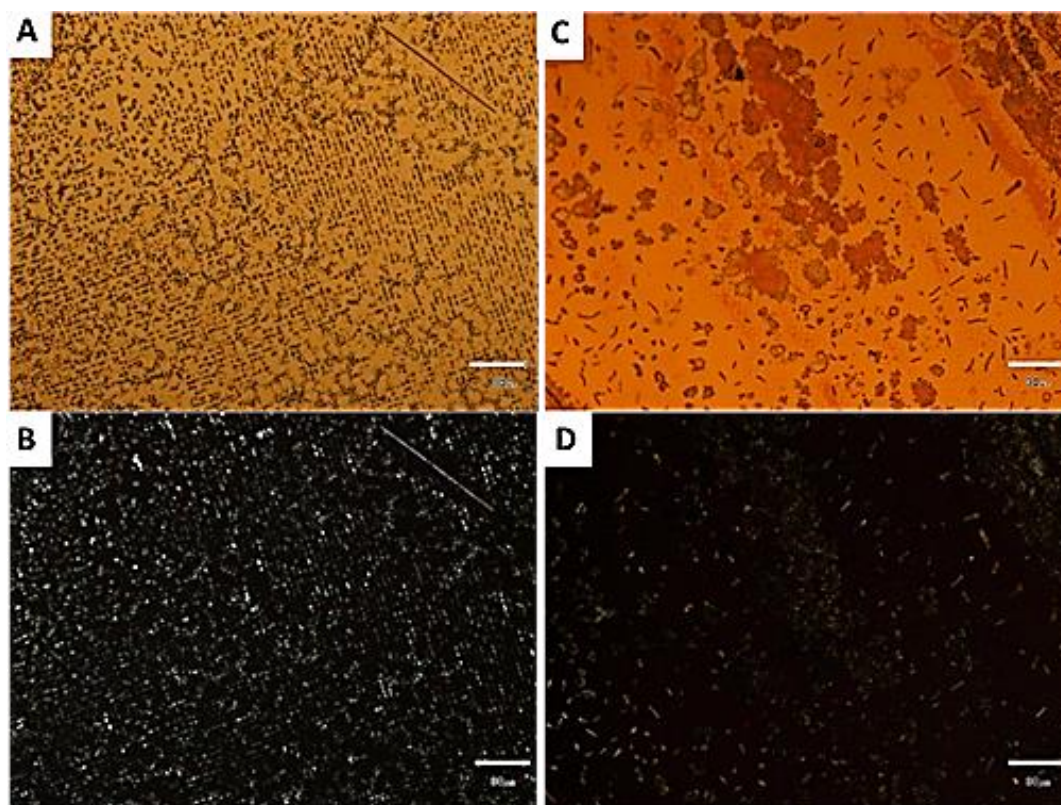
**Figure 8.1.31.** SEM images of crystals of Phencyphos on micropatterned surfaces of dots of 50 x 100  $\mu\text{m}$  of (+)-PMT and DT monolayers around. (A) (-)-Phencyphos crystals from chloroform solution. (B) (+)-Phencyphos crystals from chloroform solution. (C) (+)-Phencyphos crystals from isopropanol solution. Scale bar 20  $\mu\text{m}$ .



**Figure 8.1.32.** SEM micrographs of (A) (-) Phencyphos and (B) (+) Phencyphos on spirals pattern of 50 x 100  $\mu\text{m}$ , (C) (-) Phencyphos crystals on squares and dots 5 x 10  $\mu\text{m}$  and (D) (+) Phencyphos on crosses of 35 x 70  $\mu\text{m}$  of (+)-PMT and DT surrounded, from undersaturated solutions in chloroform under slow solvent evaporation conditions. Scale bar 30  $\mu\text{m}$ .

#### 8.1.4. Chirality and Polarity on surface

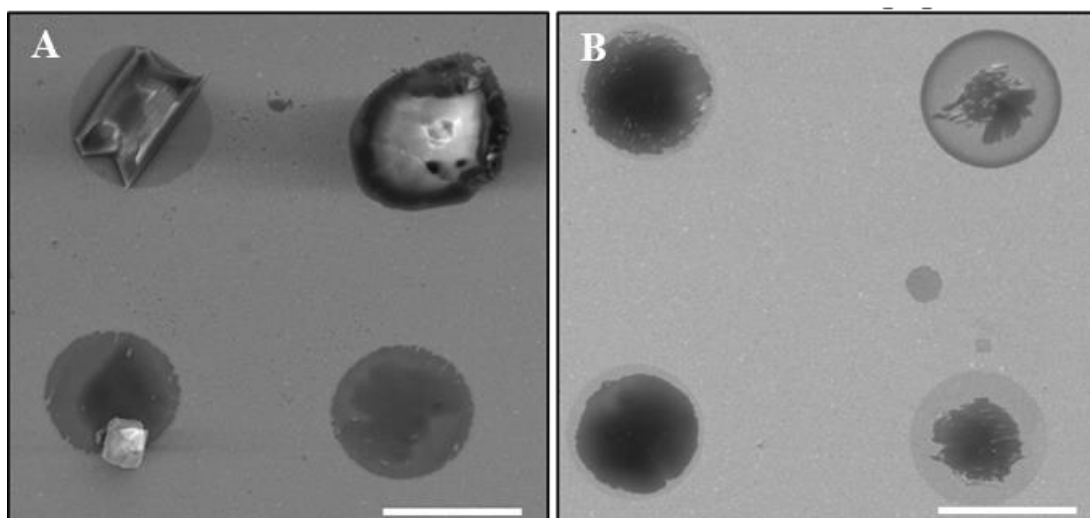
In order to test the specificity of the polar regions of the patterned surface towards the crystallization of Phencyphos, surfaces were prepared with MUA as the polar region in the same dodecanethiol surround used before. The microcontact printing method was performed as before, but using MUA as the ink, and patterns of dots of 5 x 10  $\mu\text{m}$  were used. Slow evaporation of a chloroform solution of Phencyphos results in the formation of crystal on the MUA pattern but also in between the pattern features (Figure 8.1.33), and show a significant difference from those formed on the phosphate-terminated monolayer. The heterogeneously nucleated crystals of Phencyphos follow the pattern formed by (+)-PMT almost perfectly, while those formed on the MUA pattern are largely distributed randomly. The result appears to indicate that the like-acid is important for the nucleation of the acid Phencyphos on the surface. The result emphasizes the effectiveness of the phencyphos derivative SAM in heterogeneous nucleation.



**Figure 8.1.33.** Optical microscope images of crystals of (+)-Phencyphos grown from saturated chloroform solution on different functionalized gold surfaces. (A), (B) are images of (+)-Phencyphos crystal on (+)-PMT. (C), (D) are images of (+)-Phencyphos crystals on MUA. (A) and (C) non polarized images, (B) and (D) Polarized image. Scale bar 30 microns. Notice the patterned surface in the non-polarized image of (+)-Phencyphos crystals on MUA.

### 8.1.5. Contrasting solvents in the heterogeneous nucleation of PMT on micropatterned surfaces

The combination of surface chirality and crystallizing compound chirality does not result in a well-defined diastereoselective crystal growth. When the enantiomers of Phencyphos were crystallized from isopropanol by homogeneous nucleation they formed large crystals of identical appearance to those from chloroform. The qualitative change of chiral recognition as a result of change in the solvent used is not documented for surface-based systems, although changes in discrimination between enantiomers have been observed in solution-based systems.<sup>26</sup> When the evaporation rate of the isopropanol was faster crystal nuclei were not formed significantly on the pattern, pointing to homogeneous nucleation (a fact confirmed by the presence of large crystals not correlated with the pattern). On the other hand, the use of dichloromethane - a faster evaporating solvent - resulted in the formation of crystals on the pattern, but no stereoselectivity was detected (Figure 8.1.34).



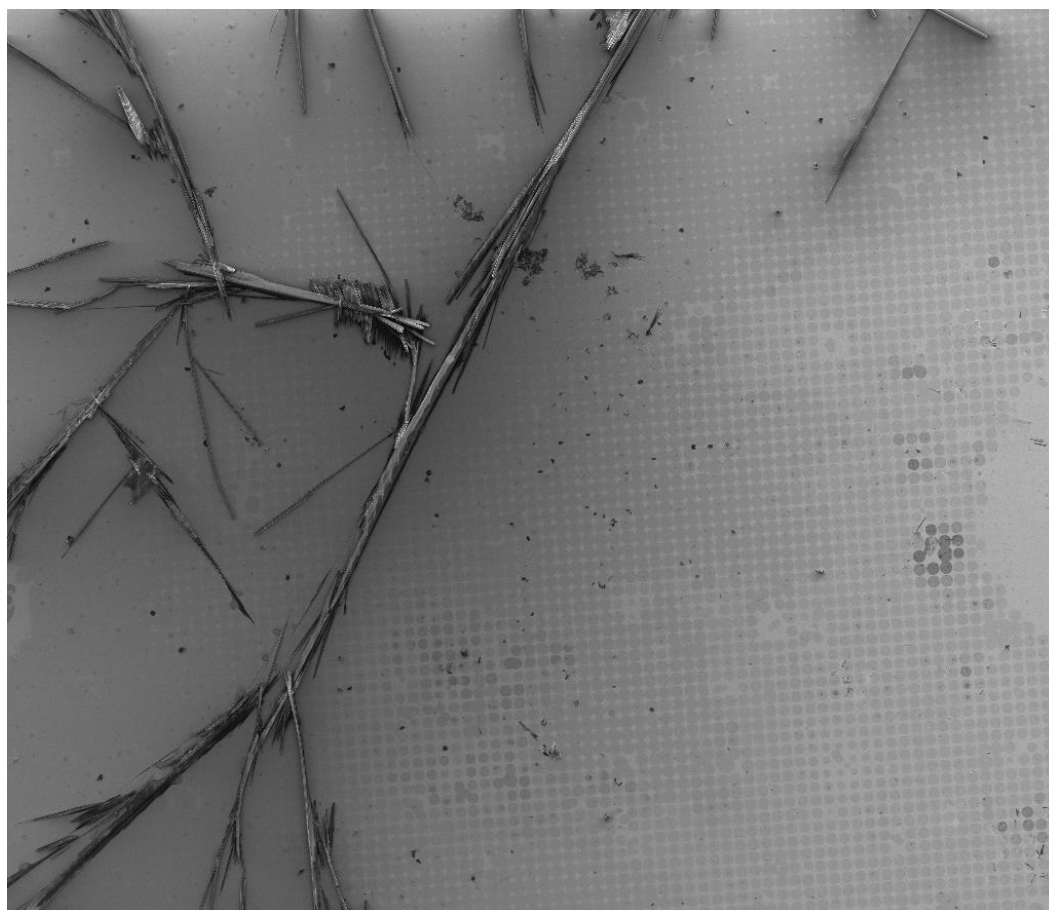
**Figure 8.1.34.** SEM images of crystals of (+) Phencyphos grown on dots of  $5 \times 10 \mu\text{m}$  (+)-PMT grown from saturated solution of (A) acetonitrile and (B) dichloromethane by slow evaporation of the solvent; the light grey zones correspond to the DT SAM. Scale bar is  $5 \mu\text{m}$ .

<sup>26</sup> H. Goto, Y. Okamoto, E. Yashima, *Macromolecules*, **2002**, *35*, 4590-4601. W. Yu, Y.G. Li, T.Y. Wang, M.H. Liu, Z.S. Li, *Acta Phys-Chim Sinica*, **2008**, *24*, 1535-1539. K. Smith, *Chem. Soc. Rev.*, **2009**, *38*, 684-694. Q.B. Wang, Y.L. Chen, P. Ma, J.T. Lu, X.M. Zhang, J.Z. Jiang, *J. Mater. Chem.*, **2011**, *21*, 8057-8065. I.C. Pintre, S. Pierrefixe, A. Hamilton, V. Valderrey, C. Bo, P. Ballester, *Inorg. Chem.*, **2012**, *51*, 4620-4635.

It seems likely that the reason for the apparently improved diastereoselectivity in isopropanol may be a result of specific interactions between monolayer and crystal nucleus mediated by the solvent, because the orientation of the crystal is also clearly different, which may point to a particular interaction between surface and growing crystal in the solvent.

This hypothesis is supported by the fact that we have not detected stereoselectivity in either dichloromethane or acetonitrile, where the morphology of the precipitate of Phencyphos is quite different to either chloroform or isopropanol. Evaporation of solutions of (+) Phencyphos onto 5 x 10  $\mu\text{m}$  dot patterns of (+)-PMT result in the formation of crystals in the micropatterned areas of different shape, but principally in the plane of the surface (Figure 8.1.34). In both cases the very dark appearance of some of the dots indicates that significant amorphous material is present there and therefore that the crystallization is not optimum from these solvents.

The use of methanol and ethanol were not suitable because Phencyphos is so soluble that the evaporation of the solutions do not lead to well-formed crystals of the compound, which is also insufficiently soluble in ethyl acetate for these experiments. The fast evaporation of isopropanol on the patterned surfaces results in the formation of large crystals (up to 1 mm in length, almost an order of magnitude larger than the pattern) which do not follow the patterned surface at all, indicating that homogeneous nucleation had taken place (Figure 8.1.35).



**Figure 8.1.35.** SEM image of crystals of (-) Phencyphos grown on dots of 5 x 10 μm (+)-PMT and DT grown from saturated isopropanol solution by slow evaporation of the solvent. Scalebar is 500 μm.

Apart from any specific interactions, such as conventional or non-conventional hydrogen bonding<sup>27</sup> or interactions involving the halogen atoms,<sup>28</sup> one could envisage that the general wetting behaviour of the solvent and the solution of Phencyphos could influence the crystallization behaviour. In Table 8.1, the wetting angles of the neat solvents used as well as the solutions containing Phencyphos (in its two enantiomeric forms) are shown for a self-assembled monolayer of (+)-PMT. The polar solvents isopropanol and acetonitrile completely wet the surface and their solutions with the solute do the same. Chloroform forms slight angle which is reduced by the presence of Phencyphos in the solvent. Dichloromethane forms the highest contact angle, which is

<sup>27</sup> I. Alkorta, I. Rozas, J. Elguero, *Chem. Soc. Rev.*, **1998**, 27, 163-170.

<sup>28</sup> A. Gavezzotti, *Mol. Phys.*, 2008, **106**, 1473-1485.



lowered slightly by the presence of Phencyphos to slightly differing extents, which might indicate another example of enantioselective wetting,<sup>29</sup> though the effect is small.

It is obvious from this data that there is no direct correlation between either the contact angle that the solutions form or their volatility and either the shape of the crystals formed or the angle that they form with respect to the templating layer plane. Again, this points to a specific solvation sphere around the nucleus and surface which leads to a growth away from the surface when the crystals are nucleated on the monolayer from chloroform and in the plane in the other cases.

**Table 8.1.** Contact angles of organic solvents and Phencyphos (PP) solutions with a monolayer of (+)-PMT on polycrystalline gold.

Solvent	Composition	Contact Angles (°)
<b>Chloroform</b>	neat	4
	(-)-PP (2.4 mM)	2
	(+)-PP (2.4 mM)	2
<b>Iso-propanol</b>	neat	0
	(-)-PP (4.8 mM)	0
	(+)-PP (4.8 mM)	0
<b>Acetonitrile</b>	neat	6
	(-)-PP (2.8 mM)	0
	(+)-PP (2.8 mM)	0
<b>Dichloromethane</b>	neat	11
	(-)-PP (6.9 mM)	9
	(+)-PP (6.9 mM)	8

<sup>29</sup> M. Rapp, W.A. Ducker, *J. Am. Chem. Soc.*, 2010, **132**, 18051–18053.

### 8.1.6. Conclusions

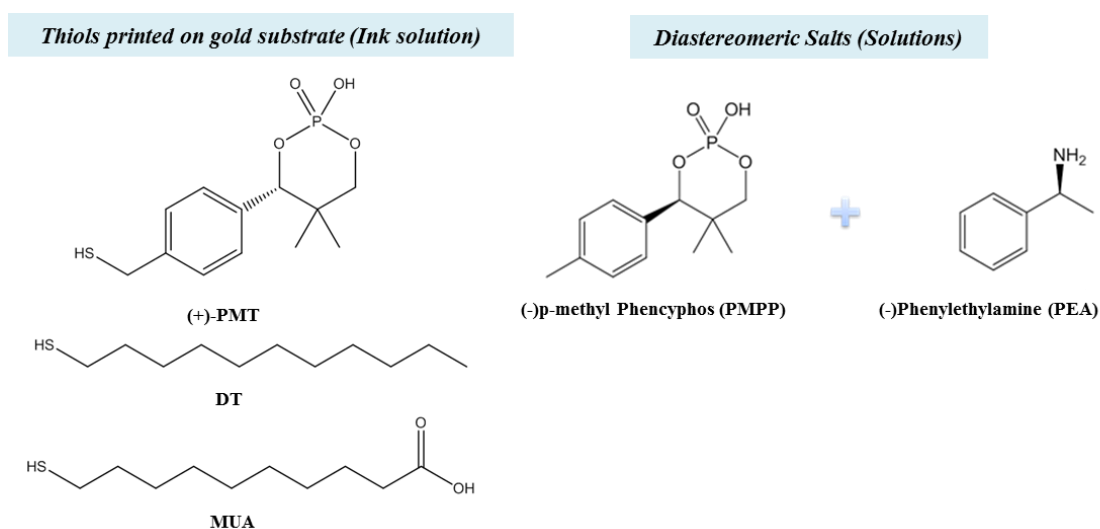
The use of chiral micropatterned SAMs to crystallise phencyphos by heterogeneous nucleation is effective when the solvent is allowed to evaporate slowly from the surface. There are several parameters which have a dramatic influence on the crystallisation process. The pattern shape and size are critical, the motif size which presents better results in favour of the nucleation is dots of 5  $\mu\text{m}$  diameter, separated by 10  $\mu\text{m}$ .

We have demonstrated the formation of chiral patterned surfaces based on a cyclic phosphate unit which has proven utility as a resolving agent. The polar group is an effective termination in a layer on gold for the heterogeneous nucleation of a similar organic compound, despite the lack of order in the monolayer. This observation points to the importance of the polarity at the surface, rather than an epitaxial model for growth. The effect that solvent plays on the crystal growth supports this idea. The apparent selectivity shown between phosphate and carboxylate termination of the pattern in the crystallization of phencyphos could indicate a way to control specific crystallization by heterogeneous nucleation. The results could be important not only for the growth of organic compounds on surfaces but also for other molecular materials presently of enormous interest. The indication of a change in the stereoselectivity of the crystallization process with the solvent because of the orientation of the crystal is particularly important, and could point to a route to stereoselective crystallization for the resolution of enantiomers.

## 8.2. Preferential Diastereomeric Salts crystallisation on micropatterned surfaces

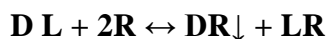
### 8.2.1. Introduction

The final objective of this Thesis was to design a selective surface able to resolve racemic mixtures of different compounds by diastereomeric salts crystallization on the same surface functionalised by different SAMs. In the previous subsection of this Chapter, we have established the fundamentals of the method for the enantiomerically pure compounds crystallisation on chiral micropatterned surfaces. Nevertheless, in this subsection the preferential crystallization of diastereomeric salts on micropatterned surfaces, as the next natural step after the study of the pure enantiomers of phencyphos on chiral micropatterned surfaces, will be described. The strategy followed was the use of the chiral enantiopure thiol (+)-PMT or the achiral MUA for the polar regions, to check whether the crystallization is a consequence of the chiral or polar recognition, respectively. To block the rest of the surface dodecanethiol was always used.



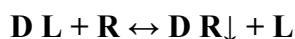
**Figure 8.2.1.** Diastereomeric salts to crystallise on micropatterned gold surfaces and thiols selected to functionalise the gold surface.

Before starting the study of the crystallization of the PMPP/PEA salt on the (+)-PMT functionalized surfaces; the salt crystallization was studied in bulk solution under homogeneous nucleation conditions. According to the optical resolution via diastereoisomeric salt formation there are three different crystallization methods: Pasteurian resolution, Marckwald method and the Pope-Peachy method<sup>1</sup>. During the classic *Pasteurian resolution*, equimolar amounts of racemic mixture and resolving agent are used so that all the material is in salt form:<sup>2</sup>

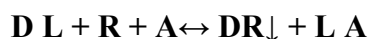


*D* and *L* represent the enantiomers of the racemic mixture, *R* represents the resolving agent.

The *Marckwald method* uses non-stoichiometric amounts (0.5 mol) of resolving agent, because only the enantiomer which forms the less-soluble salt crystallises with the resolving agent, thereby enriching the solution with the other isomer.<sup>3</sup>



The last method is the *Pope-Peachy method* which is used when there are solubility problems during the use of the Marckwald method, thus, an achiral (*A*) salt of the less preferred enantiomer can be formed.<sup>4</sup>



These three methods have been probed in our system, using the racemic mixture of phenylethylamine (PEA), p-methyl phenylphosphine (PMPP) as the resolving agent, and (+) PMT as a third component of the mixture to crystallise with one of the enantiomers of the PEA.

---

<sup>1</sup> D. Kozma, Z. Madarász, C. Kassai, E. Fogassy. *Chirality*, **1999**, *11*, 373-375.

<sup>2</sup> L. Pasteur, *Compte-rendus de l'Académie des Sciences*, **1853**, *37*, 162-166.

<sup>3</sup> W. Marckwald, *Ueber ein bequemes Verfahren zur Gewinnung der Linksweinsäure*, *Berichte der deutschen chemischen Gesellschaft*, **1896**, *29*, 42-43.

<sup>4</sup> W.J. Pope, S. J. Peachey, *J. Chem. Soc. Trans.*, **1899**, *75*, 1066-1093.

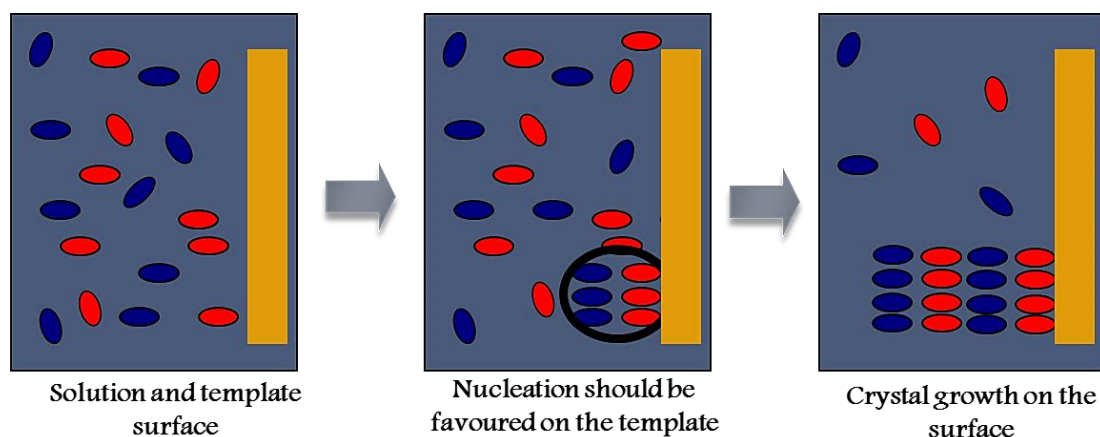
**Table 8.2.1.** Resolution experiment following the three methods: *Pasteurian resolution*, *Marckwald* and *Pope-Peachy methods*. Crystallisation conditions: 25 mM of PEA in EtOH, warm the solution up, add PMPP and the solution is left at room temperature until crystallisation.

<i>Phenylethylamine</i>	<i>PMPP</i>	<i>Pasteurian</i>	<i>Marckwald</i>	<i>Pope-Peachy</i>
(Rac) PEA	(-) PMPP	-	-	(+) PMT --
(Rac) PEA	(+) PMPP	-	-	(+) PMT --
(Rac) PEA	(-) PMPP	-	-	(+) PMT --
(Rac) PEA	(+) PMPP	-	-	(+) PMT --
(-) PEA	(-) PMPP	Crystals	-	-
(-) PEA	(+) PMPP	-	-	-
(+) PEA	(-) PMPP	-	-	-
(+) PEA	(+) PMPP	Crystals	-	-

Following the Pasteurian resolution method, only two salts of PEA and PMPP crystallised, they were: (-)-PEA/ (-)-PMPP and (+)-PEA/ (+)-PMPP. Nevertheless, when Marckwald and Pope-Peachy methods were used no crystallization was observed for any combination.

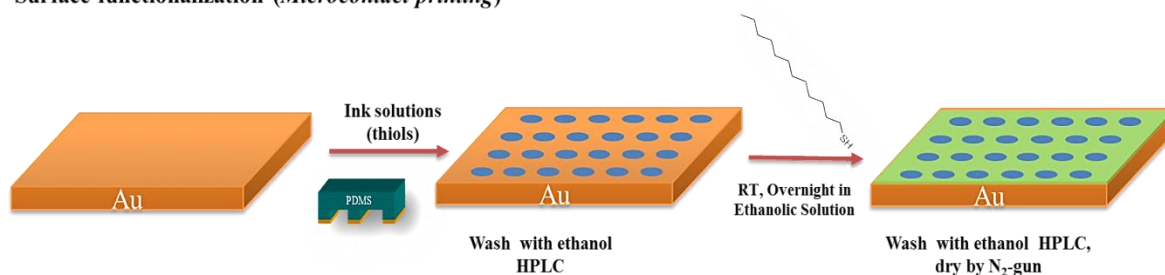
Our study is focused on the interface solution-monolayer of micropatterned surfaces (Figure 8.2.2) that corresponds to the heterogeneous nucleation which should be thermodynamically favoured providing there is a structural match of the nuclei to the monolayer at the interface.<sup>5</sup> Following the same surface procedure described in Chapter 8.1, (Figure 8.2.3), the surfaces were micropatterned with (+)-PMT or MUA, respectively, to contrast the nature of the surface. In order to prevent side-reactions or physisorption on the non-patterned areas, the surfaces were then incubated with DT to passivate the areas of the surface that had not contacted the stamp before the crystallisation step.

<sup>5</sup> Chapter 1, Introduction, Nucleation theory.



**Figure 8.2.2.** Heterogeneous nucleation favoured by the functionalised surface in solution.

**Surface functionalization (Microcontact printing)**



**Figure 8.2.3.** Microcontact printing protocol for the preparation of patterned surfaces. Each arrow implies a washing step with ethanol.

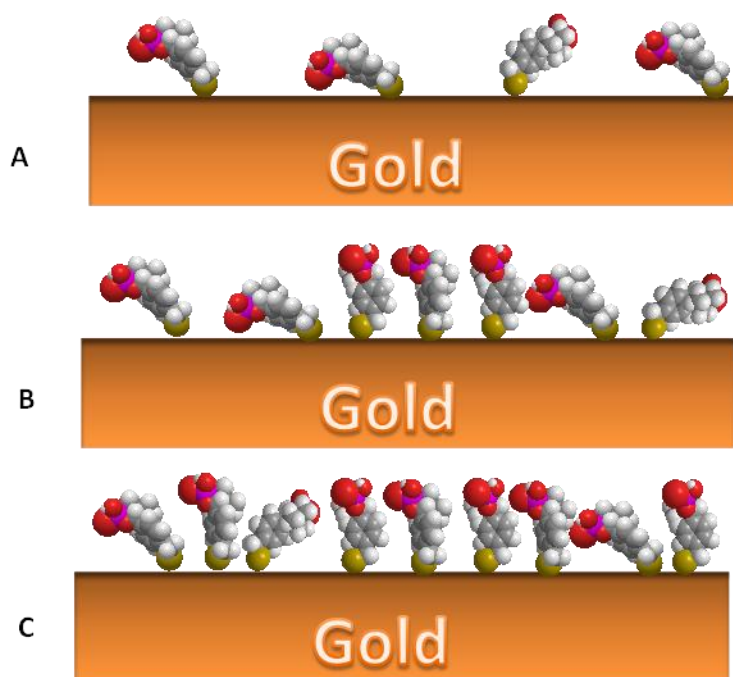
To control the crystallisation of the diastereomeric salt of PEA and PMPP on micropatterned surfaces several parameters such as solvent evaporation and formation of the micropatterned layers, among others, have to be studied. Throughout this section of the Chapter all the parameters studied and their influence on the crystallization of the PEA/PMPP diastereomeric salt will be discussed.

In the previous section we have demonstrated that the slow solvent evaporation method was the best for the crystallization of phencyphos. Therefore, the study of diastereomeric salt crystallization was performed following the same procedure. The study of the influence of the concentration of the PMPP ink solution, shape and size of the motifs, incubation time and control experiments was done first by the slow solvent evaporation method with the micropatterned surface incubated in a vertical position to ensure that the crystals grow from the surface.

## 8.2.2. The parameter influence in the diastereomeric salt crystallisation on micropatterned surfaces

### 8.2.2.1. Concentration of the ink solution influence

It is known that the packing density of printed SAMs can be modified by adjusting the ink concentration and the amount of ink solution deposited on the stamp.<sup>6</sup> The influence of the concentration of the ink solution affects the density of the monolayer as well as the density of nucleating regions (Figure 8.2.3). A very concentrated ink solution would produce a very dense monolayer, restricting the movement of the molecule's linked to the surfaces and blocking their polar positions and therefore the formation of a good template for the nucleus. Nevertheless, a low concentration of ink solution would produce a less dense monolayer with too much distance between the molecules on the monolayer<sup>7</sup> and therefore a (probably) impeded nucleating activity on the surfaces.

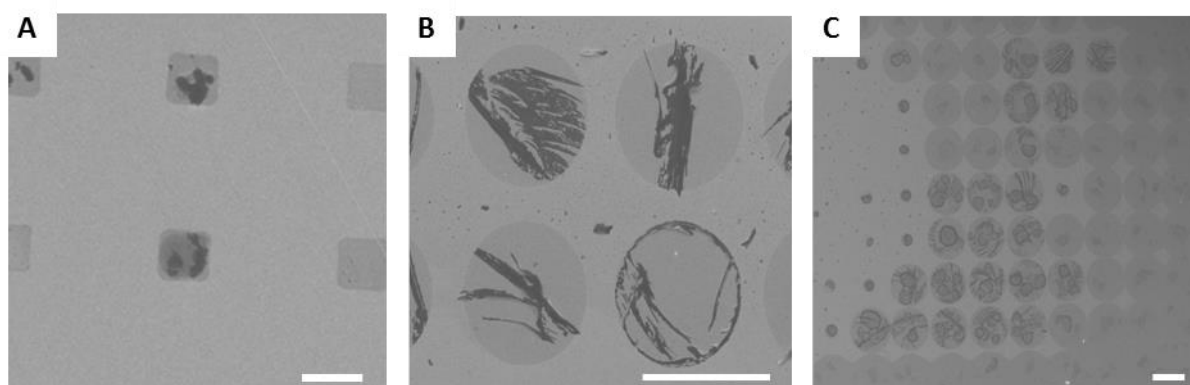


**Figure 8.2.3.** Schematic representation of the effect of variation of the density of the monolayers of (+) PMT on gold surfaces. (+)-PMT concentration: A) 0.1 mM, B) 1 mM and C) 10 mM.

<sup>6</sup> (a) D. Losic, J. G. Shapter, J. J. Gooding, *ElectroChem. Comm.*, **2001**, 3, 722-726. (b) Thomas J. Mullen, C. Srinivasan, J. N. Hohman, S. D. Gillmor, *Applied Phys. Lett.*, **2007**, 90, 063114-1-3.

<sup>7</sup> **Chapter 4**, (+)-PMT SAMs on gold, STM analysis.

The figure 8.2.4 A-C shows the micropatterned surfaces according the concentration variation of the ink solution in order to probe its influence in the nucleation process. Every micropatterned surface shows nucleation on the desired regions, nevertheless, only in the case of 1 mM (Figure 8.2.4.B) the crystal grow according to the pattern, forming well defined crystals. Thus, the most favourable concentration to get good nucleation on the dots of (+)-PMT is 1 mM, which agrees with the typical concentration used for features bigger than 1  $\mu\text{m}$ .<sup>8</sup> Moreover, higher concentration of the (+)-PMT (Figure 8.2.4.D) collapses the surface making the free movement of the molecules which form the monolayer difficult, and indicating that probably a leach out onto non-contacted regions of the surface has also occurred. The lowest concentration (Figure 8.2.4.A) is insufficient to form the ideal density of nucleating regions on the surface.



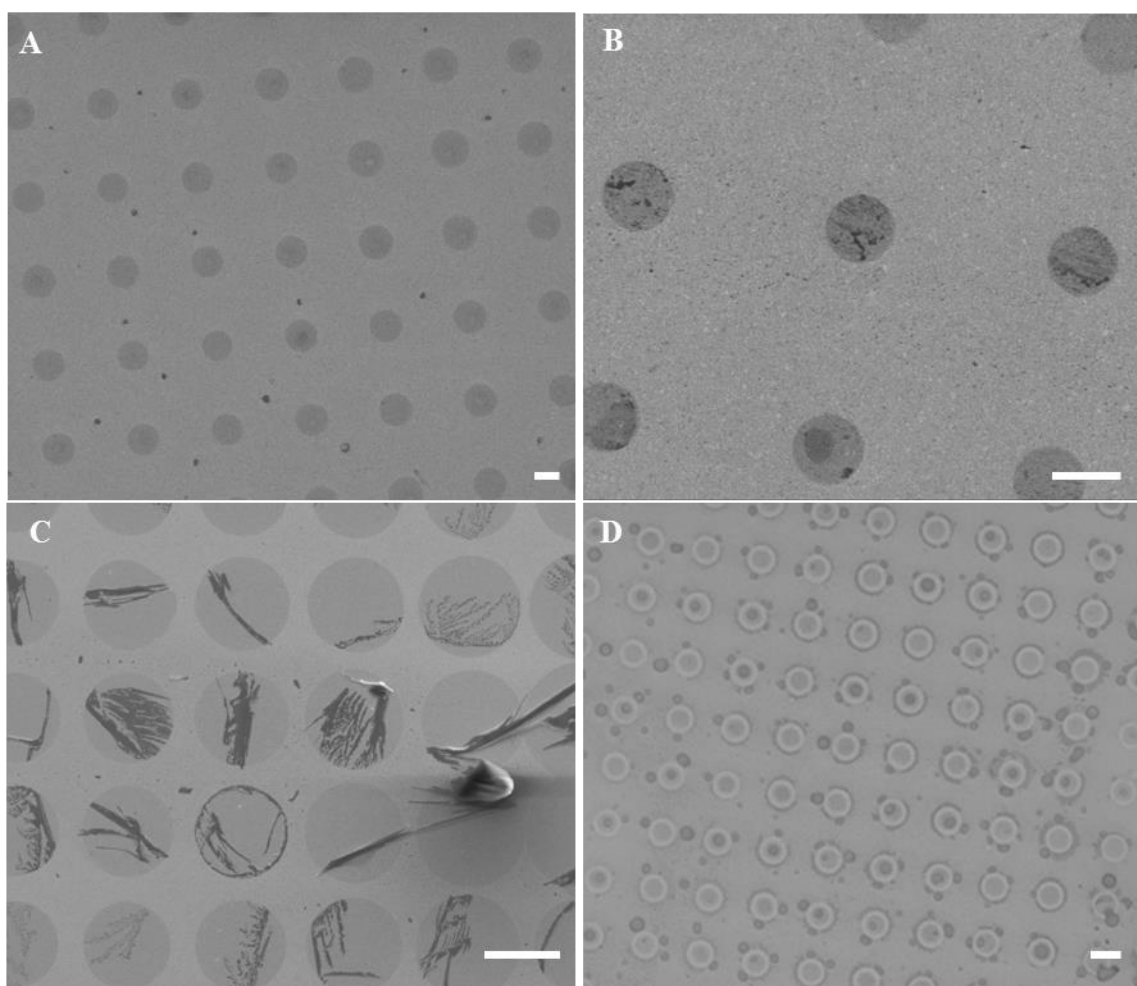
**Figure 8.2.4.** SEM micrographs of crystallization of (-) PMPP/ (-)PEA on micropatterned surfaces of squares or dots of 5 x 10  $\mu\text{m}$  of (+)-PMT as ink solutions. (+)-PMT concentration: A) 0.1 mM, B) 1 mM and C) 10 mM. Scale bar 5  $\mu\text{m}$ .

<sup>8</sup> J. C. Love, L. A. Estroff, J. K. Kriebel, R. G. Nuzzo, G. M. Whitesides, *Chem. Rev.*, **2005**, *105*, 1103-1169.



### 8.2.2.2. Control experiments

Control experiments were necessary to establish which specie crystallises on the micropattern, since PMPP and its diastereomeric salt could both form solids, while pure PEA is a liquid at room temperature. Therefore, patterned SAMs of (+)-PMT were immersed vertically for 4 hours in a solution of pure (-)-PEA (30 mM in EtOH), pure (-)-PMPP (30 mM in EtOH), mixture (-)-PEA / (-)-PMPP (30 mM in EtOH). Pure EtOH was also used to rule out impurities in the crystallization from the solvent. SEM micrographs confirmed that under these conditions crystals were only observed when the mixture of (-)-PMPP/ (-)-PEA was used, Figure 8.2.5.



**Figure 8.2.5.** SEM micrographs of control experiments. Deposition of (A) (-)-PEA, (B) (-)-PMPP, (C) (-)-PEA / (-)-PMPP and (D) EtOH on micropatterned surfaces of dots of 5  $\mu\text{m}$  separated 10  $\mu\text{m}$  (5 x 10  $\mu\text{m}$ ) of (+)-PMT. Crystals only appears when a solution of the of the diastereomeric salt was used. Scale bar is 5  $\mu\text{m}$  in all images.

### 8.2.2.3. Incubation time influence

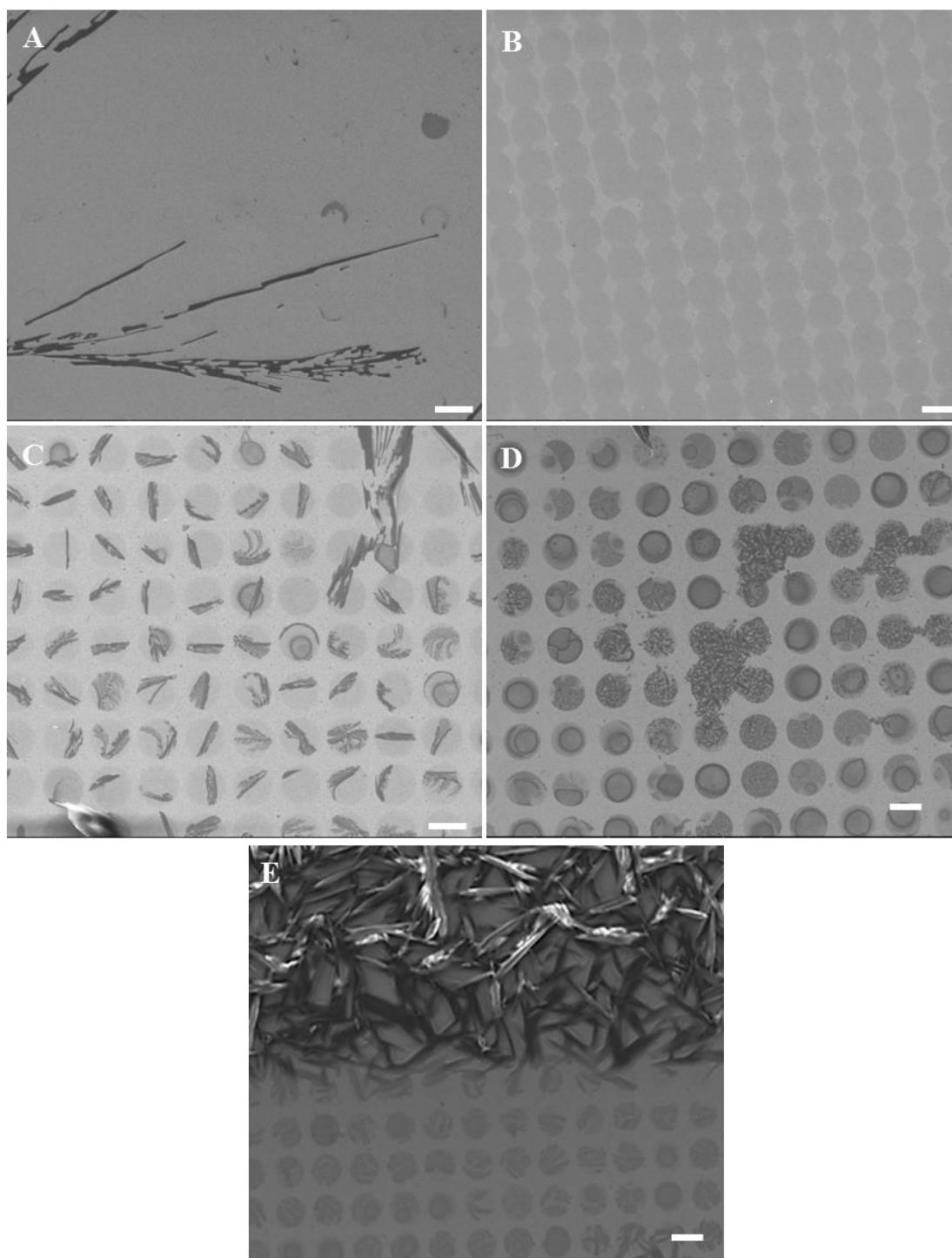
In the crystallisation process, time is a crucial parameter which could give a tool to control the crystal growth. Micropatterned surfaces in solution could provide different crystal size or amount of crystals on the surface depending on the incubation time in solution.<sup>9</sup>

In order to study the time necessary to get crystals on the surfaces, micropatterned SAMs of (+)-PMT were immersed vertically for 30 min, 1h, 4h and 26h, respectively, in a 30 mM solution of (-)PMPP/(-)PEA in EtOH at room temperature. After the incubation time the surfaces were removed from the solution carefully and placed in a closed vial, which was saturated with EtOH vapours. The solvent was slowly evaporated within 5 days to obtain the crystals. In the case of the crystallisation time of 26 hours, the crystallisation could not be controlled. In Figure 8.2.6. D-E, it can be appreciated how crystals grow outside the pattern, there are clearly many crystals also from homogeneous nucleation in the bulk solution.

SEM micrographs showed that better crystallization was achieved after 4 hours of incubation of the surface in the solution of the salt components (Figure 8.2.6.C). Shorter incubation times were apparently insufficient for well-formed diastereomeric salt nucleation and its crystallization on the surface (Figure 8.2.6.A-B). Increasing the incubation time (26h) of these micropatterned surfaces, crystals appear in and outside the micropattern, indicating that the pattern was saturated with material (Figure 8.2.6.-D-E).

---

<sup>9</sup> E. Pálóvics J. Schindler, F. Faigl, E. Fogassy, *Tetrah. Asym.*, **2010**, *21*, 2429–2434.



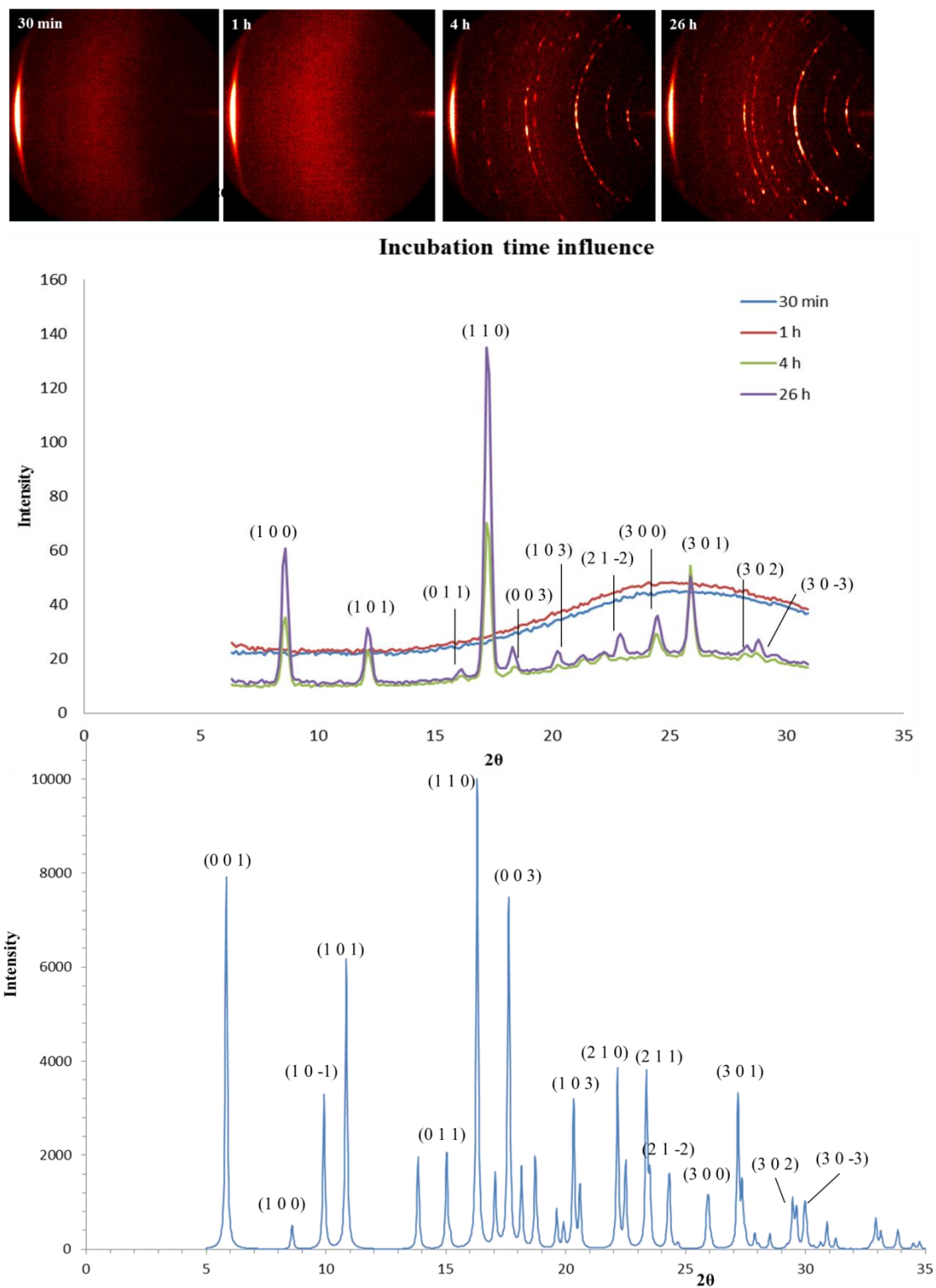
**Figure 8.2.6.** SEM micrographs of crystallization of (-)-PMPP/ (-)-PEA on micropatterned surfaces of 5  $\mu\text{m}$  dots of (+)-PMT after different incubation times: (A) 30 minutes. (B) 1 hour. (C) 4 hours. (D) 26 hours (E) 26 hours, crystals grown outside the pattern. Scale bar 5  $\mu\text{m}$  in all images.

### 8.2.2.3.1 Powder X-ray microdiffraction characterisation

The following figure 8.2.7 shows a comparison of X-ray microdiffraction pattern experimentally obtained by GADDS of the micropatterned surfaces of the influence of the incubation time in solution experiment (figure 8.2.6) to the theoretical powder X-ray diffraction pattern (calculated using Mercury programme), from a single crystal structure. X-ray microdiffraction (using a General Area Detector Diffraction System, GADDS) diffractograms confirmed the (-)-PMPP/ (-)-PEA crystal formation.

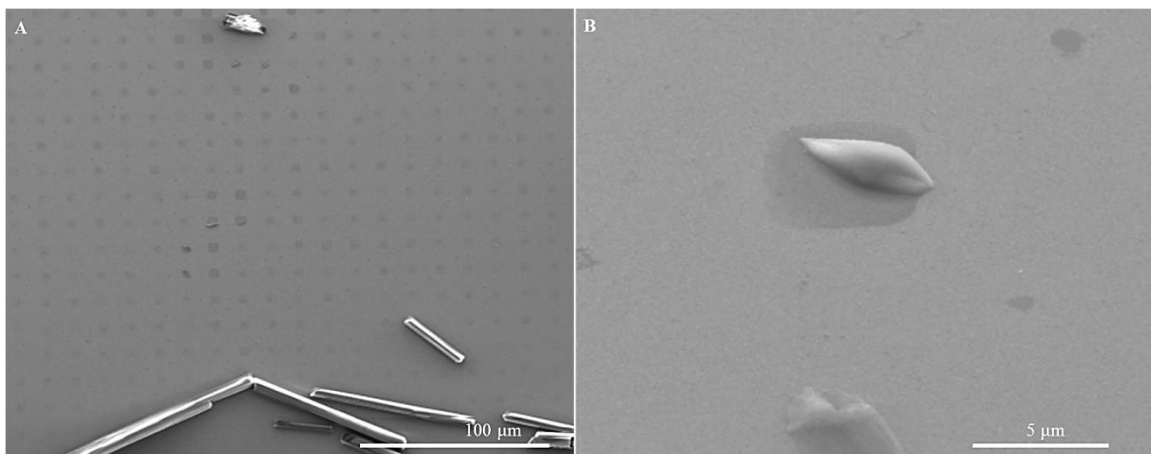
The peaks in the diffractogram are more intense as the incubation into the solution time increase. The diffractograms for the samples of lower time in solution (Figure 8.2.6 A-B; in the figure 8.2.7 blue and red curves) do not show any characteristic peak, which has sense due to the nucleation on the micropatterned surface was not significant in order to form crystals that X-ray microdiffraction (GADDS) could measure.

Only when longer times of incubation were used, signals corresponded from the salts were observed. In the 4 h sample, the peaks in the diffractogram are more intense, and they indicate the crystals grew on the micropatterned surfaces correspond to the diastereomeric salt to crystallise. The best sample to compare with the theoretical powder diffraction is the 26h sample, even though crystals on surface were from homogeneous and heterogeneous nucleation thus is not possible to distinguish the contribution of each one to the diffractogram, they provide good peaks which confirm the diastereomeric salt formation in solution and its crystallisation on the micropatterned surface.



**Figure 8.2.7.** GADDS diffractograms of (-)-PMPP/(-)-PEA crystals on micropatterned surfaces of 5  $\mu\text{m}$  dots of (+)-PMT, different incubation time: 30 minutes, 1 hour, 4 hours and 26 hours, comparison with the calculated powder X-ray diffraction (obtained from Mercury programme).

In order to decrease the incubation time, a more concentrated solution of the salt was used. The same procedure was performed with 50 mM (-)-PMPP/ (-)-PEA solution in EtOH. After 30 minutes we observed the formation of some crystals on the patterns but also big crystals in the solution and on the surfaces, indicating that the crystallization process is not controlled, Figure 8.2.8.



**Figure 8.2.8.** SEM micrographs of (-)-PMPP/ (-)-PEA crystals grown from 50 mM ethanol solution on (+)-PMT squares 5 x 10 μm pattern.

#### **8.2.2.4. Shape and size of the motif printed influence.**

As we have demonstrated previously in the phencyphos crystallization experiments, the influence of the shape of the motif and its size has an important effect on the crystal growth. The use of these different motifs to create micropatterns on surfaces provides a new way to prepare chiral surfaces due to the possibility to modulate the size and shapes of the patterns. Few examples can be found in the literature where patterned SAMs are used to control the nucleation points and crystallization process of organic compounds.<sup>10</sup> Nevertheless, to our knowledge this is the first time that patterns other than dots, squares and lines patterns are used to explore the crystallization of organic molecules.<sup>11,12</sup>

In the phencyphos crystallisation on micropatterned surfaces we concluded that the best motif were dots of 5 x 10  $\mu\text{m}$ . In the case of the diastereomeric salt of (-)-PMPP/ (-)-PEA the same study was done. We noticed when dots, squares and crosses were used, crystals grow on the micropattern in all samples following faithfully the shape (Figure 8.2.9 A, B and D), while, when spirals were used (Figure 8.2.9 C) a significant effect on the crystal growth was observed and the crystals gradually change their orientation to follow the micropattern. The micropatterns are not perfect (maybe from the PDMS stamp preparation process) and for this reason, there is growth outside the cross and spiral features.

Figure 8.2.9 shows close-up SEM images of individual motifs and emphasises their effect in the crystal growth. The dot and square features show a dendritic growth of crystals in the plane of the pattern and limited to the area where the polar SAM is present, since they provide a good area to the drop solution fits over them, wetting the interface and forming the dendritic crystals. The dark appearance of the crystallites indicates that they are in intimate contact with the underlying SAM. The nucleation point of these dendrites appears to be on the right hand side of the pattern feature in the images (Figure 8.2.9 A and B) but definitely away from the border of the pattern with the surrounding apolar SAM. The width of these crystallites is very small, approximately 200-300 nm.

---

<sup>10</sup> A. Singh, A.S. Myerson, *J. Pharm. Sci.*, **2010**, *99*, 3931-3940.

<sup>11</sup> E. Kim, G. M. Whitesides, *Chem. Mater.*, **1995**, *7*, 1257-1264.

<sup>12</sup> A. Brock, E. Chang, C. H. P. LeDuc, X. Jiang, G. M. Whitesides, D. E. Ingber, *Langmuir*, **2003**, *19*, 1611-1617.

The cross feature shown apparently favours nucleation at the centre of the pattern, because all of the crystallites (the smallest of which have similar dimensions to those seen on the dot and square features) radiate out from this point, and again do not grow beyond the frontiers of the printed region. This stamp produced patterns with a blank region around the stamp, but apparently collapse took place a few microns away from the cross, and therefore (+)-PMT is present and it can be seen that crystal formation is favoured, but again stops when the DT SAM covers the gold.

The spiral pattern– which obviously covers a much wider total area than dot or square (spirals pattern cover the 0.06% while dots pattern  $9.8 \cdot 10^{-3} \%$ )<sup>13</sup> – contains several nucleation points. In some places these seem to be very close to the frontier between (+)-PMT and DT regions. On the other hand, the growth of many crystallites seems to gradually change their orientation which processes around the shape in this particular region (Figure 8.2.9 C). In some areas of this feature the crystallites appear to be connected while in others there is not obviously any material between the crystallites, possibly meaning that this was a depletion zone during the crystallisation process. It is important to note that each crystallite is not twisted, but is linear, and the induced twist effect is on the orientation of individual crystallites. As for the cross feature, this stamp produced patterns with a blank region around the pattern where DT is present, but a collapse region during the stamping surrounds it. The effects that are seen are very much local however, as emphasised by the fact that the spiral and cross produce very different results even though they both have more (+)-PMT SAM beyond the DT surround. This apolar region is enough to favour the unique effects that are observed here.

The reason for the directional growth in the case of cross and spiral is probably a result of the directionality induced in the mass transport by these features, whereas dot and square are essentially isotropic and do not show any obvious flown effect.

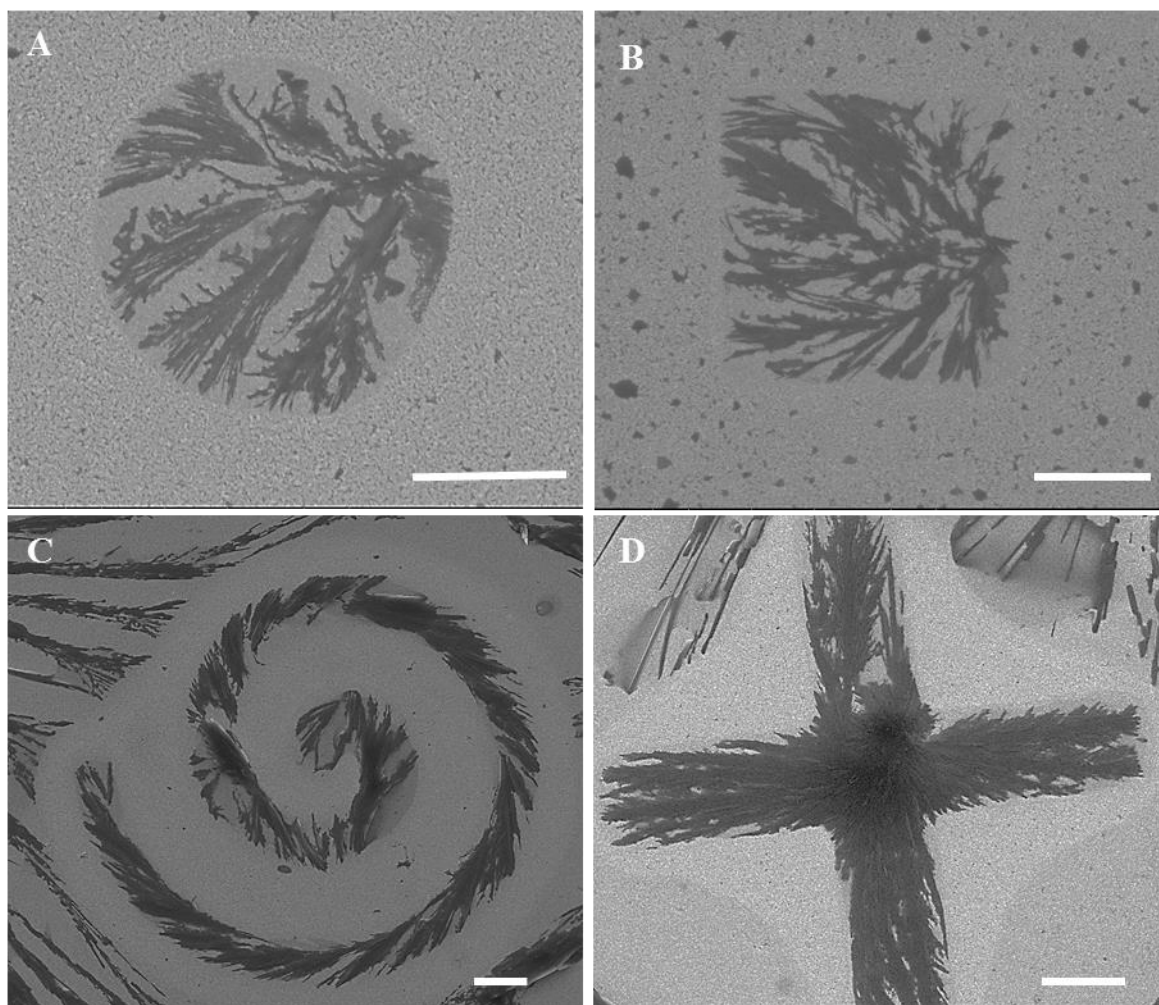
---

<sup>13</sup> To calculate the percentage of area covered of a printed motifs:  $A_{covered} = \frac{n_{motif} \cdot A_{motif}}{A_{stamp}} \cdot 100$

Pattern of spirals of 50  $\mu\text{m}$  (branch wide is 5  $\mu\text{m}$ ):  $A_{covered} = \frac{100 \cdot 655 \mu\text{m}^2}{10^8 \mu\text{m}^2} \cdot 100 = 0.06 \%$

Pattern of 5  $\mu\text{m}$  dots:  $A_{covered} = \frac{500 \cdot 19.63 \mu\text{m}^2}{10^8 \mu\text{m}^2} \cdot 100 = 9.8 \cdot 10^{-3} \%$





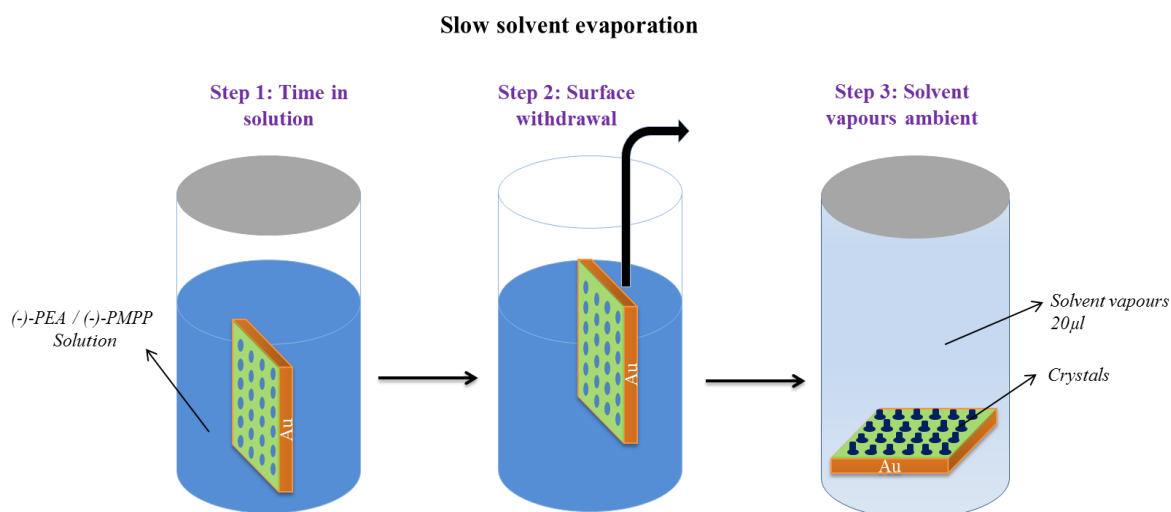
**Figure 8.2.9.** SEM micrographs of crystallization of (-)-PMPP/(-)-PEA ethanol solution (40 mM) on micropatterned surfaces of (+)-PMT (A) Dots of 10  $\mu\text{m}$ . (B) Squares of 10  $\mu\text{m}$ . (C) Spirals 50  $\mu\text{m}$ . (D) Crosses 35  $\mu\text{m}$ . The scale bar is 5  $\mu\text{m}$  in all images.

### 8.2.3. Crystallisation method

Each crystallization method employed was designed in order to study different effects on the diastereomeric salt crystallization and to get a better understanding of the process on patterned surfaces. As has been presented previously, the parameters studied have been done within the general framework of the slow solvent evaporation method developed for the phencyphos crystallization. For the diastereomeric salt crystallisation, two methods were optimised: *Slow solvent* evaporation and *Drop casting* because there are two main effects which have an influence on the crystallization process on surfaces that are the solvent evaporation rate and the diffusion over the surface.

#### 8.2.3.1. *Slow solvent evaporation*

Under slow evaporation conditions a uniform diffusion rate is achieved over the surface and the mass transport between polar and non-polar regions takes place to promote the crystallization. This method, employed to control the solvent evaporation, is based on the liquid-vapour equilibrium inside a closed vial where the surface was placed after a given time in a solution of the diastereomeric salt. The high vapour content in the vial ensures slow evaporation of the thin layer of solution in contact with the surface. These conditions allow the liquid-vapour solvent equilibrium to be established from the moment the surface is placed inside the vial.



**Figure 8.2.10.** Scheme showing the slow solvent evaporation method.

Specifically, the functionalized gold surfaces were immersed into a fresh ethanolic solution of (-)-PMPP/ (-)-PEA (30 mM). In the second step, the functionalized surface was removed from the solution carefully (ensuring a uniform film and avoiding drop formation). Finally, the wet functionalized surface - with a solution film - was placed in a closed vial, and after five days five holes were made in the lid. This vial was saturated in ethanol vapour.

All of the crystals presented up to this point in this section were obtained under these conditions. The crystals of (-)-PMPP/ (-)-PEA are formed within the patterns of PMT and do not grow across the DT SAM. Heterogeneous nucleation is favoured over homogeneous nucleation.

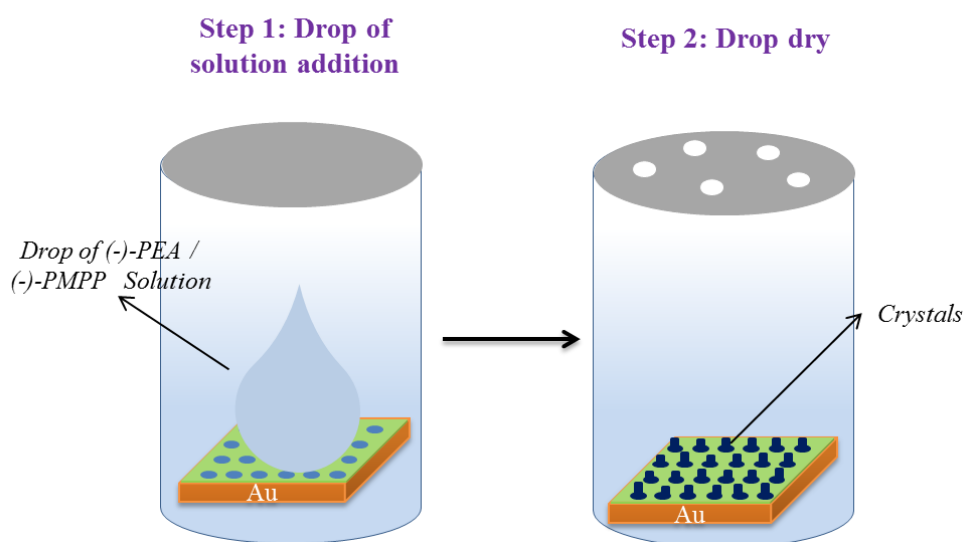
### **8.2.3.2. Drop casting**

A different crystallization strategy has been explored in order to control first the nucleation points and the crystal growth to obtain bigger crystals of the diastereomeric salt. This method is drop casting, and we have studied it under two different solvent conditions, dry and wet casting incubation-growth.

#### **8.2.3.2.1. Dry drop casting (5 mM, 10 mM, 25 and 40 mM)**

Nucleation begins when the concentration of the solute achieves supersaturation through, for instance, evaporation. Both homogeneous and heterogeneous nucleation can take place, and mass transport and local concentrations will influence dramatically which one of these is favoured. The drop casting method allows us to study the concentration limit at which heterogeneous nucleation predominates over the homogeneous nucleation in the drop. Furthermore, confirmation of whether the crystallization is constrained to the (+)-PMT patterns was sought. The protocol of this method (described in the figure 8.2.11) comprised taking a micropatterned surface and placing it in a vapour saturated vial, with a drop of 100  $\mu$ L of (-)-PMPP/ (-)-PEA of different concentrations (5, 10, 25 or 40 mM) and covering the vial with a lid with five holes to control the solvent evaporation (so that it would not be so fast that supersaturation was entered into too quickly) until complete drying at room temperature.

### Drop casting dry

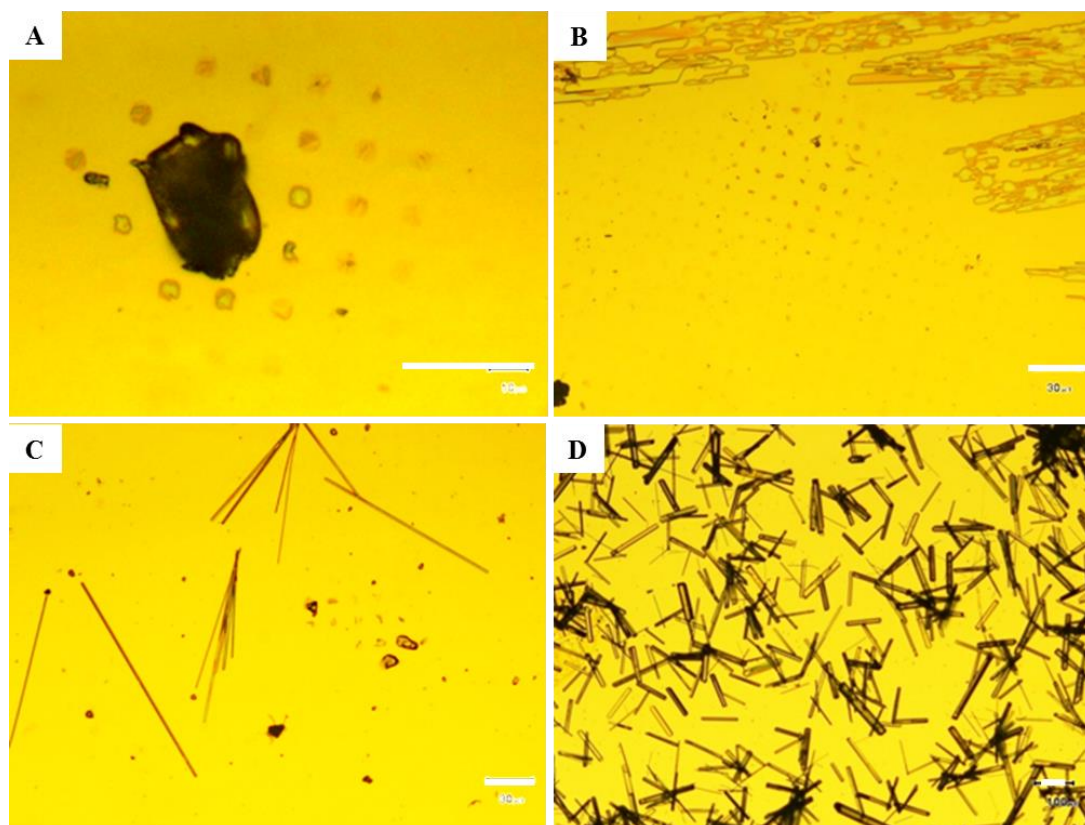


**Figure 8.2.11.** Scheme of dry drop casting method.

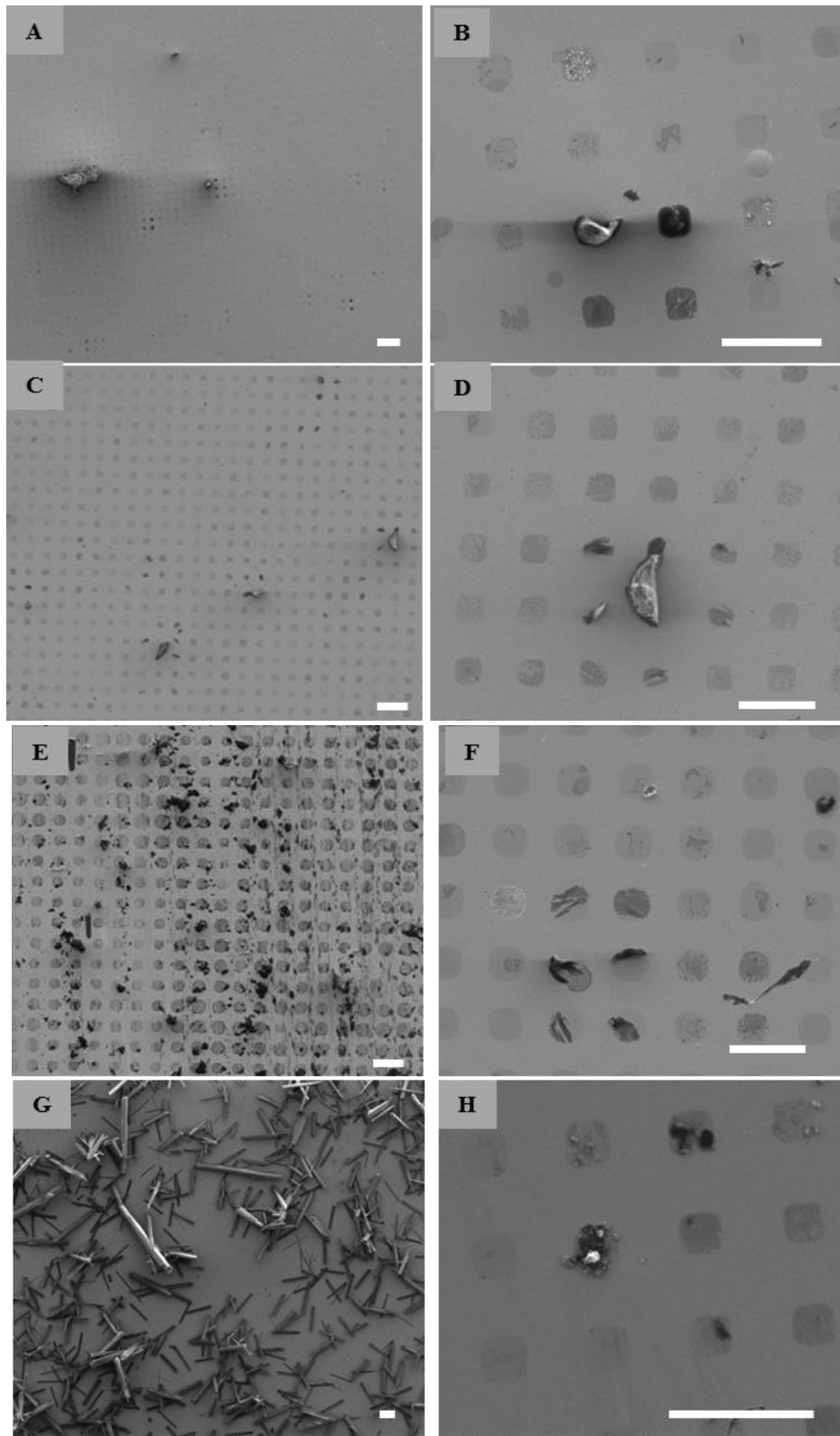
The study of this range of concentrations using the dry drop casting method conditions provides some important results (Figure 8.2.12 and 8.2.13): SEM and optical microscopy show that at the lowest concentration (5 mM) the amount of material is insufficient to promote the homogeneous nucleation over the whole micropatterned surface (Figure 8.2.12.A, and 8.2.13.A-B). On the other hand, the highest concentration, 40 mM, favours the homogeneous nucleation instead of the heterogeneous nucleation since the supersaturation level is achieved in the bulk before mass is transported to the surface (Figure 8.2.12.D, and 8.2.13.G-H).

In the case of the intermediate concentrations, 10 or 25 mM (Figure 8.2.12.B-C, and 8.2.13.C-F), heterogeneous nucleation on the micropattern is promoted leading to crystals of the diastereomeric salt on the (+)-PMT micropatterned areas. Nevertheless, the lower of these concentrations (10 mM) is still insufficient to get good crystal growth on the micropatterns. On the other hand, using a 25 mM solution, besides the heterogeneous nucleation, there is also a low proportion of homogeneous nucleation as seen by the appearance of a few relatively big crystals outside of the patterns. However, this concentration is necessary to have sufficient material to make the crystals grow. One solution which could be applied to avoid the appearance of big crystals when the 25 mM solution is used could be a slower and controlled evaporation process by decreasing the temperature or varying the number of holes of the lid. In any case, this

example shows very clearly that the homogeneous nucleation is easily distinguished from the heterogeneous case by observing the location and size of the crystals on the surface after the crystallisation experiment.



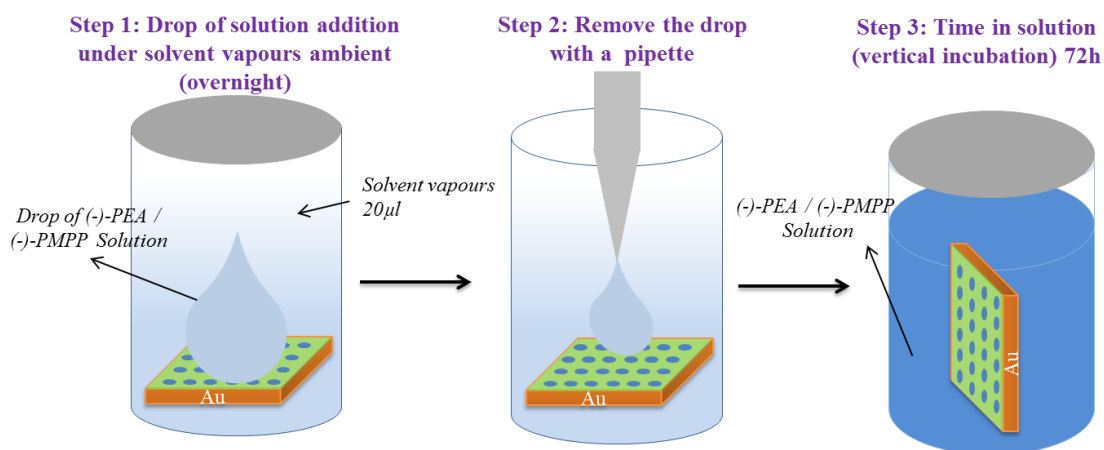
**Figure 8.2.12.** Optical micrographs of dry drop casting crystallisation method on 5 x 10  $\mu\text{m}$  squares pattern for (-)-PMPP / (-)-PEA concentrations: (A) 5 mM, (B) 10 mM, (C) 25 mM and (D) 40 mM. The scale bar is 30  $\mu\text{m}$  in all images.



**Figure 8.2.13.** SEM micrographs of dry drop casting crystallisation method on micropatterned surfaces by squares of  $5 \times 10 \mu\text{m}$  of (+)-PMT and DT surrounded, for (-)-PMPP / (-)-PEA concentrations: (A-B) 5 mM, (C-D) 10 mM, (E-F) 25 mM and (G-H) 40 mM. The scalebar is  $20 \mu\text{m}$  in all images.

### 8.2.3.2.2. Wet casting incubation-growth method

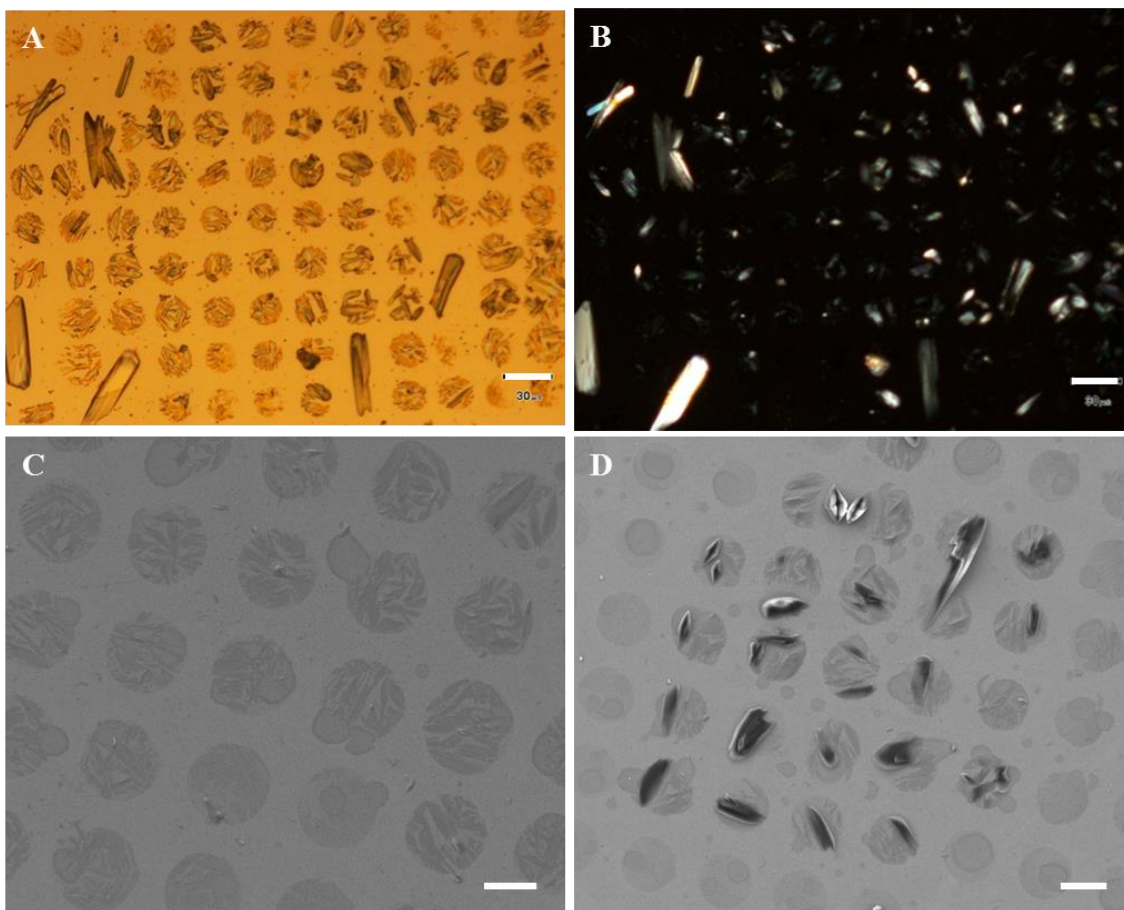
The protocol of this method composed taking a freshly micropatterned surface and placing it in a vial previously saturated in ethanol vapour (100  $\mu\text{L}$ ) with a drop (50  $\mu\text{L}$ ) of (-)-PMPP/ (-)-PEA (25.3 mM) warmed to 50  $^{\circ}\text{C}$  in ethanol on the surface overnight to promote the nucleation on the micropatterns and preventing the evaporation of the drop (Figure 8.2.14). After this time, the excess liquid was removed carefully and the surface was immersed vertically in a fresh solution of (-)-PMPP/ (-)-PEA (30 mM in EtOH) for 72h. After this time, the surface was removed from the solution and placed in an open vial at room temperature for a fast evaporation.



**Figure 8.2.14.** Scheme of the wet casting incubation-growth method.

Figures 8.2.15 and 8.2.16 show the diastereomeric salt crystallisation following the wet casting incubation-growth method on dots and spirals micropatterns. Crystals grow on the micropattern because the drop of solution left overnight in the solvent saturated vapour atmosphere induces the heterogeneous nucleation on them, rather like in the slow evaporation technique, and subsequently these nuclei presumably mature in the solution of the two components once transferred. (-)-PMPP/ (-)-PEA crystals grown on the (+)-PMT patterned region are more localised on them than in other cases, and their crystallinity is better than the crystals obtained following the dry drop casting method. There is also a more homogeneous crystallisation over the micropatterned region of whole surface. However, there are large crystals which could be from this

homogeneous nucleation. In the figure 8.2.15.D, there is a crystal which grows from one dots and still growing until a neighbour dots. As the large crystals on this sample are not large enough as the crystals from bulk crystallisation, we could conclude that these large crystals were nucleated on the pattern (figure 8.2.15.A-B).



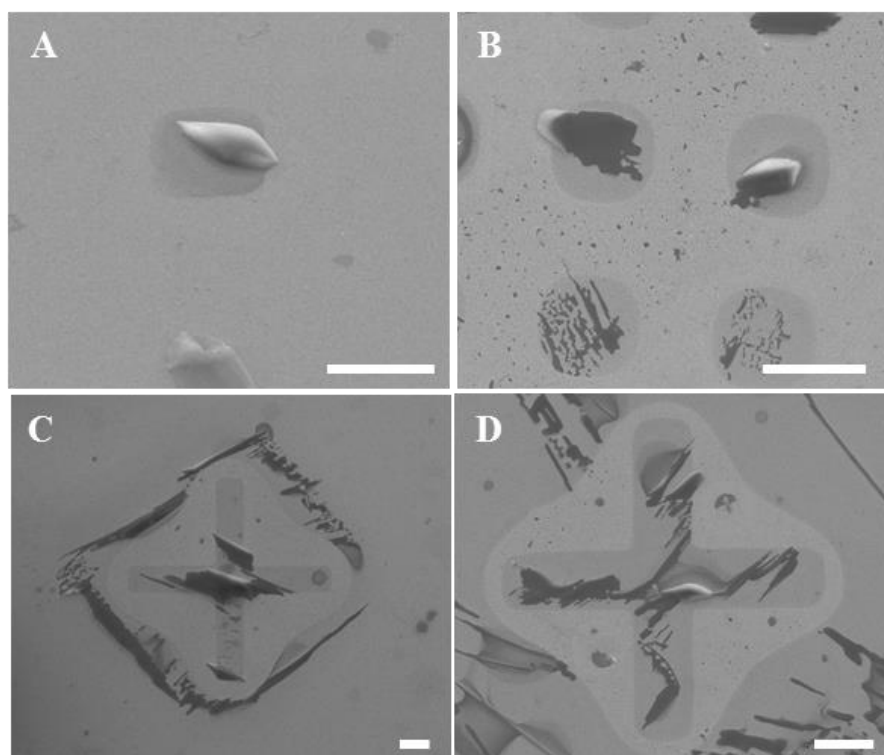
**Figure 8.2.15** Wet casting incubation-growth technique of (-)-PMPP/ (-)-PEA on micropatterned surfaces of dots 5 x 10 μm of (+)-PMT and DT surrounded. (A) Optical micrograph non-polarised. (B) Optical micrograph non-polarised. (C) and (D) SEM micrograph. The scale bar is 10 μm in all images.



## 8.2.4. Chirality at surface

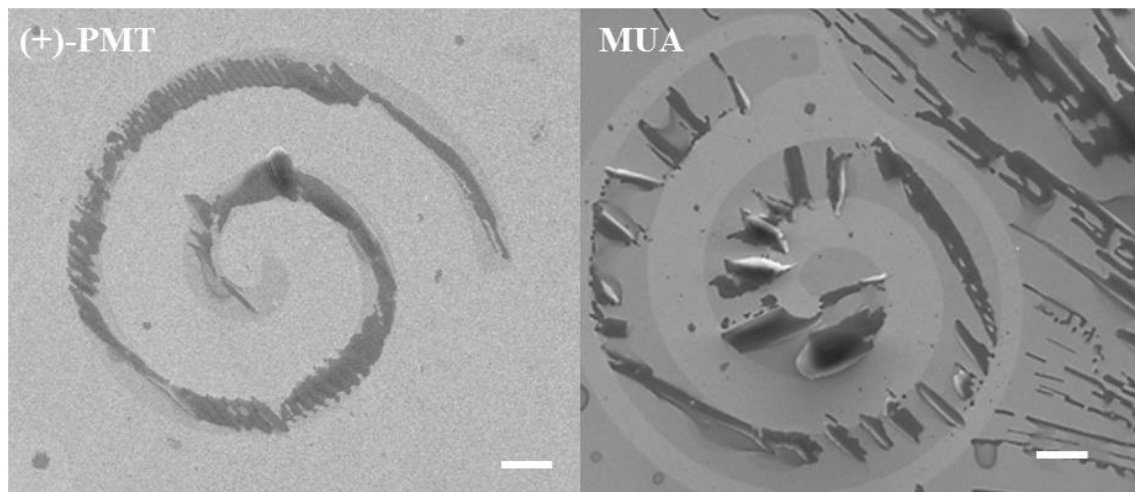
### 8.2.4.1. Same chirality on surface (full surface)

As has been shown previously, the chirality of the (+)-PMT SAMs can affect the crystal growth of phencyphos (Chapter 6). For this reason, we have also studied the influence of the chirality of the SAMs on the crystallization process of the (-)-PMPP/ (-)-PEA diastereomeric salt. The first strategy was the preparation of achiral SAMs by printing MUA and to compare the crystals obtained in the two types of template, chiral (PMT) and achiral (MUA), respectively. For these experiments, the slow evaporation method was used. Comparing the crystallization of (-)-PMPP/ (-)-PEA on micropatterned surfaces with different micropatterns of MUA or (+)-PMT, the crystal growth is slightly distinct in the two systems (Figure 8.2.16 and 8.2.17), although the difference between these surfaces is not as obvious as in the case of the crystallisation of phencyphos (Chapter 8.1). The crystals on the MUA monolayer appear darker and in general have a rather better defined shape than those grown on (+)-PMT, though it has to be said that in the case of the crosses the appearance is very similar.



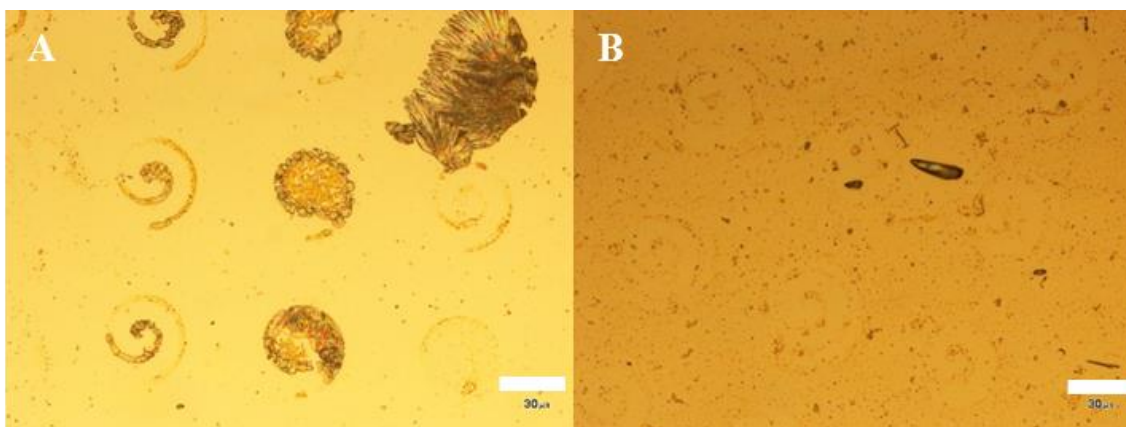
**Figure 8.2.16.** SEM micrographs of crystallization of (-)-PMPP/ (-)-PEA on micropatterned surfaces of (A), (C) (+)-PMT and (B), (D) MUA. Squares 5 x 10  $\mu\text{m}$  and crosses 35 x 70  $\mu\text{m}$  micropattern. Scale bar 5  $\mu\text{m}$ .

Crystals on the micropattern of MUA present a crystal growth which is clearly along the plane in some regions – as witnessed by the darkness of the objects – but in places the crystals grow off the surface (seen by observing bright regions which correspond to charging of the sample). Crystals grown on (+)-PMT grow mainly in the plane of the surface and are generally smaller, as seen especially for the case of the spiral micropatterns, as shown in Figure 8.2.17.



**Figure 8.2.17.** SEM micrographs of crystallization of (-)-PMPP/ (-)-PEA on micropatterned surfaces by (+)-PMT or MUA, 50 x 100  $\mu\text{m}$  spirals. The scale bar is 5  $\mu\text{m}$  in both images.

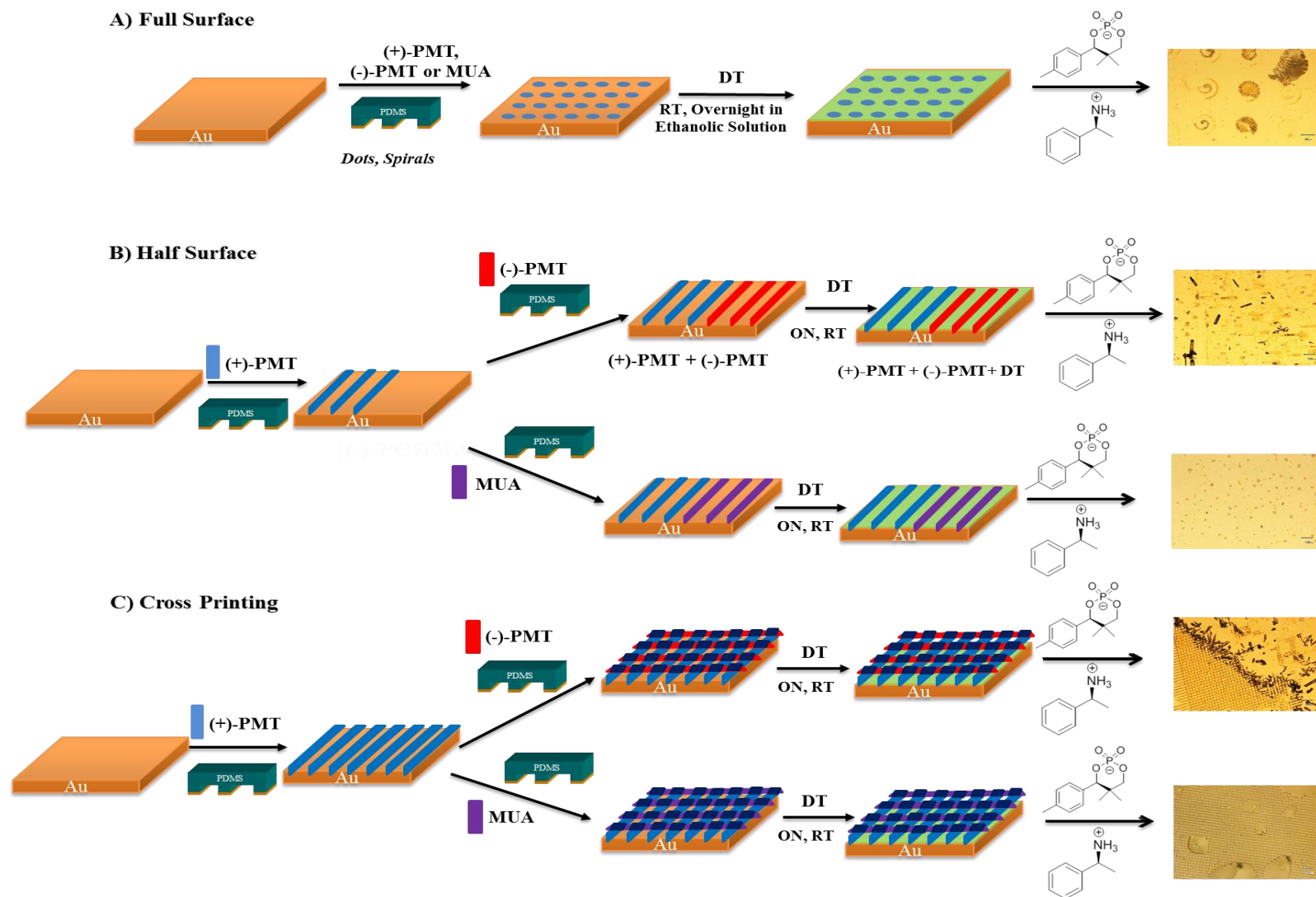
The second strategy was to compare the crystals grown on spirals patterned using (+)-PMT or (-)-PMT. For these experiments the wet casting incubation-growth technique was followed. When spirals with (+)-PMT were used and after washing the surfaces with ethanol, a significant number of crystals of (-)-PMPP/ (-)-PEA were observed on the patterns, while for the (-)-PMT patterns almost nothing remained on the surface (Figure 8.2.18). (-)-PMT offer a poorer template to the (-)-PMPP/ (-)-PEA salt because after washing the most crystals grown on (-)-PMT regions were dissolved. The interactions at the interface between the SAM and the crystal are chiral, so one of the two enantiomers of PMT will interact stronger with the salt crystal, a possible explanation for this effect.



**Figure 8.2.18.** Optical micrograph of Wet casting incubation-growth technique on 50 x 100  $\mu\text{m}$  spirals for (A) (+)-PMT and (B) (-)-PMT. (-)-PMPP / (-)-PEA concentration 25 mM. The scale bar is 30  $\mu\text{m}$  in both images.

Finally, the influence of the chirality of the micropatterned SAMs was also studied by preparation of surfaces combining either (-)-PMT and (+)-PMT or (+)-PMT and MUA. The different ability of (-)-PMPP/ (-)-PEA to differentiate between patterns of (+)-PMT and (-)-PMT was explored using either half or cross printing of both enantiomers on the same surface. Figure 8.2.19 shows all the processes used to functionalise the surface. *Full surface* refers to the habitual microcontact printing procedure, and consists of the printing of one thiol – (+)-PMT, (-)-PMT or MUA- and DT passivation of the rest of the surface. *Half surface* implies the half functionalisation – using micropatterns of lines of 5 or 10  $\mu\text{m}$  and separated 10 or 20  $\mu\text{m}$  (simplify as 5 x 10 or 10 x 20  $\mu\text{m}$ ), respectively – of the surface by one thiol, (+)-PMT, and the other half by (-)-PMT or MUA, and DT passivation of the rest of the surface. *Cross printing* comprises patterning (+)-PMT using the micropattern of lines, and then a second stamp previously inked with a solution of (-)-PMT or MUA was brought into contact with the surface with the line pattern perpendicular to the (+)-PMT or MUA lines.

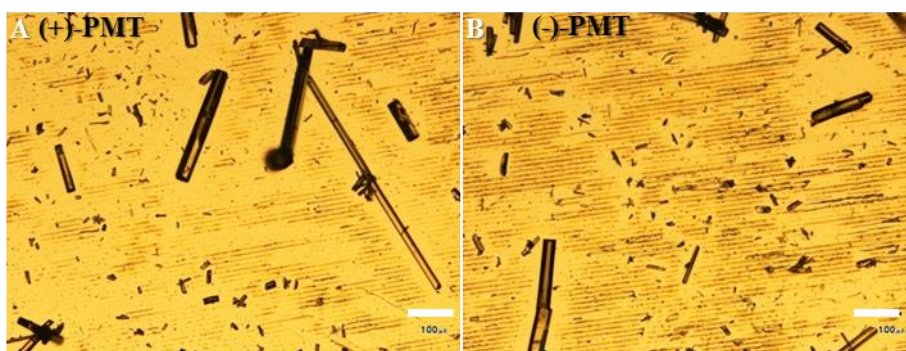
The crystallisation method selected for these experiments was the wet casting incubation-growth technique, where a drop of (-)-PMPP / (-)-PEA ethanolic solution (25 mM) was used for an incubation time of 48 hours. Micropatterns of lines of 5  $\mu\text{m}$  combining (+) and (-)-PMT on the surface as *half surface* printing and *cross printing*, are shown in Figures 8.2.20 and 21.



**Figure 8.2.19.** Surface functionalisation scheme for mono- and bi-functionalised surfaces. (A) Full surface functionalised by (-) or (+)-PMT and DT. (B) Half surface functionalised with (+)-PMT and the other half with (-)-PMT or MUA. (C) Cross printing, (+)-PMT and (-)-PMT perpendicular or (+)-PMT and MUA perpendicular.

#### 8.2.4.2. Different chirality on surface: Half and crossed printing

When the (-)-PMPP/ (-)-PEA salt was crystallized on these surfaces, crystals were observed on both patterns without any apparent selectivity in the recognition as it is shown in the following figure 8.2.20 and 8.2.21. While the different wettability and how the drop interacts with the patterned surface with spirals, lines or cross-printed lines, could be important when chiral recognition is necessary,<sup>14</sup> in the present case the growth of the salt crystals on the surface seems to be driven principally by polarity rather than any specific interaction. Large crystals observed in both figures, are from homogeneous nucleation.



**Figure 8.2.20.** Optical micrographs of (-)-PMPP/ (-)-PEA salt crystallization on half printing micropatterned surfaces of 5 x 10  $\mu\text{m}$  lines (A) (+)-PMT and (B) (-)-PMT zones. The scale bar is 100  $\mu\text{m}$  in both images.

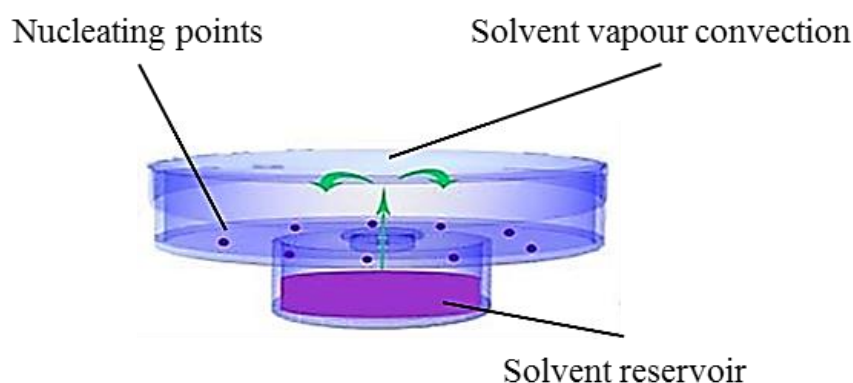


**Figure 8.2.21.** (-)-PMPP/(-)-PEA salt crystallisation on lines 5 x 10  $\mu\text{m}$  micropatterned surfaces by cross printing surface: (A) After incubation time, (B) After washing with ethanol, (C) SEM micrograph of (B). The scale bar is 100  $\mu\text{m}$  in all images.

<sup>14</sup> M. Rapp, W. A. Ducker, *J. Am. Chem. Soc.*, **2010**, *132*, 18051-18053.

### 8.2.5. Crystallisation in the Crystallisation Mushroom®

In order to reach the real final objective of the project described in this Thesis, which was to resolve several racemic mixtures by diastereomeric salt crystallisation under the same crystallisation conditions on the same functionalised surface, the wet casting incubation-growth technique was used on several surfaces (because on the same surface they were not easy to manipulate) using a *Crystallization Mushroom*®<sup>15</sup>, (Figure 8.2.22). The crystallisation mushroom has been used in the study of the heterogeneous versus homogeneous nucleation in protein crystallisation.<sup>16</sup> Using this Crystallization Mushroom, we could perform several experiments at the same time and follow the formation of the drops and the crystallization process using an optical microscope. The mushroom consists of a solvent reservoir, a platform and a crystal plate to cover it. A given quantity of ethanol was deposited into the reservoir, to saturate the atmosphere and to prevent the evaporation of the drops, and the different functionalised surfaces were left in each marked point (see Figure 8.2.22) with a drop of (-)-PMPP/ (-)-PEA salt solution on top. Then, the mushroom was covered by the glass plate, making the system closed. The solvent evaporation kept the environment wet with ethanol and diffusion for each surface was favoured in all samples.



**Figure 8.2.22.** *Crystallization Mushroom*®, from *trianatech.com*.<sup>15</sup>

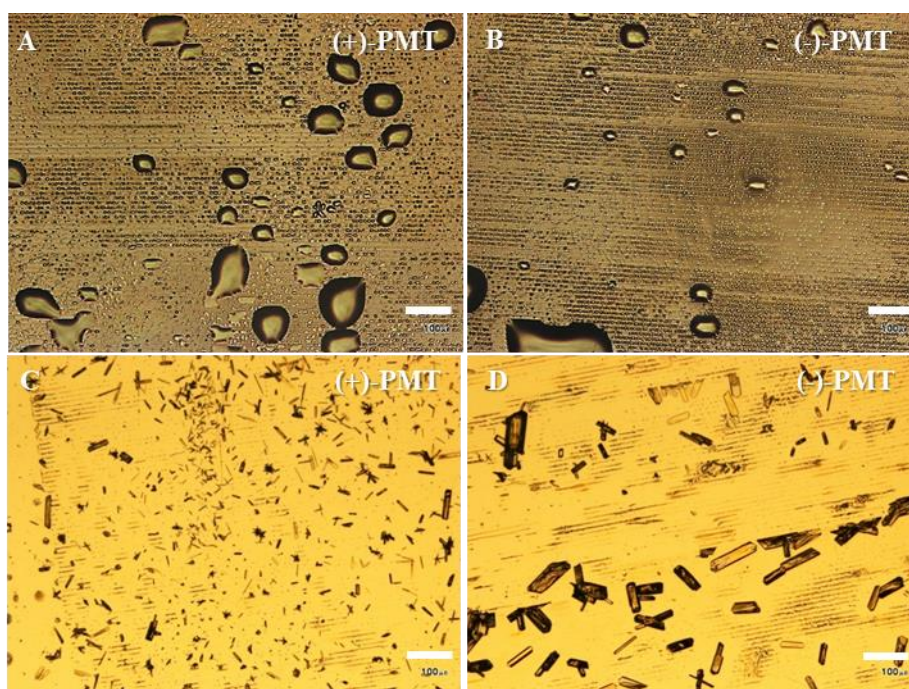
<sup>15</sup> (a) J. M. García-Ruiz, M. A. Hernández-Hernández, J. Gómez-Morales, *J. Ind. Crystallogr.*, **2008**, *27*, 99-106.  
(b) [www.trianatech.com](http://www.trianatech.com)

<sup>16</sup> G. Tosi, S. Fermani, G. Falini, J. A. Gavira, J. M. García Ruiz, *Cryst. Growth Des.*, **2011**, *11*, 1542-1548.

### 8.2.5.1. *Different chirality on surface: Half printing*

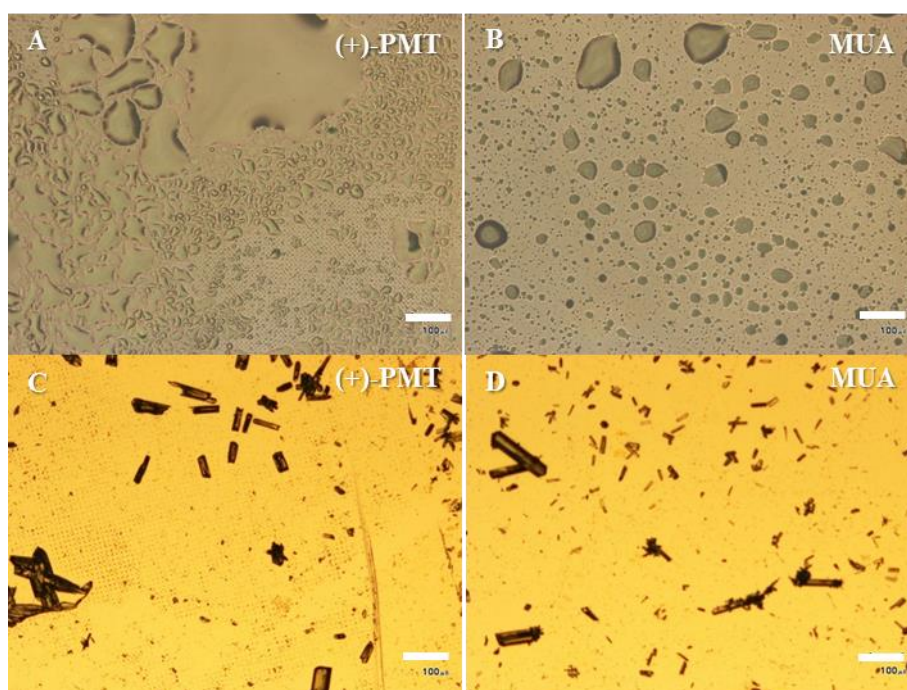
As stated previously, the crystallisation method selected for the experiments in the crystallisation mushroom was the wet casting incubation-growth technique, in which a drop (50  $\mu$ l) of 25 mM (-)-PMPP/(-)-PEA ethanol solution, incubated for 48 hours, and 2 ml of ethanol in the reservoir were used. Micropatterns of circles of 5  $\mu$ m and lines of 10  $\mu$ m alone or combined either (+) and (-)-PMT or (+)-PMT and MUA on the surface as full surface, half surface and cross printing were employed as substrates.

The comparison of the (-)-PMPP/(-)-PEA salt crystallisation on the patterned surfaces of (+) and (-) PMT is shown in the figure 8.2.23. (-)-PMPP/(-)-PEA crystals grow after 5 days of incubation in (-)-PMPP/ (-)-PEA salt solution 25 mM, however these crystals seem from homogeneous nucleation due to their big size. While, functionalised surface after the incubation time of 5 days in the crystallisation mushroom, still wet, avoiding any homogeneous nucleation indication.



**Figure 8.2.23.** (-)-PMPP/ (-)-PEA salt crystallisation on 10 x 20  $\mu$ m lines micropatterned half printing surfaces with DT surrounded: (A) (+)-PMT and (B) (-)-PMT zones after incubation time in crystallisation mushroom, (C) (+)-PMT and (D) (-)-PMT zones after 5 days of incubation in (-)-PMPP/ (-)-PEA salt solution 25 mM. The scale bar is 100  $\mu$ m in both images.

The (-)-PMPP/(-)-PEA salt crystallisation on the patterned surface of (+)-PMT and MUA comparison is shown in Figure 8.2.24. (-)-PMPP/(-)-PEA crystals grow after 5 days of incubation in (-)-PMPP/(-)-PEA salt solution (25 mM), while the functionalised surface after the incubation time of 5 days in the crystallisation mushroom, still wet, avoiding any nucleation indication. The main difference between the results in Figure 8.2.24 A and B is the drop shape. Drops on (+)-PMT are flatter and bigger than the drops on MUA which are more spherical and smaller. This difference is due to the affinity between the solution and the printed monolayer, even though both SAMs are polar. When the distinguishing parameter is the chirality, is possible to check its effects. The comparison made in the Figure 8.2.24 shows clearly the difference in the ability of the solution to wet the functionalised surface. (-)-PMPP/(-)-PEA ethanolic solution wets to (+)-PMT SAM better than MUA SAM.



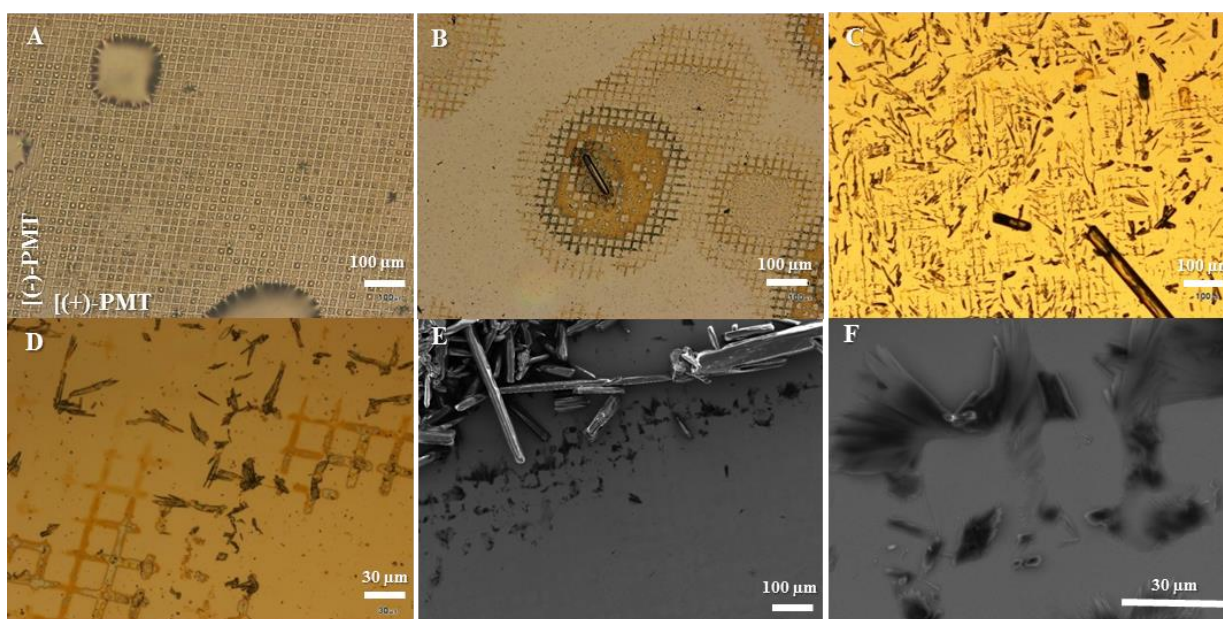
**Figure 8.2.24.** (-)-PMPP/(-)-PEA salt crystallisation on micropatterned 5 x 10 µm dots half printing surface with DT surrounded:: (A) (+)-PMT and (B) MUA zones after incubation time in crystallisation mushroom, (C) (+)-PMT and (D) MUA zones after 5 days of incubation in (-)-PMPP/ (-)-PEA salt solution 25 mM. The scale bar is 100 µm in both images.



### 8.2.5.2. Different chirality on surface: Crossed printing

In order to minimize all the effects such as as polarity, evaporation rate, microcontact printing method, temperature, solution concentration, etc., a cross printing of (+) and (-)-PMT was prepared. Figure 8.2.25 shows the cross printed surface after the crystallisation experiment in the glass mushroom. Crystals grow on both regions indiscriminately, showing that this surface is unable to demonstrate discrimination of chirality in the crystallisation of this salt.

According to the basis of the crystallisation mushroom design, the homogeneous nucleation should be avoided while the micropatterned surface is inside. The large crystal appearance from the figure 8.2.25-A to B and C was because the solvent (ethanol) dried freely, inducing the homogeneous nucleation and the uncontrolled crystallisation outside the pattern. In the figure 8.2.25-D is noticed the reduction of the crystals on surface, after 5 days in (-)-PMPP/ (-)-PEA salt solution, the crystals outside the pattern were redissolve. The figure 8.2.25-E shows that there is homogeneous nucleation which forms large needle-like crystals. As it is observed in the figure 8.2.25-F, there is no preferential crystallisation only on either (+)-PMT or (-)-PMT.



**Figure 8.2.25.** (-)-PMPP/ (-)-PEA salt crystallisation on micropatterned 10 x 20  $\mu\text{m}$  lines made by the cross printing surface route with (+) and (-)-PMT. Optical micrographs of: (A) after incubation time in crystallisation mushroom; (B) after drop drying; (C) after 5 days of incubation in (-)-PMPP/ (-)-PEA salt solution 25 mM; (D) after washing with ethanol after incubation. (E) and (F) SEM micrographs of (D).

Scale bar (A), (B), (C), (E) 100  $\mu\text{m}$ , (D) and (F) 30  $\mu\text{m}$ .

With the aim of improve the experiment, to maximize any influence of chiral recognition, a cross printed surface was made using (+)-PMT and MUA as the polar regions. Figure 8.2.26-A shows the cross printed surface after the crystallisation experiment in the glass mushroom. We observed the same phenomena as in the previous experiment (Figure 8.2.25 A-C) in the Figure 8.2.26.A-B, the homogeneous nucleation is promoted by the high solvent evaporation rate. Many crystals grow on both regions, thus even under these conditions there is no discrimination by chirality (Figure 8.2.26.C).

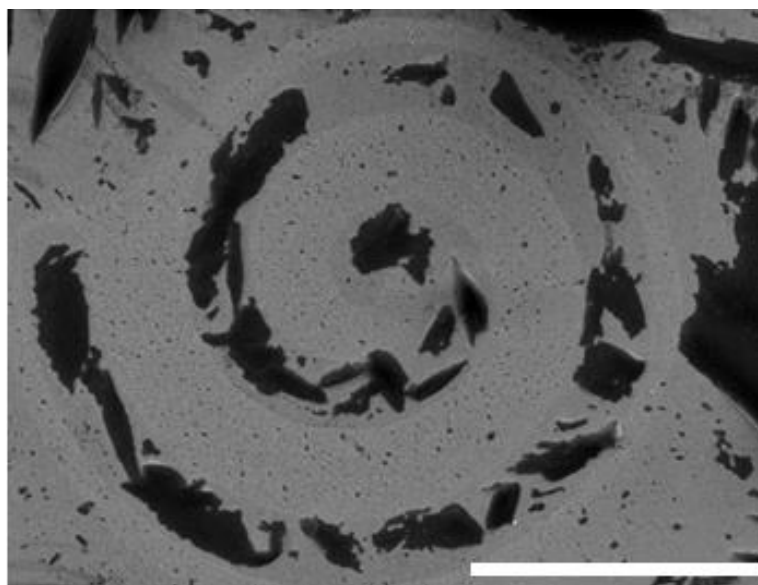


**Figure 8.2.26.** (-)-PMPP/ (-)-PEA salt crystallisation on micropatterned 10 x 20  $\mu\text{m}$  lines with the cross printing surface method using (+)-PMT and MUA. Optical micrographs of: (A) after incubation time in crystallisation mushroom; (B) after drop drying; (C) after 5 days of incubation in (-)-PMPP/ (-)-PEA salt solution 25 mM; Scale bar 100  $\mu\text{m}$ .

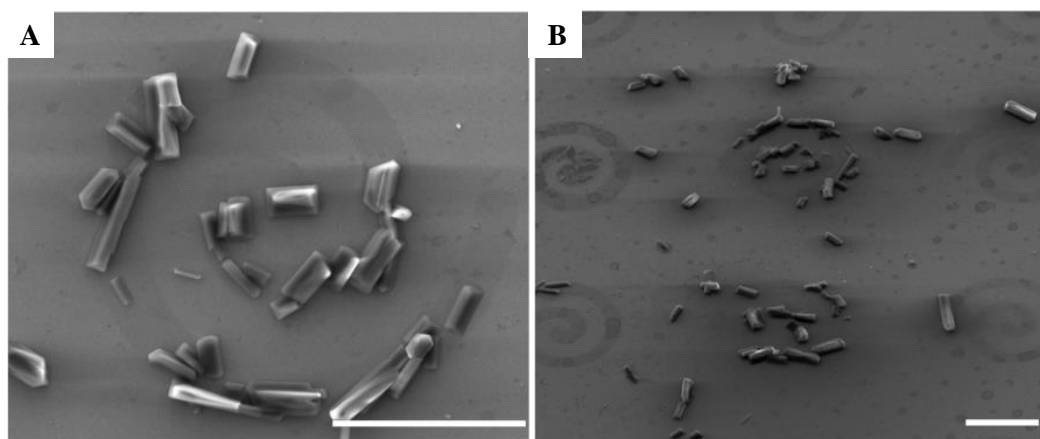
We can conclude that using the cross-printing as well as the half printing surface methods with lines of 10  $\mu\text{m}$ , no chiral recognition was observed because the wettability of the patterns also is apparently so similar in wetting ability that they are practically equally good nucleant. Furthermore, the weak interaction between the crystals and the SAMs occurred since after washing them with ethanol most of the crystals are removed. This design of the system is not ideal to check for chiral recognition because, as can be seen in Figure 8.2.26, the wetting effects leads to a directional dewetting along the lines which could force crystallisation even if a difference in interaction energy were present.

### **8.2.6. (+)-PMPP/(+)-PEA salt crystallisation**

Pasteurian crystallisation was successful with two systems: The salts (-)-PMPP/(-)-PEA and (+)-PMPP/(+)-PEA, both crystallised from ethanol. The crystallization of the (+) system was also studied. It is not possible to determine which enantiomer would interact better with the resolving agent functionalised surface, so it is possible that (+)-PMPP/(+)-PEA salt would attach better to the (+)-PMT surface than the (-)-PMT functionalised surface, or not. This study was done following the wet casting incubation-growth method: A micropatterned surface incubation overnight with a drop (50  $\mu$ L, 20 mM of salt) on top of the surfaces in vapours of 100  $\mu$ L of ethanol was used. After this time, the surface was washed and incubated in a vertical position for 68 h in a 25 mM solution of the salt; crystals appeared on the surface and in solution. Figure 8.2.27 shows the (-)-PMPP/ (-)-PEA salt crystals grown on (-)-PMT while Figure 8.2.28 shows the complementary crystallisation experiment of (+)-PMPP/ (+)-PEA salt crystals grown on (+)-PMT. In both systems there is nucleation on the micropatterned region. In the case of the crystallisation experiment showed in the figure 8.2.28, the crystal growth formed bigger crystals than in the case of the experiment showed in the figure 8.2.27, but in smaller proportion.



**Figure 8.2.27.** SEM micrograph of (-)-PMPP/ (-)-PEA salt crystallisation from solution 25 mM on micropatterned 50 x 100  $\mu$ m spirals on (-)-PMT surfaces. Scale bar 30  $\mu$ m.

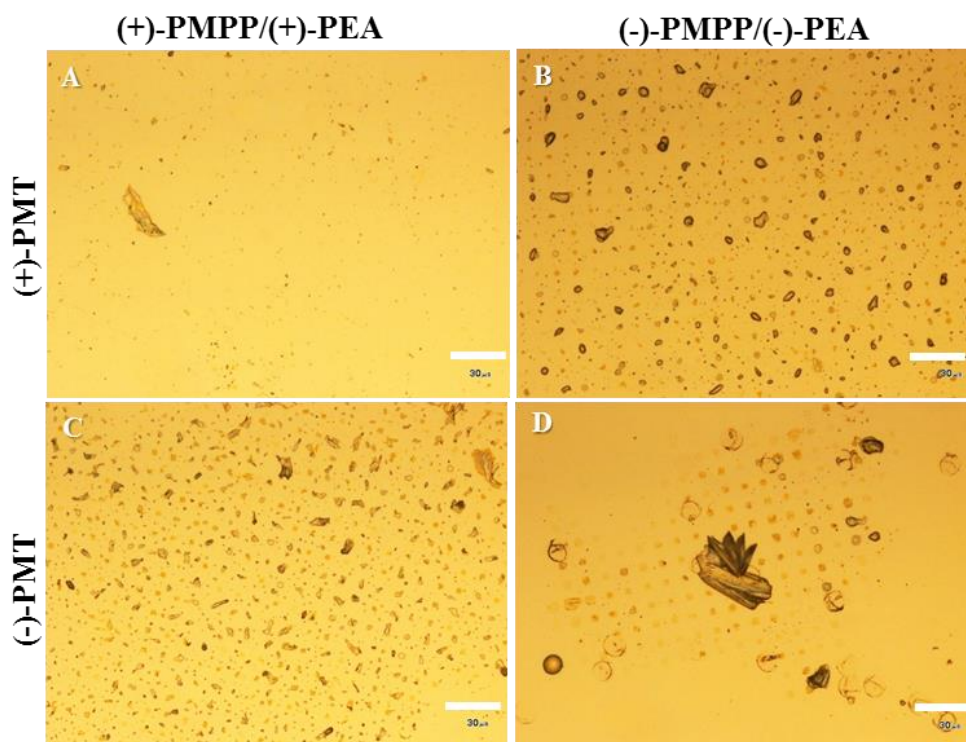


**Figure 8.2.28.** SEM micrographs after 5 days of incubation in (+)-PMPP/(+)-PEA salt solution 25 mM, salt crystallisation on micropatterned 50 x 100  $\mu\text{m}$  spirals on (+)-PMT surfaces: A) non-tilted; B) tilt 45° respect to the horizontal. The scale bar is 30  $\mu\text{m}$  in both images.

The chiral discrimination of the diastereomeric salt (+)-PMPP/(+)-PEA on micropatterned surfaces is not clear. To confirm the observations on the figure 8.2.27 and 28, a second experiments has done on micropatterned surfaces of squares of 5 x 10  $\mu\text{m}$  by either (-)-PMT or (+)-PMT and DT surrounded. The Figure 8.2.29 shows the crystals grown on (+)-PMT and (-)-PMT surface for both diastereomeric salt (+) and (-)PMPP/(-)PEA. This study was done following the wet casting incubation-growth technique.

From the four combinations, only two of them have controlled crystallisation on the micropatterned region. They are the crystallisations systems which involved the salt and the resolving agent with opposite chirality. That is, the success controlled crystallisation experiments are for the following systems: (-)-PMPP/(-)-PEA salt which crystallises on (-)-PMT and (+)-PMPP/(+)-PEA salt which crystallises on (+)-PMT preferentially (see Figure 8.2.29 B and C). The chiral recognition increases the wettability<sup>17</sup> of the solution to the surface, which favour the heterogeneous nucleation on the micropatterned surface.

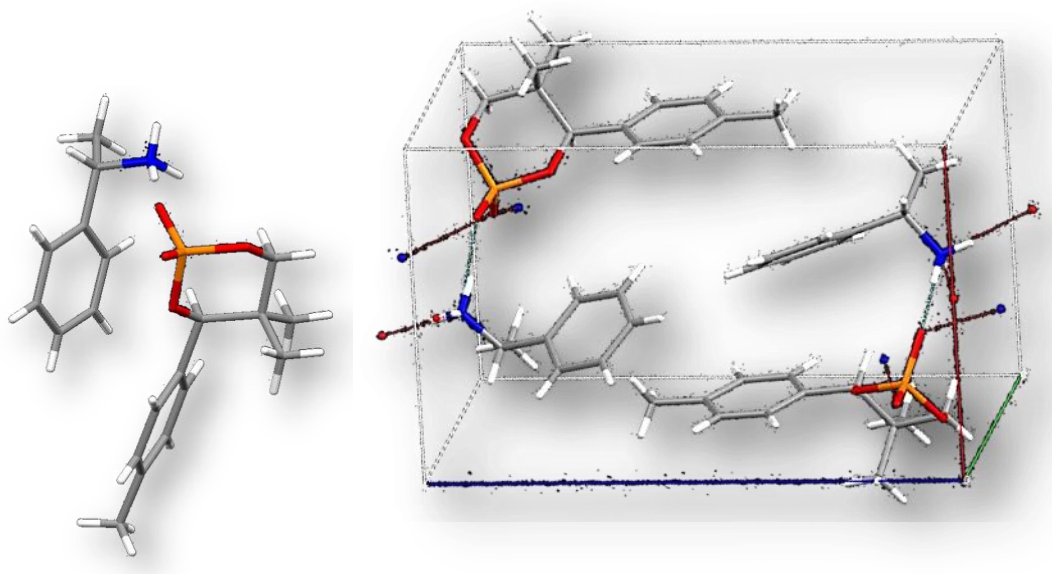
<sup>17</sup> J.M. García-Ruíz, Journal of Structural Biology, 2003, 142, 22–31.



**Figure 8.2.29.** Optical micrographs of the chiral combinations of salts and micropattern, 5 x 10  $\mu\text{m}$  squares. (A) (+)-PMPP/(+)-PEA salt on (+)-PMT. (B) (-)-PMPP/(-)-PEA salt on (+)-PMT, (C) (+)-PMPP/(-)-PEA salt on (-)-PMT. (D) (-)-PMPP/(-)-PEA salt on (-)-PMT. The scale bar is 30  $\mu\text{m}$  in all images.

### 8.2.7. Characterisation of (-)-PMPP/(-)-PEA salt crystals on micropatterned surfaces.

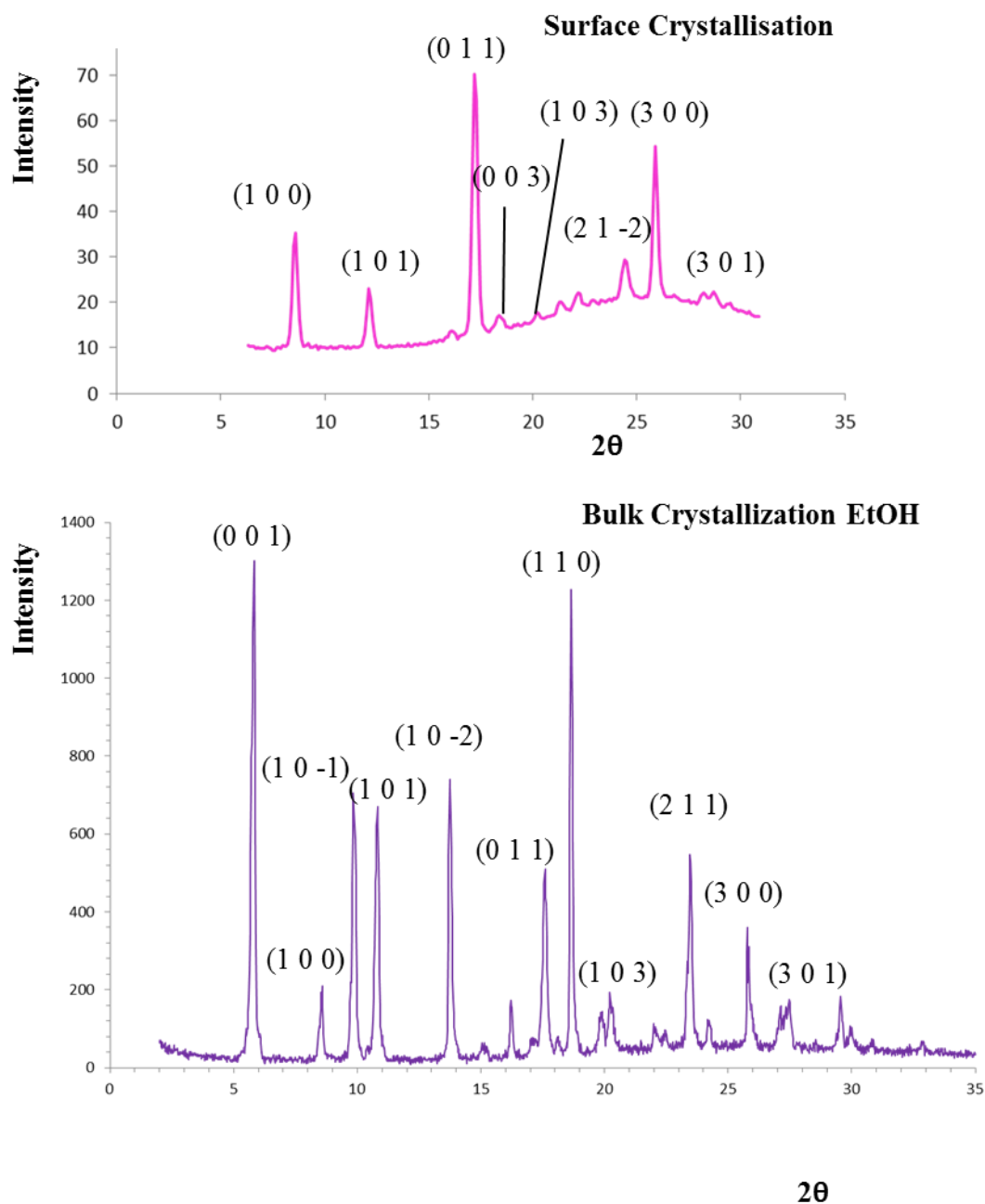
Two techniques have been used to confirm the crystallisation of the (-)-PMPP/(-)-PEA salt (Figure 8.2.30) on the micropatterned surface, powder X-ray diffraction and Raman confocal spectroscopy, and to study possible structural changes of the crystals due to the nature of the micropatterned surfaces.



**Figure 8.2.30.** Crystal X-ray structure of (-)-PMPP/ (-)-PEA diastereomeric salt.

#### 8.2.7.1 Powder X-ray microdiffraction characterisation

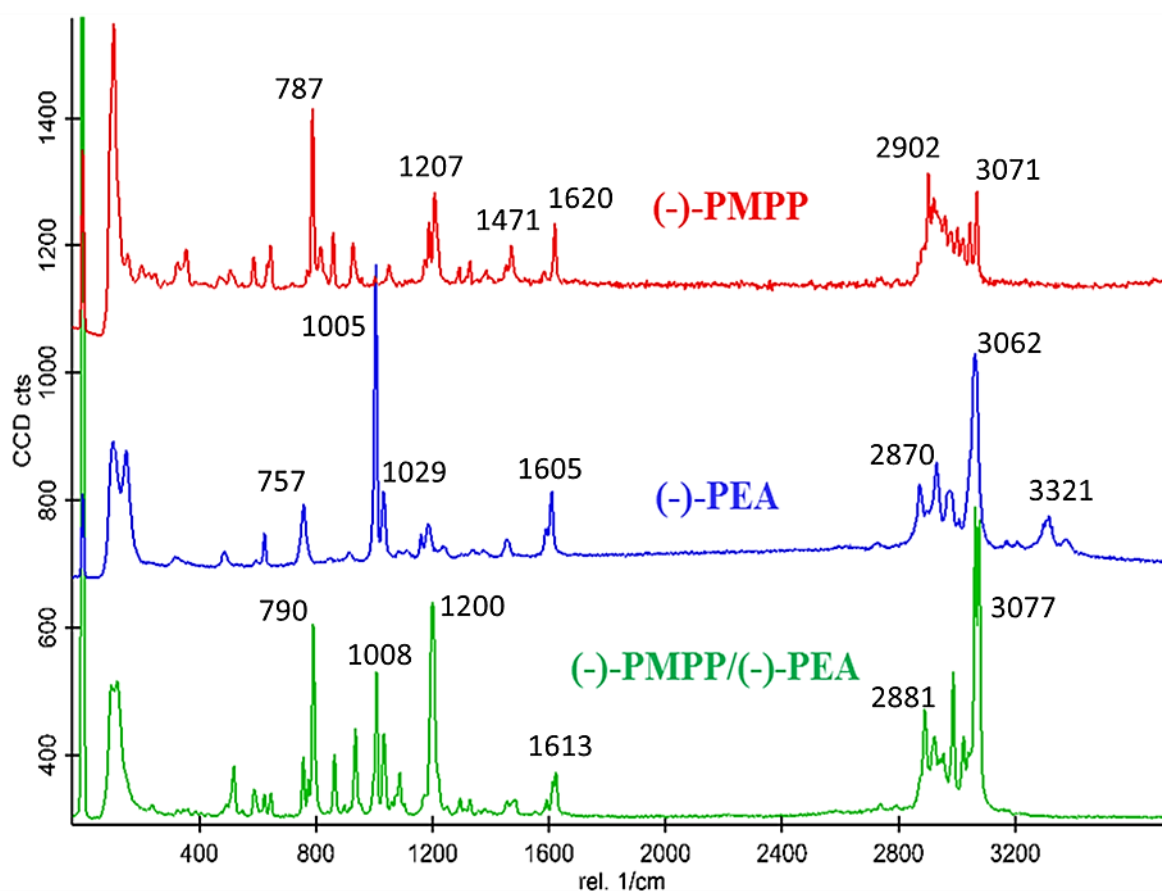
Powder X-ray diffraction confirms crystals on surface present the same crystalline structure as crystals obtained from bulk crystallisation. There are some differences in the relative intensities of the two diffractograms, although the crystalline structure is preserved. These differences are due to the preferential orientation in the growth caused by the template action of the SAMs in the micropattern and the fitting with the nucleus of the salt to start to grow. Thus, there is an effect on the orientation of growth that can be attributed to the surface. (Figure 8.2.31).



**Figure 8.2.31.** Powder diffractograms of crystals of (-)-PMPP/(-)-PEA salt crystallised from ethanol solution on surface and in bulk.

### 8.2.7.2. Raman confocal characterisation

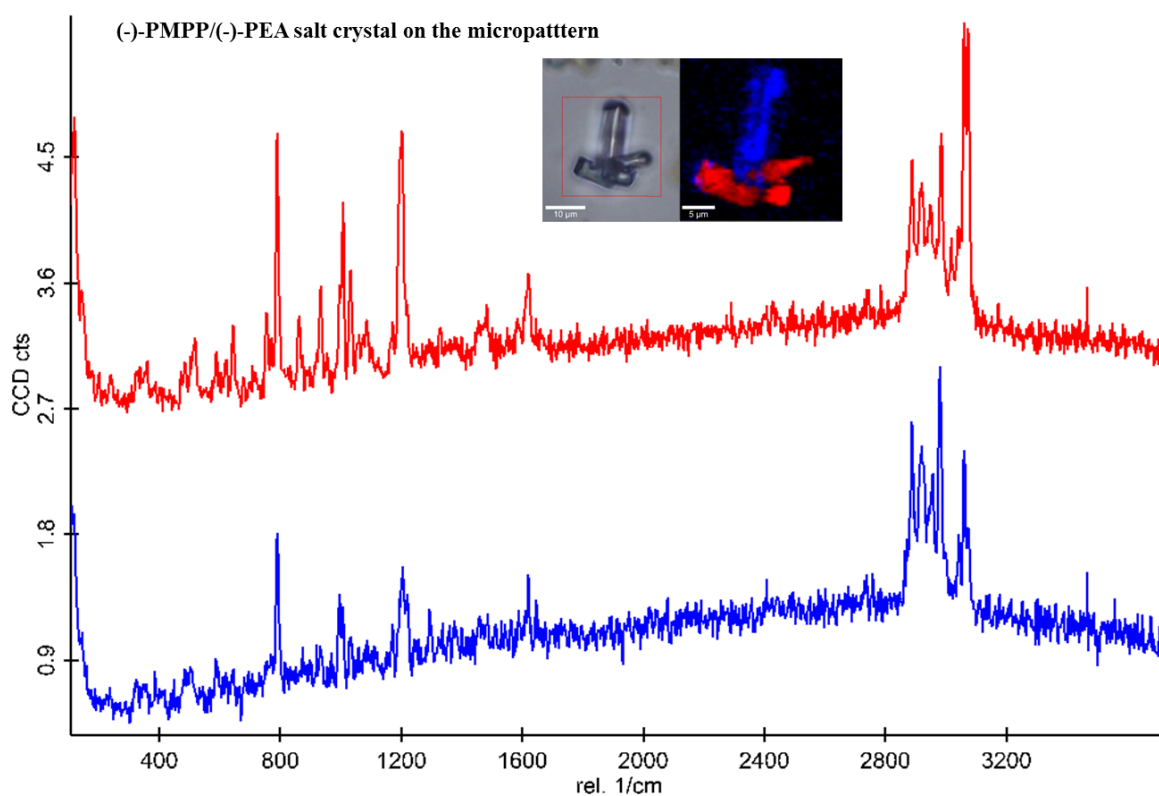
Since the crystals grown from solution and crystals grown on the micropatterns are expected to be the same, their Raman spectra should be also the same. As shown in Figures 8.2.32, 33 and 34, the Raman spectrum of (-)-PMPP/(-)-PEA grown in solution was firstly compared with the spectrum of pure (-)-PMPP and (-)-PEA, respectively. The spectrum of the salt shows peaks characteristics of (-)-PMPP and (-)-PEA, between 3077-2881, 1613, 1200, 1008 and 790  $\text{cm}^{-1}$ .



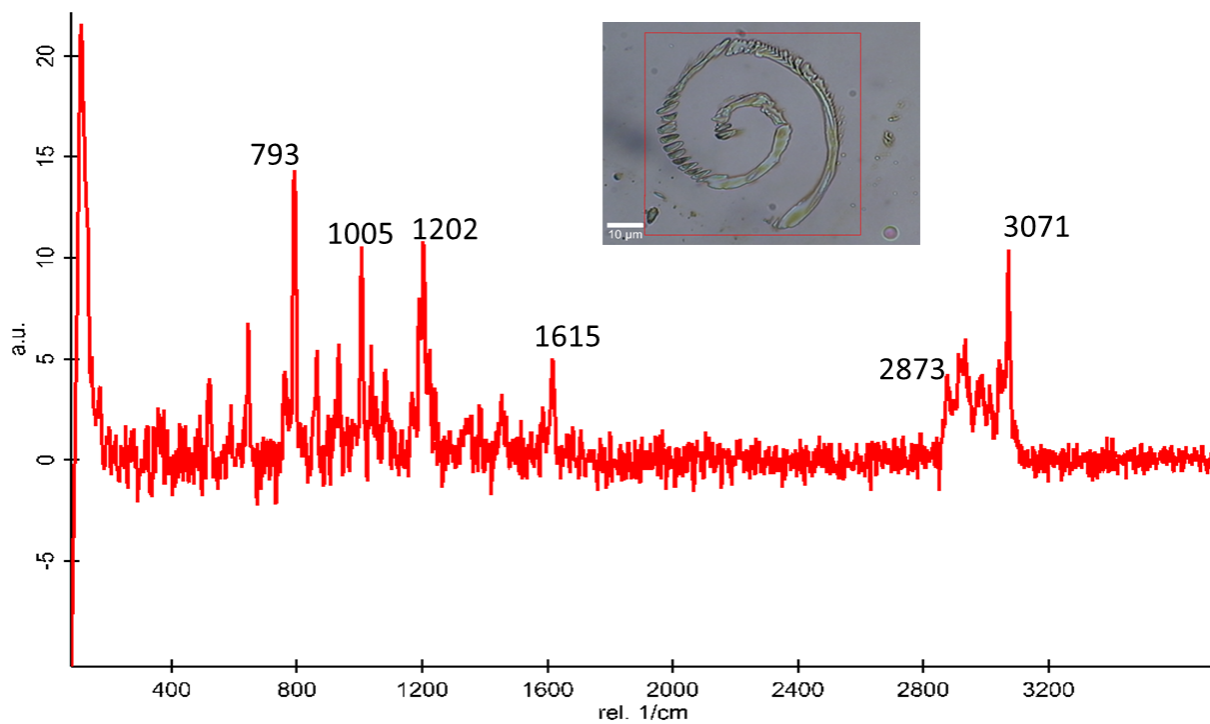
**Figure 8.2.32.** Raman spectra comparison: (-)-PMPP pure, (-)-PEA pure and (-)-PMPP/(-)-PEA salt from solution.



The Raman spectra of (-)-PMPP/(-)-PEA salts crystallised on the micropatterned surfaces with spirals or dots evidence the formation of the salt (Figures 8.234 and 8.2.34). Due to the size of the crystals, a lower intensity of signals was observed compared with bulk measurements. Nevertheless, all the main peaks of the salt are present. Slight differences in the intensity of the peaks were observed in the Raman spectra of crystals grown vertically or horizontally to the surface, as is shown in Figure 8.2.33. The red and blue spectra correspond to red and blue zones in the confocal image of the crystal showed in each Raman spectra. These differences are due to the orientation of the crystals with respect to the plane of the polarized light used, indicating that the compositions of the crystals are the same.



**Figure 8.2.33.** Raman spectra of (-)-PMPP/(-)-PEA salt crystal on the micropattern of dots 5 x 10  $\mu\text{m}$  from ethanol solution. Red and blue spectra correspond to red and blue zones in the confocal image of the crystal. They indicate different crystalline orientation of the same crystalline structure. Scalebar 10  $\mu\text{m}$ .



**Figure 8.2.34.** Raman spectra of (-)-PMPP/(-)-PEA salt crystal on the micropattern of spiral 50 x 100 μm from ethanol solution. Scalebar 10 μm.

### **8.2.8. Conclusions**

The use of chiral micropatterned SAMs to crystallise diastereomeric salts on them has been demonstrated. There are several parameters which have a dramatic influence on the crystallisation process, from the concentration of the ink solution to the crystallisation method.

The best concentration of ink solution in this system is 1 mM. The shape and size of the motif are important, as in the phencyphos crystallisation, the motif and size which present better results in terms of favouring the nucleation is for the dot pattern of 5 x 10  $\mu\text{m}$ .

In any crystallisation process, the approach to the supersaturation region is a crucial parameter; in this system the time to avoid collapse and allow a well-controlled crystallisation is 4 hours on the micropatterned surface in solution. The use of different patterns opens new possibility to study enantioselective recognition between chiral surfaces and racemates in order to develop surfaces as resolving auxiliaries, spirals motifs are the most suitable to this study.

The wet casting incubation-growth technique, where a drop of solution overnight in vapour saturated atmosphere, induces a much more homogeneous and reliable nucleation on the micropatterns.

The (-)-PMPP/ (-)-PEA salt crystallises on (+)-PMT and (+)-PMPP/ (+)-PEA salt crystallises on (-)-PMT. (+)-PMT functionalized surface presents preferred recognition than the one functionalized with (-)-PMT.

Powder X-ray diffraction and Raman confocal spectroscopy confirm the crystal growth of the (-)-PMPP/(-)-PEA on the micropatterned surface is the same salt as that grown from bulk solution.

### 8.3. Dutch Resolution on micropatterned surfaces

---

#### 8.3.1. Dutch Resolution

*Classical resolution* consists of the separation of a racemate by the exposure of this mixture of enantiomers to a resolving agent<sup>1</sup> – usually a homochiral compound which crystallises preferentially with one of the enantiomers in the racemate because of the diastereomeric relationship between the two complexes. *Dutch Resolution*<sup>2</sup> is a process whereby instead of a single resolving agent one uses a mixture of structurally related resolving agents (so-called families),<sup>3</sup> which is more effective than the single resolving agent (explained in detail in Chapter 1 of this thesis).

Having achieved the crystallization of enantiomerically pure compounds and diastereomeric salts on micropatterned surfaces by different crystallization methods, in order to reach the principals aims of this thesis, which was to probe the selective surface crystallisation of saturated solutions of different compounds. The experiments were performed in Syncom BV in Groningen (The Netherlands), the birthplace of the Dutch Resolution procedure, thus the perfect place to learn about this resolution and how it could translate to the resolution in bulk into resolution at the micropatterned surfaces.

The experiments carried out in Syncom BV. involve several thiols printed (Figure 8.3.1) on gold substrates and four different Dutch resolutions. Figure 8.3.2. shows all the combinations of monolayers and resolving agents and target racemates. The thiols selected to prepare the micropatterned surfaces are different than in the previous experiments, but all are polar and chiral. The reason to try with other thiols with similar properties is to check the importance of the effects provides for the PMT at surface. The Dutch Resolutions have a detailed protocol to follow in each experiment.<sup>3</sup> To functionalise each gold substrate we follow the same protocol of microcontact printing as in all previous experiments (Figure 8.3.1).

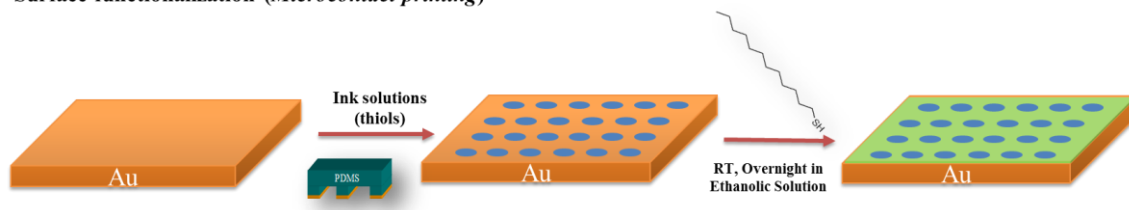
---

<sup>1</sup> T. J. Wozniak, R. J. Bopp, E. C. Jensen, *J. Pharmac. & Biomed. Anal.*, **1991**, 9, 363-382.

<sup>2</sup> R.M. Kellogg, J. W. Nieuwenhuijzen, K. Pouwer, T. R. Vries, Q. B. Broxterman, R. F.P. Grimbergen, B. Kaptein, R. M. La Crois, E. de Wever, K. Zwaagstra, A. C. van der Laana, *Synthesis*, **2003**, 10, 1626–1638.

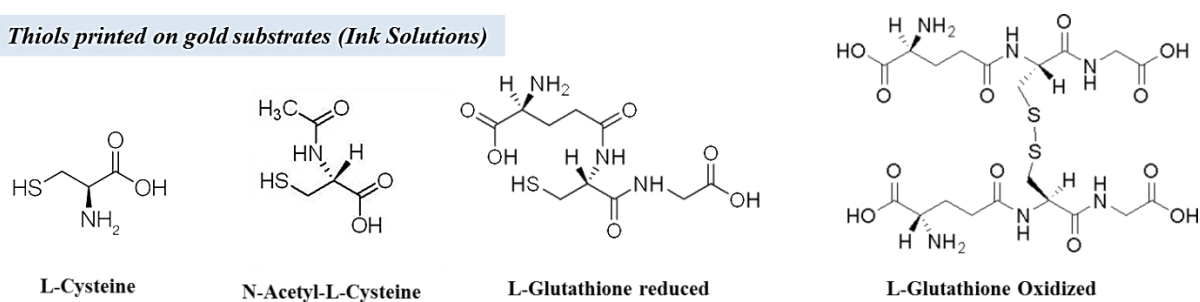
<sup>3</sup> T. Vries, H. Wynberg, E. van Echten, J. Koek, W. ten Hoeve, R. M. Kellogg, Q. B. Broxterman, A. Minnaard, B. Kaptein, S. van der Sluis, L. Hulshof, J. Kooistra, *Angew. Chem. Int. Ed.*, **1998**, 37, 2349-2354.

Surface functionalization (*Microcontact printing*)

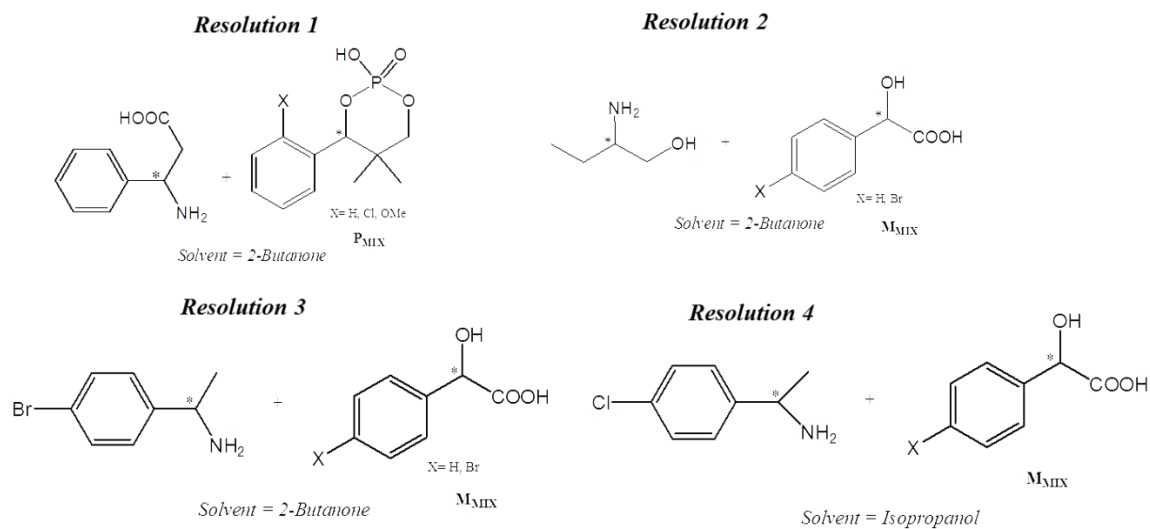


**Figure 8.3.1.** Microcontact printing protocol for the preparation of patterned surfaces. (Each arrow implies a washing by ethanol step).

Thiols printed on gold substrates (*Ink Solutions*)



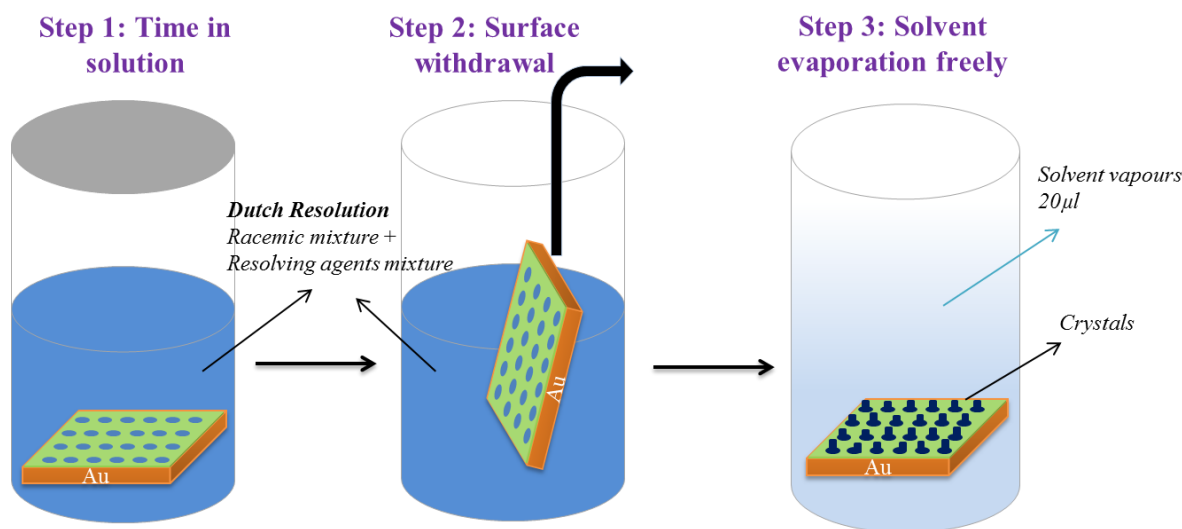
Dutch Resolution



**Figure 8.3.2.** Thiols printed on gold substrates and Dutch Resolutions.

### 8.3.2. Fast solvent evaporation method

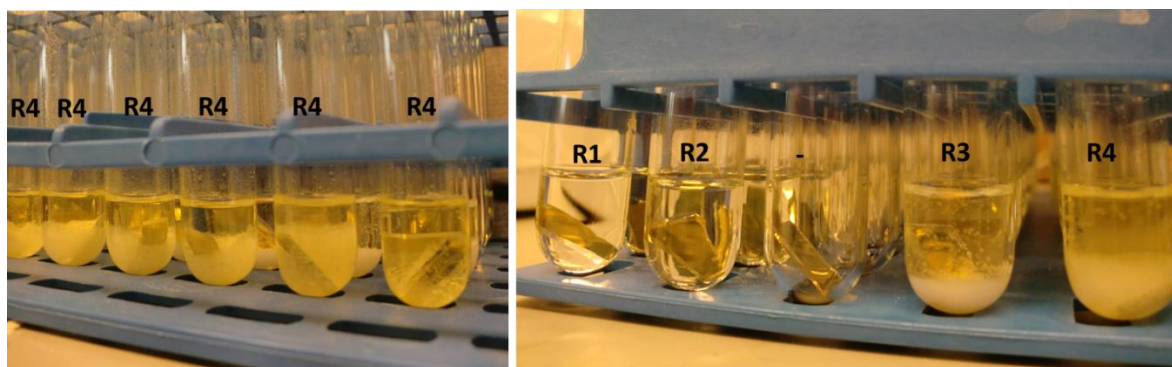
The protocol to carry out the Dutch Resolution on every micropatterned surface functionalised with the thiols in Figure 8.3.2. was identical, whereby the surfaces were immersed in supersaturated solutions of the potential salts in the solvents indicated. The quantity of each component (0.05-0.08 M for resolving agent mix and racemic mixture to resolve) necessary for obtaining a supersaturated solution was established by adding small volumes of the solvent and heating with a heatgun until complete dissolution of the solids in the hot solution was achieved. Once the solution was clear, 5 ml of the hot solution was introduced into a test tube containing the micropatterned surface. Thus, for each resolution, in order to favour the heterogeneous nucleation on the micropatterned surface, 5 ml of hot solution was in contact with each micropatterned surface functionalized by a different chiral thiol. The crystallization method followed was incubation for 30 min followed by removal and fast evaporation of the solvent (Figure 8.3.3).



**Figure 8.3.3.** Crystallization method, fast solvent evaporation.

The Dutch Resolution can be a very good method to resolve most racemic mixtures, but, occasionally, the method is less than optimum. This fact is shown pictorially in Figure 8.3.4, where it is possible to see clearly two lines of test tubes corresponding to the resolutions 1 and 2 in which no crystals were observed. Resolutions 1 and 2 were not successfully achieved and one reason could be that the nucleation inhibition effects are stronger in the compounds formed during the resolution process. In the case of resolution 3 and 4, the crystallization was almost instantaneous.

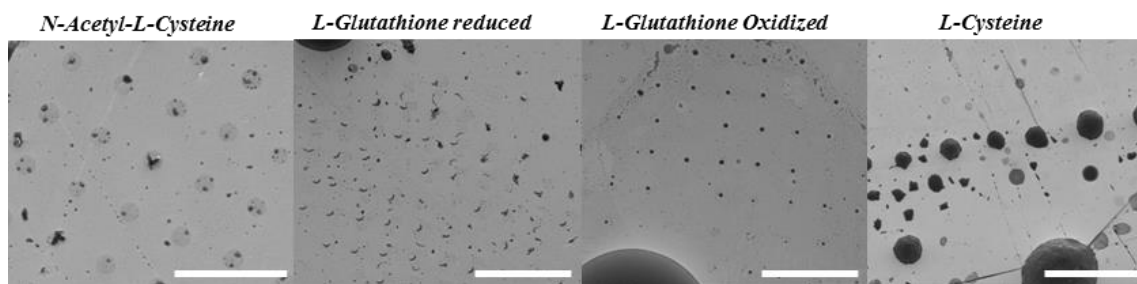
Usually this type of precipitation has a detrimental effect on the crystallization process on micropatterned surfaces, because mass is removed from the surrounding areas of the solution and does not nucleate at the surface due to the super-saturation is too high and nucleation occurs very quickly in many places before the pre-nucleus can be transported to the area of nucleation.



**Figure 8.3.4.** Micropatterned surfaces in warm Dutch Resolution solutions (R1: resolution 1; R2: resolution 2; R3: resolution 3; R4: resolution 4).

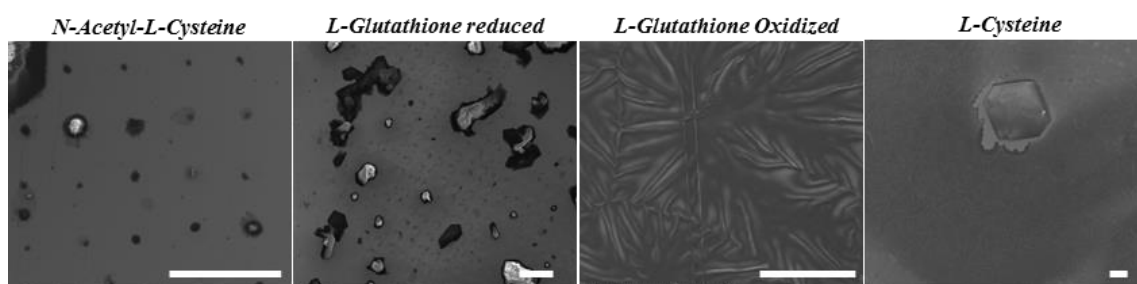
After 30 minutes in each solution, every micropatterned surface was removed and left in an empty and open vial until complete solvent evaporation from the surface. Once all the solvent had evaporated, each sample was checked by SEM (Scanning Electron Microscopy). The results are shown in Figures 8.3.5-8.3.7.

In the case of Resolution 2, the surfaces only contained stains of amorphous material and no crystalline morphology was observed at any place on the surface. The patterned areas were obvious in some cases, because material gathered there because of their polarity upon evaporation of the solvent, but the nucleation of crystals is not favoured. The lack of crystals in solution is already an indication that the crystallisation process is not controlled sufficiently under the conditions used for this experiment. The fact that only amorphous material is observed indicates that this salt does not crystallise well in the solvent used.



**Figure 8.3.5.** SEM micrographs corresponding to the micropatterned surface of each thiol after 30 min in the warm solution of the resolution 2 and solvent evaporation fast. Scalebar 30  $\mu\text{m}$ .

For resolution 3, material deposited on the patterns on the surface, and more texture was evident than in the case of resolution 2. However, the massive crystallisation in the bulk of the solution (evident in the photograph of the sample, Figure 8.3.4) as a result of homogeneous nucleation appears to have sequestered all the crystalline material, leaving the less favoured diastereomer and other components of the mixture of resolving agents – which are not good crystal formers – to deposit on the surface. The nucleation on every micropatterned surface is completely different, specially on the N-acetyl-L-cysteine the nucleation is localised on the micropatterned regions. Resolution 3 on L-Glutathione reduced micropatterned surface seems also localised and preferred on the micropatterned areas. Nevertheless, for the others (L-Glutathione oxidized and L-Cysteine) the nucleation is completely unlocalised.

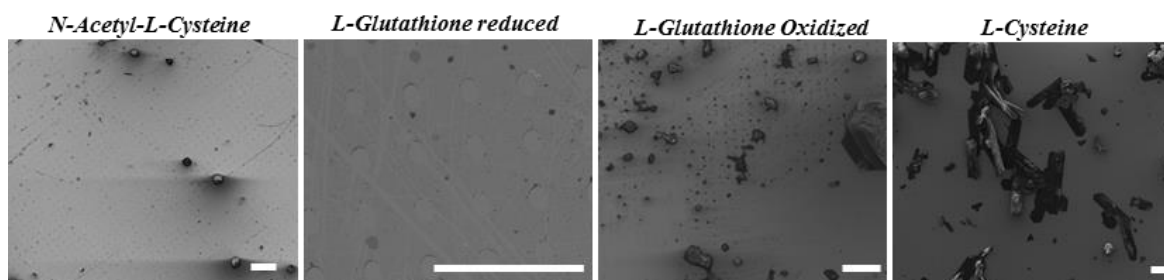


**Figure 8.3.5.** SEM micrographs corresponding to the micropatterned surface of each thiol after 30 min into the warm solution of the resolution 3 and solvent evaporation fast. Scalebar 30  $\mu\text{m}$ .

The massive crystallisation in the bulk of the solution, as in the resolution 3 case (evident in the photograph of the sample, Figure 8.3.4), as a result of homogeneous nucleation affects to the resolution 4 on the material deposited on the pattern on the surface. L-glutathione oxidized and N-acetyl-L-cysteine micropatterned surface show localised nucleation on them. L-cysteine micropatterned surface show crystals formed



from the homogeneous nucleation and felt down on the surface. On the L-glutathione reduced micropatterned surface the nucleation is completely unlocalised.



**Figure 8.3.6.** SEM micrographs corresponding to the micropatterned surface of each thiol after 30 min into the warm solution of the resolution 4 and solvent evaporation fast. Scalebar 50  $\mu\text{m}$ .

In general, for the experiments carried out in solution, the recognition between crystal nucleus and the surface is not sufficient to favour growth of the crystals on the patterns. Whether this result is caused by the slow mass transport of the nuclei through the solution or whether there is an intrinsic lack of recognition between the surface and the nucleus is not clear at this point. In any case, heterogeneous nucleation is not observed. Although in a few of the samples upon evaporation there is recognition over the micropatterned regions and material in solution – presumably because of the polarity of the areas – the material formed is not of a crystalline morphology, implying that it may be the least favoured diastereomer (and mixtures thereof) that remains in solution and is deposited upon evaporation.

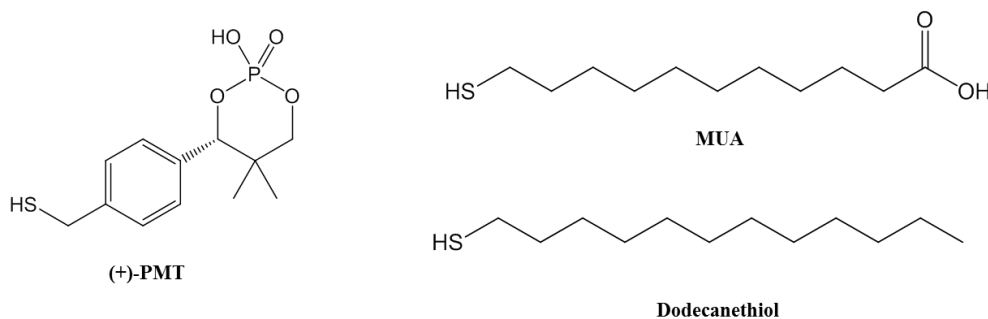
Although the objective of this work was to achieve a fast and simple procedure for the screening of Dutch resolutions on surfaces, the crystallisation process is of such complexity that it appears to be an obstacle to this goal for these systems. The precipitations are the result of many effects which are not controlled to the precision required for a perfect crystallisation during their preparation: For example, the solvent diffusion over the micropatterned surface is quite probably not optimal. Also, the concentration of the solutions for each resolution are supersaturated and hot, thus the minimum variation could promote the crystallization in bulk (for the best case) or the precipitation (in the worst case), avoiding the crystallization on the micropatterned surface in a controlled way by heterogeneous nucleation.

The solution to these challenges is to identify surface-based heterogeneous nucleants which are extremely efficient because of their interaction with the components of the final crystal, and their preference for these rather than the solvent in the medium, as well as ensuring efficient mass transport in the solution. It seems likely that more nanostructured supports will be necessary for this process to become effective.

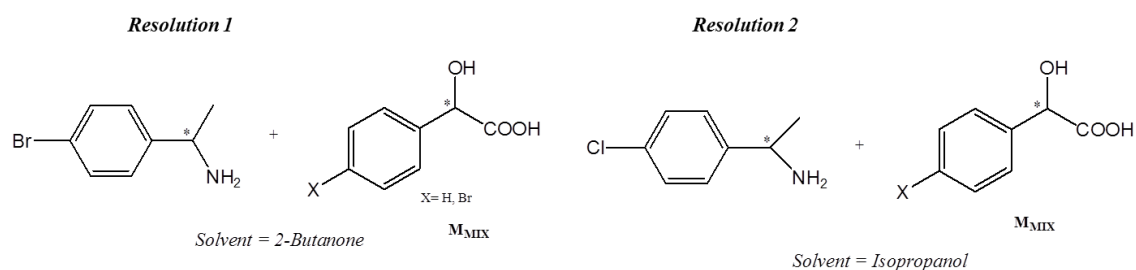
### 8.3.3. Slow solvent evaporation method

The second batch of experiments carried out to probe the Dutch resolution at a surface was carried out in clean room and included modifications of the protocol following observations from the initial experiments. The following scheme shows the thiols used to functionalise the polycrystalline gold substrates, they are the (+)-PMT, MUA and DT to form micropatterns of dots of 5  $\mu\text{m}$  and separated 10  $\mu\text{m}$ . The solutions prepared for each Dutch resolution were made slightly diluted (0.04-0.05 M), in order to delay the homogeneous nucleation when the solution grows colder and the saturated solution is formed.

#### Thiols printed on gold substrates (Ink Solutions)



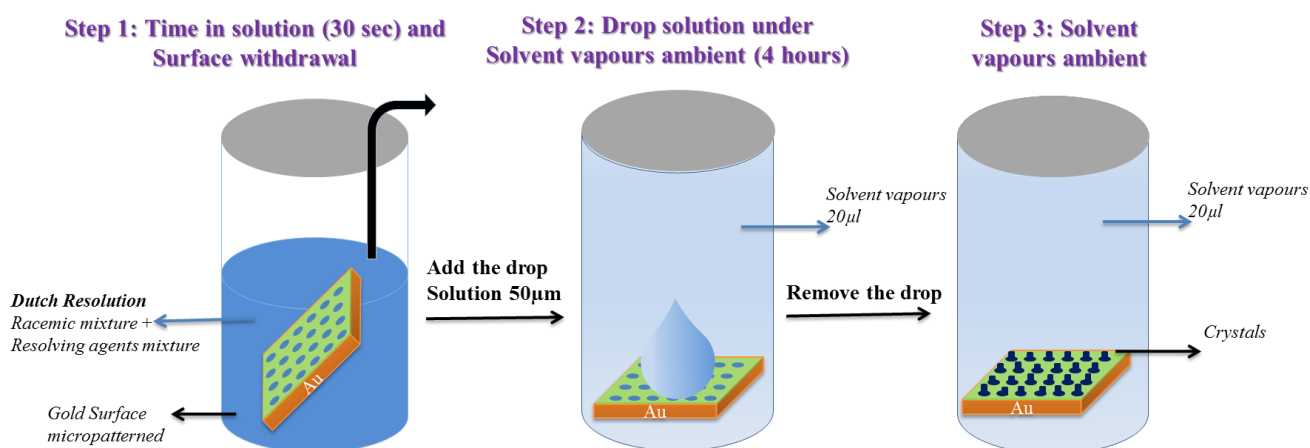
#### Dutch Resolution



**Figure 8.3.7.** Thiols printed on gold substrates and Dutch Resolutions.

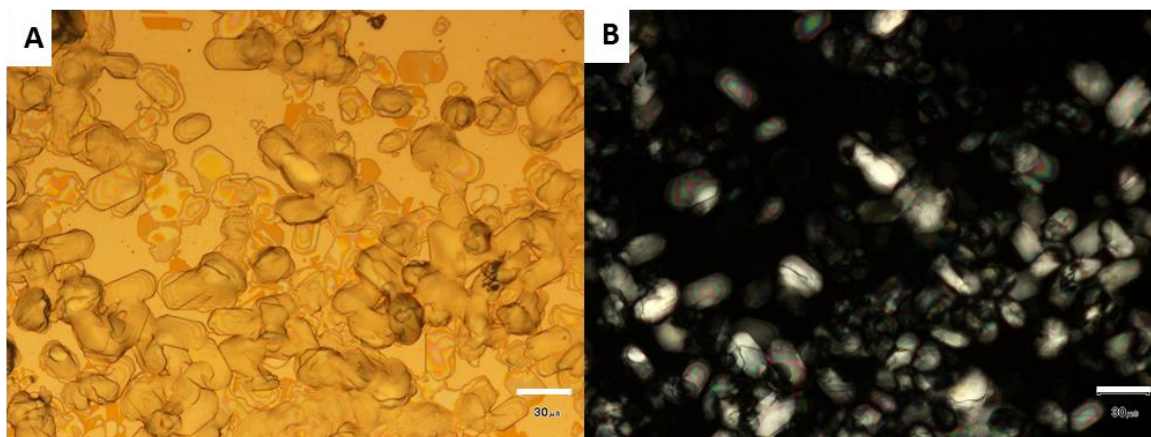
In these experiments the two resolutions that presented better results in the previous series were selected and experimental conditions were tuned to improve crystallisation on the surfaces. Under the controlled atmosphere of the clean room, the preparation of each micropatterned gold substrate was done following the same microcontact printing protocol as in the previous experiments.

The preparation of each solution was following the same protocol used in the previous experiments which follows the published protocol.<sup>3</sup> The crystallisation method followed in these experiments was *drop casting wet method*. The functionalised surfaces were placed into the hot solution for 30 seconds and then each micropatterned substrate was placed into a closed vial with a solution drop (20  $\mu\text{l}$ ) on the micropatterned surface. The vial was saturated in solvent vapour, giving an equilibrium state from the beginning. The method is showed in the next figure 8.3.8.

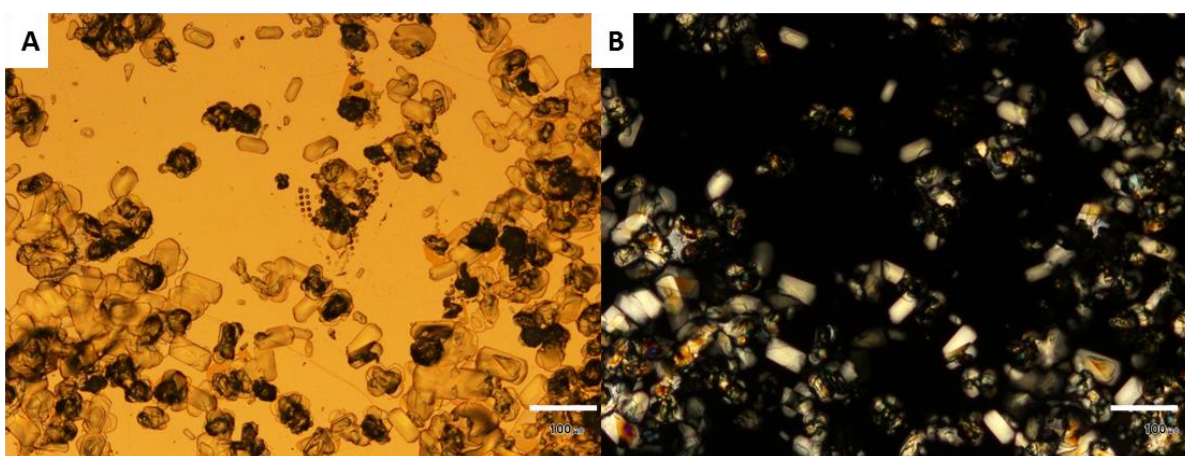


**Figure 8.3.8.** Drop casting wet crystallisation method.

After one week inside the vial, the micropatterned surfaces were dried. For the resolution 1 each micropatterned surfaces presented the same crystals from the apparent homogeneous nucleation (from solution) on surface hiding the micropattern (Figure 8.3.9 and 8.3.10). A quite homogeneous crop of rectangular crystals with rounded ends is observed (consistent with an orthorhombic space group) which are clearly birefringent even in both cases of (+)-PMT and MUA micropatterned surfaces.

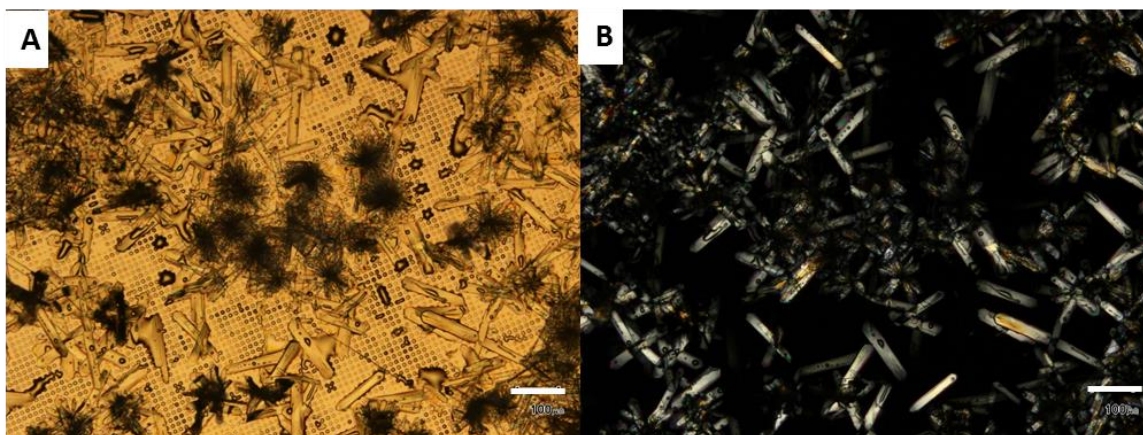


**Figure 8.3.9.** Optical micrographs of the micropatterned surface functionalised with dots of 5  $\mu\text{m}$  of (+)-PMT and DT around after one week into a closed vial vapour saturated in 2-butanone, corresponding to resolution 1. (A) non-polarised and (B) polarised reflection images. Scalebar 30 $\mu\text{m}$ .



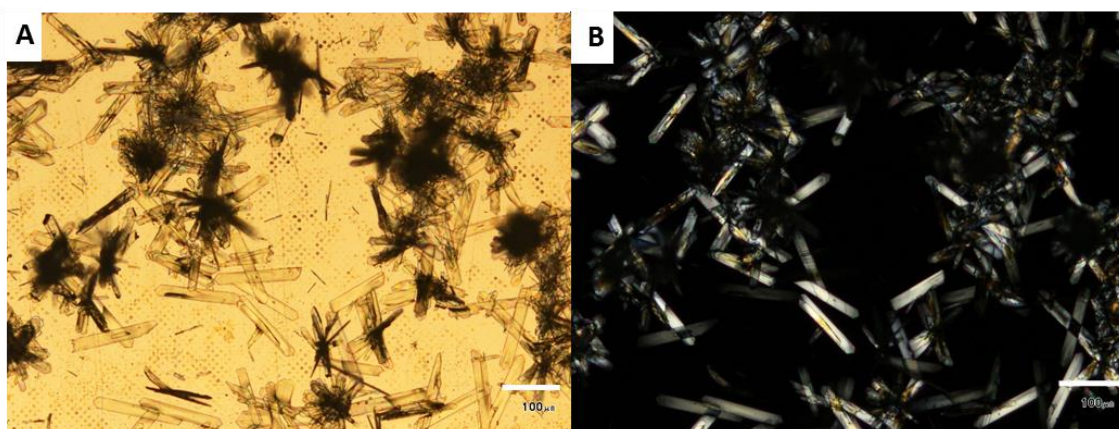
**Figure 8.3.10.** Optical micrographs of the micropatterned surface functionalised with dots of 5  $\mu\text{m}$  of MUA and DT around after one week into a closed vial vapour saturated in 2-butanone, corresponding to resolution 1. (A) non-polarised and (B) polarised reflection images. Scalebar 30  $\mu\text{m}$ .

In the case of the resolution 2, after 10 days the sample was still wet although there were crystals over the whole micropatterned surface from the solution. The homogeneous nucleation in this experiment is apparently very favoured as is observed in Figure 8.3.11 and 8.3.12, there many crystals that appear to have been formed in solution and fallen onto the micropattern and the micropattern is wet by the solution.



**Figure 8.3.11.** Optical micrographs of the micropatterned surface functionalised with dots of 5  $\mu\text{m}$  of (+)-PMT and DT around after one week in a closed vial saturated with isopropanol vapour, corresponding to resolution 2. (A) non-polarised and (B) polarised reflection images.

Scalebar 100 $\mu\text{m}$ .



**Figure 8.3.12.** Optical micrographs of the micropatterned surface functionalised with dots of 5  $\mu\text{m}$  of MUA and DT around after one week in a closed vial saturated with isopropanol vapour, corresponding to resolution 2. (A) non-polarised and (B) polarised reflection images. Scalebar

100 $\mu\text{m}$ .

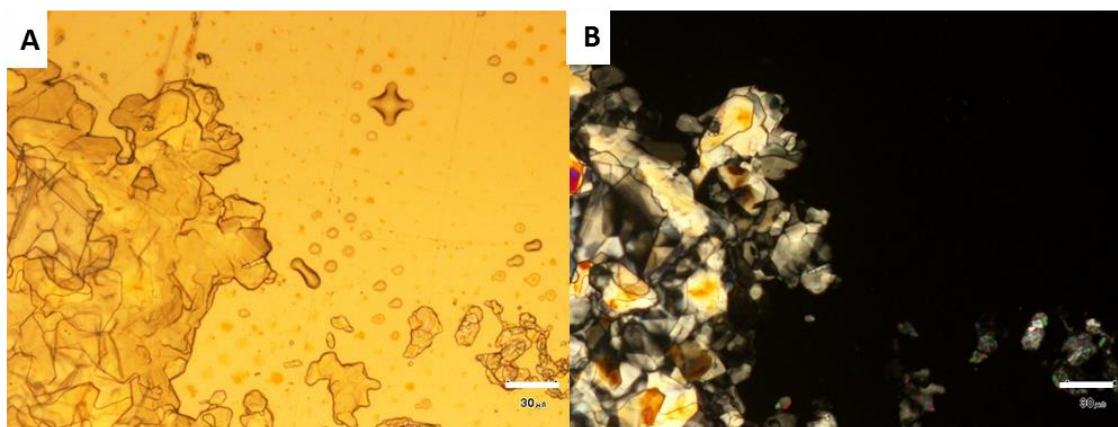
The major challenge in these systems is to favour the heterogeneous nucleation instead of the homogeneous nucleation. Thus, in order to check out which nucleation forms the crystals grown on the micropatterned surface and using the same micropatterned surfaces after washing them slightly with the same solvent (10 ml) as their solution, with several crystals on top. Then, each micropatterned surface was deposit into a closed vial saturated in their solvent vapours for a week. After these steps

(washed and incubation in vapours saturated environment), the most of crystals were washed off from the micropatterned surface, thus they were not fixed.

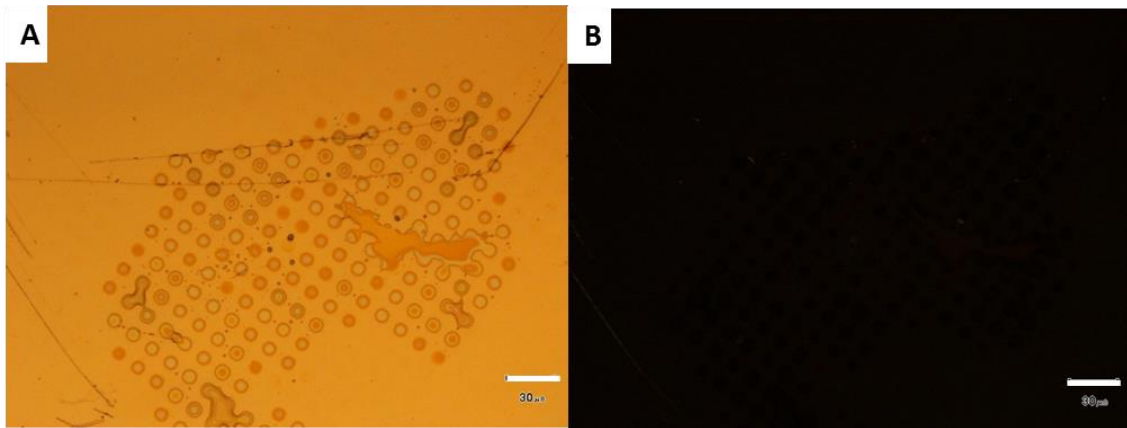
The hypothesis was that the dissolution could help to redistribute the compounds over the surface after one week of each micropatterned surface inside a closed vial saturated in vapour of their corresponding solvents. The following figures show the results of these experiments which show the redistribution over the micropatterned surface. Solvent's vapours redissolve the crystals over the surface, breaking crystals and forming news, able to fit with the thiol templates on the surface. However, the homogeneous nucleation is still favoured instead of the heterogeneous nucleation.

The micropatterned surfaces after the redissolution process of the resolution 1 are shown in the figures 8.3.13, 14 and 15. The redissolution affect mainly to the big crystals, because they were not attached to the surface so it is very easy to remove them. Moreover, on the micropatterned regions there are amorphous materials, which are clearly non birefringent in any cases of (+)-PMT neither MUA micropatterned surfaces.

The figure 8.3.13 shows crystals from homogeneous nucleation are still on the surface, notice their shape have changed, after the redissolution several crystals grown on the same point, forming this block clearly polycrystalline (Figure 8.3.13 B).

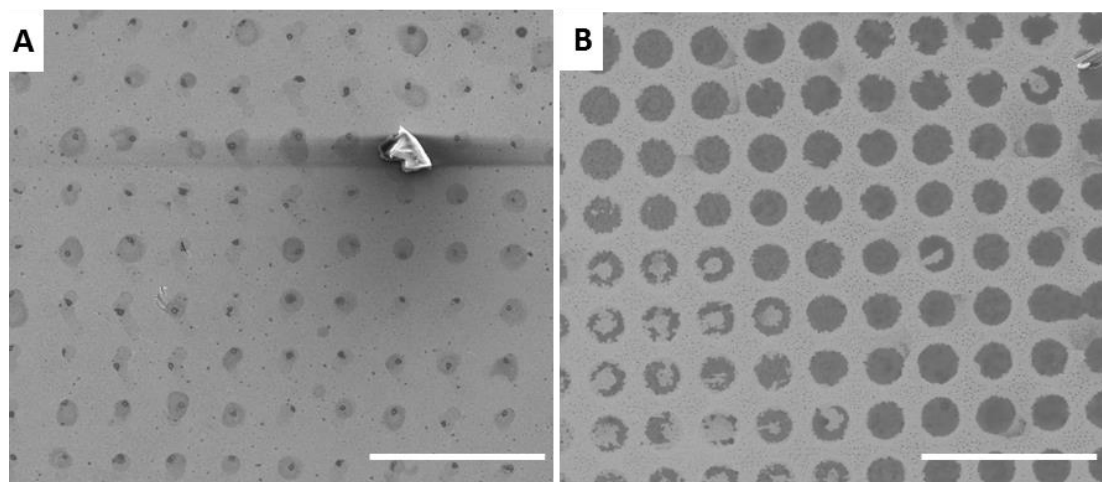


**Figure 8.3.13.** Optical micrographs of micropatterned surfaces by: (A-B) dots of 5 µm of (+)-PMT, after one week into a closed vial vapour saturated in 2-butanone, corresponding to *resolution 1*. (A) non-polarised and (B) polarised reflection images. Scalebar 30 µm.



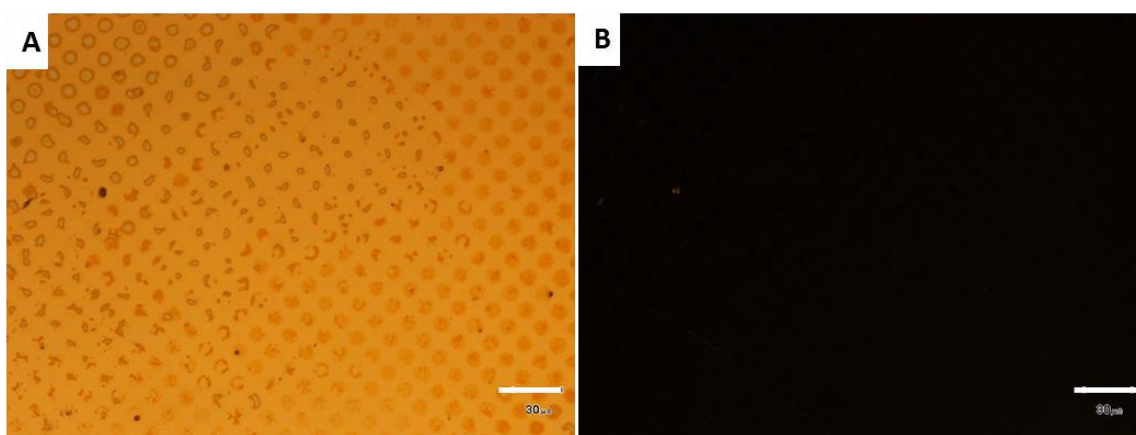
**Figure 8.3.14.** Optical micrographs of micropatterned surfaces by dots of 5  $\mu\text{m}$  of MUA; after one week into a closed vial vapour saturated in 2-butanone, corresponding to *resolution 1*. (A) non-polarised and (B) polarised reflection images. Scalebar 30  $\mu\text{m}$ .

SEM micrographs of the figure 8.3.13 confirm there is material on the micropatterned region after redissolution. Thus, there is a contribution of the heterogeneous nucleation in the crystallisation process of the resolution on micropatterned surface. Nevertheless, is not possible to confirm that the heterogeneous nucleation has a relevant influence on the Dutch resolution on micropatterned surface after the redissolution process.

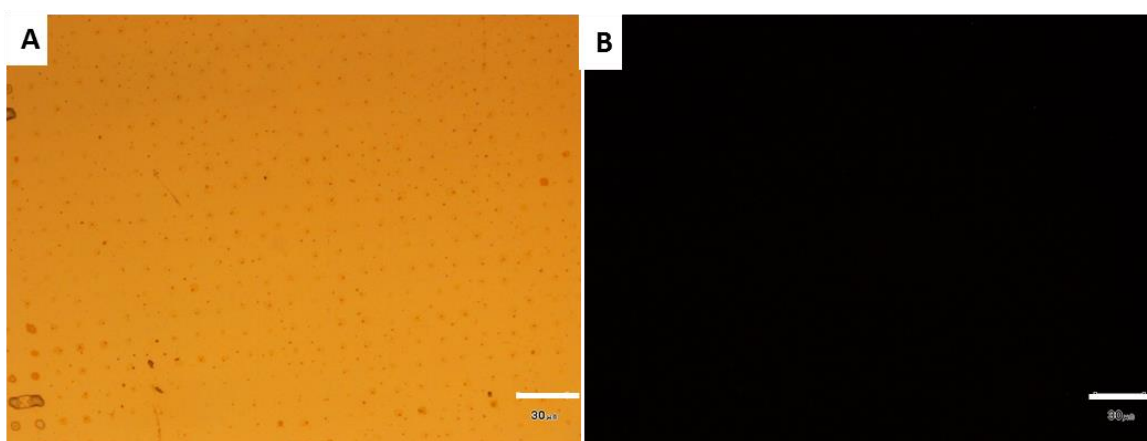


**Figure 8.3.15.** SEM micrographs of micropatterned surface comparison between the (A) (+)-PMT and (B) MUA series for the resolution 1 after redissolution. Scalebar 50  $\mu\text{m}$ .

As it has been mentioned before, the same procedure of redissolution was carried out with the *resolution 2*. The micropatterned surfaces after the redissolution process of the resolution 2 are shown in the figures 8.3.16, 17 and 18. In this case, the redissolution also affect mainly to the big crystals, presumably for the same reason than in the case of redissolution 1, because the big crystals were not attached to the surface and is very easy to remove them. Moreover, on the micropatterned regions there are amorphous materials, which are clearly non birefringent in any cases of (+)-PMT neither MUA micropatterned surfaces.



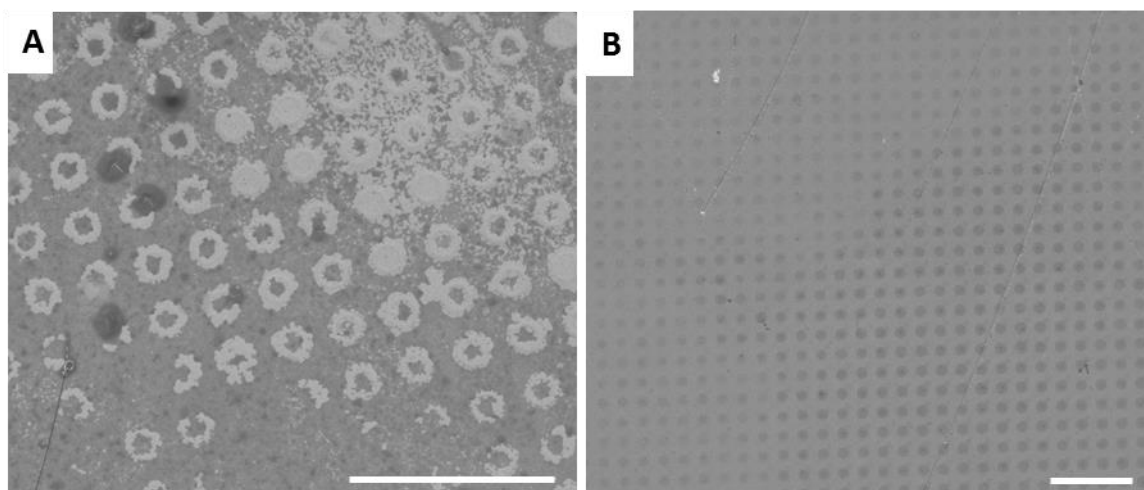
**Figure 8.3.16.** Optical micrographs of micropatterned surfaces by dots of 5  $\mu\text{m}$  of (+)-PMT, after one week into a closed vial vapour saturated in 2-butanone, corresponding to *resolution 2*. (A) non-polarised and (B) polarised reflection images. Scalebar 30  $\mu\text{m}$ .



**Figure 8.3.17.** Optical micrographs of micropatterned surfaces by dots of 5  $\mu\text{m}$  of MUA; after one week into a closed vial vapour saturated in 2-butanone, corresponding to *resolution 2*. (A) non-polarised and (B) polarised reflection images. Scalebar 30  $\mu\text{m}$ .



SEM micrographs of the figure 8.3.18 confirm there is material on the micropatterned region after redissolution, in the case of the micropatterned surface by (+)-PMT there is material outside de dots. Very high concentration could produce crystallisation on the micropatterned region and outside them.<sup>4</sup> Thus, also for the redissolution of the micropatterned surface of the resolution 2, there is a contribution of the heterogeneous nucleation after the redissolution process.



**Figure 8.3.18.** SEM micrographs of micropatterned surface if dots of 5  $\mu\text{m}$  comparison between the (A) (+)-PMT and (B) MUA for the *resolution 2* after redissolution. Scalebar 50  $\mu\text{m}$ .

<sup>4</sup> J. Aizenberg, *Adv. Matter.*, **2004**, *16*, 1295-1302

#### 8.3.4. Conclusions

Dutch resolution is a very good technique to resolve racemic mixtures using resolving agent mixtures in homogeneous media. Thus, this resolution favours strongly homogeneous nucleation and growth of specific diastereoisomers in crystals. That nucleation process is complex and specific, because of the multiple components present in the mixture. Any heterogeneous nucleation agent must be compatible with the recognition processes at play. In the patterned layers tried to date, it is clear that the interaction between nuclei and monolayers on the surface is incompatible, at least in comparison with the homogeneous process.

Control of the nucleation taking place in these systems is very complicated, because the racemic mixture and the resolving agent mixture have a very high affinity one to each other, and this nuclei must interact with the surface in order to be transformed to the critical nucleus there. Given that components of the Dutch resolution process play a critical role, the results imply that their incorporation into the heterogeneous system may be hindered. Thus their nucleation probability is much higher than any of them with the monolayer on surface.

Nevertheless, in this chapter it has been shown that both neutral compounds (phencyphos) and salts can be crystallised on a patterned surface, therefore it is foreseen that the use of modified libraries with heterogeneous nucleating agents may be practical.

# Chapter 9

## Final conclusions

---

The most significant conclusions of the crystallisation on functionalised surfaces are presented in context.

The main focus of this Thesis has been to control of the crystallisation process on functionalised surface. The family of compounds which were the focus of the study were derivatives of phencyphos, a cyclic phosphonate resolving agent. In order to understand the crystal structures of these compounds the known structural data was analysed and two new crystal structures of diastereomeric salts were obtained, from which we can conclude that:

- Both pure resolving agents and the salts with primary amines form strong hydrogen bond networks in the solid state, forming uncommon 10-membered rings in the crystal structures.
- Several potential polar faces could easily interact with polar SAMs in order for their nucleation and crystal growth to be templated.

The selected compound to functionalise a surface was the specifically designed chiral phencyphos 4-methylthiol (PMT) which was assembled on a gold substrate. From this study it was shown that:

- The self-assembled monolayer of PMT forms readily on the gold surface, and therefore the phosphoric acid group does not interfere with monolayer formation.
- The acid group is directed mainly away from the surface of the gold, in a position where it could interact with other molecules at the interface.
- The adsorbant does not form a well ordered monolayer, either because the packing cannot be

The functionalisation of gold with monolayers of this compound has provided significant results due to its demonstrated influence in the crystallisation process. Thus, the successful functionalisation of the gold substrate by this resolving agent type molecule provided the chiral property to the self-assembled monolayer on gold, and gave the following conclusions.

- PMT SAM acts as template layers for the heterogeneous nucleation and growth of a structurally related organic molecule from organic solvents.
- The influence of the monolayer is so high that as its nature coupled with evaporation rate and other solvent characteristics, influences the size distribution and morphology of the organic crystals that are formed.

- The disordered monolayer template and its tiny flexibility in between the anchoring sulphur atom and the phosphate group, and where the orientation of the groups must be understood as being random, do not allow the epitaxial growth over the PMT SAM.
- The SAM has a determining influence on the nucleation and growth of the organic crystals formed from the organic solvent. We conclude that this effect has to do with the wettability of the surface by the pre-nucleus, as inferred for the growth of an organic molecule on different polymer substrates.

The microcontact printing method favours the mass transport to the desired thiol, minimizing evaporation effect at small scale. The surface combined of PMT and dodecanethiol has been the key for the development of surfaces which can induce the nucleation process on surface. From this study we learned that:

- Phencyphos crystallisation on micropatterned surfaces demonstrates that the heterogeneous nucleation is effective when the solvent is allowed to evaporate slowly from the surface, allowing good mass transport to the desired regions.
- There are several parameters that also have a dramatic influence on the crystallisation process such as the pattern shape and size which are critical. Thus the motif size which presents better results of favour the nucleation is for dots of 5  $\mu\text{m}$  diameter spaced by 10  $\mu\text{m}$ , even for diastereomeric salt crystallisation.

Diastereomeric salt controlled crystallisation on micropatterned surfaces was the other main objective of this Thesis. The diastereomeric salt most studied and presented here is the one formed by a phencyphos derivate, *p*-methyl phencyphos which provides a pair of crystalline salts with chiral amines. X-ray crystal structure of this diastereomeric salt reveal 10-membered rings constructed through hydrogen bonds, in which two ammonium groups formally replace phencyphos molecules seen in the phencyphos hydrate structure. The hydrogen bonds are strong and provide several polar faces to the crystalline structure, thus diastereomeric salts should have their crystals templated easily on polar SAM. This effect was shown by crystallisation on patterned surfaces which showed:

- An incubation period is beneficial for crystal formation, possibly as a result of interaction of amine with the patterned monolayer. The utilization of different patterns opens new possibility to study enantioselective recognition between chiral surfaces and racemates in order to develop surfaces as resolving auxiliaries, spirals motifs are the most suitable to this study.
- The polar nature of the thiols on surface influence in the crystal growth, as (+)-PMT and MUA show different effects, depending on the compound being crystallised, pointing to a potential selectivity in crystallisation.

The final goal of the thesis was to test the possibilities of using Dutch resolution - a very good technique to resolve racemic mixture by resolving agent mixtures in bulk solutions – in a heterogeneously nucleated system. Any heterogeneous nucleation agent must be compatible with the recognition processes at play. Nevertheless, in the patterned layers tried to date, it is clear that the interaction between nuclei and monolayers on the surface is incompatible, at least in comparison with the homogeneous process. The complexity of the family type crystallisation will require the development of specific additives to favour heterogeneous nucleation.

## Bibliography

### Chapter 1

1. A. J. MacDermott, L. D. Barron, A. Brack, T. Buhse, A. F. Drake, R. Emery, G. Gottarelli, J. M. Greenberg, R. Haberle, R. A. Hegstrom, K. Hobbs, D. K. Kondepudi, C. McKay, S. Moorbath, F. Raulin, M. Sandford, D. W. Schwartzman, W. H.-P. Thiemann, G. E. Tranter, J. C. Zarnecki, *Planet. Space Sci.*, **1996**, *44*, 1441-1446.
2. R. Bentley, *Chirality*, **2010**, *22*, 1–2.
3. G. Pàlyi, C. Zucchi, L. Caglioti, *Progress in Biological Chirality*, **2004**, Elsevier Ltd.
4. L. D. Barron, *J. Am. Chem. Soc.*, **1986**, *108*, 5539.
5. A. R. Fassih, *Int. J. Pharmac.*, 1993, *92*, 1-14.
6. T. J. Wozniak, R. J. Bopp, E. C. Jensen, *J. Pharma. Biomed. Anal.*, **1991**, *9*, 363-382.
7. A. Mannschreck, R. Kiesswetter, *J. Chem. Ed.*, **2005**, *82*, 1034-1039.
8. J. Jacques, A. Collet, S. H. Wilen, *Enantiomers, Racemates and Resolution*, Krieger, Florida, **1994**.
9. R. M. Kellogg, M. Leeman, *Crystallization as a Tool in Industrial Applications of Asymmetric Synthesis*. Comprehensive Chirality, **2012**, *9*, 367-399. Elsevier.
10. M. Zhang, G. Qing, T. Sun. *Chem. Soc. Rev.*, **2012**, *41*, 1972-1984.
11. L. Pasteur, *L. Ann. Chim. Phys.*, **1848**, *24*, 442-459.
12. M. S. Leeman, *Resolutions of Racemates by Crystallization*, **2009**, University of Groningen (The Netherlands) (ISBN: 978-90-367-3842-2).
13. D. Kozma, *Optical Resolutions via diastereomeric salt formation*, CRC Press; 1st edition , **2012**.
14. Q. He, H. Goma, S. Rohani, J. Zhu, M. Jennings. *Chirality*, **2010**, *22*, 707-716.
15. S. Müller, M. Cyrus, R. de Gelder, G.J.A. Ariaans, B. Kaptein, Q.B. Broxterman, A. Bruggink, *Eur. J. Org. Chem.* **2005**, *25*, 1082–1096.
16. T. Vries, H. Wynberg, E. van Echten, J. Koek, W. W. ten Hoeve, R. M. Kellogg, Q. B. Broxterman, A. Minnard, B. Kaptein, S. van der Sluis, L. Hulshof, J. Kooistra, *Angew. Chem. Int. Ed.*, **1998**, *37*, 2349-2354.
17. R. M. Kellogg, J. W. Nieuwenhuijzen. K. Pouwer, T. R. Vries, Q. B. Broxterman, R. F. P. Grimbergen, B. Kaptein, R. M. La Crois, E. de Wever, K. Zwaagstra, A. C. van der Laan. *Synthesis*, **2003**, *10*, 1626-1638.

18. M. Leeman, G. Brasile, E. Gelens, T. Vries, B. Kaptein, R. M. Kellogg, *Angew. Chem. Int. Ed.*, **2008**, *47*, 1287–1290.
19. D. Kashchiev, *Nucleation Basic Theory with Applications*, **2000**, Butterworth-Heinemann Ed.
20. P. G. Vekilov, *Cryst. Grow. Des.*, **2010**, *10*, 5007-5019.
21. P. R. ten Wolde, D. Frenkel, *Science*, **1997**, *277*, 1975-1978.
22. D. Erdemir, A. Y. Lee, A. S. Myerson, *Accounts of Chemical Research*, **2009**, *42*, 621-629.
23. D. Erdemir, S. Chattopadhyay, L. Guo, J. Ilavsky, H. Amenitsch, C. U. Segre, A. S. Myerson, *Phys. Rev. Lett.*, **2007**, *99*, 115702.
24. S. Chattopadhyay, D. Erdemir, J. M.B. Evans, J. Ilavsky, H. Amenitsch, C. U. Segre, Allan S. Myerson, *Cryst. Growth Des.*, **2005**, *5*, 523-527.
25. P. C.J. Stephens, Y.Y. Kim, S.D. Evans, F.C. Meldrum, H.K. Christenson, *J. Am. Chem. Soc.*, **2011**, *133*, 5210-5213.
26. (a) D. W. Oxtoby, *J. Phys. Condens. Matter*, **1992**, *4*, 7627-7650. (b) D. Kashchiev, *Nucleation Basic Theory with Applications*, **2000**, 20-29, Butterworth-Heinemann Ed.
27. X. Y. Liu, *J. Chem. Phys.*, **2000**, *112*, 9949- 9955.
28. J.M. García-Ruíz, *Journal of Structural Biology*, **2003**, *142*, 22–31.
29. D. Turnbull, *J. Chem. Phys.*, **1950**, *18*, 198-203.
30. S. Sek, R. Bilewicz, K. Slowinski, *Chem. Commun.*, **2004**, 404–405.
31. C. Vericat, M. E. Vela, R. C. Salvarezza, *Phys. Chem. Chem. Phys.*, **2005**, *7*, 3258 – 3268.
32. J. C. Love, L. A. Estroff, J. K. Kriebel, R. G. Nuzzo, G. M. Whitesides, *Chem. Rev.*, **2005**, *105*, 1103-1139.
33. G. E. Poirier, *Chem. Rev.*, **1997**, *97*, 1117-1127.
34. A. Badia, R. B. Lenox, L. Reven, *Acc. Chem. Res.* **2000**, *33*, 475-481.
35. R.J. Davey, S.L.M. Schroeder, J.H. ter Horst, *Angew. Chem. Int. Ed.*, **2013**, *52*, 2166-2179.
36. (a) D. Turnbull, *J. Chem. Phys.*, **1950**, *18*, 198–203. T.E. Quested, A.L. Greer, *Acta Mater.*, **2005**, *53*, 2683–2692. (b) K. Ino, I. Udagawa, K. Iwabata, Y. Takakusagi, M. Kubota, K. Kurosaka, K. Arai, Y. Seki, M. Nogawa, A. Mariaux, M. Rappaz, *Acta Mater.*, **2011**, *59*, 927-933.



37. J. Kuther, R. Seshadri, W. Knoll, W. Tremel, *J. Mater. Chem.*, **1998**, 8, 641-650.
38. B. Pokroy, V.F. Chernow, J. Aizenberg, *Langmuir*, **2009**, 25, 14002-14006.
39. A. Y. Lee, I. S. Lee, A. S. Myerson, *Chem. Eng. Technol.*, **2006**, 29, 281-285.
40. J. R. Cox, M. Dabros, J. A. Shaffer, V. R. Thalladi, *Angew. Chem. Int. Ed.*, **2007**, 46, 1988-1991.
41. Y. Diao, A. S. Myerson, T. A. Hatton, B. L. Trout, *Langmuir*, **2011**, 27, 5324-5334.
42. (a) D.S. Tsekova, D.R. Williams, J.Y.Y. Heng, *Chem. Eng. Sci.*, **2012**, 77, 201-206. (b) O. Werzer, N. Boucher, J.P. de Silva, G. Gbabode, Y.H. Geerts, O. Konovalov, A. Moser, J. Novak, R. Resel, M. Sferrazza, *Langmuir*, **2012**, 28, 8530-8536. (c) C. Weber, C. Frank, S. Bommel, T. Rukat, W. Leitenberger, P. Schafer, F. Schreiber, S. Kowarik, *J. Chem. Phys.*, **2012**, 136, Art. No. 204709. (d) J. Martinez-Blanco, A. Mascaraque, Y.S. Dedkov, K. Horn, *Langmuir*, **2012**, 28, 3840-3844. (e) X.L. Qiao, Y.H. Geng, D.H. Yan, *J. Phys. Chem. B*, **2012**, 116, 1812-1818.
43. A. Singh, I.S. Lee, K. Kim, A.S. Myerson, *CrystEngComm*, **2011**, 13, 24-32.
44. R. Sancho, C. Minguillon *Chem. Soc. Rev.*, **2009**, 38, 797-805.
45. Y. Mastai, *Chem. Soc. Rev.*, **2009**, 38, 772-780.
46. D. H. Dressler, Y. Mastai, *Chirality*, **2007**, 19, 358-365.
47. D.H. Dressler, I. Hod, Y. Mastai, *J. Cryst. Growth*, **2008**, 310, 1718-1724.
48. M. Ejgenberg, Y. Mastai, *Chem. Commun.*, **2011**, 47, 12161-12163.
49. (a) S. Franzen, *Chem. Phys. Lett.*, **2003**, 381, 315-321. (b) X. Li, J. Huskens, D. N. Reinhoudt, *J. Mater. Chem.*, **2004**, 14, 2954-2971.
50. M. D. Eddleston, W. Jones, *Cryst. Grow. Design*, **2010**, 10, 365-370.
51. K. Kim, A. Centrone, T. A. Hatton, A. S. Myerson, *CrystEngComm*, **2011**, 13, 1127-1131.
52. D.H. Dressler, Y. Mastai, *J. Colloid Interface Sci.*, **2007**, 310, 653-660.
53. T. Nakanishi, N. Bannob, M. Matsunaga, T. Asahi, T. Osaka, *Colloids Surf. A: Physicochem. Eng. Aspects*, **2006**, 284-285, 270-275.
54. A. Singh, A.S. Myerson, *J. Pharm. Sci.*, **2010**, 99, 3931-3940.
55. L. Addadi, S. Weinstein, E. Gati, I. Weissbuch, M. Lahav, *J. Am. Chem. Soc.*, **1982**, 104, 4610-4617.
56. M. Ejgenberg, Y. Mastai, *Chem. Commun.*, **2011**, 47, 12161-12163.

57. (a) D. Turnbull, *J. Chem. Phys.*, **1950**, *18*, 198–203. (b) T.E. Quedstedt, A.L. Greer, *Acta Mater.*, **2005**, *53*, 2683–2692. (c) A. Mariaux, M. Rappaz, *Acta Mater.*, **2011**, *59*, 927–933. (d) G. Di Profio, E. Fontananova, E. Curcio, E. Drioli, *Cryst. Growth Des.*, **2012**, *12*, 3749–3757.

58. J. Aizenberg, A. J. Black, G. M. Whitesides, *Nature*, **1999**, *398*, 495–498.

59. (a) A. Singh, I.S. Lee, A.S. Myerson, *Cryst. Growth Des.*, **2009**, *9*, 1182–1185. (b) K. Kim, A. Centrone, T.A. Hatton, A.S. Myerson, *Cryst. Eng. Comm.*, **2011**, *13*, 1127–1131.

60. (a) A.Y. Lee, I.S. Lee, S.S. Dettet, J. Boerner, A.S. Myerson, *J. Am. Chem. Soc.*, **2005**, *127*, 14982–14983. (b) K. Kim, I.S. Lee, A. Centrone, T.A. Hatton, A.S. Myerson, *J. Am. Chem. Soc.*, **2009**, *131*, 18212–18213.

61. Z. Kozisek, *CrystEngComm*, **2013**, *15*, 2269–2274.

### Chapter 3

1. <http://www.ccdc.cam.ac.uk/Solutions/CSDSystem/Pages/Mercury.aspx>

2. W. Ten Hoeve, H. Wynberg, *J. Org. Chem.*, **1985**, *50*, 4508–4514.

3. R. M. Kellogg, J. W. Nieuwenhuijzen, K. Pouwer, T. R. Vries, Q. B. Broxterman, R. F. P. Grimbergen, B. Kaptein, R. M. La Crois, E. de Wever, K. Zwaagstra, A. C. van der Laan, *Synthesis*, **2003**, *10*, 1626–1638.

4. A. Herrera Fernández, R. Martínez Álvarez, *Tablas para la determinación estructural por métodos espectroscópicos*, **2000**, (ISBN 84-07-00501-0).

6. C. F. Macrae, I. J. Bruno, J. A. Chisholm, P. R. Edgington, P. McCabe, E. Pidcock, L. Rodriguez-Monge, R. Taylor, J. van de Streek and P. A. Wood, *J. Appl. Cryst.*, **2008**, *41*, 466–470.

7. (a) F. H. Allen, W. D. S. Motherwell, *Acta Cryst.*, **2002**, *58*, 407–422. (b) A. D. Bondw, *The Role of the Cambridge Structural Database in Crystal Engineering in Organic Crystal Engineering: Frontiers in Crystal Engineering*, **2010**, (eds E. R. T. Tiekink, J. Vittal and M. Zaworotko), John Wiley & Sons, Ltd, Chichester, UK. doi: 10.1002/9780470681794.ch1

8. A. M. G. Kok, H. Wynberg, J. M. M. Smits, P. T. Beurskens, V. Parthasarathi, *Acta Crystallogr., Sect. C: Struct. Commun.*, **1987**, *43*, 1328.

9. J. Dalmolen, M. van der Sluis, J.W. Nieuwenhuijzen, B. de Lange, B. Kaptein, R.M. Kellogg, Q.B. Broxterman. *Eur. J. Org. Chem.*, **2004**, 1544–1557.

10. N. Matsunaga, T. Kaku, A. Ojida, T. Tanaka, T. Hara, M. Yamaoka, M. Kusaka, A. Tasaka, *Bioorg. Med. Chem.*, **2004**, *12*, 4313.
11. (a) J. Bernstein, R. E. David, L. Shimoni, N. Chang, *Angew. Chem. Int. Ed. Engl.*, **1995**, *34*, 1555-1573. (b) M. C. Etter, *J. Phys. Chem.*, **1991**, *95*, 4601-4610.
12. <sup>1</sup> H. D. Flack, *Helvet. Chim. Acta*, **2003**, *86*, 905-921.

## Chapter 4

1. V. A. Shchukin, D. Bimberg, *Rev. Mod. Phys.*, **1999**, *71*, 1125-1171.
2. S. Hecht, *Angew. Chem. Int. Ed.*, **2003**, *42*, 24-26.
3. X. Li, J. Huskens, D. N. Reinhoudt, *J. Mater. Chem.*, **2004**, 2954-2971.
4. J. C. Love, L. A. Estroff, J. K. Kriebel, R. G. Nuzzo, G. M. Whitesides, *Chem. Rev.*, **2005**, *105*, 1103-1139.
5. A. Badia, R. B. Lenox, L. Reven, *Acc. Chem. Res.* **2000**, *33*, 475-481.
6. Thin films. Volume 24. J. Tien, Y. Xia, G. M. Whitesides. Department of Chemistry and Chemical Biology Harvard University, Cambridge, Massachusetts. 1998, Academic Press. ISBN 0-12-533024-3.
7. J. Aizenberger, *Bell Labs Technical Journal*, **2005**, *10*, 129-141.
8. A. Y. Lee, A. Ulman, A. S. Myerson, *Langmuir*, **2002**, *18*, 5886-5898.
9. K. Hinds, D.W. Grainger, *Langmuir* **1996**, *12*, 5083-5086.
10. R.M. Petoral Jr., F. Björefors, K. Uvdal, *J. Phys. Chem. B*, **2006**, *110*, 23410-23410.
11. G.E. Poirier, *Langmuir*, **1997**, *13*, 2019-2026; b) R. Yamada, K. Uosaki, *Langmuir*, **1998**, *14*, 855-861.
12. E. Torres A.T. Blumenau, P.U. Biedermann, *Phys. Rev. B.*, **2009**, *79*, 075440.
13. C. Vericat, M.E. Vela. R. C. Salvarezza, *Phys. Chem. Chem. Phys.*, **2005**, *7*, 3258-3268.
14. K. Hinds, D.W. Grainger, *Langmuir* **1996**, *12*, 5083-5086.
15. H.-S. Ahn., P. D. Cuong, S. Park, Y.-W. Kim, J.-C. Lim, *Wear* **2003**, *255*, 819-825.
16. (a) G. E. Poirier, M. J. Tarlov, *Langmuir* **1994**, *10*, 2853-2856. (b) C. Munuera, E. Barrera, C. Ocal, *J. Phys. Chem. A* **2007**, *111*, 12721-12726.
17. (a) G. E. Poirier, *Chem. Rev.* **1997**, *97*, 1117-1127. (b) C. Vericat, M.E. Vela, G. Benitez, P. Carro, R.C. Salvarezza, *Chem. Soc. Rev.* **2010**, *39*, 1805-1834. (c) E. Pensa,

E. Cortes, G. Corthey, P. Carro, C. Vericat, M.H. Fonticelli, G. Benitez, A.A. Rubert, R.C. Salvarezza, *Acc. Chem. Res.* **2012**, *45*, 1183-1192.

18. K. Hinds, D.W. Grainger, *Langmuir* **1996**, *12*, 5083-5086.

19. J. Zhou, D. A. Beattie, R. Sedev, J. Ralston, *Langmuir* **2007**, *23*, 9170-9177.

## Chapter 5

1. R. William, *pKa Data Compiled*, University of Washington at Seattle.

2. C. S. Fadley, *Nuclear Instrument and Method in Physics Research A*, **2009**, *601*, 8-31.

3. P. M. Dietrich, N. Graf, T. Gross, A. Lippitz, S. Krakert, B. Schüpbach, A. Terfortb, W. E. S. Unger, *Surf. Interface Anal*, **2010**, *42*, 1184–1187.

4. D. G. Caster, *Langmuir*, **1996**, *12*, 5083-5086.

5. R. M. Petoral, Jr. F. Björefors, K. Uvdal, *J. Phys. Chem. B*, **2006**, *110*, 23410-23416.

6. C. Dubois, F. Stellacci, *J. Phys. Chem. C*, **2008**, *112*, 7431-7435.

7. P. M. Dietrich, N. Graf, T. Gross, A. Lippitz, S. Krakert, B. Schüpbach, A. Terfortb, W. E. S. Unger, *Surf. Interface Anal*, **2010**, *42*, 1184–1187.

8. A. Atrens, A. S. Lim. *Applied Physics A*, **1990**, *51*, 411-418.

9. D. G. Caster, *Langmuir*, **1996**, *12*, 5083-5086.

10. *The microcontact printing protocol explained in detail in Chapter 7.*

11. Kun-Lin Yang et al. *Adv. Mater.* **2003**, *15*, 1819-1822.

12. D. G. Caster, *Langmuir*, **1996**, *12*, 5083-5086.

13. R. M. Petoral, Jr. F. Björefors, K. Uvdal, *J. Phys. Chem. B*, **2006**, *110*, 23410-23416.

14. D. G. Caster, *Langmuir*, **1996**, *12*, 5083-5086.

15. R. M. Petoral, Jr. F. Björefors, K. Uvdal, *J. Phys. Chem. B*, **2006**, *110*, 23410-23416.

## Chapter 6

1. R. P. Sear, *J. Phys. Chem. B*, **2006**, *110*, 4985-4989.
2. B. Pokroy, V. F. Chernow, J. Aizenberg, *Langmuir*, **2009**, *25*, 14002–14006.
3. Y. J. Han, J. Aizenberg, *Angew. Chem. Int. Ed.*, **2003**, *42*, 3668–3670.
4. R. Hiremath, J. A. Basile, S. W. Varney, J. Aizenberg. Swift, *J. Am. Chem. Soc.*, **2005**, *127*, 18321-18327.
5. F. Zhang, J. Liu, H. Huang, B. Du, T. He, *Eur. Phys. J. E*, **2002**, *8*, 289-297.
6. (a) A. Al-Mahboob, J.T. Sadowsk, T. Nishihara, Y. Fujikawa, Q.K. Xu, K. Nakajima, T. Sakurai, *Surf. Sci.*, **2007**, *601*, 1311-1318; (b) P. De Marco, F. Fioriti, F. Bisti, P. Parisse, S. Santucci, L. Ottaviano, *J. Appl. Phys.*, **2011**, *109*, 063508.
7. Chapter 3, *Crystal structure analysis*.

## Chapter 7

1. P. Arjan, E. Quist, E. Pavlovic, S. Oscarsson, *Anal Bioanal Chem*, **2005**, *381*, 591–600.
2. (a) P, Zorlutuna, N, Annabi, G. Camci-Unal, M. Nikkhah, JM. Cha, JW. Nichol, A. Manbachi, HJ. Bae, SC. Chen, A. Khademhosseini, *Adv. Mat.*, **2012**, *24*, 1782-1804. (b) M. Mrksich, G. M. Whiteside, *Trends in biotechnology*, **1995**, *13*, 228–235.
3. T. Kaufmann, B. J. Ravoo, *Polym. Chem.*, 2010, *1*, 371–387.
4. Y.N. Xia, G.M. Whitesides, *Angew. Chem. Int. Ed.* **1998**, *37*, 551-575.
5. Y. Xia, G, M. Whitesides, *Langmuir*, **1997**, *13*, 2059-2067.
6. J. Aizenberg, A. J. Black, G. M. Whitesides, *Nature*, **1998**, *394*, 868-871.
7. J. Aizenberg, A. J. Black, G. M. Whitesides, *Nature*, **1999**, *398*, 495-498.
8. J. Aizenberg, *Adv. Matter.*, **2004**, *16*, 1295-1302.
9. <http://www.wieweb.com/ns6/index.html>
10. <http://www.photonics.com/plab/photonics/>
11. A. Perl, D. N. Reinhoudt, J. Huskens, *Adv. Mater*, **2009**, *21*, 2257-2268.
12. G. M. Wallraff, W. D. Hinsberg, *Chem. Rev.*, **1999**, *99*, 1801.
13. D. B. Weibel, W. R. DiLuzio, G. M. Whitesides, *Nature Reviews Microbiology*, **2007**, *5*, 209–218.

14. A. Perl, D. N. Reinhoudt, J. Huskens, *Adv. Mater.*, **2009**, *21*, 2257-2268.
15. H. Schmid, B. Michel, *Macromolecules*, **2000**, *33*, 3042-3049.
16. E. E. Hamurcu, B. M. Baysal, *Polymer*, **1993**, *34*, 5163-5167.
17. <http://www.dowcorning.com>
18. J.N. Lee, C. Park, G.M. Whitesides, *Anal. Chem.*, **2003**, *75*, 6544-6554.

## Chapter 8

### Chapter 8.1.

1. D. H. Dressler, Y. Mastai, *Chirality*, **2007**, *19*, 358-365.
2. K. Kim, A. Centrone, T. A. Hatton, A. S. Myerson, *Cryst. Eng. Comm.*, **2010**.
3. R. Hiremath, J. A. Basile, S. W. Varney, J. A. Swift, *J. Am. Chem. Soc.*, **2005**, *127*, 18322- 18327.
4. (a) C. J. Stephens, Y. Kim, S. D. Evans, F. C. Meldrum, H. K. Christenson, *J. Am. Chem. Soc.*, **2011**, *133*, 5210–5213. (b) J. Aizenberg, *Bell Labs Technical Journal*, **2005**, *10*, 129–141.
5. N. Erdemir, A. Y. Lee, A. S. Myerson, *Acc. Chem. Res.*, **2009**, *42*, 621-629.
6. (a) A. Y. Lee, A. Ulman, A. S. Myerson. *Langmuir*, **2002**, *18*, 5886-5898. (b) D. J. Turnbull, *Chem. Phys.* **1949**, *18*, 198.
7. J. Aizenberg, A. J. Black ; G. M. *Nature*, **1999**, *398*, 495-498.
8. A. Y. Lee, I. S. Lee, A. S. Myerson, *Chem. Eng. Technol.* **2006**, *29*, 281-285.
9. K. Kim, A. Centrone, T. A. Hatton, A. S. Myerson, *Cryst. Eng. Comm.*, **2011**, *13*, 1127.
10. R. B. A Sharpe, *Controlling mass transport in microcontact printing*, **2005**, University of Twente, the Netherlands (ISBN: 90-356-2320-6).
11. Y. Xia, G. M. Whitesides, *Angew. Chem.*, **1998**, *37*, 550-575.
12. D. H. Dressler, Y. Mastai, *J. Colloid Interface Sci.* **2007**, *310*, 653–660.
13. ] Nakanishi, T.; Bannob, N.; Matsunaga M.; Asahi, T.; Osaka, T. *Colloids Surf. A: Physicochem. Eng. Aspects* **2006**, *284–285*, 270–275.
14. A. Singh, A.S Myerson, *J. Pharm. Sci.* **2010**, *99*, 3931-3940.

15. (a) L. Addadi, J. Vanmil, M. Lahav, *J. Am. Chem. Soc.* **1981**, *103*, 1249-1251. (b) L. Addadi, S. Weinstein, E. Gati, I. Weissbuch, M. Lahav, *J. Am. Chem. Soc.* **1982**, *104*, 4610-4617.

16. M. Ejgenberg, Y. Mastai, *Chem. Commun.*, **2011**, *47*, 12161–12163.

17. A. Bejarano-Villafuerte, M. van der Meijden, M. Lingenfelder, K. Wurst, R.M. Kellogg, D. B. Amabilino, *Chem. Eur. J.*, 2012, *18*, 15984-15993.

18. (a) Leeman, M.; Querniard, F.; Vries, T.R.; Kaptein, B.; Kellogg, R.M. *Org. Proc. Res. Dev.* **2009**, *13*, 1379-1381. (b) Nieuwenhuijzen, J.W.; Grimbergen, R.F.P.; Koopman, C.; Kellogg, R.M.; Vries, T.R.; Pouwer, K.; van Echten, E.; Kaptein, B.; Hulshof, L.A.; Broxterman, Q.B.; *Angew. Chem. Int. Ed.* **2002**, *41*, 4281-4286.

19. Singh, A.; Lee, I.S.; Myerson, A.S. *Cryst. Growth Des.* **2009**, *9*, 1182-1185.

## 20. Chapter 1, Introduction.

21. (a) G. Berteloot, A. Hoanga, A. Daerr, H. P. Kavehpour, F. Lequeux, L. Limat, *J. Colloid Interf. Scie*, **2012**, *370*, 155–161. (b) H. Y. Erbil, *Adv. Colloid Interf. Scie*, **2012**, *170*, 67–86.

22. H. Imai, Y. Oaki, *Angew. Chem. Int. Ed.*, **2004**, *43*, 1363 –1368.

23. H. Imai, Y. Oaki, *CrystEngComm*, **2010**, *12*, 1679-1687.

24. J. C. Love, L. A. Estroff, J. K. Kriebel, R. G. Nuzzo, G. M. Whitesides, *Chem. Rev.*, **2005**, *105*, 1103-1169.

25. A. Bejarano-Villafuerte, M. van der Meijden, M. Lingenfelder, K. Wurst, R.M. Kellogg, D.B. Amabilino, *Chem. Eur. J.*, 2012, **18**, 15984-15993.

26. H. Goto, Y. Okamoto, E. Yashima, *Macromolecules*, **2002**, *35*, 4590-4601. W. Yu, Y.G. Li, T.Y. Wang, M.H. Liu, Z.S. Li, *Acta Phys-Chim Sinica*, **2008**, *24*, 1535-1539. K. Smith, *Chem. Soc. Rev.*, **2009**, *38*, 684-694. Q.B. Wang, Y.L. Chen, P. Ma, J.T. Lu, X.M. Zhang, J.Z. Jiang, *J. Mater. Chem.*, **2011**, *21*, 8057-8065. I.C. Pintre, S. Pierrefixe, A. Hamilton, V. Valderrey, C. Bo, P. Ballester, *Inorg. Chem.*, **2012**, *51*, 4620-4635.

27. I. Alkorta, I. Rozas, J. Elguero, *Chem. Soc. Rev.*, **1998**, *27*, 163-170.

28. A. Gavezzotti, *Mol. Phys.*, 2008, **106**, 1473-1485.

29. M. Rapp, W.A. Ducker, *J. Am. Chem. Soc.*, 2010, **132**, 18051–18053.

## Chapter 8.2.

1. D. Kozma, Z. Madarász, C. Kassai, E. Fogassy. *Chirality*, **1999**, *11*, 373-375.

2. L. Pasteur, *Compte-rendus de l'Académie des Sciences*, **1853**, *37*, 162-166.

3. W. Marckwald, *Ueber ein bequemes Verfahren zur Gewinnung der Linksweinsäure*, *Berichte der deutschen chemischen Gesellschaft*, **1896**, 29, 42–43.

4. W.J. Pope, S. J. Peachey, *J. Chem. Soc, Trans.*, **1899**, 75, 1066-1093.

5. **Chapter 1**, *Introduction, Nucleation theory*.

6. (a) D. Losic, J. G. Shapter, J. J. Gooding, *ElectroChem. Comm.*, **2001**, 3, 722-726. (b) Thomas J. Mullen, C. Srinivasan, J. N. Hohman, S. D. Gillmor, *Applied Phys. Lett.*, **2007**, 90, 063114-1-3.

7. **Chapter 4**, *(+)-PMT SAMs on gold, STM analysis*.

8. J. C. Love, L. A. Estroff, J. K. Kriebel, R. G. Nuzzo, G. M. Whitesides, *Chem. Rev.*, **2005**, 105, 1103-1169.

9. E. Pálovics J. Schindler, F. Faigl, E. Fogassy, *Tetrah. Asym.*, **2010**, 21, 2429–2434.

10. A. Singh, A.S. Myerson, *J. Pharm. Sci.*, **2010**, 99, 3931-3940.

11. E. Kim, G. M. Whitesides, *Chem. Mater.*, **1995**, 7, 1257-1264.

12. A. Brock, E. Chang, C. H, P. LeDuc, X. Jiang, G. M. Whitesides, D. E. Ingber, *Langmuir*, **2003**, 19, 1611-1617.

13. M. Rapp, W. A. Ducker, *J. Am. Chem. Soc.*, **2010**, 132, 18051-18053.

14. (a) J. M. García-Ruiz, M. A. Hernández-Hernández, J. Gómez-Morales, *J. Ind. Crystallogr.*, **2008**, 27, 99-106. (b) [www.trianatech.com](http://www.trianatech.com)

15. G. Tosi, S. Fermani, G. Falini, J. A. Gavira, J. M. García Ruiz, *Cryst. Growth Des.*, **2011**, 11, 1542-1548.

16. J.M. García-Ruiz, *Journal of Structural Biology*, 2003, 142, 22–31.

### **Chapter 8.3.**

1. T. J. Wozniak, R. J. Bopp, E. C. Jensen, *J. Pharmac. & Biomed. Anal.*, **1991**, 9, 363-382.

2. R.M. Kellogg, J. W. Nieuwenhuijzen, K. Pouwer, T. R. Vries, Q. B. Broxterman, R. F.P. Grimbergen, B. Kaptein, R. M. La Crois, E. de Wever, K. Zwaagstra, A. C. van der Laana, *Synthesis*, **2003**, 10, 1626–1638.

3. T. Vries, H. Wynberg, E. van Echten, J. Koek, W. ten Hoeve, R. M. Kellogg, Q. B. Broxterman, A. Minnaard, B. Kaptein, S. van der Sluis, L. Hulshof, J. Kooistra, *Angew. Chem. Int. Ed.*, **1998**, 37, 2349-2354.

4. J. Aizenberg, *Adv. Matter.*, **2004**, 16, 1295-1302.